

# CELLULAR INTERACTIONS UNDERPINNING THE IMMUNOMODULATORY ACTION OF MESENCHYMAL STROMAL CELLS IN MODELS OF LIVER TRANSPLANT INJURY

by

ANDREW PHILIP OWEN

A thesis submitted to  
The University of Birmingham  
for the degree of  
DOCTOR OF PHILOSOPHY

Institute of Immunology and Immunotherapy  
College of Medical and Dental Sciences  
The University of Birmingham  
28th January 2018

UNIVERSITY OF  
BIRMINGHAM

**University of Birmingham Research Archive**

**e-theses repository**

This unpublished thesis/dissertation is copyright of the author and/or third parties. The intellectual property rights of the author or third parties in respect of this work are as defined by The Copyright Designs and Patents Act 1988 or as modified by any successor legislation.

Any use made of information contained in this thesis/dissertation must be in accordance with that legislation and must be properly acknowledged. Further distribution or reproduction in any format is prohibited without the permission of the copyright holder.

## Abstract

End stage liver disease represents a common end point for a number of disease processes, the only current treatment for which is liver transplantation, but the demand for donor organs exceeds the supply. This has led to the use of more marginal donors with an increase in the rates of complications. Mesenchymal stem/stromal cells (MSC) are a multipotent cell capable of modulating the immune system through a number of different processes and represent a potential therapy in post transplantation liver injury.


In this study I describe the prospective isolation and culture expansion of murine MSC. In *in vitro* assays MSC suppressed T lymphocytes and following stimulus with inflammatory cytokines MSC secreted a number of cytokines including Il-10. In the MDR2<sup>-/-</sup> model intravenous MSC therapy led to a reduction in liver injury with an increase in restorative macrophages. Subcutaneous administration of MSC showed no beneficial effect. MSC were also tested in a hepatic ischaemia reperfusion injury model where no effect was seen.

In summary MSC were able to suppress lymphocyte proliferation and secrete anti-inflammatory cytokines *in vitro*, and *in vivo* they were able to reduce liver injury in the MDR2<sup>-/-</sup> model but not the hepatic ischaemia reperfusion injury mode.

This thesis is dedicated to my wife Molly  
and my children Florence and Jacob who  
believed in me and supported me throughout  
my studies.

## ACKNOWLEDGEMENTS

I would like to thank my supervisors Professor Newsome and Professor Frampton for their help and support. I would also like to thank the staff in the Centre for Liver Research for welcoming me into their department and in particular I would like to thank Dr Vasanthi Vigneswara and Mr Mohammed Alfaifi for their assistance with my animal work, Dr Daniel Patten for his assistance with a variety of laboratory techniques and Dr Chris Weston and Dr Patricia Lalor for their assistance in troubleshooting when things were not working as expected.

I would also like to thank the staff at the  as the *in vivo* work would not have been possible without their support, and the biochemistry team at the Birmingham Women's Hospital for analysing serum samples.

Finally I would like to thank Professor Julian Bion for his mentorship during my academic career and the MRC for providing the funding to carry out this research.

# CONTENTS

<b>1</b>	<b>Introduction</b>	<b>1</b>
1.1	Overview . . . . .	1
1.2	End-stage liver disease . . . . .	1
1.3	Anatomy and function of the human liver . . . . .	3
1.3.1	Surfaces and functional anatomy of the liver . . . . .	3
1.3.2	Blood supply to the liver and biliary drainage . . . . .	4
1.3.3	Microscopic anatomy of the liver . . . . .	5
1.3.4	Comparison of mouse and human liver . . . . .	6
1.4	Current therapeutic strategies in patients with end stage liver disease . . .	6
1.4.1	Cell therapy for end stage liver disease . . . . .	6
1.4.2	Liver transplantation . . . . .	7
1.4.3	Marginal organ donation . . . . .	8
1.4.4	Complications of liver transplantation . . . . .	9
1.4.4.1	Perioperative complications . . . . .	9
1.4.4.2	Acute and chronic rejection . . . . .	10
1.4.4.3	Biliary complications . . . . .	10
1.5	Hepatic ischaemia reperfusion injury . . . . .	11
1.5.1	Ischaemic injury to the liver . . . . .	12
1.5.2	Hepatic reperfusion injury . . . . .	14
1.5.3	Strategies to limit ischaemia reperfusion injury . . . . .	17
1.5.3.1	Ischaemic preconditioning . . . . .	17

1.5.3.2	Treatment with xanthine oxidase inhibitors . . . . .	17
1.5.3.3	Cyclophilin D inhibitors . . . . .	18
1.6	Animal models of liver injury . . . . .	18
1.6.1	Carbon tetrachloride . . . . .	19
1.6.2	MDR2 <sup>-/-</sup> . . . . .	19
1.6.3	Hepatic ischaemia reperfusion injury . . . . .	19
1.6.4	Liver transplantation . . . . .	20
1.7	Immune system . . . . .	20
1.7.1	Innate immunity . . . . .	21
1.7.2	Adaptive immunity . . . . .	22
1.7.2.1	T lymphocytes . . . . .	22
1.7.2.2	B lymphocytes . . . . .	25
1.7.2.3	Natural killer T cells . . . . .	26
1.8	Mesenchymal stromal cells . . . . .	26
1.8.1	Evolution of a bone marrow stromal cell niche . . . . .	27
1.8.2	Isolation techniques for MSC . . . . .	29
1.8.3	MSC and immunomodulation . . . . .	31
1.9	MSC in liver disease . . . . .	33
1.9.1	Liver fibrosis and cirrhosis . . . . .	34
1.9.2	Acute liver failure . . . . .	35
1.9.3	Ischaemia reperfusion injury and transplantation . . . . .	36
1.9.4	Acute hepatitis . . . . .	37
1.9.5	Chronic hepatitis . . . . .	38
1.9.6	Concerns about tumour formation . . . . .	38
1.9.7	Route of administration and homing . . . . .	39
1.9.8	Cell therapy without administering cells . . . . .	40
1.9.9	Tracking MSC <i>in vivo</i> . . . . .	41
1.10	Aims and Objectives . . . . .	42

1.10.1	Hypotheses . . . . .	42
1.10.2	Specific aims . . . . .	43
<b>2</b>	<b>Methods</b>	<b>44</b>
2.1	Preparation of buffers and culture media . . . . .	44
2.1.1	P2 buffer . . . . .	44
2.1.2	FACS buffer . . . . .	44
2.1.3	MACS buffer . . . . .	44
2.1.4	C10 media . . . . .	45
2.1.5	HBSS <sup>+</sup> . . . . .	45
2.1.6	$\alpha$ -MEM culture medium . . . . .	45
2.2	Animal husbandry . . . . .	45
2.2.1	Wildtype mice . . . . .	46
2.2.2	OT-1 mice . . . . .	46
2.2.3	MDR2 <sup>-/-</sup> mice . . . . .	46
2.2.4	Genotyping . . . . .	46
2.3	Prospective isolation of murine P $\alpha$ S MSC by cell sorting . . . . .	47
2.3.1	Long bone removal and preparation . . . . .	47
2.3.2	Preparation of cell suspension . . . . .	48
2.3.3	Red cell lysis . . . . .	49
2.3.4	Labelling of MSC with fluorescent antibodies . . . . .	49
2.3.5	Cell sorting of fluorescently labelled MSC . . . . .	50
2.4	P $\alpha$ S MSC culture . . . . .	51
2.5	P $\alpha$ S MSC passage . . . . .	51
2.6	<i>In vitro</i> naive lymphocyte immunosuppression assay . . . . .	52
2.6.1	Isolation of CD4 <sup>+</sup> CD25 <sup>-</sup> T lymphocytes using MACS MicroBeads . . . . .	52
2.6.2	Isolation of CD19 <sup>+</sup> B lymphocytes using MACS MicroBeads . . . . .	53
2.6.3	Proliferation and flow cytometric analysis . . . . .	54
2.7	<i>In vitro</i> splenocyte reaction . . . . .	55



2.7.1	Isolation of bulk splenocytes . . . . .	55
2.7.2	Stimulation of CD8 <sup>+</sup> lymphocytes with OVA <sub>257-264</sub> peptide . . . . .	56
2.7.3	Flow cytometric analysis . . . . .	56
2.8	MDR2 <sup>-/-</sup> knockout model of liver injury . . . . .	57
2.8.1	Treatment of MDR2 <sup>-/-</sup> mice with PαS MSC . . . . .	58
2.9	Murine model of hepatic ischaemia reperfusion injury . . . . .	58
2.9.1	Surgical technique . . . . .	58
2.10	Collection of murine blood and tissue . . . . .	59
2.11	Analysis of serum liver enzymes . . . . .	60
2.12	Western blotting . . . . .	60
2.12.1	Liver tissue lysis . . . . .	60
2.12.2	Determination of protein concentration using the biuret assay . . . . .	61
2.12.3	Western blotting for CK19 . . . . .	61
2.12.3.1	Loading controls . . . . .	63
2.13	Liver immune cell isolation . . . . .	63
2.13.1	Isolation of liver immune cells using Lympholyte <sup>®</sup> . . . . .	64
2.13.2	Isolation of liver immune cells using Optiprep <sup>™</sup> . . . . .	64
2.13.3	Isolation of immune cells from whole blood . . . . .	65
2.13.4	Viability and surface antibody staining of isolated circulating or liver immune cells for flow cytometry . . . . .	65
2.13.5	Intracellular staining for FoxP3 . . . . .	66
2.14	MSC surface markers . . . . .	67
2.15	Protein array . . . . .	67
2.16	QDot <sub>605</sub> experiments . . . . .	68
2.16.1	Labelling PαS MSC with QDot <sub>605</sub> . . . . .	68
2.16.2	Cryoimaging . . . . .	68
2.17	Immunohistochemistry . . . . .	69
2.17.1	Processing of paraffin samples . . . . .	69

2.17.2	Processing of frozen samples . . . . .	69
2.17.3	Haematoxylin and eosin staining . . . . .	70
2.17.4	Periodic acid-Schiff staining . . . . .	70
2.17.5	Chromogenic immunohistochemistry . . . . .	71
2.17.6	Structural fluorescence staining . . . . .	72
2.17.7	Slide scanning and analysis . . . . .	73
2.18	Statistical analysis . . . . .	73
2.19	Supplier information . . . . .	74
<b>3</b>	<b><i>In vitro</i> phenotype and properties of P<math>\alpha</math>S mesenchymal stromal cells</b>	<b>86</b>
3.1	Introduction and aims . . . . .	86
3.1.1	Specific chapter aims . . . . .	88
3.2	Results . . . . .	89
3.2.1	Prospective isolation of murine P $\alpha$ S MSC . . . . .	89
3.2.2	Surface marker expression of P $\alpha$ S MSC . . . . .	91
3.2.3	Developing an <i>in vitro</i> immunosuppression assay . . . . .	92
3.2.3.1	C57BL/6 MSC do not suppress purified lymphocytes when stimulated . . . . .	92
3.2.3.2	Development of a bulk splenocyte reaction to test the efficacy of P $\alpha$ S MSC . . . . .	93
3.2.3.3	<i>In vitro</i> efficacy of P $\alpha$ S MSC in a bulk splenocyte reaction	101
3.2.4	The effects of an inflammatory stimulus on P $\alpha$ S MSC . . . . .	104
3.2.4.1	P $\alpha$ S MSC morphology . . . . .	105
3.2.4.2	Cytokines secreted by P $\alpha$ S MSC . . . . .	106
3.3	Discussion . . . . .	109
3.3.1	Isolation, culture expansion and phenotype of murine P $\alpha$ S MSC . .	109
3.3.2	The ability of murine P $\alpha$ S MSC to suppress lymphocyte proliferation <i>in vitro</i> . . . . .	110
3.3.3	The secretome of P $\alpha$ S MSC exposed to an inflammatory stimulus .	111

3.3.4	Chapter summary . . . . .	113
<b>4</b>	<b>The <i>in vivo</i> efficacy of P<math>\alpha</math>S MSC in the MDR2<sup>-/-</sup> model of liver injury</b>	<b>115</b>
4.1	Chapter introduction and aims . . . . .	115
4.1.1	Non-anastomotic biliary complications following liver transplantation	115
4.1.2	MDR2 <sup>-/-</sup> mouse model of liver injury . . . . .	116
4.1.3	MSC as a therapy in immune mediated liver injury . . . . .	117
4.1.4	Specific chapter aims . . . . .	117
4.2	Results . . . . .	119
4.2.1	Genotyping of MDR2 <sup>-/-</sup> breeding pairs . . . . .	119
4.2.2	Time course of liver injury in the MDR2 <sup>-/-</sup> mouse model . . . . .	119
4.2.2.1	Serum markers of liver injury over time . . . . .	119
4.2.2.2	Liver immunohistochemistry over time . . . . .	122
4.2.2.3	Western blotting for CK19 expression . . . . .	127
4.2.2.4	Characterisation of liver lymphocytes by flow cytometry . . . . .	128
4.2.3	<i>In vivo</i> efficacy of P $\alpha$ S MSC in the MDR2 <sup>-/-</sup> model . . . . .	132
4.2.3.1	Effects of P $\alpha$ S MSC on serum markers of liver injury in the MDR2 <sup>-/-</sup> model . . . . .	132
4.2.3.2	Histological changes in MDR2 <sup>-/-</sup> mouse livers when treated with P $\alpha$ S MSC . . . . .	134
4.2.3.3	Effects on ductular proliferation in MDR2 <sup>-/-</sup> mouse livers when treated with P $\alpha$ S MSC . . . . .	142
4.2.3.4	Characterisation of immune cell populations in MDR2 <sup>-/-</sup> mice following treatment with P $\alpha$ S MSC . . . . .	143
4.3	Discussion . . . . .	150
4.3.1	Characterisation of the injury pattern MDR2 <sup>-/-</sup> mouse model . . . . .	150
4.3.1.1	Classical markers of injury in the MDR2 <sup>-/-</sup> mouse model . . . . .	150
4.3.1.2	Liver immune cell profile in the MDR2 <sup>-/-</sup> model . . . . .	151
4.3.2	P $\alpha$ S MSC reduce markers of injury in the MDR2 <sup>-/-</sup> model . . . . .	152

4.3.2.1	Timing and dose of P $\alpha$ S MSC . . . . .	152
4.3.2.2	Reduction in markers of liver injury with P $\alpha$ S MSC therapy	154
4.3.2.3	Changes in infiltrating immune cells in MDR2 <sup>-/-</sup> mouse livers	155
4.3.3	Chapter summary . . . . .	158
<b>5</b>	<b>The Distribution and remote action of P<math>\alpha</math>S MSC</b>	<b>159</b>
5.1	Chapter introduction and aims . . . . .	159
5.1.1	Distribution of parenterally administered mesenchymal stem cells .	159
5.1.2	Remote effects of mesenchymal stem cells . . . . .	160
5.1.3	Specific chapter aims . . . . .	161
5.2	Results . . . . .	162
5.2.1	<i>In vivo</i> tracking of systemically administered P $\alpha$ S MSC . . . . .	162
5.2.1.1	The effects of QDot <sub>605</sub> staining on P $\alpha$ S MSC . . . . .	162
5.2.1.2	Tracking QDot <sub>605</sub> labelled P $\alpha$ S MSC in the MDR2 <sup>-/-</sup> model of liver injury . . . . .	164
5.2.2	<i>In vivo</i> efficacy of subcutaneously administered P $\alpha$ S MSC in the MDR2 <sup>-/-</sup> model of liver injury . . . . .	171
5.2.2.1	Effects of subcutaneous P $\alpha$ S MSC on serum markers of liver injury in the MDR2 <sup>-/-</sup> model . . . . .	171
5.2.2.2	Histological changes in MDR2 <sup>-/-</sup> mouse livers when treated with subcutaneous P $\alpha$ S MSC . . . . .	172
5.2.2.3	Effects on ductular proliferation in MDR2 <sup>-/-</sup> mouse livers when treated with P $\alpha$ S MSC . . . . .	178
5.2.2.4	Characterisation of liver and serum immune cell popu- lations in MDR2 <sup>-/-</sup> mouse livers following subcutaneous treatment with P $\alpha$ S MSC . . . . .	179
5.3	Discussion . . . . .	182
5.3.1	Tracking systemically administered P $\alpha$ S MSC . . . . .	182

5.3.2	The effect of P $\alpha$ S MSC administered subcutaneously in the MDR2 <sup>-/-</sup> model . . . . .	184
5.3.3	Chapter summary . . . . .	185
<b>6</b>	<b>Development and <i>in vivo</i> efficacy testing of P<math>\alpha</math>S MSC in a model of hepatic ischaemia reperfusion injury</b>	<b>187</b>
6.1	Chapter introduction and aims . . . . .	187
6.1.1	Hepatic ischaemia reperfusion injury . . . . .	187
6.1.2	Mouse models of liver ischaemia reperfusion injury . . . . .	189
6.1.3	Specific chapter aims . . . . .	189
6.2	Results . . . . .	191
6.2.1	Developing a model of hepatic ischaemia reperfusion injury . . . . .	191
6.2.2	Time course of hepatic ischaemia reperfusion injury . . . . .	193
6.2.2.1	Serum transaminases in hepatic ischaemia reperfusion injury	193
6.2.2.2	Histochemical analysis in hepatic ischaemia reperfusion injury . . . . .	194
6.2.2.3	Analysis of liver infiltrating immune cells by flow cytometry in hepatic ischaemia reperfusion injury . . . . .	204
6.2.3	The effect of clamp duration in ischaemia reperfusion injury . . . . .	206
6.2.3.1	Serum transaminases following different clamp durations in hepatic ischaemia reperfusion injury . . . . .	206
6.2.3.2	Histochemical analysis of different clamp durations in hepatic ischaemia reperfusion injury . . . . .	207
6.2.3.3	The effect of clamp duration on liver infiltrating immune cells in hepatic ischaemia reperfusion injury . . . . .	213
6.2.4	<i>In vivo</i> efficacy of P $\alpha$ S MSC in the hepatic ischaemia reperfusion model . . . . .	215
6.2.4.1	Serum transaminases in hepatic ischaemia reperfusion injury following P $\alpha$ S MSC therapy . . . . .	216

6.2.4.2	Histochemical analysis in hepatic ischaemia reperfusion injury following P $\alpha$ S MSC therapy . . . . .	216
6.2.4.3	The effect of P $\alpha$ S MSC therapy on circulating and liver infiltrating immune cells in hepatic ischaemia reperfusion injury . . . . .	222
6.3	Discussion . . . . .	226
6.3.1	Injury pattern in the hepatic ischaemia reperfusion model . . . . .	227
6.3.1.1	Liver immune cell populations in ischaemia reperfusion injury . . . . .	229
6.3.2	The effects of clamp duration on ischaemic injury in the hepatic ischaemia reperfusion injury model . . . . .	231
6.3.3	The effects of P $\alpha$ S MSC therapy on hepatic ischaemia reperfusion injury . . . . .	232
6.3.4	Chapter summary . . . . .	234
<b>7</b>	<b>Discussion and Conclusions</b>	<b>235</b>
7.1	Summary of the main findings . . . . .	235
7.1.1	Phenotype and immunosuppressive action of P $\alpha$ S MSC <i>in vitro</i> . . . . .	236
7.1.2	The <i>in vivo</i> effects of P $\alpha$ S MSC in hepatic ischaemia reperfusion injury . . . . .	237
7.1.3	The <i>in vivo</i> effects of P $\alpha$ S MSC in biliary injury . . . . .	239
7.1.4	P $\alpha$ S MSC trafficking and remote effects in biliary injury . . . . .	240
7.2	Future work . . . . .	241
7.2.1	What is the mechanism of P $\alpha$ S MSC mediated immunosuppression in the MDR2 <sup>-/-</sup> model? . . . . .	241
7.2.2	Can P $\alpha$ S MSC be primed to respond depending on the inflammatory microenvironment? . . . . .	241
7.2.3	Can P $\alpha$ S MSC reduce injury in ischaemia reperfusion injury? . . . . .	242
7.2.4	Is MSC therapy a double edged sword? . . . . .	242

7.2.5	What are the effects of xenotransplantation and are murine cells a better model for further study? . . . . .	243
7.3	Final conclusions . . . . .	243
<b>Bibliography</b>		<b>245</b>

# LIST OF FIGURES

1.1	Diagram representing the functional anatomy of the liver . . . . .	4
1.2	Graphics depicting the microarchitecture of the liver . . . . .	5
1.3	Equation to calculate the UKELD score . . . . .	8
1.4	Diagram showing the main cellular ion changes in ischaemia and reperfusion injury . . . . .	16
1.5	Diagram showing the subsets of CD4 <sup>+</sup> T lymphocytes . . . . .	25
1.6	Diagram showing the effects of MSC on the immune system . . . . .	33
1.7	Diagram showing the effects of MSC in liver fibrosis . . . . .	35
1.8	Diagram of the effects of MSC in ischaemia reperfusion injury . . . . .	37
3.1	Representative flow cytometry plots demonstrating the gating strategy for isolating P $\alpha$ S MSC from collagenase digested bone marrow. . . . .	90
3.2	Representative image of the morphology of murine P $\alpha$ S MSC in culture. . . . .	90
3.3	Cultured P $\alpha$ S MSC express MSC surface antigens when assessed using flow cytometry . . . . .	91
3.4	P $\alpha$ S MSC isolated from C57BL/6 mice do not suppress purified naive lymphocytes unlike those isolated from BALB/c mice . . . . .	93
3.5	Optimisation of OVA <sub>257-264</sub> dose and splenocyte number in a splenocyte reaction . . . . .	95
3.6	CellTrace <sup>TM</sup> violet levels were reduced by similar amounts in CD8 <sup>+</sup> cells following stimulation with either 2 $\mu$ g/ml or 10 $\mu$ g/ml of OVA <sub>257-264</sub> . . . . .	96



3.7	A significantly greater percentage of CD8 lymphocytes proliferated when stimulated with OVA <sub>257-264</sub> . . . . .	97
3.8	Quantification of the numbers of immune cells on day 0 of a bulk splenocyte reaction . . . . .	98
3.9	Quantification of the numbers of immune cells on day 1 of a splenocyte reaction . . . . .	99
3.10	Quantification of the numbers of immune cells on day 4 of a bulk splenocyte reaction . . . . .	100
3.11	CellTrace <sup>TM</sup> violet fluorescence was reduced in CD8 <sup>+</sup> cells 96 hours after stimulation in the splenocyte reaction . . . . .	101
3.12	PαS MSC suppress CD8 <sup>+</sup> proliferation in a bulk splenocyte reaction . . . .	102
3.13	PαS MSC reduce CD8 <sup>+</sup> and CD8 <sup>+</sup> CD25 <sup>+</sup> numbers in a bulk splenocyte reaction . . . . .	103
3.14	PαS MSC reduce CellTrace <sup>TM</sup> violet fluorescence in CD8 <sup>+</sup> cells in a bulk splenocyte reaction . . . . .	104
3.15	Representative fluorescent histochemical images of PαS MSC stimulated with TNFα and IFN-γ . . . . .	106
3.16	Cytokine profile in the secretome of PαS MSC following stimulation with TNFα and IFN-γ . . . . .	107
3.17	Chemokine and adhesion molecule profile of PαS MSC following stimulation with TNFα and IFN-γ . . . . .	108
4.1	MDR2 <sup>-/-</sup> serum markers of liver injury show changes over time . . . . .	121
4.2	Representative haematoxylin and eosin staining of MDR2 <sup>-/-</sup> livers between 7 and 14 weeks . . . . .	123
4.3	Time course quantification of CD45 and F4/80 staining levels in MDR2 <sup>-/-</sup> mice . . . . .	124
4.4	Representative immunohistochemical staining for CD45 of MDR2 <sup>-/-</sup> livers between 7 and 14 weeks . . . . .	125

4.5	Representative immunohistochemical staining for F4/80 of MDR2 <sup>-/-</sup> livers between 7 and 14 weeks . . . . .	126
4.6	Western blot of the time course of CK19 levels in the MDR2 <sup>-/-</sup> mouse model	128
4.7	Flow cytometric analysis of immune cell numbers from 8 week old MDR2 <sup>-/-</sup> mouse liver following extraction with Lympholyte <sup>®</sup> . . . . .	129
4.8	Optiprep <sup>™</sup> yields a greater number of immune cells from liver digest then Lympholyte <sup>®</sup> in MDR2 <sup>-/-</sup> mice . . . . .	130
4.9	FACS analysis of MDR2 <sup>-/-</sup> mouse livers demonstrating the immune cell profile between 7 and 11 weeks of age . . . . .	131
4.10	PαS MSC significantly reduce ALT and ALP but not Bile acids in MDR2 <sup>-/-</sup> mice . . . . .	133
4.11	Representative images of haematoxylin and eosin staining in MDR2 <sup>-/-</sup> mice treated with either PBS or PαS MSC at 6-8 weeks of age and culled 2 weeks later . . . . .	135
4.12	CD45 expression in the livers of MDR2 <sup>-/-</sup> mice treated with either PBS or PαS MSC at 6-8 weeks of age and culled 2 weeks later . . . . .	136
4.13	Representative images of CD45 staining in MDR2 <sup>-/-</sup> mice treated with either PBS or PαS MSC at 6-8 weeks of age and culled 2 weeks later . . . . .	137
4.14	F4/80 expression in the livers of MDR2 <sup>-/-</sup> mice treated with either PBS or PαS MSC at 6-8 weeks of age and culled 2 weeks later . . . . .	138
4.15	Representative images of F4/80 staining in MDR2 <sup>-/-</sup> mice treated with either PBS or PαS MSC at 6-8 weeks of age and culled 2 weeks later . . . .	139
4.16	Representative images of CK19 staining in MDR2 <sup>-/-</sup> mice treated with either PBS or PαS MSC at 6-8 weeks of age and culled 2 weeks later . . . . .	141
4.17	CK19 quantification by western blotting in MDR2 <sup>-/-</sup> mice treated with PαS MSC . . . . .	143
4.18	Flow cytometric analysis of immune cell infiltrates in the livers of MDR2 <sup>-/-</sup> mice treated with PαS MSC . . . . .	145

4.19	Flow cytometric analysis of regulatory immune cell infiltrates in the livers of MDR2 <sup>-/-</sup> mice treated with PαS MSC . . . . .	147
4.20	Flow cytometric analysis of circulating regulatory immune cells in MDR2 <sup>-/-</sup> mice treated with PαS MSC . . . . .	148
4.21	The CD4/CD8 ratio assessed by flow cytometry in the livers and whole blood of MDR2 mice aged 6-8 weeks old were treated with PαS MSC and culled after 2 weeks . . . . .	149
5.1	QDot <sub>605</sub> staining of PαS MSC demonstrates no effect on viability and a small reduction in intensity over a 7 day period . . . . .	164
5.2	Representative bright field and fluorescent images of QDot <sub>605</sub> labelled PαS MSC injected <i>ex-vivo</i> into MDR2 <sup>-/-</sup> lung tissue . . . . .	165
5.3	Representative images from whole mouse CryoViz <sup>TM</sup> imaging showing bright field, fluorescent and 3 dimensional reconstructions in MDR2 <sup>-/-</sup> mice injected with QDot <sub>605</sub> labelled PαS MSC . . . . .	167
5.4	PαS MSC cell numbers decline rapidly in all organs following systemic administration in MDR2 <sup>-/-</sup> mice . . . . .	169
5.5	Subcutaneous treatment with PαS MSC does not reduce ALT, ALP or bile acids in MDR2 <sup>-/-</sup> mice . . . . .	172
5.6	Representative images of haematoxylin and eosin staining in MDR2 <sup>-/-</sup> mice treated with either subcutaneous PBS or PαS MSC at 6-8 weeks of age and culled 2 weeks later . . . . .	173
5.7	CD45 expression in the livers of MDR2 <sup>-/-</sup> mice treated with either subcutaneous PBS or PαS MSC at 6-8 weeks of age and culled 2 weeks later . .	174
5.8	Representative images of CD45 staining in MDR2 <sup>-/-</sup> mice treated with either subcutaneous PBS or PαS MSC at 6-8 weeks of age and culled 2 weeks later	175
5.9	F4/80 expression in the livers of MDR2 <sup>-/-</sup> mice treated with either subcutaneous PBS or PαS MSC at 6-8 weeks of age and culled 2 weeks later . .	176

5.10	Representative images of F4/80 staining in MDR2 <sup>-/-</sup> mice treated with either subcutaneous PBS or PαS MSC at 6-8 weeks of age and culled 2 weeks later . . . . .	177
5.11	CK19 quantification by western blotting in MDR2 <sup>-/-</sup> mice treated with subcutaneous PαS MSC . . . . .	178
5.12	Flow cytometric analysis of immune cell infiltrates in the livers of MDR2 <sup>-/-</sup> mice treated with subcutaneous PαS MSC . . . . .	180
5.13	The CD4/CD8 ratio assessed by flow cytometry in the livers of MDR2 mice aged 6-8 weeks old were treated with subcutaneous PαS MSC and culled after 2 weeks . . . . .	181
6.1	Graphic of 70% partial liver ischaemia . . . . .	191
6.2	Images demonstrating hepatic ischaemia reperfusion surgery . . . . .	192
6.3	Time course of serum ALT following 60 minutes of hepatic ischaemia . . .	194
6.4	Representative haematoxylin and eosin staining of ischaemic mouse livers following 60 mins ischaemia and varied reperfusion injury . . . . .	196
6.5	Representative haematoxylin and eosin staining of non-ischaemic mouse liver lobes following 60 mins ischaemia and varied reperfusion injury . . .	198
6.6	Histogram showing the time course of glycogen depletion in ischaemic and non-ischaemic livers of mice after hepatic ischaemia reperfusion injury assessed by PAS staining . . . . .	199
6.7	Representative histology of PAS stained ischaemic liver lobes following 60 minutes of 70% ischaemia . . . . .	201
6.8	Representative histology of PAS stained non-ischaemic liver lobes following 60 minutes of 70% ischaemia. . . . .	203
6.9	Flow cytometric analysis of mouse livers following ischaemia reperfusion injury . . . . .	205
6.10	Time course of serum ALT following either 30 or 60 minutes of hepatic ischaemia . . . . .	207

6.11	Representative haematoxylin and eosin staining of non-ischaemic mouse liver lobes following 30 minutes ischaemia and varied duration of reperfusion injury . . . . .	209
6.12	Histogram showing the time course of glycogen depletion in ischaemic and non-ischaemic livers of mice after either 30 or 60 minutes of hepatic ischaemia reperfusion injury assessed by PAS staining . . . . .	211
6.13	Representative PAS staining of ischaemic and non-ischaemic mouse liver lobes following 30 minutes of ischaemia and varied duration of reperfusion injury . . . . .	212
6.14	Flow cytometric analysis of mouse livers following 30 minutes of ischaemia and a variable duration of reperfusion injury . . . . .	214
6.15	Serum ALT in mice following 60 minutes of ischaemia and treatment with P $\alpha$ S MSC . . . . .	216
6.16	Representative images of haematoxylin and eosin staining in C57BL/6 mice having undergone 60 minutes of ischaemia treated with either PBS or P $\alpha$ S MSC . . . . .	218
6.17	PAS staining in the livers of C57BL/6 mice following 60 minutes 70% ischaemia and treatment with either PBS or P $\alpha$ S MSC . . . . .	219
6.18	Representative images of PAS staining in C57BL/6 mice having undergone 60 minutes of ischaemia treated with either PBS or P $\alpha$ S MSC . . . . .	221
6.19	Flow cytometric analysis of ischaemic liver lobes of mice treated with P $\alpha$ S MSC and undergoing 60 minutes of 70% hepatic ischaemia . . . . .	223
6.20	Flow cytometric analysis of the non-ischaemic liver lobes of mice treated with P $\alpha$ S MSC and undergoing 60 minutes of 70% hepatic ischaemia . . . .	224
6.21	Flow cytometric analysis of the whole blood of mice treated with P $\alpha$ S MSC and undergoing 60 minutes of 70% hepatic ischaemia . . . . .	225

# LIST OF TABLES

1.1	List of causes of end stage liver disease . . . . .	2
1.2	A list of functions of the human liver . . . . .	3
1.3	List of surface markers for human and mouse MSC . . . . .	29
2.1	List of primers used for genotyping mice . . . . .	47
2.2	Table of mouse strains used in this study . . . . .	74
2.3	Table of software used in this study . . . . .	74
2.4	Table of antibodies and dilution factors used in this study . . . . .	75
2.5	Table of reagents used in this study . . . . .	80
2.6	Table of consumables used in this study . . . . .	84
5.1	Quantification of QDot <sub>605</sub> labelled PαS MSC in different organs following tail vein injection into MDR2 <sup>-/-</sup> mice . . . . .	168
5.2	Tables demonstrating the rate of decline and percentages in different organs of PαS MSC when administered to MDR2 <sup>-/-</sup> mice . . . . .	170
6.1	A table of methodological variables seen in hepatic ischaemia reperfusion injury in the published literature . . . . .	226
6.2	A list of considerations to improve recovery from surgery. . . . .	227

# GLOSSARY

**$\alpha$ -MEM**  $\alpha$  Modified Minimum Essential Medium (Eagle).

**$\alpha$ -SMA**  $\alpha$  Smooth Muscle Actin.

**$\beta$ ME**  $\beta$ -mercaptoethanol.

**ALP** Alkaline Phosphatase.

**ALT** Alanine Transaminase.

**AMP** Adenosine Monophosphate.

**APS** Ammonium Persulphate.

**ATP** Adenosine Triphosphate.

**BCA** Bicinchoninic Acid.

**CCL** Chemokine (C-C motif) Ligand.

**CCL<sub>4</sub>** Carbon Tetrachloride.

**CFU-F** Colony Forming Unit Fibroblast.

**CXCL** Chemokine (C-X-C motif) Ligand.

**CXCR** CXC Chemokine Receptor.

**DAB** 3,3'-Diaminobenzidine.

**DAMP** Damage Associated Molecular Pattern.

**DAPI** 4',6-diamidino-2-phenylindole.

**DBD** Donation after Brainstem Death.

**DCD** Donation after Cardiac Death.

**DMEM** Dulbecco's Modified Eagle's Medium.

**DMSO** Dimethylsulfoxide.

**ECM** Extracellular Matrix.

**EDTA** Ethylenediaminetetraacetic Acid.

**FACS** Fluorescence Activated Cell Sorting.

**FBS/FCS** Foetal Bovine/Calf Serum.

**G-CSF** Granulocyte colony stimulating factor.

**GFP** Green Fluorescent Protein.

**H & E** Haematoxylin and Eosin.

**H<sub>2</sub>O<sub>2</sub>** Hydrogen Peroxide.

**HBSS** Hank's Balanced Salt Solution.

**HCELL** Hematopoietic Cell E-/L-Selectin Ligand.

**HGF** Hepatocyte Growth Factor.

**HO1** Haem Oxygenase 1.

**HRP** Horseradish Peroxidase.

**HSC** Haematopoietic Stem Cells.



**IDO** Indoleamine 2,3-dioxygenase.

**IFN- $\gamma$**  Interferon  $\gamma$ .

**IMC** Isotype Matched Control.

**IMS** Industrial Methylated Spirits.

**iNOS** inducible Nitric Oxide.

**IP** Intraperitoneal.

**ISCT** International Stem Cell Therapy Society.

**IV** Intravenous.

**JNK** c-Jun N-terminal kinase.

**LNGFR** Low-affinity Nerve Growth Factor.

**LPS** Lipopolysaccharide.

**MACS** Magnetic Activated Cell Sorting.

**MDSC** Myeloid Derived Suppressor Cells.

**MHC** Major histocompatibility complex.

**MMP** Matrix metalloproteinase.

**MPT** Mitochondrial permeability transition.

**MRI** Magnetic Resonance Imaging.

**MS** Multiple sclerosis.

**MSC** Mesenchymal Stem/Stromal Cell.

**NGF** Nerve Growth Factor.

**NHSBT** National Health Service Blood and Transplant Service.

**NK** Natural Killer.

**NKT** Natural Killer T Lymphocyte.

**NSAIDs** Non-Steroidal Anti-Inflammatory Drugs.

**OCT** Optimal Cutting Temperature.

**OFR** Oxygen Free Radicals.

**OH** Hydroxyl.

**PAMP** Pathogen Associated Molecular Patterns.

**PAS** Periodic Acid-Schiff.

**PBS** Phosphate Buffered Saline.

**PGE<sub>2</sub>** Prostaglandin E<sub>2</sub>.

**PI** Propidium Iodide.

**PRR** Pattern Recognition Receptors.

**PSC** Primary Sclerosing Cholangitis.

**PSG** Penicillin-Streptomycin-Glutamine.

**RAAS** Renin Angiotensin Aldosterone System.

**ROS** Reactive Oxygen Species.

**RPMI** Rosewell Park Memorial Institute.

**SC** Subcutaneous.

**SCA-1** Stem Cell Antigen.

**SDS** Sodium Dodecyl Sulphate.

**TBS** Tris Buffered Saline.

**TCR** T Cell Receptor.

**TEMED** N,N,N',N'-Tetramethylethylenediamine.

**TGF $\beta$**  Transforming Growth Factor  $\beta$ .

**T<sub>H</sub>** T helper.

**TLR** Toll Like Receptor.

**TNF $\alpha$**  Tumour Necrosis Factor  $\alpha$ .

**UK** United Kindgom.

**UKELD** United Kingdom End Stage Liver Disease.

**USA** United States of America.

**VCAM** Vascular Cellular Adhesion Molecule.

# CHAPTER 1

## INTRODUCTION

### 1.1 Overview

Liver disease is an endemic problem found in both developing and developed countries and whilst the aetiology may be different depending on a countries human development index the progression to end stage liver disease yields the same outcome. Once this progression reaches its end stage transplantation is the only option and there is an urgent need for better therapies to improve outcomes in these patients.

In this thesis I focus on the isolation and characterisation of murine Mesenchymal Stem/Stromal Cell (MSC), and their use as a therapy in models of post transplantation liver injury with the aim of identifying novel ways to improve outcomes from marginal donor liver transplantation. In this introduction some sections are taken from a commissioned review in the field that I designed and wrote during my research time [1].

### 1.2 End-stage liver disease

End-stage liver disease represents a common end point for many chronic disease processes of the liver. Repeated injury of liver parenchyma leads to scar formation and fibrosis. Due to changes in liver architecture associated with fibrosis liver function can be impaired [2]. There are a number of different causes of liver fibrosis (table 1.1) with histologically

different patterns of scar formation, however functional impairment due to capillarisation of sinusoids, deposition of extra-cellular matrix and impairment of normal bile transport are common in all pathologies [3]. Progression of fibrosis to cirrhosis is seen as a move from potentially reversible to irreversible pathology, although there exists some debate as to whether cirrhosis may be reversible [4]. There exists some differences in the description of cirrhosis in the literature, however the formation of fibrotic nodules of regenerative parenchyma surrounded by fibrotic septa coupled with disruption of the hepatic vascular architecture is a commonly used pathological description of cirrhosis [5]. Key therapeutic strategies for patients who develop fibrosis focus on treating the underlying cause in order to prevent the progression from fibrosis to cirrhosis. The rate of progression from fibrosis to cirrhosis is determined by a number of factors including the underlying pathology, environment and genetics. Patients who develop cirrhosis are deemed to have end stage liver disease, the only recognised treatment for which is liver transplantation. In the United Kingdom (UK) two percent of all deaths are due to liver disease, and whilst all other leading causes of death are decreasing, those from end stage liver disease have increased by 400% since 1970 [6]. Liver disease is the leading cause of premature death in the UK, and given the relatively young age of patients developing end stage liver disease, is responsible for the loss of a greater number of life years than other major causes of death in the UK. There is a clear need for novel therapeutic options in order to reduce the global impact of liver diseases.

Pathology		
Alcohol related liver disease	Non-alcoholic fatty liver disease	Glycogen storage disease
Chronic hepatitis (B, C and D)	Wilson's disease	Budd-Chiari syndrome
Primary biliary cirrhosis	Haemochromatosis	Glycogen storage disease
Primary sclerosing cholangitis	Biliary obstruction	Autoimmune hepatitis

**Table 1.1 – List of causes of end stage liver disease.**

## 1.3 Anatomy and function of the human liver

The liver is the largest internal organ in the human body and the second largest overall after the skin. It lies inferior to the diaphragm on the right hand side and on average weighs approximately 1500 g which accounts for 2.5% of the total body weight [7]. The liver is an organ found in vertebrates and is responsible for hundreds of metabolic functions including absorption, digestion, steroid hormone metabolism, protein synthesis and detoxification (figure 1.2). The liver also represents a major store of glycogen and is involved in glucose metabolic pathways including glycogenolysis and gluconeogenesis. Another important function of the liver is to regulate the immune system [8].

Function		
Bile production	Absorption of vitamin K	Vitamin storage (A, D, E, K, B12)
Fat absorption	Protein digestion	Ferritin storage
Cholesterol absorption	Bilirubin metabolism	Copper homeostasis
Digestion of fats	Carbohydrate metabolism	Metabolism and excretion
Synthesis of clotting factors	Protein synthesis	Xenobiotic detoxification

**Table 1.2 – A list of functions of the human liver.**

### 1.3.1 Surfaces and functional anatomy of the liver

The liver has a diaphragmatic surface which is in opposition to the inferior surface of the diaphragm and a visceral surface which is found on the inferior aspect separated from the diaphragmatic surface by its inferior border. The liver is broadly separated into 4 anatomical lobes (left, right, caudate and quadrate) with a functionally independent right and left side of roughly equal size which receives independent blood supply from the hepatic vessels. The liver can also be divided into 8 segments based on its blood supply (figure 1.1).

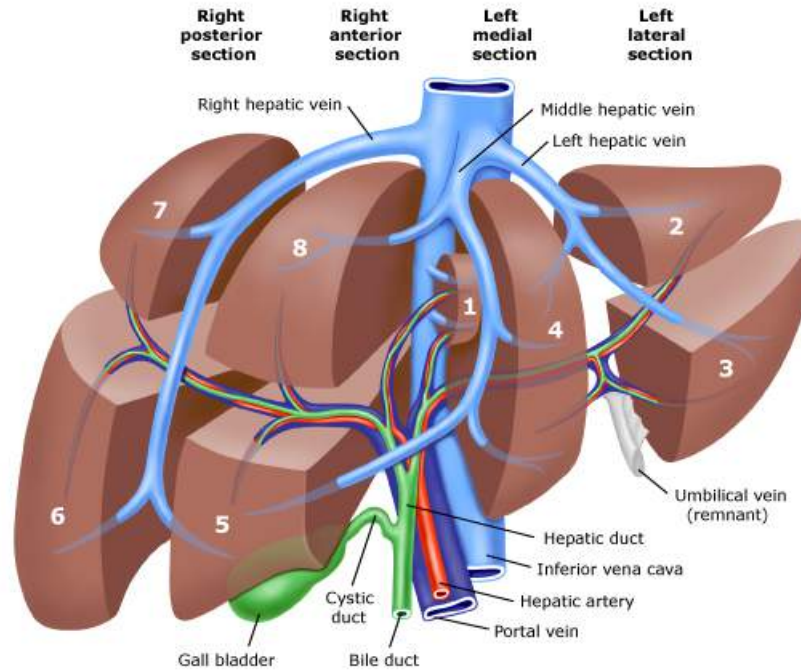


**Figure 1.1 – Diagram representing the functional anatomy of the liver.** The liver is split into 8 different segments determined by their blood supply from the hepatic artery and hepatic portal vein. Figure taken from wikimedia [9].

### 1.3.2 Blood supply to the liver and biliary drainage

The liver has a dual blood supply with 70 % of it's supply coming from the hepatic portal vein and 30% from the hepatic artery [8]. The portal vein is formed by the superior mesenteric vein and the splenic veins as they join and as it enters the liver it divides into the right and left branches which subsequently ramify. Venous drainage from the liver is via the right, middle and left hepatic veins which subsequently drain into the inferior vena cava.

Bile is produced in the hepatocytes and flows along the bile canaliculus into the bile duct. Small bile ducts join together eventually forming the right and left hepatic ducts outside of the liver. The right and left hepatic ducts join to form the common hepatic duct and this is joined by the cystic duct to form the common bile duct. The cystic duct connects to the gallbladder where bile can be stored, and the common bile duct joins the small intestine at the ampulla of Vater where bile can be secreted into the intestines [10].

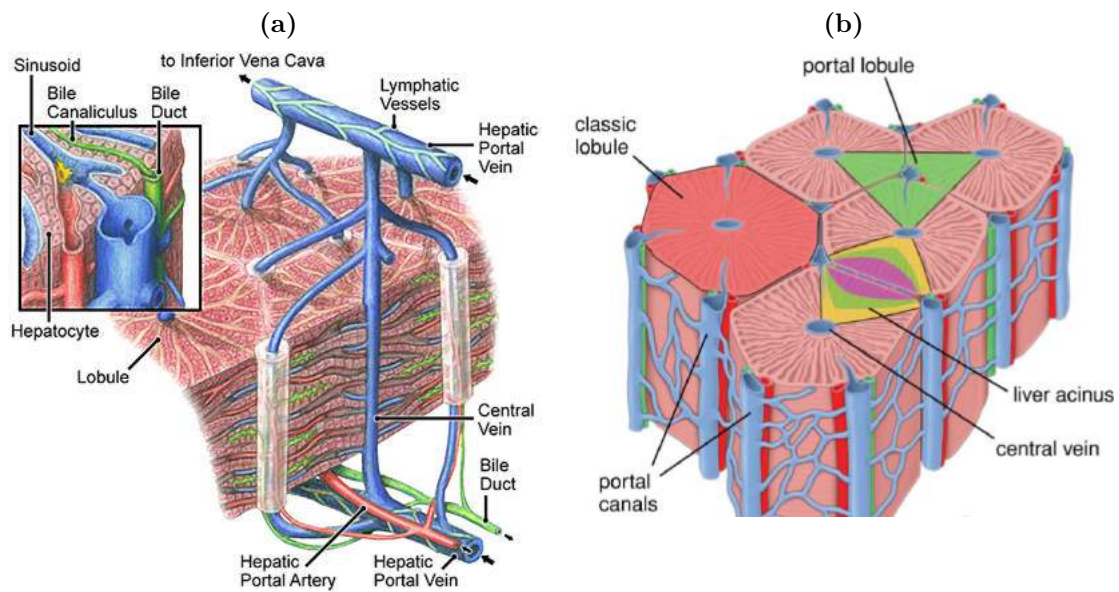


**Figure 1.2 – Graphics depicting the microarchitecture of the liver.** (a) The liver microarchitecture can be organised as an anatomic lobule with the hepatic vein at the centre and the portal triad at the edges. (b) Other representations include the portal lobule with the portal vein at the centre or the functional representation called the acinus. Figures taken from easy card and Spirstein [11, 12].

### 1.3.3 Microscopic anatomy of the liver

The liver is composed of five main types of specialised cells which can be divided into parenchymal and non-parenchymal with hepatocytes being the only parenchymal cell type, and the non-parenchymal cells being made up of Kupffer cells, stellate cells, cholangiocytes and sinusoidal endothelial cells. The two dimensional microarchitecture of the liver can be viewed from three different perspectives; the classical lobule, the portal lobule or the hepatic acinus, with the lobule being an anatomical representation of the microarchitecture and the acinus being a functional representation (figure 1.2). The classical lobule is hexagonal in shape and has the central vein at the centre and is a purely anatomical representation, the portal lobule is a triangular shape with the portal vein at the centre and the central veins making up each corner and follows the flow of bile through the liver and the the acinus is a diamond shape and follows the flow of blood through the liver as a purely functional representation.



### **1.3.4 Comparison of mouse and human liver**

Mouse liver anatomy is similar to human liver anatomy. Whilst mice tend to have a greater number of anatomical lobes (usually 6) each lobe still retains its own blood supply as in the human liver. The microscopic architecture of the mouse liver has a lobar structure surrounding a central vein again showing remarkable similarity to the human liver. Recent advances in micro computed tomography have allowed for accurate examination of the anatomy of the murine liver, further demonstrating the similarities between human and mouse livers [13].

## **1.4 Current therapeutic strategies in patients with end stage liver disease**

The development of cirrhosis currently marks a step down an irreversible pathway. In the pre-cirrhotic stage the main therapeutic strategies are targeted at the underlying pathology, however there are some novel therapies under investigation to attempt to slow or reverse fibrosis development and progression. Due to the involvement of the Renin Angiotensin Aldosterone System (RAAS) in hepatic stellate cells and their production of reactive oxygen species Reactive Oxygen Species (ROS), modulating this pathway has been shown in animal models to reduce the development of fibrosis [14]. In patients with cirrhosis levels of Lipopolysaccharide (LPS) have been found to be elevated [15], and Toll Like Receptor (TLR) signalling, particularly via TLR4 has been demonstrated to be important in animal models suggesting that TLR4 inhibitors may have a roll in treating liver fibrosis [16, 17].

### **1.4.1 Cell therapy for end stage liver disease**

A number of cell types have the potential for use as therapy in fibrosis and end stage liver disease. During liver injury hepatocytes are able to divide and replace injured areas,

however this mechanism can be compromised in a cirrhotic liver. The liver also contains liver progenitor cells which are able to divide and differentiate into new hepatocytes to replace injured areas [18], however this mechanism may be impaired in alcohol related liver disease [19]. Finally bone marrow derived and circulating non-hepatic stem cells are able to enter the liver and differentiate into hepatocytes although how and when this occurs *in vivo* is still not fully understood [20].

Hepatocyte transplantation in order to repopulate an injured liver has been studied in a number of models and has been shown to improve survival in rats with decompensated liver cirrhosis [21]. Whilst some success has been demonstrated using hepatocyte transplantation as a therapy in patients with metabolic liver diseases [22], these patients have normal liver architecture and as yet there has been no benefit shown using hepatocyte transplantation in patients with liver cirrhosis. The use of Granulocyte colony stimulating factor (G-CSF) in order to stimulate the proliferation of hepatic progenitor cells has been demonstrated with success in patients suffering from alcohol related steatohepatitis [23], however this therapy has yet to be translated into a treatment that improves outcome or reduces liver injury. Trials of haematopoietic stem cells as a therapy in mouse models of liver fibrosis showed promise with resolution of fibrosis seen following therapy [24], however a recent clinical trial combining G-CSF and haematopoietic stem cell therapy showed no benefit in patients with liver cirrhosis [25].

### 1.4.2 Liver transplantation

Liver transplantation currently represents the only curative strategy for patients with end-stage liver disease. A liver transplant is a major surgical undertaking requiring accurate risk stratification due to the limited pool of donor organs available. The decision to list a patient for liver transplantation is complex with a multitude of factors contributing to the final decision but the United Kingdom End Stage Liver Disease (UKELD) score (figure 1.3), a physiological scoring system, is a major component of this decision in the UK with patients who have a predicted 5 year mortality of greater than 50% generally excluded

from transplantation [26, 27].

$$(5.395 \times \ln(INR)) + (1.485 \times \ln(Creatinine)) + (3.13 \times \ln(Bilirubin)) - (81.565 \times \ln(Sodium)) + 435$$

**Figure 1.3 – Equation to calculate the UKELD score.**

Recent publications from the National Health Service Blood and Transplant Service (NHSBT) show the impact of the paucity of donor organs which leads to long delays from meeting the transplant criteria to receiving a liver transplantation. Between 2005 and 2015 almost 49,000 have waited for a transplant and over 6,000 patients have died before a donor organ has become available. There are currently around 600 patients on the UK organ transplant waiting list and 130 of these have been waiting over 1 year with the average wait for an adult currently 137 days [28]. As a result of the limited donor organs transplant centres have begun to use more marginal organs.

### 1.4.3 Marginal organ donation

Traditionally liver transplantation has been performed using Donation after Brainstem Death (DBD) organs, the so called 'heart beating' donors. With a shortage of donor organs worldwide the use of more marginal organs has become widespread. Donor organs from 'non-heart beating' donors such as those from Maastricht class III and IV Donation after Cardiac Death (DCD) has increased in recent years [29]. Whilst using more marginal donor organs has led to controversy in the literature with some studies demonstrating significantly worse outcomes and reduced long term survival [30], although these findings are debated and centres who use careful donor selection criteria have been able to demonstrate comparable outcomes between DBD and DCD organs [31]. The less favourable survival figures seen in both graft and recipient in patients who receive a DCD liver transplant are a reflection of the more profound ischaemic injury inflicted on the donor organ during donor death. The initial generation of ROS coupled with early neutrophil migration and release

of further ROS, further augmented by the slightly delayed adaptive immune response leads to a characteristic injury pattern and loss of hepatocytes [32], compared with the predominantly endothelial related injury which occurs during the ‘cold ischaemic’ phase demonstrated in DBD donor organs. This injury pattern represents the early ischaemic damage seen in liver transplantation.

#### **1.4.4 Complications of liver transplantation**

Liver transplantation is a major surgical undertaking in a patient population who are at high surgical and anaesthetic risk due to the underlying disease process and its effects on a multitude of organ systems. There are a number of potential complications which can occur either during a liver transplant operation, in the immediate post operative period, or over a longer time frame. The incidence of some of these complications can be different depending on whether a DBD or DCD liver is used.

##### **1.4.4.1 Perioperative complications**

There are a number of complications commonly seen during liver transplantation surgery. Almost all major perioperative complications occur following organ reperfusion and whilst most complications seem to have a similar incidence the number of some of these complications vary depending on the donor source [33].

Bleeding is a complication in almost all types of surgery, however major blood loss can occur during a liver transplant operation due to the combination of surgery involving major blood vessels and a patient population who usually have abnormal clotting function and bone marrow suppression leading to low platelet numbers. This leads to a requirement for blood products which itself brings a risk of infection, graft failure, multi-organ failure and an increased mortality, therefore strategies are implemented in order to minimise blood loss and therefore requirement of transfusion of blood products [34].

The use of vasopressors and inotropes is common in liver transplant surgery due to

rapid shifts in fluid and changes in vascular tone and remaining on inotrope therapy in the early postoperative period whilst seen as a complication is commonplace and similar between DBD and DCD transplantation surgery [35, 33].

Post reperfusion syndrome is a state of cardiovascular collapse originally described by Aggarwal 40 years ago [36] with further more specific definitions being postulated, the most recent by Fukazawa [37]. Both post reperfusion syndrome and post reperfusion hyperkalaemia have been shown to occur more frequently following DCD liver transplantation [33].

#### **1.4.4.2 Acute and chronic rejection**

Rejection post liver transplantation is an immunological phenomenon and can be categorised as acute or chronic. Acute cellular rejection occurs in up to 25% of transplants however does not pose major problems as it can be readily treated with corticosteroids [38]. Acute reaction is a consequence of transplanting Major histocompatibility complex (MHC) incompatible organs and leads to a T cell mediated response which is characterised by ductular injury and T cell infiltration [39]. Chronic rejection occurs in up to 17% of liver transplants and is a major source of morbidity leading to graft loss [40]. In contrast to acute rejection the pathophysiology is not well understood but probably involved a mixture of antibody mediated damage and vascular occlusion [41].

#### **1.4.4.3 Biliary complications**

Biliary complications following a liver transplant occur in the medium term and DCD liver transplants have a significantly greater incidence of these when compared with DBD transplants [42]. The most common biliary complication seen following DCD liver transplantation is ischaemic cholangiopathy, whereas common bile duct leak or strictures tend to be the most common in DBD transplants [42]. The development of biliary complications appears to be related to donor age with age greater than 40 being linked to an increased risk of biliary complications. Ischaemic cholangiopathy seems to be increased

when the cold ischaemic time is greater than 6.5 hours [42].

Ischaemic cholangiopathy is characterised by multiple intra-hepatic strictures in the absence of hepatic artery insufficiency [43]. The underlying aetiology of ischaemic cholangiopathy is unclear but there is likely a combination of microvascular obstruction and immune mediated injury [44]. Ischaemic cholangiopathy leads to significant morbidity with an increased hospital stay, increased re-transplantation rate and reduced quality of life in transplant recipients suffering from this complication [45]. Ischaemic cholangiopathy is also a cause of non-anastomotic biliary strictures, however the commonest cause of this complication is hepatic artery thrombosis.

Bile leak post liver transplant usually occurs at the anastomotic site and can be a result of ischaemia, downstream obstruction or following T tube removal [46]. Biliary strictures following liver transplant are commonly categorised as anastomotic; being related to the biliary tract surgical anastomosis, and non-anastomotic; being at site not related to the anastomosis [47]. Anastomotic stenosis occurs due to a combination of inadequate mucosal surface contact coupled with ischaemia and can be related to surgical technique [48]. Non-anastomotic biliary complications tend to be more extensive and the underlying aetiology is less clear. There is an increased incidence as cold ischaemic time increases, however an immune mediated injury is thought to be likely due to the higher incidence when ABO mismatching occurs [47].

## **1.5 Hepatic ischaemia reperfusion injury**

Ischaemia and reperfusion injury are important concepts with clinical relevance. The main reason for graft dysfunction following liver transplantation is ischaemia reperfusion injury [49]. Ischaemia (figure 1.4a) and reperfusion injury (figure 1.4b) can be thought of as two separate but related processes.

### 1.5.1 Ischaemic injury to the liver

Ischaemia is not a new concept and can be defined as:

'an inadequate blood supply to an organ' [50]

The word originating from the Greek word iskhaimos meaning 'to stop blood' as early as the 19th century. It was not until the 1980's however, that the concept of reperfusion injury was postulated. The first description of reperfusion injury which described an injury occurring as a result of superoxide generation used a feline model of gastrointestinal tract ischaemia and reperfusion [51]. Since this publication nearly 40 years ago there has been a considerable amount of work done to illicit the causes of reperfusion injury. Ischaemic injury to the liver usually occurs during both liver resection and liver transplantation, either due to organ preservation and transport, major haemorrhage or deliberate vascular inflow occlusion with an aim to reduce surgical blood loss [52, 53, 54, 55]. One of the first descriptions of occluding the liver vasculature was by Pringle, who described a process of retracting the liver to occlude its blood supply in patients with major haemorrhage [56], the eponymous Pringle manoeuvre, or a variation of the original description is still used today in liver surgery. In the context of liver transplantation ischaemia can be categorised as either warm or cold ischaemia. Cold ischaemia occurs during cold preservation of the explanted liver and is defined as occurring from the beginning of cold preservation to the removal from 4°C cold storage. Warm ischaemia can be further categorised into donor warm ischaemic time, occurring between withdrawal of life support and the initiation of cold storage, or graft warm ischaemic time which occurs between removal from cold storage and establishment of reperfusion [57]. In a DBD transplant donor warm ischaemic time should not exist as cold preservation occurs whilst blood flow is still maintained.

Whilst there are some organ specific differences in the response to ischaemia broadly speaking the responses are the same. Ischaemic injury to an organ occurs following an interruption of the supply of oxygen usually as a result of an interruption to the blood supply. The extent of the cell dysfunction and death seen is thought to be related to

the extent and the duration of the ischaemic period [58]. Usually ischaemia occurs in a sterile environment, although the resultant inflammatory stimulus resembles that seen following invasion by an external pathogen [59]. Humans rely on aerobic metabolism utilising oxygen as an electron acceptor in order to generate Adenosine Triphosphate (ATP) which is required for almost all metabolic processes. When the oxygen supply is interrupted a process of glucose fermentation (often called anaerobic respiration) is used to generate further ATP which involves the conversion of glucose to lactate without the need for a terminal electron acceptor. This process is considerably less efficient than aerobic respiration and leads to an increase in  $H^+$  ions and a reduction in cellular pH as lactate is converted into lactic acid. There is activation of the  $Na^+/H^+$  transporters in an attempt to correct the raised intracellular  $H^+$  concentration and in the process of pumping  $H^+$  ions out of the cell the intracellular  $Na^+$  concentration increases [60]. The result of this increase in intracellular  $Na^+$  ions leads to an osmotic gradient favouring water movement into the cell causing cellular swelling, oedema and subsequently cell death. The lack of oxygen as a terminal electron carrier leads to the electron transport chain becoming reduced with interruption of electron flow. This leads to reduction of pyridine nucleotides and results in an increase in the ratio of  $NADH/NAD^+$  [49]. As ATP is depleted there is also an increase in ATP breakdown products such as adenosine, xanthine and hypoxanthine. There is also an increase in cellular cyclic Adenosine Monophosphate (AMP), an important intracellular messenger responsible for signalling in carbohydrate metabolism [61]. Other cellular ion pumps are effected by the lack of ATP, one important pump being the ATP dependent  $Ca^{2+}$  pump which removes  $Ca^{2+}$  from the cytoplasm by either expulsion from the cell or uptake into the endoplasmic reticulum. Once inactive intracellular  $Ca^{2+}$  accumulates further distorting the osmotic gradient and also causing the activation of  $Ca^{2+}$  dependent proteases which cause disruption of the cellular structure and can lead to cell death [62]. Hypoxia also leads to priming of the Mitochondrial permeability transition (MPT) pore which opens at reperfusion and leads to a change in electrical gradient within the mitochondria causing further impairment of mitochondrial function



and therefore reduced ATP production [63], although MPT pores can also be opened due to cellular  $\text{Ca}^{2+}$  overload. Hepatocytes are particularly prone to warm ischaemia and changes occur in hepatocytes at the mitochondrial level. The extent of ischaemia injury has been shown to be in part related to the amount of blood supply/oxygen delivery lost and the duration of the ischaemic period [64].

### 1.5.2 Hepatic reperfusion injury

Whilst restoration of blood flow and oxygen delivery as quickly as possible has been the mainstay of treatment for ischaemia it was first noticed in the 1960s that this came with it's own problems when studying myocardial ischaemia in canine models [65]. ROS were first discovered to be important in reperfusion injury in the early 1980's when superoxide generation was demonstrated to contribute to reperfusion injury in a feline model of gastrointestinal tract ischaemia and reperfusion [51]. ROS or Oxygen Free Radicals (OFR) include superoxide, Hydroxyl (OH) and Hydrogen Peroxide ( $\text{H}_2\text{O}_2$ ) and are produced early on following reperfusion. The primary sources of ROS in the early phase of reperfusion is intracellular xanthine oxidase, Kupffer cells and infiltrating polymorphonuclear cells [66]. Kupffer cells become activated following exposure to damage associated molecular patterns released from neighbouring hepatocytes [67]. Following activation Kupffer cells also release pro-inflammatory cytokines including Tumour Necrosis Factor  $\alpha$  ( $\text{TNF}\alpha$ ), Interferon  $\gamma$  ( $\text{IFN-}\gamma$ ) and Il-12 [68] which leads to further neutrophil recruitment and a cycle of ROS release, inflammatory cytokine release and immune cell recruitment and activation [49]. Activated hepatic endothelial cells also express a number of surface adhesion molecules as well as MHC which primes the endothelium for accumulation of immune cells as well as platelet binding and aggregation which can lead to microvascular occlusion [69]. Damage Associated Molecular Pattern (DAMP) are also able to bind to TLR4 and trigger an inflammatory cascade via an MyD88 independent pathway [70]. Mice treated with a TLR4 inhibitor have been shown to have lower levels of liver injury following ischaemia reperfusion injury [71]. The extent to which the initial cellular injury contributes to

the inflammatory response seen in ischaemia reperfusion injury is not fully understood, however it has been shown that there is an important link between DAMPs released during cell damage and the subsequent inflammatory response[70]. T cell mediated injury is an important cause of reperfusion related liver injury and blocking T cell co-stimulation or using T cell deficient mice shows a reduction in liver injury [72]. Following reperfusion there appears to be an increase in  $CD4^+$  T cells but not in  $CD8^+$  T cells suggesting a role for  $CD4^+$  cells in reperfusion injury [73]. T cells may have a role in neutrophil recruitment to injured liver, but treatment of mice with Il-10 leads to a reduction in T cell numbers and a dramatic reduction in liver injury following reperfusion which can be reversed by transplanting further T cells into the injured mice [74]. When examining subsets of  $CD4^+$  cells it appears that T cells contribute to neutrophil recruitment, Natural Killer T Lymphocyte (NKT) cells are able to directly injure the liver, whereas Natural Killer (NK) cells and Treg cell appear to have little effect in liver reperfusion injury [75], and in models of stroke Tregs appear to have a protective effect [76]. It is not clear the exact mechanism by which T cells become activated in hepatic ischaemia reperfusion injury, although it is thought that this occurs without exposure to 'cognate' antigens[77]. Platelet aggregation and activation also plays an important role in reperfusion injury, both due to occlusion of the microvasculature, but also through their ability to stimulate regeneration through the release of serotonin [78]. The final result of these injury pathways is structural damage to the hepatic parenchyma and hepatocellular dysfunction.

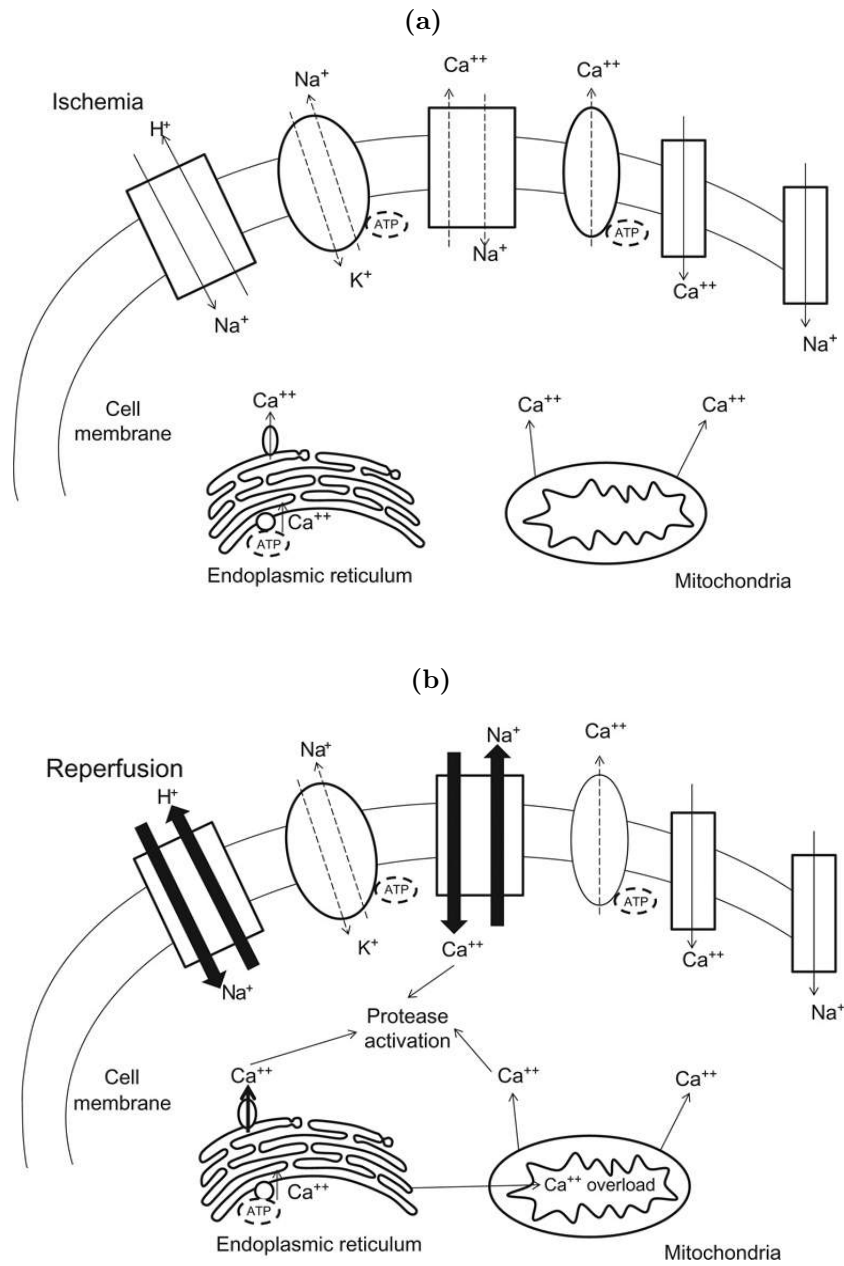


**Figure 1.4 – Diagram showing the main cellular ion changes in ischaemia and reperfusion injury.** (a) During an ischaemic insult cells deplete their oxygen reserves and begin using anaerobic pathways which leads to an accumulation of  $H^+$  ions. This leads to activation of  $Na^+/H^+$  transporters to correct the electrochemical imbalance. Inactivation of the  $Ca^{2+}$  transporters leads to accumulation of  $Ca^{2+}$ . (b) Following reperfusion  $H^+$  ions are rapidly washed out of the ischaemic tissue and the oxygen supply is restored. Figures taken from Kalogeris [58].

### **1.5.3 Strategies to limit ischaemia reperfusion injury**

Ischaemia reperfusion injury has long been recognised as a major source of morbidity following organ transplantation but is a necessary evil due to the nature of transplant surgery and the need for cold preservation and transport of donor organs. As such considerable research has been undertaken with an aim at reducing the injury sustained during ischaemia and reperfusion [79].

#### **1.5.3.1 Ischaemic preconditioning**

Ischaemic preconditioning was originally proposed as a means to reduce infarct size in ischaemic myocardium however it was subsequently suggested as a means of mitigating injury from ischaemia reperfusion injury [80]. It involves subjecting an organ to a brief ischaemic period in an attempt to reduce subsequent ischaemic injury. Small animal studies have shown that ischaemic preconditioning of the liver can lead to a reduction in hepatocyte and sinusoidal endothelial cell apoptosis by reducing caspase activity independent of Bcl-2 expression [81]. It seems that the protective effect of ischaemic preconditioning is due to nitric oxide generation and adenosine supplementation of animals undergoing ischaemia is able to mimic this effect due to its ability to stimulate nitric oxide release [82, 83]. Clinical studies have also shown a reduction in markers of liver injury when using ischaemic preconditioning [84], however recent reviews of clinical trials have shown no proven benefit in the use of ischaemic preconditioning in liver surgery [85] or liver transplant operations [86], but both conclude that further research is required to confirm these findings.

#### **1.5.3.2 Treatment with xanthine oxidase inhibitors**

The generation of intracellular ROS has been shown to occur in animal models of ischaemia reperfusion injury [87]. Due to this finding the xanthine oxidase inhibitor allopurinol was tested successfully in small animal models of hepatic ischaemia reperfusion injury [88]. Unfortunately this therapy has not been translated into clinical practice. There are

potentially a number of reasons for this. Firstly the doses used in animal experiments required a number of high doses, considerably more than the single low dose of allopurinol required to completely inhibit xanthine oxidase. This implies that the effects are off target and not related to xanthine oxidase inhibition. Further work has demonstrated a beneficial effect of allopurinol which appears to inhibit mitochondrial injury although the mechanism by which this happens has not been elucidated [89]. Secondly the clinical importance of xanthine oxidase as a means of generating ROS has been challenged as the enzyme requires xanthine and hypoxanthine to act as substrates. Whilst these substances have been shown to accumulate in ischaemic tissue they are quickly metabolised and unlikely to provide adequate substrate to xanthine oxidase to generate enough ROS to cause significant damage [90].

#### **1.5.3.3 Cyclophilin D inhibitors**

Mitochondria present in hepatic parenchyma play an important role in warm ischaemia reperfusion injury as they are able to trigger cellular necrosis by opening their membrane permeability transition pores leading to a loss of the mitochondrial membrane potential inhibiting the production of ATP. Mitochondria also release cytochrome C following injury through mitochondrial outer-membrane permeabilisation which has pro apoptotic effects [91]. Mitochondrial permeabilisation transition is regulated by cyclophilin D, and inhibitors of cyclophilin D have been shown in rat models of liver ischaemia to reduce injury [92]. So far this finding has not been translated.

## **1.6 Animal models of liver injury**

A number of models of liver injury exist in the literature, however few truly recapitulate the injury seen in DCD liver transplantation. There are no models described to demonstrate the biliary complications seen following liver transplantation.

### 1.6.1 Carbon tetrachloride

The Carbon Tetrachloride ( $\text{CCL}_4$ ) model is a model of liver fibrosis originally described in the 1930's [93]. First described as a chronic model the  $\text{CCL}_4$  model has been modified to demonstrate acute injury. Administration of  $\text{CCL}_4$  to mice causes hepatocyte injury and centrilobular necrosis followed by hepatic fibrosis. In the early stages of the  $\text{CCL}_4$  model ROS are generated which contribute to the damage seen [94], as such  $\text{CCL}_4$  can be used as a model of oxidative stress.

### 1.6.2 $\text{MDR2}^{-/-}$

The  $\text{MDR2}^{-/-}$  Mouse model is a model of biliary injury which has been used to model Primary Sclerosing Cholangitis (PSC) due to similarities in the phenotype seen [95, 96]. The  $\text{MDR2}^{-/-}$  model has a targeted disruption of the multi-drug resistance gene 2 (*Abcb4*) which leads to an absence of biliary phospholipids. This leads to bile acid leak and a cytotoxic injury to the biliary tree. A pattern of onion skin fibrosis is seen in the peri-portal regions in the first few weeks which continues to develop with widespread fibrosis being seen at 4-5 months of age [95, 97, 98]. In female mice gallstone formation occurs and seems to be more prevalent from 15 weeks of age [99]. Immune mediated injury occurs early on in the model with higher levels of lymphocytes seen in the first few weeks of life [98]. Microvascular injury and biliary fibrosis is seen, similar to that in post transplant liver injury [100].

### 1.6.3 Hepatic ischaemia reperfusion injury

Ischaemia reperfusion injury has been studied for the last 4 decades with small animal models being used widely. Whilst ischaemia reperfusion injury is relatively simple to induce surgically there is a variety of heterogeneity in the literature making comparison between studies difficult [101]. Clamping of the blood supply to the liver for a predetermined period of time followed by release and a period of reperfusion leads to a warm ischaemic and

reperfusion injury with generation of ROS and resultant immune cell infiltration [102]. Whilst a good model of warm ischaemia due to the fact that no vessels are divided it would be challenging to model cold ischaemia in standard hepatic ischaemia reperfusion models.

#### **1.6.4 Liver transplantation**

A number of models of liver transplantation have been described in the literature, mainly using rats due to their larger size than mice making surgery more straightforward [103, 104]. Whilst the surgical technique is similar to that in human liver transplantation it was noticed that in mice failure to reconnect the hepatic artery did not lead to ischaemic injury or complications [105]. This finding was also confirmed in rat models and due to the technical challenge of reconnecting the hepatic artery models tended not to do this. Recent studies however have found that whilst ischaemic damage does not seem to occur as a result of leaving the artery tied off there is an effect on the immune system, in particular graft function with greater levels of rejection in those animals who do not have the arterial supply reconnected [106]. Whilst transplantation models recapitulate a lot of the clinical environment and include both warm and cold ischaemia there are few published papers which demonstrate a prolonged period of warm ischaemia such as that seen in DCD liver transplantation.

### **1.7 Immune system**

The immune system is a complex collection of cells, tissues and organs which perform a number of vital function in man including prevention of infection from micro organisms and suppression of tumour formation. The immune system develops in three main components the macrophage, lymphatic and haematopoietic systems which originate independently of each other. The macrophage system arises from the coelomic cavity as mesenchymal amoeboid cells and has the ability to recognise self from foreign antigens. The lymphoid system develops from the endoderm of the pharyngeal pouches. Lymphocytes that originate

here retain the ability to divide and seed all lymphatic organs. The final component of the immune system is the haematopoietic component which originates from the splanchnic mesoderm of the yolk sac [107]. Early haematopoiesis occurs in the umbilical vesicle in the foetus but quickly move to the liver. The spleen and bone marrow subsequently take over production.

There are a number of classifications for the immune system including anatomical and functional but a commonly used system is to separate into the innate and adaptive components.

### **1.7.1 Innate immunity**

The innate immune system is traditionally thought of as the first line of defence against invading pathogens and consists of phagocytic cells such as macrophages and dendritic cells [108]. The innate immune system is responsible for the presentation of antigen to the adaptive immune system, the clearance of foreign substances by phagocytosis and activation of the complement cascade. Whilst it was originally thought that the innate immune system is non-specific this is not entirely true as it has the ability to differentiate between self and non-self. The innate immune system uses a small number of Pattern Recognition Receptors (PRR) in order to recognise non-self organisms. Pathogen Associated Molecular Patterns (PAMP) are specific patterns that react with PRR. One extensively studied group of PRR are the TLR which can be divided into several subfamilies related to the PAMP that they are able to recognise. TLRs utilise the same signalling molecules as those used for IL-1R [109]. Antigen presenting cells such as macrophages and dendritic cells are the main source of TLR expression, however antigen presenting cells are also able to activate the adaptive immune system and activated dendritic cells are able to control differentiation of naive  $CD4^+$  T cells into T helper ( $T_H$ ), either  $T_H1$  or  $T_H2$  cells [108].

The complement system forms a distinct part of the innate immune system which consists of circulating proteins and glycoproteins predominantly formed in the liver. The complement system has a classical and alternative pathway of activation and its main



functions are to bind to foreign pathogens and mark them for removal by phagocytic cells and to attack bacterial cell membranes leading to cell wall rupture [110].

NK cells, whilst a type of lymphocyte, are a part of the innate immune system. They have an ability to control the spread of infection and tumour preventing tissue damage. They also have an immunomodulatory role by interacting with T cells, macrophages and dendritic cells and are therefore able to both increase and decrease immune responses. NK cells are able to recognise stress induced self ligands. They also possess TLRs and CD16, an Fc receptor which enables them to recognise cells coated with antibody [111].

## **1.7.2 Adaptive immunity**

Whilst the innate immune system provides an ability to rapidly sense and eliminate pathogens, the adaptive immune system is able to provide a broader reaching system able to deal with variability in pathogens and their ability to mutate in an attempt to evade the body's defences. Broadly speaking the adaptive immune system is composed of T cells which mature in the thymus and B cells, which are able to produce antibody. Cells of the adaptive immune system begin in the thymus and bone marrow and once mature migrate to secondary lymphoid tissue such as the spleen and lymph nodes. Adaptive immune responses are often triggered by innate immune responses due to circulating antigen presentation cells. Trafficking of immune cells is then regulated by adhesion molecules and chemokine receptors.

### **1.7.2.1 T lymphocytes**

T cells, so called because they mature in the thymus, are distinct from other cells in the adaptive immune system due to the presence of a T Cell Receptor (TCR) on their cell surface. In humans the TCR consists of a number of subunits. The majority of TCRs are composed of  $\alpha$  and  $\beta$  chains, with a smaller proportion being composed of  $\gamma$  and  $\delta$  chains, the so called  $\gamma\delta$  T cells. The T cell receptor allows T cells to recognise

and bind to foreign antigens presented by cells in specialised glycoproteins. These MHC antigen complexes are expressed on the cell surface and allow recognition of intra-cellular pathogens or endocytosed antigen. TCRs are diverse and intricate structures made from a combination of V, D and J gene segments and recombination of these variable segments leads to a large number of potential combinations allowing for recognition of a broad range of antigens [112].

During development the thymic microenvironment directs differentiation and positive and negative selection leading to T cells which are restricted and self-tolerant. Originally produced from haematopoietic stem cells in the bone marrow, lymphoid progenitor cells travel to the thymus to complete a process of antigen independent maturation into functional T cells. Cells entering the thymus are termed double (or sometimes triple) negative cells due to the lack of CD3, CD4 and CD8 expression [113]. These cells can be subdivided based on their expression of CD44 and CD25 and pass through a number of stages leading to rearrangement of the TCR mediated by RAG1 and RAG2. Following successful rearrangement the TCR  $\beta$  chain associates with a pre-TCR  $\alpha$  chain and CD3 to form the pre-TCR complex [114, 115]. Double positive  $\alpha\beta$  T cells undergo positive and negative selection in the thymus. Positive selection requires that the rearranged  $\alpha\beta$  TCR be able to bind to cortical epithelial cells expressing either MHC class I or class II along with self peptide. If binding occurs with enough affinity survival signals are sent and apoptosis is prevented[116]. Development to either cytotoxic or TH cells is dependent on which class of MHC is recognised and is in part mediated by Notch signalling[117]. T cells which survive positive selection pass further into the thymus where they encounter bone marrow derived antigen presenting cells with high expression of MHC-self peptide complexes. T cells with a high affinity for this complex undergo negative selection and die by apoptosis[116].

T cells are activated by binding of their receptor with antigen complexed with MHC. In the case of CD8<sup>+</sup> T cells this is MHC class I, expressed by all cells and in CD4<sup>+</sup> T cells this is MHC class II, expressed by antigen presenting cells. Once bound the TCR requires

co-stimulation in order to trigger down stream effects. The best characterised pathway for co-stimulation in T cells is CD28 which binds to CD86 and CD80 [118]. Activation of T cells is supported by the T cell co-receptor CD3 and the TCR  $\zeta$  chain accessory molecules [119]. Whilst this signalling process leads to gene transcription within the T cell further co-stimulation is required for activation as without this T cell anergy occurs, a way of protecting against self recognition by T cells. Whilst a number of co-stimulatory molecules have been discovered CD28 is one of the best known and studied [120].

CD4<sup>+</sup> T cells have been shown to have a number of phenotypically different subsets (figure 1.5) with differing roles in the immune system. T helper cells are CD4<sup>+</sup> cell with an  $\alpha\beta$  TCR. T helper cells are able to divide and produce two main subsets of T helper cell, TH1 cells which are produced in response to IFN- $\gamma$ , Il-12 and Il-18 and are able to secrete Il-2 and IFN- $\gamma$ , and TH2 cells which are produced in response to Il-4 and are able to secrete a number of interleukins including Il-4, Il-5, Il-10 and Il-13 [121]. Regulation of T cell responses is performed in part by the subset of CD4<sup>+</sup> cells known as regulatory T cells. These cells are known to express CD4, CD25 and FoxP3 [122].

A pro-inflammatory T cell subtype can be generated following stimulation with Transforming Growth Factor  $\beta$  (TGF $\beta$ ) and Il-6. Known as TH17 cells they have the ability to secrete Il-17 and are thought to be important in autoimmunity. Exposing TH2 cells to a combination of TGF $\beta$  and Il-4 can cause them to secrete Il-9. These so called TH9 cells are thought to be important in helminth infection.

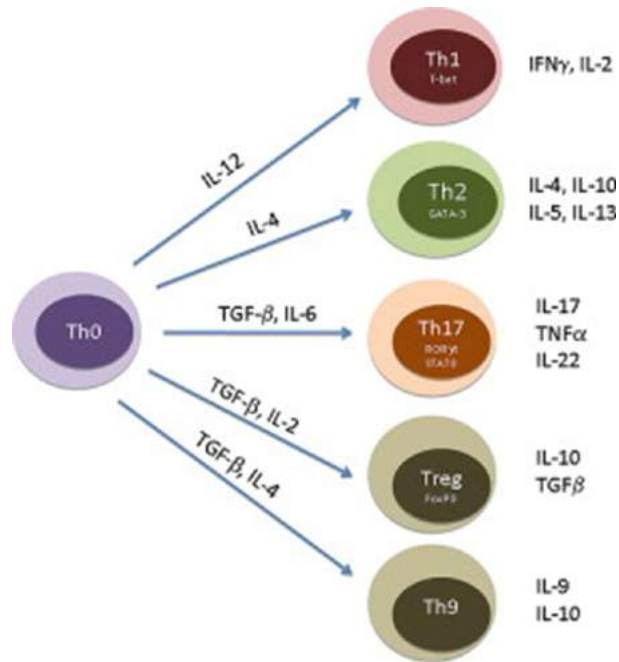


**Figure 1.5 – Diagram showing the subsets of CD4<sup>+</sup> T lymphocytes.** CD4<sup>+</sup> cells expressing the  $\alpha\beta$  TCR are able to divide and produce a variety of different effector cells. Whilst initially it was thought that CD4<sup>+</sup> cells secreted a broad range of cytokines it has been since shown that the secretome of CD4<sup>+</sup> cells is dependent on which subset of cells is present. Image taken from Bonilla[121].

### 1.7.2.2 B lymphocytes

Production of B lymphocytes occurs in the bone marrow and it is during their development that they acquire their antigen specificity. B cells leave the bone marrow in an immature state and on maturity they become naive B cells expressing both IgD and IgM. B cell development occurs without exposure to antigens. Following this antigen independent phase B cells will become activated when they are exposed to antigen and this is termed the antigen dependent phase. Following activation B cells can either acquire memory of the antigen to which they were exposed and become memory B cells, or differentiate into plasma cells and produce antibodies. B cell activation can occur in a T cell dependent or T cell independent fashion, although the former accounts for the majority of B cell activity. The interaction between B cells and T cells occurs via co-stimulatory molecules such as CD40, CD80 and CD86 and following this interaction B cells can migrate to a follicle and form a germinal centre which enables class switching from IgM and IgD to

IgA, IgG or IgE. Mutations in immunoglobulin heavy chains in the germinal centre can lead to higher affinity antibodies against a particular antigen [123].

#### **1.7.2.3 Natural killer T cells**

NKT are a subset of T lymphocytes which are restricted to recognise lipid antigens presented by CD1d molecules. They have two functional subtypes determined by their TCR. NKT cells have a TCR and express CD3, as well as CD44 and CD122. There exists considerable heterogeneity within the NKT cell lineage but as their name suggests NKT cells share functional and phenotypic properties with both NK cells and T cells. NKT cells have been shown to have both pro and anti-inflammatory actions [124].

## **1.8 Mesenchymal stromal cells**

The definitions of MSC have developed over time due to advances in isolation techniques and a greater functional understanding of how MSC exert their effect. Whilst no clear consensus exists as to exactly what MSC are the International Stem Cell Therapy Society (ISCT) have developed a set of minimal criteria for describing MSC [125, 126]. It has been argued more recently that these criteria are dated and require updating [127] with ongoing debate as to whether the term 'stem cell' should be used or whether MSC represent a type of stromal cell [128]. It has even been suggested that MSC are a type of fibroblast [129]. Criticism of the ISCT criteria focus on their inability to account for heterogeneous populations of cells which commonly occur following traditional isolation techniques. Whilst cells can be isolated from wide variety of tissues using different techniques and culture methods, they are still able to meet the minimum criteria for an MSC as defined by the ISCT [130]. Whilst debate will almost certainly continue as to what exactly constitutes an MSC it is generally agreed that MSC are multipotent, self-renewing cells originating in the mesoderm or the neural crest, their differentiation potential being limited to chondrocytic, osteocytic and adipocytic lineages [131]. Until recently the ability of MSC

to self renew has been inferred from their behaviour in culture as techniques to isolate purified populations of cells have been lacking and heterogeneous populations of cells were cultured following plastic adherence [130]. MSC exist in a number of adult tissues, albeit in low numbers [132], and whilst traditional isolation techniques have relied on their ability to adhere to tissue culture plastic and proliferate [133], prospective isolation with cell sorting based on specific cell surface markers is gaining popularity as the isolation method of choice.

### **1.8.1 Evolution of a bone marrow stromal cell niche**

Whilst modern day research into MSC dates back over 50 years one of the first hypotheses regarding their existence can be dated back over 100 years. In 1908 a description of the ability of bone marrow stroma to create an environment in which haematopoietic precursors are able to differentiate was first suggested in 1908 by Maximov [134, 135]. The osteogenic potential of bone marrow was demonstrated in experiments by Tavassoli in the 1960s. In these experiments Tavassoli showed that serial transplantation of bone marrow fragments in rats, rabbits and dogs led to complete reconstitution of the bone marrow and the eventual establishment of a micro-circulation and haematopoiesis. These experiments were limited however as it was not possible to identify which cellular constituents within the bone marrow were responsible for this reconstitution [136]. It took a further 2 years before Friedenstein was able to demonstrate that a rare population of bone marrow cells with fibroblastic properties were responsible and confirm Tavassoli's hypothesis and the term Colony Forming Unit Fibroblast (CFU-F) was used to describe them [137]. These bone marrow cells have subsequently been shown to be multi-potent [138] and able to differentiate into different mesenchymal cells at the colony forming level by modifying the culture conditions, but their complex interplay with haematopoietic stem cells has only recently been demonstrated [139]. The term MSC was first used in 1991 when it was introduced by Caplan [140], and the idea of a stem cell niche within the bone marrow was further developed by the discovery of a rare, self-renewing population of cells [132]. The

MCAM/CD146 expressing cells found in the sub-endothelium of human bone marrow were found to be capable of recapitulating the haematopoietic micro-environment following transplantation to heterotopic sites, which began the currently ongoing debate regarding the correct criteria with which to judge MSC. More recently cells who do not express CD146, but do express CD271 have also been shown to be MSCs[141]. Due to their mixture of stem and stromal like properties both stem and stromal cell have been suggested as correct terms, although the ability to self-renew and tri-lineage differentiation potential (osteogenic, chondrogenic, adipogenic) appear in most definitions [142, 126].

The descriptive criteria for human MSC are focused on their ability to adhere to tissue culture plastic, their multi-potency and their expression of specific cell surface antigens (table 1.3). The minimal criteria described by the ISCT in 2006 defined a population of human MSC as needing to be greater than 95% positive for positive antigens and less than 2% positive for negative antigens [126]. In mice however, CD105, CD90 and VCAM-1 have been described as important markers of MSC purity (table 1.3), although as discussed next the successful isolation of MSC from murine bone marrow has been considerably more challenging with robust and reproducible techniques only recently being discovered [143]. These difficulties have led to a number of studies using markedly heterogeneous cell populations with inconsistent results in pre-clinical studies making comparison between them difficult. Prospective isolation of MSC using cell sorting techniques and specific surface markers has been demonstrated. In humans and mice, MSC can also be isolated based on their expression of Low-affinity Nerve Growth Factor (LNGFR) along with Thy1 and Vascular Cellular Adhesion Molecule (VCAM). Cells with an LNGFR<sup>+</sup> (CD271), THY-1<sup>+</sup>, VCAM-1<sup>hi</sup> expression profile have also been shown to meet the ISCT criteria for an MSC due to their ability to undergo tri-lineage differentiation and self-renewal [144]. The intermediate filament protein nestin has also been shown to identify a population of perivascular MSC which are able to support the haematopoietic niche and may also be used as a marker for prospective isolation. Notably the overlap between P $\alpha$ S MSC and nestin<sup>+</sup> cells is not complete, with the majority of nestin<sup>+</sup> cells not expressing Stem

Cell Antigen (SCA-1), suggesting some phenotypic differences [139]. Cells expressing nestin were also shown to form clonal mesenspheres and following serial transplantation these mesenspheres were able to self renew and generate haematopoietic activity. More recently Zhou et al.[145] have described the expression of the leptin receptor on murine bone marrow derived MSC. It is clear from the description of various sub-populations of CFU-Fs that early work demonstrated a heterogeneous population of cells and that MSC only represent a small fraction of this.

Surface Antigens			
Positive		Negative	
<i>Human</i>	<i>Mouse</i>	<i>Human</i>	<i>Mouse</i>
CD105	CD105	CD86	CD45
CD90 (Thy1)	CD90	CD80	Ter119
CD73	VCAM	CD79 $\alpha$ or CD19	
CD73	PDGFR $\alpha$	CD45	
CD71	SCA-1	CD40	
CD44	Leptin receptor	CD34	
GD2		CD14 or CD11b	
LNGFR (CD271)		HLA-DR	
		PDGFR $\alpha$	

**Table 1.3 – List of surface markers for human and mouse MSC.**

### 1.8.2 Isolation techniques for MSC

The MSC literature has been hampered by an inability to isolate purified populations of cells. Whilst there are hundreds of studies published assessing the effects of MSC in various models of disease, the heterogeneity of cell types, isolation methods and culture techniques makes comparison between studies challenging. Studies using MSC have focussed on human cells, in part due the notion that findings should be readily translatable, but mainly due to the difficulties in isolating murine MSC [131, 146]. There are obvious advantages to the use of MSC isolated from mice including the avoidance of xenotransplantation and



the ability to use genetic knockout models enabling finer study of the mechanism of action of MSC which until recently has been lacking. Traditional techniques for MSC isolation involve their ability to adhere to plastic. Following plastic adherence serial changes of media enable the depletion of haematopoietic cells and allows the culture expansion of a heterogeneous population of cells with colony forming potential [147]. Whilst this technique has been successful for the isolation of human MSC, plastic adherence techniques in murine MSC leads to a considerable number of contaminating cells [143, 148]. Techniques to enrich the population of MSC have been demonstrated including immunodepletion and positive selection. Immunodepletion using haematopoietic markers led to a population of cells capable of tri-lineage differentiation, however cell growth was slowed due to a down regulation of genes responsible for cell proliferation [149]. Recent techniques have investigated the prospective isolation of MSC based on a variety of markers thought to represent more purified populations of stem/stromal cells. Morikawa was one of the first to develop a technique for prospective isolation of murine bone marrow MSC based on prospective markers [150]. The markers used were PDGFR $\alpha$  and SCA-1 with negative markers for the haematopoietic markers CD45 and Ter119. Study of these cells *in vivo* demonstrated a perivascular location and *in vitro* studies of isolated cells demonstrated the ability to form colonies and undergo tri-lineage differentiation. Using a genetic mouse model combining the intracellular filament protein nestin with Green Fluorescent Protein (GFP) Méndez-Ferrer demonstrated a population of cells able to undergo tri-lineage differentiation which could be propagated as clonal mesospheres. This study also demonstrated the functional *in vivo* link between MSC and Haematopoietic Stem Cells (HSC) [139]. As isolation of cells expressing nestin requires a transgenic mouse, Pinho demonstrated that cells isolated using PDGFR $\alpha$  and CD51 and that did not express endothelial markers or haematopoietic markers are highly positive for nestin, suggesting an alternative technique to isolate these cells [151]. Whilst all of these techniques produce cells that demonstrate the properties of MSC and meet the ISCT definition, overlap between these populations is not complete suggesting that heterogeneity still exists, however whether a truly homogeneous

population of MSC will ever be described remains to be seen. It is certainly possible that these cells do represent the same population of cells but in a different state of differentiation.

MSC can be isolated from a variety of tissue including bone marrow, umbilical cord, umbilical blood and adipose tissue. Whilst sometimes seen as comparable due to being described as MSC and meeting all of the basic requirements to be refereed to as MSC, cells isolated from different tissues show differences in proliferation capacity and their ability to modulate the immune system [152].

### 1.8.3 MSC and immunomodulation

The evolution of the MSC field has been directed around their ability to undergo differentiation into tissue in the mesodermal lineage and the potential uses for this in regenerative medicine. The ability of MSC to secrete trophic factors coupled with the low level of MHC expression makes them an ideal candidate for use as a cell therapy [153]. In recent years however the ability of MSC to modulate the immune system has gained widespread interest. MSC have broad reaching immunomodulatory properties and have been shown to exert effects on both the adaptive and the innate immune systems mediated by a combination of paracrine signalling and more remote effects the mechanism of which has not yet been elicited [139, 154, 155]. A number of the mechanisms by which MSC have been demonstrated to modulate the immune system in predominantly pre-clinical studies are described below (figure 1.6).

MSC are able to inhibit T cell proliferation and activation and a number of mechanisms have been proposed and demonstrated to explain this finding. Early cell cycle arrest of T cells may have a role in their suppressive action, and MSC have been shown to inhibit cyclin D2 and up regulate p27Kip1. The mechanism by which MSC achieve this is not entirely clear although it has been shown to be independent of MHC expression [156]. The suppressive activity of MSC is not however limited to a specific subset of T cells, and has also been shown to occur during CD40L and Il-4 stimulation of B cells, which likely reflects the role of cyclin D2 in driving B cell proliferation [157, 158]. Notably,

an inflammatory environment is required for MSC to exert their immune-suppressive effect as otherwise MSC have been shown paradoxically to exert a pro-inflammatory effect on T cells [159]. MSC have been shown to inhibit the maturation of dendritic cells [160, 161, 162] and decrease their expression of MHC class 1, MHC class 2 and other co-stimulatory molecules. This leads to a reduction in the ability of dendritic cells to present antigen to other immune cells. *In vitro* assays have been able to demonstrate that MSC can stimulate plasmacytoid dendritic cells to increase their production of Il-10 and can also inhibit the release of  $\text{TNF}\alpha$  from dendritic cells via a Prostaglandin  $\text{E}_2$  ( $\text{PGE}_2$ ) dependent pathway [163]. This mechanism has been proposed for the success of MSC in graft versus host disease [164, 165]. MSC are able to inhibit and promote the release of soluble factors such as Indoleamine 2,3-dioxygenase (IDO),  $\text{TGF}\beta$ ,  $\text{PGE}_2$  and Il-10. This inhibitory effect has been shown to prevent activation of NK cells by Il-2, however once NK cells are activated the inhibitory effect of MSC is only partial. Reductions in  $\text{IFN-}\gamma$  secretion by NK cells has been used to demonstrate the activity of MSC on activated NK cells [166]. MSC can be induced to increase their production of MHC class 1 and 2 by activation using  $\text{IFN-}\gamma$ , and inhibition of MHC production has been shown to protect MSC from NK induced apoptosis [166]. It has recently been suggested that need MSC to be induced to undergo perforin dependent apoptosis by host cytotoxic cells in order to exert their immunosuppressive effects[167].

Whilst the phenotypic differences between human and mouse MSC are relatively well described, and there is a clear difference in expression profiles and phenotype, differences between strains of mice and rats with respect to their mode of immunomodulation have also been demonstrated, with BALBc mice predominantly secreting inducible Nitric Oxide (iNOS) as opposed to IDO being a proposed mechanism of immunosuppression in other models [168, 169]. Parallels between some human and mouse cells have been seen with human MSC also secreting IDO, a potential mechanism by which they exert their immunosuppressive effect [170]. An understanding of the similarities and differences between human and mouse MSC as well as the strain differences is critical when choosing

mice for MSC isolation, particularly when carrying out studies with a translational objective.

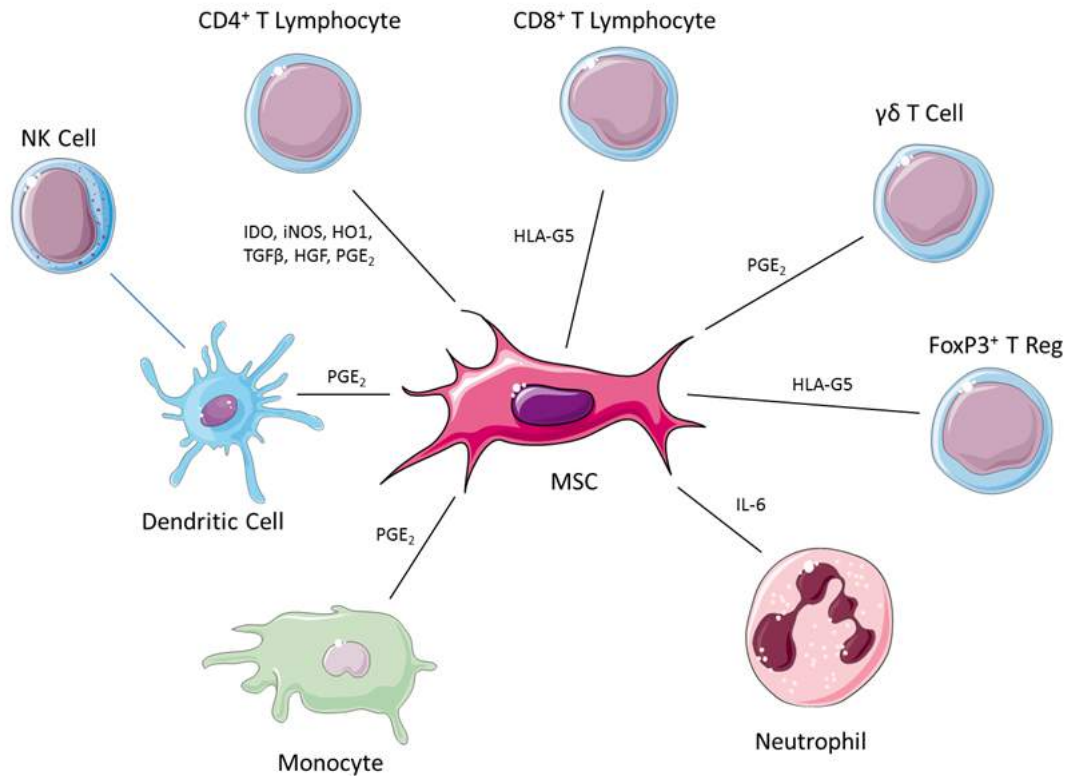


**Figure 1.6 – Diagram showing the effects of MSC on the immune system.** MSC have been shown to have the ability to exert an effect on a range of cells involved in the immune response. Direct effects can be exerted on CD4<sup>+</sup>, CD8<sup>+</sup>, γδT cells, FoxP3<sup>+</sup> regulatory T cells, neutrophils and monocytes. Indirect effects are also exerted on NK cells via their action on dendritic cells. Picture taken from Owen [1].

## 1.9 MSC in liver disease

MSC have been investigated in both pre-clinical and more recently clinical trials of liver and gastrointestinal disease. Mechanisms studied in this context range from paracrine trophic signalling, reduction of oxidative stress and modulation of immune responses including a reduction in liver fibrosis. In the last decade whilst there has been a rapid increase in the number of pre-clinical and clinical trials [146] in the MSC literature, few robust clinical

trials have been undertaken in liver disease and there is clear need for well conducted clinical trials in this area [1].

MSC therapy has been examined in a number of different liver pathologies with some encouraging results.

### **1.9.1 Liver fibrosis and cirrhosis**

Chronic liver disease is characterised by progression from injury to fibrosis and finally cirrhosis. It is generally accepted that fibrosis represents a reversible phase and may be amenable to therapies to prevent or reverse this stage [171]. Cirrhosis marks the final clinical pattern in chronic liver disease and is generally accepted as a move towards irreversible liver damage. During fibrosis stellate cell activation leads to deposition of Extracellular Matrix (ECM) along with collagen and proteins [172]. When activated, stellate cells express P75, a receptor which can trigger apoptosis in response to stimulation by Nerve Growth Factor (NGF). MSC are able to release NGF and therefore stimulate stellate cell apoptosis. Binding of NGF to P75 leads to induction of the NF- $\kappa$ B and c-Jun N-terminal kinase (JNK) pathways [173]. Inflammation and fibrosis are not mutually exclusive and both fibrosis and immune mediated injury can occur simultaneously, particularly in ongoing injury. MSC have been used in models of fibrotic liver disease with an aim to reverse fibrosis, however due to the nature of the models used ongoing immune injury is usually present and so determining whether beneficial effects seen are due to reversal of the fibrosis or immunomodulation is debated (figure 1.7). MSC are able to initiate stellate cell apoptosis, and due to their role in ECM deposition and subsequent fibrosis this has been suggested as a possible mechanism by which MSC could improve fibrotic liver disease [174]. In rat models of liver cirrhosis human umbilical cord MSC have been shown to decrease the expression of markers of fibrosis including  $\alpha$  Smooth Muscle Actin ( $\alpha$ -SMA) [175]. MSC are also able to secrete the Matrix metalloproteinase (MMP) MMP9, a protease which is able to breakdown the ECM and in mouse models of fibrosis MSC have been shown to increase expression of MMP9 along fibrous septa leading to a reduction in

fibrosis [176]. It has been suggested that MSC can differentiate into hepatocytes and are able to repopulate fibrotic or cirrhotic liver, however this mechanism seems unlikely due to the low numbers of MSC administered and the even lower number of cells which actually arrive at the liver [177]. Clinical trials in liver fibrosis have shown conflicting results with early observational studies demonstrating an increase in liver volume but later randomised control trials demonstrating no beneficial effect of MSC therapy [178, 179].

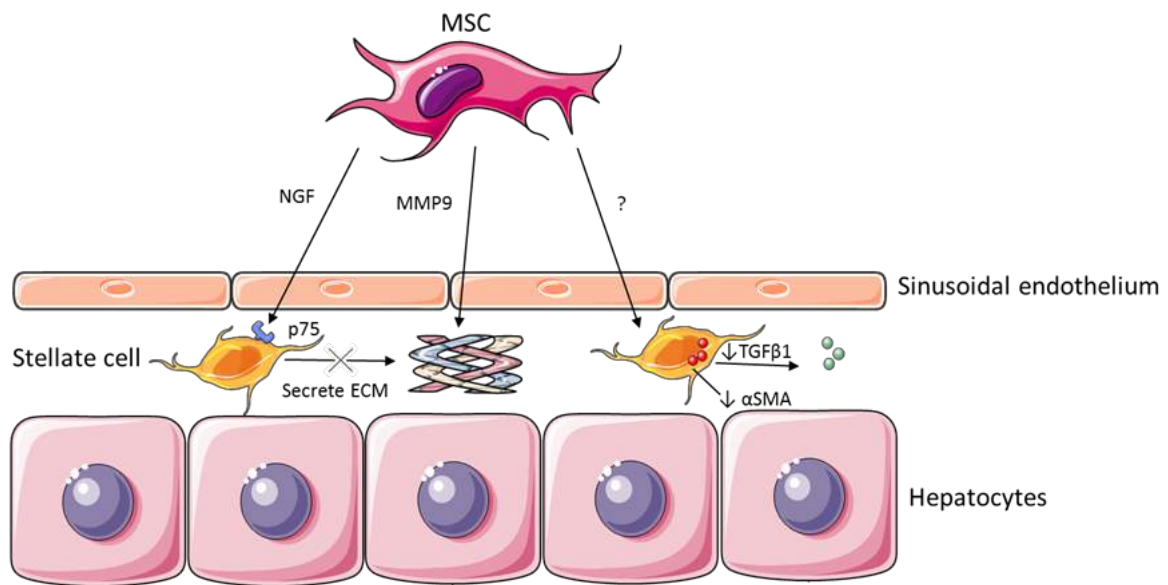


**Figure 1.7 – Diagram showing the effects of MSC in liver fibrosis.** MSC are able to secrete NGF which binds to p75 expressed on activated stellate cells. This causes stellate cell apoptosis and therefore a reduction in ECM due to less stellate cell production. MSC also secrete MMP9 which is a protease able to cleave collagen in the ECM. MSC may also act via an as yet undiscovered mechanism to reduce the secretion of stellate cell  $\alpha$ -SMA and TGF $\beta$ 1. Image taken from Owen [1].

### 1.9.2 Acute liver failure

Acute liver failure is relatively rare but has a high morbidity and mortality. There are a number of causes of acute liver failure and the prevalence of these varies between developed and developing countries with drug induced liver injury being the most common in the developed world whereas hepatitis induced acute liver failure is the commonest aetiology in developing countries [180]. Drug induced liver failure accounts for over 50% of cases of acute liver failure in the United States of America (USA) and across Europe with

the commonest drug being paracetamol [181, 182]. In both CCL<sub>4</sub> and concanavalin A induced liver failure MSC therapy has been shown reduce liver injury through a reduction in pro-inflammatory cytokines such as TNF $\alpha$  and IFN- $\gamma$  with a greater effect seen with repeated dosing of MSC [183, 184, 185]. In the acute CCL<sub>4</sub> model oxidative stress has been demonstrated as discussed earlier. MSC have been shown to have the ability to act as free radical scavengers in the CCL<sub>4</sub> model and reduce liver injury by reducing oxidative stress [186]. In mouse models of paracetamol induced liver failure MSC have been shown to reduce liver injury by inhibition of JNK, a change that has been shown to persist along with reduction in overall hepatic JNK and TNF $\alpha$  whilst levels of glutathione seem to be preserved [187, 188].

### 1.9.3 Ischaemia reperfusion injury and transplantation

Ischaemia reperfusion injury occurs due to trauma, blood loss and during liver surgery [189]. The broad mechanisms of injury which occur in ischaemia reperfusion injury have been described earlier with one important component of reperfusion injury being the infiltration of CD4<sup>+</sup> T cells and their subsets including NK cells and  $\gamma\delta$ T cells [190]. A number of potential roles for MSC therapy have been investigated (figure 1.8). A therapy that has been studied in hepatic ischaemia reperfusion injury is hepatocyte transplantation and using MSCs in this setting appears to increase the survival of transplanted hepatocytes as well as maintain their function [191, 192]. MSC have also been shown to reduce the number of TUNEL positive hepatocytes in a rat model of ischaemia reperfusion injury [193]. MSC have been shown to inhibit neutrophil apoptosis via modulation of the Bcl-2:Bax pathway *in vitro* [194], possibly through secretion of Il-6 leading to increased phosphorylation of STAT3 [1], the relevance of this in ischaemia reperfusion injury needs consideration due to the role of neutrophils in reperfusion injury.

MSC that have been transfected to enable them to overexpress Hepatocyte Growth Factor (HGF) have been shown to improve survival in models of small for size liver transplantation although it is not clear if this is an effect of HGF alone [195, 196]. In

reduced size liver transplantation MSC have been shown to prolong graft survival, although the mechanism by which they achieve this is not clear [197].

In models of liver transplantation MSC have been shown to induce tolerance by suppressing cytotoxic T cell levels whilst increasing the levels of regulatory T cells [198, 154]. So far these results have not been translated into clinical practice, however results from small studies in renal transplant have shown that MSC may improve graft survival [199, 200].

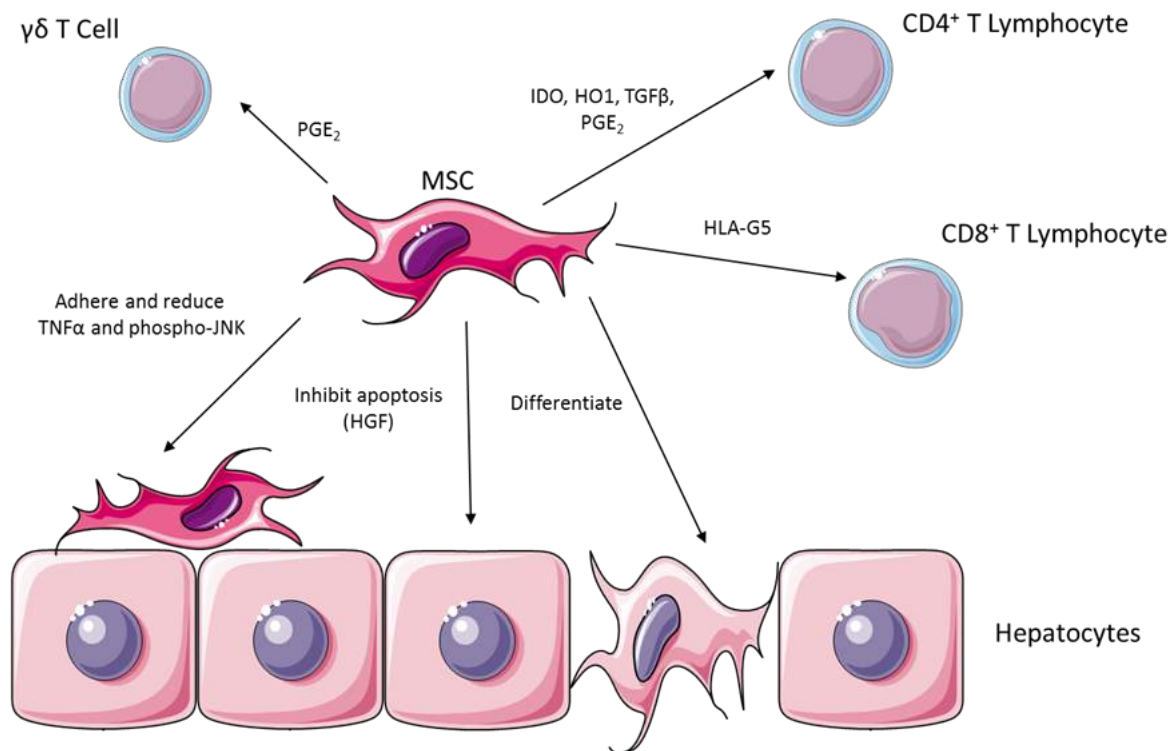


**Figure 1.8 – Diagram of the effects of MSC in ischaemia reperfusion injury.** MSC are able to inhibit CD4<sup>+</sup>, CD8<sup>+</sup> and  $\gamma\delta$  T lymphocytes by secreting a number of anti-inflammatory cytokines including LHA-G5, IDO, Haem Oxygenase 1 (HO1),  $TGF\beta$  and  $PGE_2$ . MSC may also differentiate into hepatocytes, although this occurs in low numbers and is unlikely to be a significant mechanism of action. Hepatocyte apoptosis is also inhibited by MSC due to their ability to secrete HGF. MSC may also adhere to hepatocytes and reduce  $TNF\alpha$  and phospho-JNK. Image taken from Owen [1].

#### 1.9.4 Acute hepatitis

In the developing world acute liver failure is commonly caused by viral infection with hepatitis A and hepatitis E [201, 202, 203]. Whilst predominantly a cause of chronic



hepatitis viral infection with hepatitis B has also been shown to cause acute on chronic liver failure [204]. In a case control study MSC therapy has been shown to reduce liver volume, as well as improve liver function tests and albumin production in patients with acute on chronic hepatitis B [205]. Due to the design of this study it is difficult to infer causality and so further work is needed to ascertain if MSC are a viable therapy in acute on chronic liver failure.

### **1.9.5 Chronic hepatitis**

MSC may have a role in patients suffering from chronic hepatitis B and C infection. In patients with hepatitis B related cirrhosis MSC have been shown to improve liver function tests when compared with anti-viral therapy alone [206]. The mechanism proposed for the beneficial effects of MSC in hepatitis B are an increase in regulatory T cells and a reduction in Il-17 secreting T helper cells [207]. In hepatitis C small clinical trials have shown a reduction in markers of fibrosis along with a decrease in pro-inflammatory cytokines and an increase in anti-inflammatory cytokines in patients treated with a combination of MSC and G-CSF [208]. Hepatitis B virus is able to infect MSC without any apparent effect on their ability to modulate the immune system, the clinical significance of this needs further study [209].

### **1.9.6 Concerns about tumour formation**

There has always been a concern with stem and stromal cell therapy about the theoretical risk of tumour formation. Indeed any immunosuppressive treatment can potentially lead to an increased risk of tumour formation due to the complex role that the immune system plays in prevention and removal of abnormal cells. MSC have also been demonstrated to secrete pro-angiogenic factors including platelet derived growth factor and vascular endothelial growth factor which could support tumour growth [210]. MSC have been shown to inhibit tumour growth in hepatocellular carcinoma by stimulating the down

regulation of factors associated with the Wnt signalling pathway, but in other models MSC seem to promote tumour growth by secreting trophic factors [211].

Transformation of MSC has been shown to occur and is a possible explanation for the heterogeneity seen in pre-clinical and clinical studies. It is seen more commonly in murine MSC and more commonly when using plastic adherent isolation techniques [212].

There were two reports which described spontaneous transformation of human MSC following transplantation which led to the suspension of a number of clinical trials [213, 214]. These reports were subsequently retracted after it was demonstrated that the MSC used in these studies had been cross contaminated with the HT1080 human fibrosarcoma cell line [215, 216].

Studies into murine MSC have been able to generate more robust data indicating a potential problem with MSC therapy. Late passage MSC (passage 65) have been shown to be able to bypass senescence and generate fibrosarcomas in multiple organs after being injected into mice and early passage MSC have been shown to exhibit genetic instabilities which can go on to form tumours [217]. Whilst the increased susceptibility of inbred murine cells to malignant transformation is well documented, human cells appear to be relatively resistant. Human fibroblasts have been shown to require mutations in 6 different signalling pathways in order to undergo malignant transformation whereas mouse fibroblasts only require mutations in 2 pathways [218]. Whilst some of these findings may raise concern it is worth noting that so far no clinical trials have demonstrated malignant transformation of human MSC when used as a cell therapy.

### **1.9.7 Route of administration and homing**

Delivery of MSC into animals and humans has been achieved using a number of different routes of administration. Conventional routes of administration such as Intravenous (IV) have been tested extensively, however other routes of administration such as intra-portal and Intraperitoneal (IP) are an attractive prospect as they enable bypassing of the pulmonary circulation which is responsible for trapping the majority of systemically

administered MSC [219]. Strategies to improve homing of MSC to target organs have been trialled with some success. In CCL<sub>4</sub> induced liver injury MSC use CD29 and CD44 to mediate adhesion to the sinusoidal endothelium leading to increased engraftment [220]. Human MSC are able to express a number of molecules involved in adhesion and trafficking including the CXC Chemokine Receptor (CXCR)s CXCR4, CXCR5 and CXCR6, however the *in vivo* relevance of this requires further study [221]. In standard culture conditions MSC quickly lose expression of CXCR4, however culture in hypoxic conditions CXCR4 expression is increased which may aid in homing to hypoxic tissues expressing SDF-1 $\alpha$  [222]. By converting surface CD44 on MSC into Hematopoietic Cell E-/L-Selectin Ligand (HCELL) MSC can be modified using glycosyltransferase-programmed stereosubstitution to adhere to endothelial tissue expressing E-Selectin aiding recruitment to therapeutic targets[223]. MSC encapsulated in alginate have been shown to survive longer *in vivo* and in models of graft versus host disease are able to reduce the injury seen suggesting that paracrine signalling plays an important role in the effects of MSC in systemic inflammatory conditions [155].

### 1.9.8 Cell therapy without administering cells

Due to the potential risks of administering live cells and the potential unpredictability of the response *in vivo* work has been undertaken to find alternative ways to achieve the same clinical outcomes without administering cells. MSC conditioned media is media taken from cultured cells and along with MSC based extra corporeal membranes have been shown to have similar effects to administering cells. In a study using the d-galactosamine model of acute liver failure extracorporeal membranes containing MSC showed the greatest reduction in liver injury, followed by MSC conditioned media with systemic administration of MSC alone showing the least improvement in liver function [224]. Studies in other diseases have shown a benefit from the MSC secretome with models of Multiple sclerosis (MS) showing an improvement [225]. Whilst encouraging, MSC derived conditioned media contains a large number of cytokines and further work needs to be done to elicit which of

these are important in order to effectively reduce liver injury.

Extracellular vesicles were first described in the 1980's and it was believed that they were a means for cells to excrete waste products [226]. Recent studies have demonstrated that cells are able to use extracellular vesicles to facilitate cell to cell communication by transferring biomolecules [227]. MSC secrete extra cellular vesicles and administration of MSC derived extra cellular vesicles has been shown to increase hepatocyte proliferation and cell viability in an acute CCL<sub>4</sub> model [228].

### 1.9.9 Tracking MSC *in vivo*

Due to the lack of clarity as to whether MSC need to be located in an area of inflammation in order to exert immunomodulatory effects it is important to be able to accurately track the location of systemically administered MSC in order to gain further insight into their mechanism of action. Early techniques to allow for the tracking of MSC required magnetoporation of MSC to enable labelling with super-magnetic iron oxide allowing visualisation in a Magnetic Resonance Imaging (MRI) scanner [229]. Whilst promising initially it has subsequently been discovered that magnetoporation inhibits MSC migration and differentiation making this tracking technique unusable [230]. An alternative technique involves the use of manganese oxide nanoparticles and this technique has been used with success in models of glioblastoma [231]. Quantum dots are a stable nanoparticle which can be used to label cells for an extended period of time without significant deleterious effects on cell function. Recent studies have successfully used quantum dots to track MSC in rat lung injury models, however further work is required in order to demonstrate that quantum dots are truly inert in murine MSC [232].

## 1.10 Aims and Objectives

With the paucity of donor organs available for liver transplantation and the increasing incidence of liver disease in the developed world there is an urgent need for novel therapies in order to reduce the morbidity and mortality from liver disease and liver transplantation. MSC have great potential as an immunomodulatory therapy which may be able to reduce the immune mediated injury that occurs in liver transplantation operations and the resulting medium term complications that occur as a result of ischaemia reperfusion injury to the donor liver. The pre-clinical MSC literature demonstrates a huge amount of heterogeneity in both the isolation techniques used for MSC and the type of cell used with a mixture of the xenotransplantation of human MSC into mouse models and the allotransplantation mouse MSC into mouse models.

In order to test the potential of MSC as a potential therapy for improving liver transplantation outcomes I opted to use murine bone marrow derived MSCs prospectively isolated based on their expression of PDGFR $\alpha$  and SCA-1 (P $\alpha$ S) and test them in models of liver injury.

### 1.10.1 Hypotheses

In order to investigate the hypothesis that MSC represent a translatable therapy for marginal donor liver transplantation I first considered a number of hypotheses. The hypotheses for this study were:

1. P $\alpha$ S MSC are able to suppress lymphocyte proliferation *in vitro*
2. P $\alpha$ S MSC are able to reduce hepatobiliary injury in the MDR2<sup>-/-</sup> mouse model
3. P $\alpha$ S MSC are able to exert their immunomodulatory effects via a remote action
4. P $\alpha$ S MSC are able to reduce immune mediated injury in a model of hepatic reperfusion injury

### 1.10.2 Specific aims

The specific aims for this study were to:

1. Isolate and characterise P $\alpha$ S MSC from murine bone marrow
2. Optimise an *in vitro* splenocyte reaction and test the *in vitro* efficacy of P $\alpha$ S MSC
3. Characterise the MDR2<sup>-/-</sup> model of biliary injury and test the *in vivo* efficacy of P $\alpha$ S MSC in this model
4. Investigate the trafficking of P $\alpha$ S MSC following systemic administration and test their ability to exert remote immunomodulatory effects
5. Develop a model of hepatic ischaemia reperfusion injury and test the *in vivo* efficacy of P $\alpha$ S MSC in this model

## CHAPTER 2

## METHODS

### **2.1 Preparation of buffers and culture media**

All buffers and media were made and stored refrigerated at 4°C for a maximum of 2 weeks unless otherwise stated.

#### **2.1.1 P2 buffer**

P2 buffer was prepared by combining sterile Phosphate Buffered Saline (PBS) with 2% Foetal Bovine/Calf Serum (FBS/FCS) (Gibco<sup>®</sup>, UK).

#### **2.1.2 FACS buffer**

Fluorescence Activated Cell Sorting (FACS)buffer was prepared by combining sterile PBS with 2% FBS/FCS

#### **2.1.3 MACS buffer**

Magnetic Activated Cell Sorting (MACS)buffer was prepared by combining sterile PBS with 2% FBS/FCS and 1mM Ethylenediaminetetraacetic Acid (EDTA) (Sigma-Aldrich, UK).

### **2.1.4 C10 media**

C10 medium was prepared by combining Rosewell Park Memorial Institute (RPMI) (Gibco, UK) with 10% FBS/FCS, 1% Penicillin-Streptomycin-Glutamine (PSG) (Gibco<sup>®</sup>, UK) and 50 mM  $\beta$ -mercaptoethanol ( $\beta$ ME) (Sigma-Aldrich, UK).

### **2.1.5 HBSS<sup>+</sup>**

A solution of Hank's Balanced Salt Solution (HBSS) (Gibco<sup>®</sup>, UK) was prepared with the addition of 2% FBS/FCS, 1% PSG and 10 mM of HEPES buffer (Sigma-Aldrich, UK).

### **2.1.6 $\alpha$ -MEM culture medium**

$\alpha$  Modified Minimum Essential Medium (Eagle) ( $\alpha$ -MEM) culture medium was prepared by combining  $\alpha$ -MEM (Gibco<sup>®</sup>, UK) with 10% FBS/FCS and 1% PSG.

## **2.2 Animal husbandry**

All mice were maintained at the [REDACTED]. Care was undertaken using the standard established care protocols at our institution. Mice were housed in cages of no greater than 5 animals. The environment was controlled, with a 12 hour light/dark cycle and a temperature of 22°C. Any procedures carried out on animals were done so in accordance with the Animals (Scientific Procedures) Act 1986, UK and all procedures underwent ethical review prior to being performed. Procedures were performed under project license numbers 707707 and 708302, and personal license number IBB240811.



### 2.2.1 Wildtype mice

Male C57BL/6 mice and male FVB mice were purchased from [REDACTED] and male BALB/c mice were purchased from [REDACTED]. Animals were purchased at age 7 weeks and acclimatised for 1 week prior to use in experiments. Genotyping was not required in our institution.

### 2.2.2 OT-1 mice

Male OT-1 mice were purchased from [REDACTED]. A breeding colony was established and maintained at [REDACTED]. OT-1 mice were maintained on a C57BL/6 background as homozygotes. Genotyping was performed by TransnetYX<sup>®</sup> as described.

### 2.2.3 MDR2<sup>-/-</sup> mice

The MDR2<sup>-/-</sup> mouse colony was already established on an FVB background in [REDACTED]. As this is a genetic knockout model injury develops from birth and does not recover. Whilst animals were regularly observed for signs of distress this is a mild non-fatal model and distress was not expected or seen. Whilst genotyping of all mice were not required due to this being a homozygous colony occasional genotyping of breeding pairs was undertaken to ensure there was no genetic drift. Genotyping was performed by TransnetYX<sup>®</sup> as described.

### 2.2.4 Genotyping

Genotyping was undertaken by TransnetYX<sup>®</sup> (TransnetYX<sup>®</sup>, US). Ear clippings were removed from breeding pairs by animal handling staff at the [REDACTED] labelled and shipped to TransnetYX<sup>®</sup> for analysis. Zygosity testing using

real time PCR was undertaken using the primers in table 2.1. One probe per allele was run and results were uploaded online.

Mouse strain	Forward primer	Reverse primer
OT-1	5' - CAG CAG GTG AGA CAA AGT - 3'	5' - GGC TTT ATA ATT AGC TTG GTC C - 3'
MDR2 <sup>-/-</sup>	5' - CTC GTT AAC ATG CAG ACA GCA G - 3'	5' - GAC CAG GGA GAA CAT GTT ACA C - 3'

**Table 2.1** – List of primers used for genotyping mice.

## 2.3 Prospective isolation of murine P $\alpha$ S MSC by cell sorting

The prospective isolation of murine P $\alpha$ S MSC was originally described by Morikawa et al in 2009 [150]. The technique for isolation of P $\alpha$ S MSC was further optimised by our group [233] to ensure consistency and reproducibility in our laboratory. Prospective isolation using this technique yields a highly purified population of P $\alpha$ S MSC (>99% pure).

### 2.3.1 Long bone removal and preparation

Each isolation was performed using 10 male wild type mice aged between 8 and 12 weeks as following earlier optimisation this number represented the most efficient and least wasteful number of mice to ensure adequate cell yield. Following sacrifice mice were sprayed with 70% ethanol. A transverse incision was made in the abdomen through the skin layer and extended to each hind limb. Forceps were used to grip the knee joint and the skin was folded back over the foot and then the foot removed and discarded. The tibia was exposed by blunt dissection using scissors and the fibula discarded. An incision was made through the knee joint and the tibia removed and cleaned by gentle rolling between a piece of tissue paper until all soft tissue had been removed. The tibia was then placed into a 50 ml Falcon<sup>TM</sup> (Corning, US) conical centrifuge tube containing PBS and kept on ice. The femur was then exposed by a combination of blunt dissection and careful incisions in the soft tissue. A further incision was made through the hip joint aiming to preserve the

femoral head. The femur was then cleaned in the same manner as the tibia and again placed into PBS. This process was then repeated for the other hind limb. Each mouse was sacrificed individually just prior to long bone removal.

Following removal of all long bones the bones were washed 3 times in PBS by gentle agitation in a conical tube. The bones were then placed into a pestle and mortar and each bone broken with a single break in the middle. A bony paste was then produced by cutting the bones with dissection scissors until there was no resistance felt (approximately 5-10 minutes). The bony paste was then washed with 5 ml of PBS and the bones transferred into a further 50 ml Falcon<sup>TM</sup> tube containing 20 ml of Dulbecco's Modified Eagle's Medium (DMEM) (Gibco<sup>®</sup>, UK) with 0.2% crude collagenase (Wako, Germany) and treated with PSG, pre-warmed to 37°C. The mixture was then placed in a rocking incubator at 37°C with an oscillatory frequency of 110 rpm for 60 minutes.

### **2.3.2 Preparation of cell suspension**

On removal from the incubator the tube was immediately placed on ice to stop the collagenase reaction. The bone fragments were filtered using a 70 µm sterile filter (Corning, US) into a new conical tube and kept on ice. The remaining bone fragments/bone paste are returned to the mortar. HBSS<sup>+</sup> solution is added to the bone fragments. The bone fragments were then gently crushed using the pestle with repeated light tapping for 100 taps. This was followed by the addition of a further 2.5 ml of the HBSS<sup>+</sup> solution was added using a pipette. The total of 5 ml of solution was pipetted up and down 3 times to aid with cell release. Gentle swirling of the bone fragments and liquid was carried out using the pestle for 30 seconds. Further mixing with the pipette was carried out with repeat up and down transfer. The solution was then carefully drawn up into the pipette being sure to leave the remaining bone fragments and the solution filtered through a 70 µm filter into the conical tube containing the previous filtrate, remaining on ice at all times. This process was repeated a further 5 times until a total of 50 ml of solution had been collected in the conical tube. The solution was subsequently spun in a pre-chilled centrifuge at 4°C

for 7 minutes at 280g (1350 rpm). Following centrifugation the supernatant was discarded and the cell pellet resuspended as previously described but no medium added.

### **2.3.3 Red cell lysis**

Red blood cell lysis was required in order to remove all of the red blood cells, which are not being collected, and therefore improve the efficiency of the later sorting step. Whilst the technique described is a non-standard technique it has been found through meticulous optimisation to give the greatest yield of P $\alpha$ S MSC compared with other methods of red cell lysis. The resuspended pellet present in a 50 ml conical tube had 1 ml of cold (approximately 4°C) sterile water (Sigma-Aldrich, UK) added whilst continuous rotating of the tube was carried out by hand. After 5 seconds of contact with the water 1 ml of double strength PBS solution (with 4% FBS/FCS added) was added followed by 13 ml of HBSS<sup>+</sup> solution to make a total volume of 15 ml in order to quench the reaction. The cell suspension was then filtered through a sterile 70  $\mu$ m filter before further spinning in a pre-chilled centrifuge at 4°C for 5 minutes at 280g (1350 rpm). Following this the supernatant was again discarded and the cell pellet resuspended as described previously in 1ml of the HBSS<sup>+</sup> solution.

### **2.3.4 Labelling of MSC with fluorescent antibodies**

The staining colours were determined after careful analysis of the requirements of the MoFlo<sup>TM</sup> XDP cell sorter (Beckman Coulter, US) at the university of Birmingham along with the availability of stains for the relevant markers. The antibody panel used was as described in the literature. All antibodies were purchased from eBioscience in the UK. The antibodies used were as follows; CD45-PE (1  $\mu$ l/mouse), Ter119-PE (1  $\mu$ l/mouse), SCA-1-FITC (1  $\mu$ l/mouse) and PDGFR $\alpha$ -APC (1.5  $\mu$ l/mouse). Propidium Iodide (PI) (Sigma-Aldrich, UK) solution was also used as described later. Sterile FACS tubes (Corning, US) were used for all samples and controls. Staining of the main sample was

carried out in the conical tube and transferred to a cuvette as described later. All samples were kept on ice during the staining process. Staining was carried out in a standard hood with the light switched off and all antibodies were protected from light exposure. Control tubes were as follows; negative control (cells only), positive control for PE (cells and PE antibody), positive control for FITC (cells and FITC antibody), and positive control for APC (cells and APC antibody). Each control tube (4 in total) had 100  $\mu$ l of HBSS<sup>+</sup> solution, 4  $\mu$ l of the cell suspension and 1  $\mu$ l of the relevant antibody. The main sample tube staining was achieved with the addition of 1 $\mu$ l per mouse of each of the 4 antibodies (CD45-PE, Ter119PE, SCA-1-FITC and PDGFR $\alpha$ -APC). All samples were then incubated on ice in the dark for 30 minutes. Following incubation the control samples were washed by the addition of a further 1ml of HBSS<sup>+</sup> solution. The control samples were then spun at 2000 rpm for 5 minutes. The supernatant was discarded and the resulting cell pellets resuspended as described earlier. The main sample conical tube was spun in a pre-chilled centrifuge at 4°C for 5 minutes at 280g (1350 rpm). Following this the supernatant was discarded and the resulting cell pellet resuspended. A solution of PI stain and HBSS<sup>+</sup> was made with a concentration of 2  $\mu$ l of PI per ml of HBSS<sup>+</sup>. The control tubes each had 500  $\mu$ l of PI/HBSS<sup>+</sup> solution added. The main sample had 1 ml PI/HBSS<sup>+</sup> solution per mouse added (10-15 ml). Each control tube was filtered into a new FACS cuvette through a sterile 50  $\mu$ m filter (Partec, DE). The main sample was filtered into multiple FACS cuvette tubes through a sterile 50  $\mu$ m filter aiming for 3-4 ml in each cuvette. All samples were then stored on ice in the dark ready for cell sorting.

### 2.3.5 Cell sorting of fluorescently labelled MSC

A MoFlo<sup>TM</sup> XDP cell sorter was used for cell sorting. The cell sorter was configured to the manufacturer's exact specifications and calibrated extensively prior to use and the machine allowed to reach a stable working temperature. Whilst many lasers are available on this particular machine only the 488 nm and 647 nm lasers are used in this protocol. Voltage, fanning, laser alignment and drop delay were all calibrated as per

manufacturer specifications. The negative control was run through to ensure detection of events without any significant detection by the lasers. Following this each single antibody control/compensation tube was run starting with PE, then FITC then APC. Each of these channels was compensated against the others in order to prevent significant colour bleed between the fluorescent antibodies. Once compensation was complete gating was carried out. Gating on PI allowed for the live cells to be selected. Negative gates for PE and Ter119 were created and positive gates for PDGFR $\alpha$  and SCA-1 in order to select the P $\alpha$ S cells. Finally a gate was drawn in order to select the central population of P $\alpha$ S cells based on previous optimisations and experience from the literature. The positively selected cells P $\alpha$ S were collected in a small collecting tube containing  $\alpha$ -MEM media with added PSG and 10% FBS/FCS. The mixture was then transferred into a FACS cuvette following completion of the sort and spun in a centrifuge at 2000 rpm for 5 minutes. The resulting pellet was resuspended and the appropriate amount of culture medium added for seeding onto 6 well plates (Corning, US).

## 2.4 P $\alpha$ S MSC culture

Following cell sorting isolated purified P $\alpha$ S MSC were cultured in  $\alpha$ -MEM. Media was changed every 3 days and cells were assessed under light microscopy daily. Cells were cultured in a humidified incubator at 37°C in 5% carbon dioxide. When cells reached 90% confluency they were passaged and separated into larger containers. A minimum seeding density of 5x10<sup>3</sup> cells per cm<sup>2</sup> was used.

## 2.5 P $\alpha$ S MSC passage

Cell passage was performed when signs of confluence were detected. All media was removed and the cells were washed 3 times with PBS whilst still adherent to the container or plate they were housed in. A combination of trypsin and EDTA (TrypLE Express; Gibco®),

UK) was added to the container and left covered in an incubator at 37°C for 3 minutes. Loss of adherence was encouraged by gentle tapping and confirmed by microscopy. The trypsin mixture was neutralised by the addition of an equal volume of  $\alpha$ -MEM. The cell suspension was transferred by pipette into either a 15 ml or 50 ml Falcon™ Conical Centrifuge tube depending on the volume of suspension being separated. Cells were spun by centrifuge at 2000 rpm for 5 minutes. The supernatant was discarded and the cells were then resuspended by vigorous tapping of the conical tube until a homogeneous cell suspension remained. An appropriate volume of medium was then added and the suspension agitated to achieve a homogeneous mixture. The cells were then seeded onto larger plates to allow for continued growth.

## **2.6 *In vitro* naive lymphocyte immunosuppression assay**

The *in vitro* immunosuppression assay used isolated naive CD4<sup>+</sup> cells stimulated with CD3e with co-stimulation provided by CD19<sup>+</sup> B lymphocytes. Graded numbers of P $\alpha$ S MSC isolated from C57BL/6 mice were added and cultured for 72 hours. Analysis was by flow cytometry.

### **2.6.1 Isolation of CD4<sup>+</sup>CD25<sup>-</sup> T lymphocytes using MACS MicroBeads**

Isolation of CD4<sup>+</sup>CD25<sup>-</sup> T cells was undertaken using a CD4<sup>+</sup>CD25<sup>-</sup> T cell isolation kit (Miltenyi Biotec, DE). Lymph nodes were removed from 8-12 week old C57BL/6 mice following cervical dislocation. Lymph nodes were immediately placed into P2 buffer and stored on ice. Lymph nodes were dissociated by passing through a 70  $\mu$ m filter into 1 ml of P2 buffer. and an aliquot taking for counting. Cells were washed in excess P2 buffer and centrifuged at 1400 rpm for 7 minutes in a refrigerated centrifuge at 4°C. The cell pellet was resuspended in 40  $\mu$ l of P2 buffer per 10<sup>7</sup> total cells. 10  $\mu$ l of Biotin-Antibody

Cocktail per  $10^7$  cells was added and the sample incubated for 5 minutes at  $4^{\circ}\text{C}$ . Following incubation 20  $\mu\text{l}$  of P2 buffer, 20  $\mu\text{l}$  of Anti-Biotin MicroBeads and 10  $\mu\text{l}$  of CD25-PE MicroBeads per  $10^7$  cells were added and the sample mixed well and incubated for 10 minutes at  $4^{\circ}\text{C}$ . The samples were then quenched in excess P2 buffer and centrifuged at 1400 rpm for 7 minutes in a refrigerated centrifuge at  $4^{\circ}\text{C}$ . Cell pellets were resuspended in 500  $\mu\text{l}$  of MACS buffer.

The first pass magnetic separation was then carried out using LD columns (Miltenyi Biotec, DE). Columns were placed onto a stand containing a magnetic field and washed with 2 ml of MACS buffer. 500  $\mu\text{l}$  of the cell suspension was then placed onto the column followed by 2 1 ml washes with MACS buffer and the flow through collected. The flow through was washed in excess P2 buffer and centrifuged at 1400 rpm for 7 minutes in a refrigerated centrifuge at  $4^{\circ}\text{C}$ . The cell pellet was resuspended in 90  $\mu\text{l}$  MACS buffer and 10  $\mu\text{l}$  of anti-PE MicroBeads per  $10^7$  cells was added and the sample incubated at  $4^{\circ}\text{C}$  for 15 minutes. Following incubation the sample was quenched with excess MACS buffer and centrifuged at 1400 rpm for 7 minutes in a refrigerated centrifuge at  $4^{\circ}\text{C}$ . The cell pellet was resuspended in 500  $\mu\text{l}$  of MACS buffer.

The second pass magnetic separation was carried out using MS columns (Miltenyi Biotec, DE). Columns were placed onto a stand containing a magnetic field and washed with 500  $\mu\text{l}$  of MACS buffer. 500  $\mu\text{l}$  of cell suspension followed by three 500  $\mu\text{l}$  washes of MACS buffered were passed over the columns and the flow through collected containing the  $\text{CD4}^+\text{CD25}^-$  naive T lymphocytes. Cells were washed in MACS buffer and centrifuged at 1400 rpm for 7 minutes in a refrigerated centrifuge at  $4^{\circ}\text{C}$ . The cell pellet was resuspended in C10 media and the resulting suspension kept on ice until required.

### **2.6.2 Isolation of $\text{CD19}^+$ B lymphocytes using MACS MicroBeads**

Isolation of  $\text{CD19}^+$  B lymphocytes was undertaken using MACS MicroBeads (Miltenyi Biotec, DE). Spleens were removed from 8-12 week old C57BL/6 mice following cervical dislocation. Spleens were immediately placed into P2 buffer and stored on ice. Spleens



were dissociated by passing through a 70  $\mu\text{m}$  filter into red cell lysis buffer (Sigma-Aldrich, UK). Cell filtrate was pipetted up and down to ensure adequate mixing with lysis buffer and then quenched in excess P2 buffer. Samples were centrifuged at 1400 rpm for 7 minutes in a refrigerated centrifuge at 4°C.

An aliquot was removed for counting and then the cell pellet was resuspended in P2 buffer at a concentration of 90  $\mu\text{l}$  buffer per  $10^7$  cells. 10  $\mu\text{l}$  of CD19 MicroBeads were added per  $10^7$  total cells and mixed well. Samples were incubated for 15 minutes at 4°C. Cells were washed in 2 ml of P2 buffer per  $10^7$  cells and centrifuged at 1400 rpm for 7 minutes in a refrigerated centrifuge at 4°C. The cell pellet was resuspended in 500  $\mu\text{l}$  of P2 buffer.

Magnetic separation was then carried out using LS columns (Miltenyi Biotec, DE). Columns were placed onto a stand containing a magnetic field and washed with 3 ml of P2 buffer. 500  $\mu\text{l}$  of the cell suspension was then placed onto the column. The column wash then washed three times each with 3 ml of P2 buffer to wash out the unlabelled cells. The column was then removed from the magnetic field and placed onto a collecting tube. 5 ml of P2 buffer was flushed through the column with a plunger to wash out the labelled cells. The cell suspension was then washed in excess P2 and centrifuged at 1400 rpm for 7 minutes in a refrigerated centrifuge at 4°C. Cells were then resuspended in C10 media and stored on ice until required.

### **2.6.3 Proliferation and flow cytometric analysis**

Isolated CD4<sup>+</sup>CD25<sup>-</sup> naive T lymphocytes were cultured in 96 well round bottomed plates (Starstedt, DE) at a seeding density of  $2.5 \times 10^4$  cells per well. CD19<sup>+</sup> B lymphocytes selected by magnetic columns were added at a ratio of 2:1 ( $5 \times 10^4$  B cells). T lymphocytes were stimulated by the addition of 0.8  $\mu\text{g}/\text{ml}$  anti-CD3e antibody (BD Bioscience, US). Culture was carried out in C10 medium. P $\alpha$ S MSC were added to some of the wells in varying ratios and culture carried out for 72 hours in a standard humidified incubator at 37°C with 5% CO<sub>2</sub>.

Following incubation samples in each group were created by merging 3 wells. Media from each well was pipetted up and down to wash off the non-adherent cells and collected in FACS tubes leaving behind the MSC which are plastic adherent. Non-adherent cells were washed in FACS buffer and centrifuged at 2000 rpm for 5 minutes. The cell pellet was resuspended in 100  $\mu$ l of FACS buffer for staining. Fluorescent antibodies to CD4 (PerCP, BD Bioscience) and CD19 (APC, BD Bioscience) were added to the samples and appropriate controls and incubated for 30 minutes in the dark at 4°C. Following incubation excess FACS buffer was added and centrifuged at 2000 rpm for 5 minutes in a refrigerated centrifuge at 4°C. Cell pellets were resuspended in 400  $\mu$ l of FACS buffer and Flow Cytometry was undertaken on a Cyan ADP (Beckman Coulter, US).

## **2.7 *In vitro* splenocyte reaction**

Due to difficulties found when using a naive lymphocyte reaction I developed a splenocyte reaction in order to allow for MSC to use intermediary cells in order to exert their effects. By utilising immune cells extracted from the spleens of transgenic OT-1 mice [234] I was able to use OVA peptide to stimulate T cell proliferation.

### **2.7.1 Isolation of bulk splenocytes**

Spleens were removed from male OT-1 transgenic mice aged 8-10 weeks. On average one spleen would yield  $7-9 \times 10^7$  splenocytes, requiring 1-2 OT-1 mice per experiment. Spleens were placed in C10 medium at 4°C. Spleens were pushed through a 70  $\mu$ m with a syringe plunger into a 6 well plate containing 1 ml of red cell lysis buffer (Sigma-Aldrich, UK). The resulting mixture was pipetted up and down in order to encourage mixing and then transferred to a 15 ml Falcon<sup>TM</sup> conical tube and filled up to 15 ml with C10 media, inverting gently to encourage mixing. The cell suspension was centrifuged at 1400 rpm in a refrigerated centrifuge at 4°C for 7 minutes. The resulting cell pellet was resuspended in 5 ml of C10 media. The resulting cell suspension was filter through a 50  $\mu$ m filter and

cells counted using a haemocytometer. An aliquot of 2-3 million cells were removed to be used as unstained and single colour controls. The cell suspension was centrifuged at 1400 rpm for 7 minutes at 4°C. The resulting cell pellet was resuspended in PBS at a concentration of  $1 \times 10^6$  cells per ml. Staining for proliferation analysis was undertaken using a CellTrace™ Violet Proliferation Kit (Molecular Probes, US). CellTrace™ Violet was reconstituted as per the kit instructions and in Dimethylsulfoxide (DMSO) and added to the sample at a concentration of 1  $\mu$ M per ml. The cell suspension was covered in foil and incubated in the dark at 37°C on a rocking incubator with an oscillatory frequency of 50 rpm for 30 minutes. Following incubation 5x the staining volume of C10 media was added to the suspension and a further 5 minutes of incubation undertaken. The suspension was then centrifuged at 1400 rpm at 4°C for 7 minutes. The resultant cell pellet was resuspended in C10 media.

### **2.7.2 Stimulation of CD8<sup>+</sup> lymphocytes with OVA<sub>257-264</sub> peptide**

Bulk splenocytes were cultured in 96 well round bottomed plates (Starstedt, DE). Either  $1 \times 10^5$  or  $2 \times 10^5$  bulk splenocytes were cultured in a total working volume of 200  $\mu$ l per well. In order to stimulate cell proliferation OVA<sub>257-264</sub> peptide (AnaSpec, US) was added. Different doses were tested based on the broad ranges found in the literature [235]. Low and high doses of OVA<sub>257-264</sub> peptide were used (2  $\mu$ g/ml and 10  $\mu$ g/ml) and supplemental Il-2 was added at a concentration of 50 units/ml. Cells were cultured in a humidified incubator at 37°C in 5% carbon dioxide. After 24 hours in culture variable numbers of P $\alpha$ S MSC were added to the stimulated lymphocytes and then cultured for a further 72 hours. Cells were then stained and analysed by flow cytometry.

### **2.7.3 Flow cytometric analysis**

After 96 hours in culture cells were stained for surface antigens and analysed by flow cytometry. Wells were pooled to enable more accurate analysis so that 3 wells represent

one data point. Wells were pipetted up and down to free the non-adherent lymphocytes leaving P $\alpha$ S MSC attached to the plate and then placed into FACS tubes. Cells were washed in PBS and centrifuged at 1400 rpm in a refrigerated centrifuge at 4°C for 7 minutes. The resultant cell pellet was resuspended in 500  $\mu$ l of PBS and viability staining was undertaken using a live/dead marker. Cells were incubated at 4°C for 30 mins in the dark. The reaction was quenched with the addition of 2 ml of FACS buffer per tube and then two washing steps performed with FACS buffer. Cells were centrifuged at 2000 rpm at 4°C for 5 minutes. Following washing the resultant cell pellet was resuspended in 100  $\mu$ l of FACS buffer and surface staining undertaken. Antibodies were added and tubes were incubated at 4°C for 30 minutes in the dark. The reaction was quenched with the addition of 2 ml of FACS buffer per tube and then a washing step performed with FACS buffer. Cells were centrifuged at 2000 rpm at 4°C for 5 minutes. Following washing the resultant cell pellet was resuspended in 400  $\mu$ l of FACS buffer and samples were filtered through a 50  $\mu$ m filter and analysed using a Cyan ADP flow cytometer. Compensation beads (BD Biosciences, US) were run at the same time as the samples and compensation and analysis was performed offline using FlowJo version X.0.7 (TreeStar, US). A complete list of antibodies and dilutions is provided in table 2.4.

## 2.8 MDR2<sup>-/-</sup> knockout model of liver injury

The MDR2<sup>-/-</sup> Mouse model is a model characterised by Fickert et al [96] to demonstrate sclerosing cholangitis. With targeted disruption of the multi-drug resistance gene 2 (Abcb4), an absence of biliary phospholipids is seen leading to the leaking of bile acids and cytotoxic injury to the biliary tree. The MDR2<sup>-/-</sup> mouse colony was maintained as homozygotes on an FVB background. Genotyping to confirm breeding pair genotypes was carried out by TransnetYX<sup>®</sup> as previously described. All animals were cared for in the  using standard care protocols as previously described.

### **2.8.1 Treatment of MDR2<sup>-/-</sup> mice with P $\alpha$ S MSC**

Male MDR2<sup>-/-</sup> mice aged 6-8 weeks old were injected with either PBS or P $\alpha$ S MSC at passage 4. To prepare P $\alpha$ S MSC flasks were washed with sterile PBS and then incubated with enough TrypLE Express (Gibco<sup>®</sup>, UK) to cover the bottom of the flask until cells were no longer adherent (approximately 5 minutes). The reaction was quenched with the same volume of  $\alpha$ -MEM and then cells transferred to a Falcon<sup>™</sup> tube and centrifuged at 2000 rpm for 5 minutes. The resultant cell pellet was resuspended in PBS and following counting and dilution aliquoted into Eppendorf's and kept on ice. Either 1x10<sup>5</sup> or 2x10<sup>5</sup> P $\alpha$ S MSC were used and diluted into a volume of 100  $\mu$ l for intravenous injection and 200  $\mu$ l of subcutaneous injection. Prior to injection P $\alpha$ S MSC were pipetted up and down in order to reduce clumping of cells. A 29 gauge insulin needle (Terumo, US) was used for IV injections and a 25 gauge needle (Terumo, US) was used for Subcutaneous (SC) injections. Animals had free access to food and water and were monitored for 2 weeks for any signs of distress. On day 14 all animals were sacrificed and analysed as described below.

## **2.9 Murine model of hepatic ischaemia reperfusion injury**

In order to model the initial warm ischaemic injury seen in DCD liver transplantation I developed a surgical model of hepatic ischaemia reperfusion injury based on previously published literature and experience in our facility with this type of mouse model.

### **2.9.1 Surgical technique**

The surgical model used male C57BL/6 mice aged between 8 and 10 weeks. Mice were weighed and given a single dose of buprenorphine (Temgesic) 1 hour prior to surgery in order to provide post operative analgesia. Timing of analgesia was important as adequate analgesia needed to be onboard due to the extent of the surgery to ensure a

quick recovery after surgery, however giving analgesia too close to induction of analgesia led to unpredictable anaesthesia and a risk of intraoperative apnoea. Mice were then placed into a warmer at 37°C as pre-operative temperature optimisation led to more stable intraoperative temperature. Mice were anaesthetised with isoflurane anaesthesia with pure oxygen as a carrier gas. An initial concentration of 5% was used for induction and maintenance achieved with a concentration between 0.5% and 1.5% titrated to loss of pedal reflex. After shaving and sanitising with chlorhexidine a 1.5-2cm incision was made inferior to the epigastrium. Following insertion of a retractor the bowel was deflected distally with the use of wet cotton wool buds. A 1-2 mm atraumatic micro-arterial clamp (Harvard Apparatus, US) capable of an occlusion pressure of 15-29g was applied to the portal vein and hepatic artery proximal to the inferior lobes allowing for the occlusion of 70% of the hepatic blood flow. Occlusion was confirmed by observing lobar colour change. A moist piece of gauze was placed over the abdominal incision to reduce fluid loss and an infra red heating lamp used to maintain core temperature at 36.5-37°C. A rectal thermometer was used for continuous core temperature monitoring. Five minutes prior to clamp removal 500 µl of warm 0.9% saline was administered into the peritoneal cavity. After 30-60 minutes of warm ischaemia the clamp was removed and a two layer closure performed with surgical sutures for the deep layer and staples for the superficial layer. Mice were recovered and given free access to food and water. Following surgery mice were individually housed in a warmed recovery area at 25°C. Mice were given a second dose of buprenorphine at 4 hours following surgery or sooner if required. No further doses of analgesia were required after this. Reperfusion was allowed for up to 24 hours and mice culled as described below. Regular monitoring for signs of distress was undertaken.

## 2.10 Collection of murine blood and tissue

At the appropriate predetermined time point for the completion of the experiment animals underwent general anaesthesia with isoflurane. Induction of anaesthesia was undertaken

with 4% isoflurane using pure oxygen as a carrier gas. Maintenance of anaesthesia was carried out with 2% isoflurane with oxygen. Confirmation of anaesthesia was carried out by pedal reflex testing. Cardiac puncture was undertaken with a 25 gauge needle under terminal anaesthesia. Blood samples were placed in a 1.5 ml Eppendorf and left to stand at room temperature for 2 hours to allow clot formation. Samples were then spun twice at 15,000 rpm in a micro-centrifuge for 10 minutes. Serum was taken and sent for analysis at the Birmingham Women's Hospital Laboratory. Excess serum was stored at -80°C.

## **2.11 Analysis of serum liver enzymes**

Mouse serum was extracted and analysis for Alanine Transaminase (ALT), Alkaline Phosphatase (ALP) and bile acids carried out. Analysis was performed by the biochemistry department at the Birmingham Women's Hospital Laboratory. Analysis was performed using a clinical grade automated analyser.

## **2.12 Western blotting**

Western blotting was carried out to quantify levels of Cytokeratin 19 (CK19), a marker of biliary injury/proliferation. Protein lysates were made as described below and diluted and then western blotting carried out as described below.

### **2.12.1 Liver tissue lysis**

At the end of the 2 week MDR2<sup>-/-</sup> experiment small pieces of the caudate and right lateral lobes were flash frozen in liquid nitrogen for later use. A small piece of frozen liver was weighed and trimmed to a target weight of 70-90mg and then placed into a gentleMACS M-tubes (Miltenyi Biotec, DE). A lysis buffer containing CelLytic™ MT lysis reagent (Sigma-Aldrich, UK), 1% v/v phosphatase inhibitor cocktail 3 (Sigma-Aldrich, UK), 1% v/v protease inhibitor cocktail (Sigma-Aldrich, UK) and 5U/ml DNase 1 (Sigma-Aldrich,

UK) was added in the amount of 20 µl per mg of liver tissue. The samples were kept on ice at all times. Following addition of the lysis buffer the tissue was homogenised on a gentleMACS (Miltenyi Biotec, DE) using the programme Protein.01. Tubes were then spun on a centrifuge at 1000g for 2 minutes. Following centrifugation tissue samples were placed into eppendorfs and left on a vibrating platform, on ice for 1 hour. Eppendorfs were then spun in a micro-centrifuge at 15000 rpm for 10 minutes. The supernatant was then transferred into a clean eppendorf and protein concentration determined using the biuret assay.

### **2.12.2 Determination of protein concentration using the biuret assay**

A working solution was prepared combining 50 parts Bicinchoninic Acid (BCA) solution (Sigma-Aldrich, UK) to 1 part Copper (II) Sulphate pentahydrate 4% (Sigma-Aldrich, UK). 200 µl of working solution was added to 25 µl of protein solution and then placed in the corresponding well on a 96 well flat bottomed plate. A protein standard of known concentration (Sigma-Aldrich, UK) was used for comparison. The plate was placed briefly on a plate shaker for 5 minutes and then incubated at 37°C for 30 minutes. The plate was immediately read on a plate reader (Synergy HT; BioTek, UK) at 562nm. The protein concentration curve was calculated and the protein concentration determined for each of the samples. Samples were then diluted with CellLytic™ MT buffer to a working concentration of 1 µg per µl.

### **2.12.3 Western blotting for CK19**

Gel tanks for western blotting (Bio-Rad, UK) were assembled as per manufactures instructions. A 1.5mm 12% resolving gel was formed using a mixture of 30% Degassed Acrylamide (ProtoGel; National Diagnostics, US), Resolving gel buffer (National Diagnostics, US), 10% w/v Sodium Dodecyl Sulphate (SDS) (Sigma-Aldrich, UK), and double deionised water.



The gel was set by the addition of a 10% Ammonium Persulphate (APS) (Sigma-Aldrich, UK) and N,N,N',N'-Tetramethylethylenediamine (TEMED) (Sigma-Aldrich, UK). Once set a 4% stacking gel (National Diagnostics, US) was added on top using a stacking buffer (National Diagnostics, US) and made in the same way as the resolving buffer with 30% Degassed Acrylamide, 10% w/v APS, and double deionised water. The gel was again set with TEMED and APS with the addition of a comb in order to form suitable wells. Once set the comb was removed and the gel transferred to a gel electrophoresis tank (Bio-Rad, UK) and assembled as per the manufacturer's instructions. A running buffer (National Diagnostics, US) was added to the tank fill line. 20 µl of protein sample was added to 5 µl of loading buffer (Promega, UK) and incubated at 100°C for 2 minutes. Samples were then loaded into individual wells in the gel and a molecular weight marker (Amersham™ ECL™ Rainbow™ Marker; Sigma-Aldrich, UK) used as a reference. Samples were run at 200 volts for 30 minutes. The gel was then removed and carefully placed onto a nitrocellulose membrane and assembled between filter paper and scotch pads into the transfer apparatus. The transfer apparatus was placed into a clean tank with transfer buffer (National Diagnostics, US) and an ice block with a magnetic stirrer and run at 100 volts for 1 hour. Following this transfer was confirmed by the addition of Ponceau red solution (Sigma-Aldrich, UK) to the membrane.

Blocking of non-specific binding was achieved by incubating the membrane in 20ml of a 5% milk solution (Premiere International Foods, UK) diluted in PBS containing 0.02% TWEEN 20 (Sigma-Aldrich, UK) for 1 hour at room temperature. Primary antibody for CK-19 (Cell Signalling Technologies, US) was added to 10 ml of Milk/PBS/TWEEN solution and incubated overnight at 4°C. Three 5 minute washing steps were then performed using PBS with 0.02% TWEEN 20. A secondary Horseradish Peroxidase conjugated antibody (Cell Signalling Technologies, US) was then added at varying concentrations to 10ml of the Milk/PBS/TWEEN solution and incubated at room temperature for 1 hour. Following this two 5 minute and one 30 minute wash steps were performed. The membrane was then developed using Pierce ECL 2 developer solution (Thermo Fisher

Scientific, US) as per the manufacturer instructions. Immediately following development the membrane was imaged using X-Ray imaging and then scanned as an image file for further analysis. Analysis was undertaken using Image Studio™ Lite software package (LI-COR Biotechnology, US).

#### **2.12.3.1 Loading controls**

In order to generate protein loading controls membranes were stripped and re-probed. Immediately following X-Ray imaging two 5 minute and one 30 minute wash steps were performed. Following washing membranes were soaked in Restore™ Western Blot Stripping Buffer (Thermo Fisher Scientific, US) for 15 minutes. Stripping buffer was removed and two 5 minute and one 30 minute wash steps were performed. The blotting process described above was repeated beginning with blocking of non-specific binding. Primary antibody against  $\alpha$ -actinin (Cell Signalling Technologies, US) was used and incubation carried out for 1 hour. Secondary antibody use and developing proceeded as previously described.

### **2.13 Liver immune cell isolation**

Routine protocols in our laboratory to isolate murine lymphocytes involved density gradient centrifugation using Lympholyte® (Cedarlane, US) which has demonstrated good results in the OVA-Bil and CCL<sub>4</sub> mouse models of liver injury. Unfortunately when using this technique with MDR2<sup>-/-</sup> mice the number of lymphocytes isolated was very low. This warranted a change of technique and the use of Optiprep™ (Sigma-Aldrich, UK) as well as a reduction in the number of spin steps. Both techniques are described below. First a cell suspension was generated as described prior to either the Lympholyte® or Optiprep™ technique.

Following sacrifice, 10 ml of sterile 0.9% sodium chloride was injected through the portal vein in order to wash out any remaining blood within the liver tissue. The liver was then removed and two thirds of the median lobe was removed and weighed. The liver

segment was then placed into a bijou containing RPMI media and placed on ice. Liver segments were transferred into gentleMACS C-tubes (Miltenyi Biotec, DE) with 3 ml of RPMI and then dissociated using the “Mouse spleen 1.01” programme. Samples were then passed through a 70 µm sieve and collected in a 50 ml conical centrifuge tube.

### **2.13.1 Isolation of liver immune cells using Lympholyte®**

Following collection in a 50 ml centrifuge tube the contents were made up to 50 ml with RPMI and then a slow ‘hepatocyte’ spin was undertaken to remove hepatocytes. Samples were centrifuged at 54g for 5 minutes with the brake set to 3 for a slow stop. The supernatant was collected in a new 50 ml conical centrifuge tube and made up to a volume of 50 ml with RPMI. Samples were then centrifuged at 2000 rpm for 5 minutes and the resultant cell pellet resuspended in 50 ml of RPMI. A further wash was undertaken at the same centrifuge settings in order to remove fatty cells. The resultant cell pellet was resuspended in 7 ml of RPMI and filtered through a 50 µm filter. A fresh 15 ml conical centrifuge tube was placed on a rack in a dark tissue culture cabinet and 5 ml of Lympholyte® was added ensuring the Lympholyte® was at room temperature prior to use. The 7 ml of sample was carefully layered on top of the Lympholyte®. The samples were then centrifuged at 2000 rpm for 30 minutes with a brake of 0. Following centrifugation two thirds of the media at the interphase was removed and placed into a fresh 15 ml conical centrifuge tube. The volume of the sample was made up to 15 ml with RPMI and the sample centrifuged at 2000 rpm for 5 minutes. The resultant cell pellet was resuspended in 500 µl of PBS and placed on ice ready for staining.

### **2.13.2 Isolation of liver immune cells using Optiprep™**

Following collection in a 50 ml centrifuge tube the contents were made up to 30 ml with RPMI. The filtrate was transferred into two 15 ml conical centrifuge tubes and spun in a centrifuge at 2000 rpm for 5 minutes. The supernatant was then discarded and

the resultant pellet resuspended in 10 ml of RPMI. For each sample two 15 ml conical centrifuge tubes were prepared containing 7 ml of Optiprep<sup>TM</sup> at a concentration of 1.09 g/ml at room temperature. A 5 ml layer of cell suspension was then carefully layered on top and the tubes spun at 1000g for 25 minutes with no brake. This allowed the formation of an immune cell layer at the interface. Following centrifugation two thirds of the media at the interphase was removed and placed into a fresh 15 ml conical centrifuge tube. The volume of the sample was made up to 15 ml with RPMI and the sample centrifuged at 2000 rpm for 5 minutes. The resultant cell pellet was resuspended in 500 µl of PBS and placed on ice ready for staining.

### **2.13.3 Isolation of immune cells from whole blood**

Animals underwent general anaesthesia with isoflurane. Induction of anaesthesia was undertaken with 4% isoflurane using pure oxygen as a carrier gas. Maintenance of anaesthesia was carried out with 2% isoflurane with oxygen. Confirmation of anaesthesia was carried out by pedal reflex testing. Cardiac puncture was undertaken with a 25 gauge needle under terminal anaesthesia. Blood samples were placed in a clinical grade collecting tube containing EDTA. Red cell lysis was undertaken by adding 500 µl of red cell lysis buffer (Sigma-Aldrich, UK) to 500 µl of whole blood in a 1.5 ml Eppendorf and left to stand at room temperature for 5 minutes. Samples were then spun at 15,000 rpm in a micro-centrifuge for 10 minutes. This process was repeated and the resultant cell pellet was resuspended in PBS.

### **2.13.4 Viability and surface antibody staining of isolated circulating or liver immune cells for flow cytometry**

Throughout the staining process samples were kept on ice when possible and the procedure carried out in a cell culture cabinet with the light turned off. Live/dead staining was carried out using an intracellular live/dead marker for 30 minutes at 4°C. Following incubation

excess MACS buffer containing FBS/FCS was added at 5x the staining volume and samples centrifuged at 2000 rpm for 5 minutes. The resultant cell pellet was resuspended in 100  $\mu$ l of MACS buffer for cell surface staining. Fluorescent antibodies against multiple cell surface antigens were used including CD3, CD4 and CD8 were used. A complete list of antibodies and dilutions used is included in table 2.4. Isotype control samples were also used by pooling aliquots of all samples in an experiment. Samples were incubated for 30 minutes at 4°C. Following incubation 5x the staining volume of MACS buffer was added and samples centrifuged at 2000 rpm for 5 minutes. The resultant pellet was resuspended in 400  $\mu$ l of MACS buffer and filtered using a 50  $\mu$ m filter prior to flow cytometric analysis on a Cyan ADP analyser. Analysis of flow cytometric data was carried out using FlowJo vX.0.7 software.

### **2.13.5 Intracellular staining for FoxP3**

In a subset of experiments intracellular staining was undertaken to examine regulatory T-Cells. Following cell surface staining fixation and permeabilization was undertaken. Fixation and permeabilization working solution was prepared by adding 1 part of Fixation/Permeabilization Concentrate (ebioscience, UK) to 3 parts of Fixation/Permeabilization Diluent (ebioscience, UK). Samples were prepared in FACS tubes and following centrifugation pellets were resuspended in 100  $\mu$ l of workings solution and incubated in the dark for 30 minutes at 4°C. Following incubation 1 ml of permeabilization buffer, made from diluting Permeabilization Buffer 10X (ebioscience, UK) with deionised water, was added and the samples centrifuged at 2000 rpm for 5 minutes. The resulting pellet was resuspended in 100  $\mu$ l of dilute permeabilization buffer containing intracellular antibodies and incubated for 30 minutes in the dark at 4°C. The reaction was quenched with dilute permeabilization buffer and centrifuged at 2000 rpm for 5 minutes. The resulting cell pellet was resuspended in 400  $\mu$ l of MACS buffer ready for flow cytometric analysis.

## 2.14 MSC surface markers

Following prospective isolation using cell sorting and culture in  $\alpha$ -MEM as previously described P $\alpha$ S MSC were removed from their culture environment by the addition of TrypLE as described for cell passaging. Following quenching of the reaction and centrifugation at 2000 rpm for 5 minutes cells were washed in PBS with a further centrifugation step. Cells were then resuspended in 500  $\mu$ l of PBS and placed on ice ready for staining.

Throughout the staining process samples were kept on ice when possible and the procedure carried out in a cell culture cabinet with the light turned off. Live/dead staining was carried out using an intracellular live/dead marker for 30 minutes at 4°C. Following incubation excess MACS buffer containing FBS/FCS was added at 5x the staining volume and samples centrifuged at 2000 rpm for 5 minutes. The resultant cell pellet was resuspended in 100  $\mu$ l of MACS buffer for cell surface staining. Fluorescent antibodies against multiple cell surface antigens were used. A complete list of antibodies and dilutions used is included in table 2.4. Isotype control samples were also used by pooling aliquots of all samples in an experiment. Samples were incubated for 30 minutes at 4°C. Following incubation 5x the staining volume of MACS buffer was added and samples centrifuged at 2000 rpm for 5 minutes. The resultant pellet was resuspended in 400  $\mu$ l of MACS buffer and filtered using a 50  $\mu$ m filter prior to flow cytometric analysis on a Cyan ADP analyser. Analysis of flow cytometric data was carried out using FlowJo vX.0.7 software.

## 2.15 Protein array

Protein profiling was undertaken on cell supernatant using a Proteome Profiler<sup>TM</sup> (R&D Systems, US). P $\alpha$ S MSC cultured to passage 5 and some flasks stimulated with 20 ng/ml of murine IFN- $\gamma$  (PeproTech, UK) and 20 ng/ml murine TNF $\alpha$  (PeproTech, UK). After 24 hours supernatant was collected and centrifuged at 2000 rpm for 5 minutes to remove any debris. Protein profiling was carried out on 1 ml of each sample using a Proteome Profiler<sup>TM</sup> following the manufacturers instructions. Blots were processed using X Ray

imaging and images were scanned and analysed with ImageJ. Pixel density was recorded and background intensity subtracted from negative control spots. Mean pixel density was calculated between replicates.

## 2.16 QDot<sub>605</sub> experiments

In order to examine the bio-distribution of systemically administered P $\alpha$ S MSC I decided to use the novel CryoViz<sup>TM</sup> system. As such intracellular labelling of P $\alpha$ S MSC was required.

### 2.16.1 Labelling P $\alpha$ S MSC with QDot<sub>605</sub>

P $\alpha$ S MSC were cultured as previously described. Cells were removed from flasks by incubation with TrypLE Express and washed. Labelling was carried out using Qtracker<sup>TM</sup> 605 Cell Labelling Kit (Thermo Fisher Scientific, US). Labelling solution was prepared as per the manufacturers instructions. For every 1x10<sup>6</sup> P $\alpha$ S MSC 1.5 ml of labelling solution and 0.2 ml of standard medium were combined. Cells were incubated at 37°C for 60 minutes in a standard culture incubator in the dark. Following incubation cells were washed twice with standard medium at 2000 rpm. Cells were either resuspended in PBS for staining and FACS or injection in to mice or were resuspended in standard medium and placed in flasks for further culture. In a subset of experiments Live/dead staining was performed prior to cell labelling as previously described.

### 2.16.2 Cryoimaging

Cryoimaging was undertaken on whole mice and individual organs. Organs were carefully removed from sacrificed mice and injected *ex vivo* with QDot<sub>605</sub> labelled P $\alpha$ S MSC. Organs were then placed in foil baths and immersed in optimal cutting temperature compound (OCT; Sakura FineTek, US). Organs were then frozen on dry ice and stored at -80°C prior

to shipping to BioInVision (BioInVision, US) for analysis. MDR2<sup>-/-</sup> mice were injected with QDot<sub>605</sub> labelled PαS MSC and culled at different time points using a CO<sub>2</sub> chamber. Following confirmation of death whole mice were placed in foil baths and completely submerged in OCT. Mice were then frozen on dry ice and stored at -80°C prior to shipping to BioInVision. Samples were sectioned and imaged on the CryoViz<sup>TM</sup> instrument and quantification and image generation undertaken by the technical staff at BioInVision.

## **2.17 Immunohistochemistry**

Following confirmation of death the whole liver was divided and dissected. The distal one third of the median lobe was placed in formalin solution for fixation and half of the left lateral lobe snap frozen with liquid nitrogen.

### **2.17.1 Processing of paraffin samples**

Formalin fixed samples were embedded in paraffin in accordance with local protocols. Tissue blocks were then sectioned into 5 µm sections and fixed onto glass microscope slides (X-tra adhesive; Leica, UK). De-waxing and rehydration for staining was achieved by passing through three sequential Xylene (PFM medical, UK) baths for 2 minutes each, followed by two Industrial Methylated Spirits (IMS) (PFM medical, UK) baths for 2 minutes each and finally one water bath for 2 minutes. Dehydration of slides following staining was achieved by reversing the rehydration steps described earlier. Mounting of cover slips was carried out using DPX (Leica, UK) and left to dry before imaging by conventional light microscopy.

### **2.17.2 Processing of frozen samples**

Snap frozen tissue was embedded in Optimal Cutting Temperature (OCT). Frozen blocks were cut into 7 µm sections and mounted on coated glass slides (Thermo Fisher Scientific,



US). Following mounting sections were fixed by submersion in acetone for 10 minutes. Excess acetone was then removed by washing in Tris Buffered Saline (TBS) containing 0.05% TWEEN<sup>®</sup> 20 for two 5 minute washes. Slides were kept wrapped in foil at -20°C until required.

### **2.17.3 Haematoxylin and eosin staining**

Haematoxylin and Eosin (H & E) staining of paraffin sections was carried out on all samples using local staining protocols. De-waxing and rehydration was carried out first as previously described and immediately following on slides were moved sequentially through baths of reagents as follows: Harris Haematoxylin (Leica, UK) for 4 minutes; water for 2 minutes; Acid Alcohol (Leica, UK) for 30 seconds; water for 2 minutes; Scott's Tap Water Substitute (Leica, UK) for 30 seconds; Eosin (Leica, UK) for 1 minute; and 2 water baths for 2 minutes each. Dehydration and mounting was undertaken as previously described.

### **2.17.4 Periodic acid-Schiff staining**

De-waxing and rehydration was carried out first as previously described. Wax rings were drawn around slides and the staining steps carried out in a humidified container. Periodic Acid Solution (Sigma-Aldrich, UK) was added at room temperature and the container covered and placed on a rocker for 5 minutes. Slides were rinsed in a distilled water bath for three 5 minute washes with changes of water between each wash. Slides were then placed back into a humidified container and wax rings redrawn if required. Schiff's Reagent was added and the container covered and placed on a rocker for 15 minutes at room temperature. Slides were rinsed in a tap water bath for three 5 minute washes with changes of water between each wash. Slides were then placed back into a humidified container and wax rings redrawn if required. Counter staining was undertaken with Mayer's Haematoxylin (Leica, UK) for 90 seconds. Slides were rinsed in a tap water bath for two 5 minute washes one with warm water and one with cold water. Dehydration and

mounting was undertaken as previously described.

### **2.17.5 Chromogenic immunohistochemistry**

De-waxing and rehydration was carried out first as previously described. Wax rings were drawn around slides and the staining steps carried out in a humidified container. Blocking of endogenous peroxidases was carried out by adding 200 µl of Peroxidase-Blocking Solution (Dako, DK) to each slide and the humidified container covered and placed on a rocker for 40 minutes. Slides were then washed in a water bath containing TBS with 0.1% TWEEN<sup>®</sup> 20 for three 5 minute washes with changes of wash fluid between each wash. Antigen retrieval was then performed. Antigen unmasking solution (Vector Laboratories, US) was diluted from 10x stock with TBS and a volume of 1 litre added to a plastic bucket. The unmasking solution was then heated in a microwave on full power for 5 minutes. Slides were transferred to a plastic holder and placed in the warm unmasking solution and the bucket loosely covered and heated on full power for 15 minutes. The slides were allowed to passively cool for 10 minutes and then cool water slowly added until the solution reached room temperature. Slides were then washed in a water bath containing TBS with 0.1% TWEEN<sup>®</sup> 20 for three 5 minute washes with changes of wash fluid between each wash. Wax rings were redrawn on the slides if required and the slides transferred into a humidified container. Blocking of non-specific staining was carried out by adding 150 µl of 10x Casein (Vector Laboratories, US) diluted to a 1x solution with TBS. The humidified container was covered and placed on a rocker for 60 minutes. Following blocking 150 µl of the primary antibody was added with out washing. Antibodies were diluted in TBS, a full list of antibodies and dilutions is included in table 2.4. The humidified container was covered and placed on a rocker for 60 minutes. Slides were then washed in a water bath containing TBS with 0.1% TWEEN<sup>®</sup> 20 for three 5 minute washes with changes of wash fluid between each wash. One drop of secondary antibody (Vector Laboratories, US) was added and the humidified container was covered and placed on a rocker for 60 minutes. Slides were then washed in a water bath containing TBS with 0.1% TWEEN<sup>®</sup> 20 for three 5 minute

washes with changes of wash fluid between each wash. 3,3'-Diaminobenzidine (DAB) substrate (AbD Serotec, UK) was prepared following the manufacturers instructions and 150 µl added to each slide. Incubation for up to 2.5 minutes was undertaken observing for a colour change in the slides or the Isotype Matched Control (IMC). Slides were then washed for 5 minutes in tap water. Counter staining was undertaken with filtered Mayer's Haematoxylin which was added to the slides for 30 seconds. Following counter staining slides were washed for 2.5 minutes in cold tap water followed by a further wash for 2.5 minutes in warm tap water. Dehydration and mounting was undertaken as previously described.

### **2.17.6 Structural fluorescence staining**

Frozen slides were thawed on the bench for 15 minutes. Slides were then fixed in acetone for 5 minutes. Wax rings were drawn around the slides and slides were then washed in a water bath containing TBS with 0.1% TWEEN® 20 for three 5 minute washes with changes of wash fluid between each wash. Cytoskeletal staining was undertaken by adding Phalloidin (Thermo Fisher Scientific, US). Slides were place in a humidified container with a lid and covered in foil. The container was then placed on a rocker for 20 minutes. Slides were then washed in a water bath containing TBS with 0.1% TWEEN® 20 for three 5 minute washes with changes of wash fluid between each wash. Slides were then stained with 4',6-diamidino-2-phenylindole (DAPI) (Sigma-Aldrich, UK) at a concentration of 0.5µg/ml in water. Slides were place in a humidified container with a lid and covered in foil. The container was then placed on a rocker for 2 minutes. Slides were then washed in a water bath containing TBS with 0.1% TWEEN® 20 for three 5 minute washes with changes of wash fluid between each wash. Mounting of cover slips was then performed using fluorescence mounting medium (Dako, DK).

### **2.17.7 Slide scanning and analysis**

After mounting slides were left and adequate amount of time to dry. Slides were scanned with a Zeiss Axio Scan Z.1 (Zeiss, DE) onto a PC running Carl Zeiss Microscopy Zen 2 software (Zeiss, DE). Whole slides were scanned using the 20x lens and images stitched by the software. Representative images were taken from whole slide images using Carl Zeiss Microscopy Zen 2 software. Multiple images were taken for analysis and converted to portable network graphic format for analysis using GNU Image Manipulation Project Software (GNU Image Manipulation Project Software, US). Quantification of staining was undertaken using ImageJ Software (NIH, US).

## **2.18 Statistical analysis**

Statistical analysis was carried out using Prism 6.0 (Graphpad Software). Normally distributed data were analysed using an unpaired Student's t-test when comparing two groups. For multiple group comparison one-way analysis of variance (ANOVA) testing was used. A p-value of  $\leq 0.05$  (\* -  $p < 0.05$ , \*\* -  $p < 0.01$ , \*\*\* -  $p < 0.001$ , \*\*\*\* -  $p < 0.0001$ ) was taken as significant. Bonferroni's correction was used when undertaking multiple comparison testing.

## 2.19 Supplier information

All mouse strains, consumables, reagents and antibodies used in this study are described in the following tables.

**Table 2.2 – Table of mouse strains used in this study.**

Type	Background	Supplier	Catalogue Number
C57BL/6	-	Charles River Laboratories, UK	027
FVB	-	Charles River Laboratories, UK	207
BALB/c	-	The Jackson Laboratory, US	000651
OT-1	C57BL/6	The Jackson Laboratory, US	003831
MDR2 <sup>-/-</sup>	FVB	N/A	N/A

**Table 2.3 – Table of software used in this study.**

Name	Version	Supplier	Location
FlowJo	X.0.7	TreeStar	US
Image Studio <sup>TM</sup> Lite	5.2	LI-COR Biotechnology	US
ImageJ	1.51j	NIH.gov	US
Carl Zeiss Zen 2 software	2	Zeiss	DE
GNU Image Manipulation Project	2.8.18	GIMP	US
Summit	4.3	Beckman-Coulter	US
LyX	2.2.2	LyX Team	US

**Table 2.4 – Table of antibodies and dilution factors used in this study.**

Antibody	Fluorophore	Concentration	Use	Supplier	Location	Catalogue number
CD105	FITC	5 µg/ml	FC	eBioscience	UK	12-1051
CD11b	PE	1.25 µg/ml	FC	eBioscience	UK	12-0112
CD11b	FITC	0.025 µg/ml	FC	eBioscience	UK	11-0112
CD11c	PE	0.05 µg/ml	FC	eBioscience	UK	12-0114
CD19	APC	1:100	FC	BD Biosciences	US	561738
CD19	PE	0.0125 µg/ml	FC	eBioscience	UK	12-0193
CD25	PE	1.25 µg/ml	FC	eBioscience	UK	12-0251
CD25	APC	1.25 µg/ml	FC	eBioscience	UK	17-0251
CD29	PE	10 µg/ml	FC	eBioscience	UK	12-0291
CD3	PE	5 µg/ml	FC	eBioscience	UK	12-0031
CD3	APC	2.5 µg/ml	FC	eBioscience	UK	17-0031
CD3	PE-Cy7	10 µg/ml	FC	eBioscience	UK	25-0031
CD3	BV500	5 µl/test	FC	Biolegend	UK	100233
CD34	FITC	10 µg/ml	FC	eBioscience	UK	11-0341
CD3e	V500	4 µg/ml	FC	BD Biosciences	US	560771
CD4	BV450	5 µl/test	FC	Biolegend	UK	100544
CD4	FITC	2.5 µg/ml	FC	eBioscience	UK	11-0042
CD4	PerCP	1:100	FC	BD Biosciences	US	561090
CD4	V450	4 µg/ml	FC	BD Biosciences	US	560468
CD41	APC	0.025 µg/ml	FC	eBioscience	UK	17-0411

CD44	FITC	5 µg/ml	FC	eBioscience	UK	11-0441
CD45	PerCP-Cy5.5	0.0125 µg/ml	FC	eBioscience	UK	45-0451
CD49e	PE	5 µg/ml	FC	eBioscience	UK	12-0493
CD62L	APC	0.6 µg/ml	FC	eBioscience	UK	17-0621
CD69	FITC	5 µg/ml	FC	eBioscience	UK	11-0691
CD69	Pacific Blue	2.5 µg/ml	FC	Invitrogen	UK	HM4028
CD8a	PE-Cy7	5 µg/ml	FC	eBioscience	UK	25-0081
CD8a	APC	1.25 µg/ml	FC	eBioscience	UK	17-0081
CD8a	APC-Cy7	1:100	FC	BD Biosciences	US	561967
CD8a	FITC	0.05 µg/ml	FC	eBioscience	UK	11-0081
CD90	PE	0.3 µg/ml	FC	eBioscience	UK	12-0902
CTV pro- liferation kit	450 nm	1 µm/ml	FC	Molecular Probes	US	C34557
F4/80	FITC	5 µg/ml	FC	eBioscience	UK	11-4801
F4/80	APC	0.2 µg/ml	FC	eBioscience	UK	17-4801
FoxP3	PE	10 µg/ml	FC	eBioscience	UK	12-5773
Gr-1	APC	0.05 µg/ml	FC	eBioscience	UK	17-9668
Live/Dead Marker	eFluor®780	1 µl/ml	FC	eBioscience	UK	65-0865
NK1.1	APC	0.0125 µg/ml	FC	eBioscience	UK	17-5941
Qtracker™ 605	605 nm	N/A	FC	Thermo Fisher	US	Q25001MP
Ly6G	V510	5 µg/ml	FC	Biolegend	UK	127633

Ly6C	V421	5 µg/ml	FC	Biolegend	UK	128032
CD45	PE	1 µl/mouse	FACS	eBioscience	UK	12-0451
PDGFR $\alpha$	APC	1 µl/mouse	FACS	eBioscience	UK	17-1401
Sca-1	FITC	1 µl/mouse	FACS	eBioscience	UK	11-5981
Ter-119	PE	1 µl/mouse	FACS	eBioscience	UK	12-5921
Armenian hamster IgG isotype	PE-Cy7	Variable	FC	eBioscience	UK	25-488
Armenian hamster IgG isotype	FITC	Variable	FC	eBioscience	UK	11-488
Golden syrian hamster IgG isotype	PE	Variable	FC	eBioscience	UK	12-4914
Mouse IgG2a K isotype	APC	Variable	FC	eBioscience	UK	17-4724
Rat IgG K isotype	PerCP-Cy5.5	Variable	FC	eBioscience	UK	45-4031



Rat IgG1 K isotype	APC	Variable	FC	eBioscience	UK	17-4301
Rat IgG2b K isotype	PE	Variable	FC	eBioscience	UK	12-4031
Rat IgG1 isotype	V421	Variable	FC	Biolegend	UK	401911
Rat IgG1 isotype	V510	Variable	FC	Biolegend	UK	400435
Rat IgG2a $\lambda$ isotype	V450	Variable	FC	BD Biosciences	US	560723
Rat IgG2a $\kappa$ isotype	V500	Variable	FC	BD Biosciences	US	560786
F4/80	Purified	1:100	IHC	ABD Serotec	UK	MCA497R
CK19	Purified	1:500	IHC	Origene	US	TA300867
CD45	Purified	1:200	IHC	eBioscience	UK	14-0451
Alexa Fluor™ 633 Phalloidin	633 nm	N/A	IHC	Thermo Fisher	US	A22284
HRP conjugated anti-rabbit Ig	N/A	Pre-diluted	IHC	Vector Labs	US	MP-7401

HRP conjugated anti-rat Ig	N/A	Pre-diluted	IHC	Vector Labs	US	MP-7444
Keratin 17/19	N/A	1:500	WB	CST	US	12434
$\alpha$ -Actinin Antibody	N/A	1:1000	WB	CST	US	3134
Polyclonal Goat Anti- Rabbit IG/HRP	N/A	1:2000	WB	Dako	DK	P0448
CD3e	Purified	0.8 $\mu$ g/ml	Functional	BD Biosciences	US	553057

**Table 2.5 – Table of reagents used in this study.**

Item	Supplier	Country	Catalogue Number
10x Casein Solution	Vector Laboratories	US	SP-5020
4',6-diamidino-2-phenylindole (DAPI)	Sigma-Aldrich	UK	28718-90-3
Absolute ethanol	Sigma-Aldrich	UK	459844
Acid Alcohol	Leica	UK	3803651E
Amersham <sup>TM</sup> ECL <sup>TM</sup> Rainbow <sup>TM</sup>	Sigma-Aldrich	UK	GERPN800E
Ammonium persulfate	Sigma-Aldrich	UK	A3678
Antigen Unmasking Solution, Tris-Based	Vector Laboratories	US	H-3301
Anti-rat/hamster compensation beads	BD Bioscience	US	552845
Bicinchoninic Acid solution	Sigma-Aldrich	UK	B9643-1L
Blue/Orange Loading Dye, 6X	Promega	UK	G1881
CD3/CD28 Dynabeads <sup>®</sup>	Gibco	UK	11452
CD4 <sup>+</sup> CD25 <sup>-</sup> T cell isolation kit	Miltenyi Biotec	DE	130-091- 041
CellLytic <sup>TM</sup> MT	Sigma-Aldrich	UK	C3228
Copper(II) sulfate pentahydrate	Sigma-Aldrich	UK	203165- 10G
DAB substrate	AbD Serotech	UK	BUF022

Dako Fluorescence Mounting Medium	Dako	DK	S3023
DMEM	Gibco	UK	41965-039
DNase I	Sigma-Aldrich	UK	AMPD1
DPX Mounting Medium	Leica	UK	08600E
EDTA	Sigma-Aldrich	UK	E6758
Eosin	Leica	UK	3801602E
FBS	Gibco	UK	10500
Fixation/Permeabilization Concentrate	eBioscience	UK	00-5123-43
Fixation/Permeabilization Diluent	eBioscience	UK	00-5223-56
Harris Haematoxylin	Leica	UK	3801562E
HBSS	Gibco	UK	14170-088
HEPES	Sigma-Aldrich	UK	H0887
Industrial Methylated Spirit	PFM Medical	UK	PRC/R/101
Lympholyte <sup>®</sup> Mouse	Cedarlane	US	CL5035
Marvel Milk Powder	Premier International Foods	UK	N/A
Mayers Haematoxylin Nuclear Stain	Leica	UK	3801582E
Mouse Il-2 Recombinant Protein	eBioscience	UK	16-7022
Murine recombinant IFN- $\gamma$	PeproTech	UK	315-05
Murine recombinant TNF $\alpha$	PeproTech	UK	315-01A

N,N,N',N'- Tetramethylethylenediamine	Sigma-Aldrich	UK	T9281
OptiPrep™ Density Gradient Medium	Sigma-Aldrich	UK	D1556
OVA (257-264) peptide	AnaSpec	US	60193-5
Penicillin/Streptomycin/Glutamine	Gibco	UK	10378-016
Periodic acid	Sigma-Aldrich	UK	210064
Permeabilization Buffer (10X)	ebioscience	UK	00-8333-56
Phosphatase Inhibitor Cocktail 3	Sigma-Aldrich	UK	P0044
Ponceau S solution	Sigma-Aldrich	UK	P7170
Propidium Iodide	Sigma-Aldrich	UK	P4170
Protease Inhibitor Cocktail	Sigma-Aldrich	UK	P8340
Protein Standard	Sigma-Aldrich	UK	P0914
Proteome Profiler™ Mouse XL	R&D Systems	US	ARY028
ProtoGel (30%)	National Diagnostics	US	EC-890
ProtoGel Resolving Buffer (4X)	National Diagnostics	US	EC-892
ProtoGel Stacking Buffer	National Diagnostics	US	EC-893
RBC lysis buffer	Sigma-Aldrich	UK	R7757
REAL Peroxidase-Blocking Solution	Dako	DK	S202386

Restore <sup>TM</sup> Western Blot Stripping Buffer	Thermo Fisher Scientific	US	21059
RNase-Free DNase Set	Qiagen	US	79254
RNase-Free DNase Set (50)	Qiagen	US	69506
RNeasy <sup>®</sup> Mini Kit	Qiagen	US	74104
RPMI	Gibco	UK	31870-025
Schiff Reagent	Sigma-Aldrich	UK	2818-71
Scott's Tap Water Substitute	Leica	UK	3802901E
Sodium dodecyl sulfate	Sigma-Aldrich	UK	436143
ECL 2 Western Blotting Substrate	Thermo Fisher Scientific	US	PI80196
Tissue-Tek <sup>®</sup> O.C.T. Compound	Sakura FineTek	US	4583
Tris-Glycine SDS PAGE Buffer (10X)	National Diagnostics	US	EC-870
Tris-Glycine Electroblothing Buffer (10X)	National Diagnostics	US	EC-880
TrypLE Express	Gibco	UK	12605010
TWEEN 20	Sigma-Aldrich	UK	P2287
Water	Sigma-Aldrich	UK	W3500
Xylene	PFM Medical	UK	PRC/R/201
$\alpha$ -MEM	Gibco	UK	32561-029
$\beta$ -mercaptoethanol	Sigma-Aldrich	UK	M6250

**Table 2.6 – Table of consumables used in this study.**

Item	Supplier	Location	Catalogue Number
70 $\mu$ m cell strainer	Corning	US	352350
1 ml Insulin Syringe & Needle 25g	Terumo	US	01H2516
1 ml Insulin Syringe & Needle 29g	Terumo	US	05M2913
15 ml polypropylene Falcon <sup>TM</sup> tubes	Corning	US	430791
50 ml polypropylene Falcon <sup>TM</sup> tubes	Corning	US	430829
50 $\mu$ m cell strainer	Partec	DE	04-004-2327
6 well plate	Corning	US	3516
96 well flat bottom plate	Corning	US	353072
96 well U-bottom plate	Sarstedt	DE	83.18357.500
FACS tubes	BD Biosciences	US	352002
gentleMACS <sup>TM</sup> C tubes	Miltenyi Biotec	DE	130-096-334
gentleMACS <sup>TM</sup> M tubes	Miltenyi Biotec	DE	130-096-335
LD Columns	Miltenyi Biotec	DE	130-042-901
LS Columns	Miltenyi Biotec	DE	130-042-401
MACS Separators	Miltenyi Biotec	DE	130-042-302
Micro Vascular Clip for 1-2 mm diameter vessels	Harvard Apparatus	US	610196
MS Columns	Miltenyi Biotec	DE	130-042-201

RNeasy Mini Kit	Qiagen	US	74104
Sterile FACS tubes	BD Biosciences	US	352063
T175 Culture flask	Corning	US	353112
T25 Culture flask	Corning	US	430639
T75 Culture flask	Corning	US	430641
X-tra Adhesive Slides	Leica	US	38002032



## CHAPTER 3

# *IN VITRO* PHENOTYPE AND PROPERTIES OF P $\alpha$ S MESENCHYMAL STROMAL CELLS

### 3.1 Introduction and aims

MSCs were first postulated over 100 years ago, however their ability to regulate immune cell function is a more recent discovery. Whilst traditional techniques for isolating MSCs have focussed on exploiting their plastic adherence this leads to a heterogeneous population of cells. In 2005 the ISCT defined minimal criteria for characterising MSC [125, 126], although recently it has been proposed that these be further refined[127]. Developments in isolation techniques to include prospective isolation using cell surface markers have allowed for more defined populations of cells to be isolated. A number of prospective isolation techniques for murine MSC have been described in the literature focussing on different combinations of surface markers, however the uptake of these as techniques for the generation of cells to be studied in *in vivo* experiments still seems low. This is likely due to the complexity of the techniques, requirement for high speed cell sorting and the relatively low yield of cells requiring extensive culture expansion. Originally described by Morikawa [150], MSC isolated using the markers PDGFR $\alpha$  and SCA-1 (P $\alpha$ S MSC) demonstrate all of the properties required by the ISCT including tri-lineage differentiation, self renewal and plastic adherence. Since the description of P $\alpha$ S MSC in the literature there has been little further research done on these cells likely due to the reasons described

above. Whilst descriptions of murine MSC have shown overlap between P $\alpha$ S MSC and other populations such as nestin<sup>+</sup> cells [139], almost no work has been carried out to assess the function of these cells, or their ability to act as immunomodulatory cells in the context of cell therapy. Whilst work has already been undertaken in our institution to isolate [233], characterise [236] and test the efficacy of P $\alpha$ S MSC [237], these cells were mostly isolated from BALB/c mice. When attempting to assess the ability of P $\alpha$ S MSC isolated from C57BL/6 mice to suppress lymphocyte proliferation no suppression could be demonstrated. The propensity of BALB/c mice to adopt a TH2 response to inflammation could mean that P $\alpha$ S MSC isolated from these mice have a different mechanism of immunosuppression and indeed, work in our lab has demonstrated that these cells have a different mechanism of action when compared with human MSC. The benefit of using P $\alpha$ S MSC isolated from C57BL/6 mice may mean a closer analogue of human MSC aiding in subsequent translation from pre-clinical to clinical research. So far robust *in vitro* testing of MSC isolated from C57BL/6 mice has not been undertaken.

The MSC literature has demonstrated that MSC exposed to an inflammatory environment are able to modulate inflammation [238], as well as release chemokines including the Chemokine (C-C motif) Ligand (CCL) CCL2, CCL3 and CCL12 [239]. There are a number of conflicting reports relating to MSC and Il-10 with some studies demonstrating that MSC secrete Il-10 [240, 241], whilst others disagree with this [242, 243]. It has been suggested that MSC can polarise macrophages down a M2 route leading to the secretion of Il-10 by M2 macrophages rather than MSC themselves [244, 128]. No studies so far have demonstrated the secretome of P $\alpha$ S MSC and understanding the response of this type of MSC may aid with an understanding of their immunomodulatory abilities and potential as a cell therapy.

In order to address these needs I set out to prospectively isolate murine P $\alpha$ S MSC by cell sorting and use these cells to study MSC biology and trafficking in the context of post transplant liver injury. In particular I wished to study the use of exogenous P $\alpha$ S MSC as a cell therapy models of liver injury that recreate features found after DCD liver

transplantation. In the first instance I aimed to develop a robust technique to assess the ability of these cells to suppress lymphocyte proliferation *in vitro*.

### 3.1.1 Specific chapter aims

Having described a novel and underutilised population of murine MSC I began this study by assessing the function and phenotype of P $\alpha$ S MSC. The specific aims of this chapter were:

1. To optimise the methodology to prospectively isolate and culture murine P $\alpha$ S MSC
2. To optimise the methodology of an *in vitro* assay for assessing MSC immunosuppressive efficacy
3. To demonstrate the *in vitro* immunosuppressive efficacy of P $\alpha$ S MSC
4. To assess the secretome of P $\alpha$ S MSC following exposure to an inflammatory stimulus

## 3.2 Results

### 3.2.1 Prospective isolation of murine P $\alpha$ S MSC

I first sought to isolate and culture expand murine P $\alpha$ S MSC using a technique previously described by Morikawa [150], and optimised in our laboratory [233, 245]. Long bones were removed from C57BL/6 mice and following crushing were digested with collagenase. Antibody staining for positive (PDGFR $\alpha$  and SCA-1) and negative markers (CD45 and Ter119) was carried out and the cells were sorted by flow cytometry with the exclusion of dead cells. The gating strategy, represented in figure 3.1, started by excluding all dead cells, resulting in a viability of 60-80% of the total number of events. The haematopoietic fraction was then removed by selecting cells negative for PE which was used to highlight CD45 and Ter119, approximately 0.7-1% of the live cells. Finally the cells positive for FITC and APC (SCA-1 and PDGFR $\alpha$ ) were selected by cell sorting and represented 10-15% of the live non-haematopoietic cells or 0.05% of the total bone marrow cells (data representative of 20 replicates each using ten mice). There was a large amount of variability in this technique in keeping with prior experience with the number of cells sorted ranging from 8-10x10<sup>3</sup> per mouse when using ten mice, with a purity of 95-99% based on flow cytometry data (data representative of 20 replicates each using ten mice).

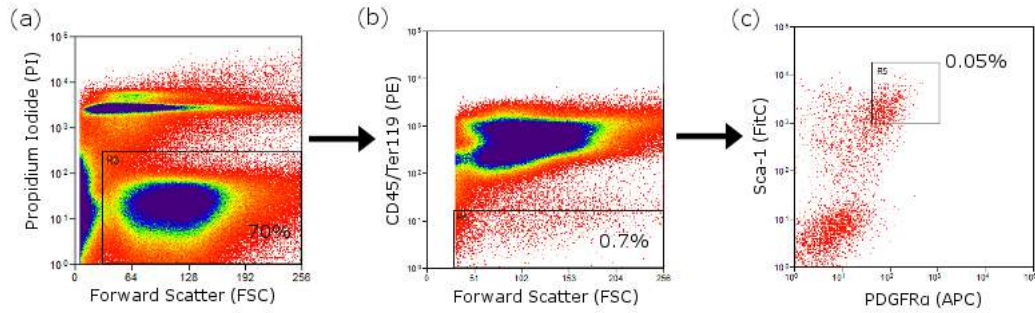


**Figure 3.1 – Representative flow cytometry plots demonstrating the gating strategy for isolating P $\alpha$ S MSC from collagenase digested bone marrow.** (a) Cells were isolated from the long bones of ten C57Bl/6 mice. Gating for live cells was carried out using PI to exclude dead cells resulting in a viability of 60-80%. (b) Next the haematopoietic fraction were excluded with a negative gate against PE stained CD45 and Ter119 cells leaving 0.7-1% of live cells. (c) Finally cells positive for PDGFR $\alpha$  (APC) and SCA-1 (FITC) were selected which represented 0.05% of all cells with a yield of  $8-10 \times 10^3$  cells per mouse when using ten mice, with a purity of 95-99%. Values on the plots represent percentage of total cells in each gate. Data are representative of 20 replicates each using ten mice.

Following isolation cells were incubated in standard media in 6 well coated tissue culture plates at a concentration 50,000 cells per well. Colonies formed as previously described [150]. Colony forming ability and spindle shaped morphology developed early on after isolation however (figure 3.2), by passage 4 colony forming ability was lost.

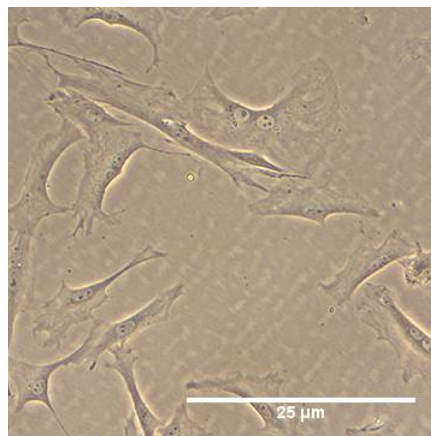


**Figure 3.2 – Representative image of the morphology of murine P $\alpha$ S MSC in culture.** The panel shows a representative image of P $\alpha$ S MSC that were isolated by fluorescent cell sorting and plated into 6 well coated plates at a seeding density of  $5 \times 10^4$  per well and cultured in standard media for 72 hours. Images were captured at 72 hours following a media change at 100x original magnification. The bar indicates 25 $\mu$ m.

I will next demonstrate the phenotype of isolated murine P $\alpha$ S MSC.

### 3.2.2 Surface marker expression of P $\alpha$ S MSC

Previous work in our lab in conjunction with Shankar Suresh has demonstrated that surface marker expression was examined in cultured P $\alpha$ S MSC at passage one by flow cytometry. Surface antigen staining was undertaken by me for positive MSC lineage markers (CD29, CD44, CD49e, CD90, CD105, CD140a and SCA-1) as well as the negative haematopoietic and leucocyte markers (CD34, CD45 and Ter119). P $\alpha$ S MSC showed expression of all of the positive markers tested for and none of the haematopoietic markers (figure 3.3) in keeping with the ISCT description of murine MSC [126, 125].

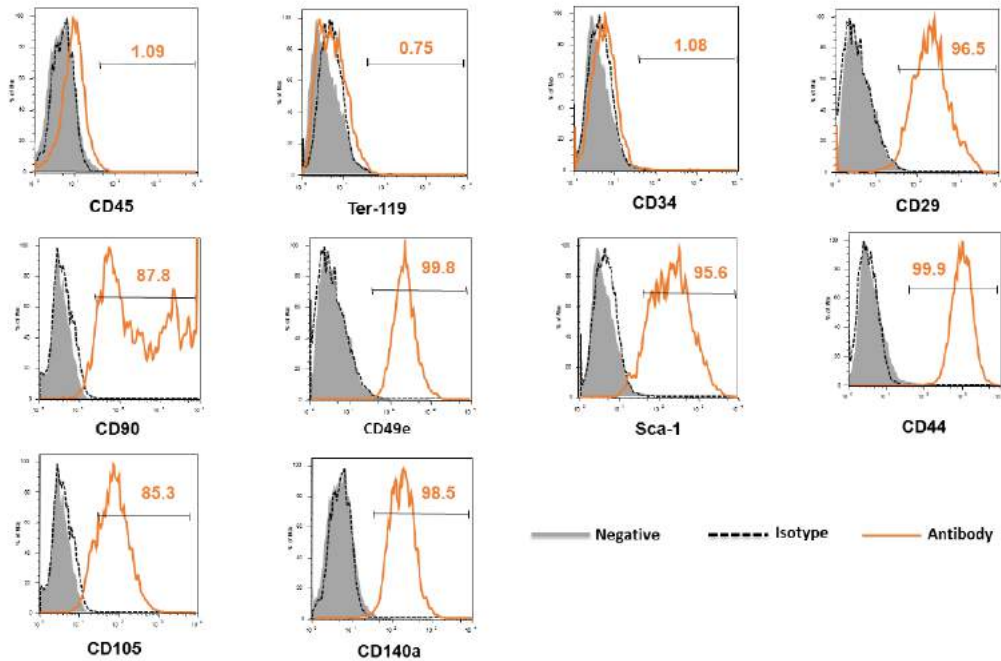


**Figure 3.3 – Cultured P $\alpha$ S MSC express MSC surface antigens when assessed using flow cytometry.** Representative flow cytometry histograms for P1 P $\alpha$ S MSC cultured in standard media. MSC were trypsinised, stained for cell surface markers and analysed by flow cytometry. Representative plots shown demonstrate high positivity for positive MSC markers (CD29, CD44, CD49e, CD90, CD105, CD140a and SCA-1) as well as no expression of the negative markers (CD34, CD45 and Ter119). Plots shown demonstrate positive fluorescence (orange lines), negative fluorescence in unstained controls (grey lines) and isotype matched controls (dotted lines) superimposed for each marker. Percentages indicate the proportion of positive cells and are representative of 3 experiments. Figure taken from Suresh [237].

I next sought to develop an assay for examining the immunomodulatory properties of murine P $\alpha$ S MSC.

### 3.2.3 Developing an *in vitro* immunosuppression assay

MSC have been shown to exert effects on a broad range of immune cells, however one important effect when considering their use as a cell therapy is their ability to suppress T cell proliferation. In their paper in 2002 Nicola et al demonstrated that human MSC can suppress CD4<sup>+</sup> and CD8<sup>+</sup> T cells in an *in vitro* assay and the effect was dose dependent [246]. Work from our lab has demonstrated that murine MSC can suppress T cell proliferation and activation in a splenocyte reaction when isolated from BALB/c mice [237].

#### 3.2.3.1 C57BL/6 MSC do not suppress purified lymphocytes when stimulated

Previous work with P $\alpha$ S MSC isolated from BALB/c mice in our lab has demonstrated their ability to suppress T lymphocytes in a dose dependent manner [237]. To test the ability of purified P $\alpha$ S MSC to suppress T cells P4 MSC isolated from either BALB/c or C57BL/6 mice were added to T cell suppression assays in graded concentrations. MSC were co-cultured with isolated CD4<sup>+</sup>CD25<sup>-</sup> T lymphocytes and CD19<sup>+</sup> B cells. Stimulation of the lymphocytes was undertaken using 0.8  $\mu$ g/ml anti-CD3e antibody. After 72 hours of co-culture cells were stained and analysed by flow cytometry (figure 3.4). Results were normalised to a stimulated lymphocyte culture containing no MSC with the non-suppressed sample being referred to as 100% proliferation. Multiple replicates were undertaken (n=6) and confirmed that in a purified T cell suppression assay MSC isolated from C57BL/6 appear to be unable to suppress proliferation of CD4<sup>+</sup> lymphocytes and indeed there was a significant increase in T lymphocyte numbers (p=0.001). This increase is not in keeping with the majority of the published literature suggesting that either P $\alpha$ S MSC isolated from C57BL/6 are unable to suppress lymphocyte proliferation, or this assay is not the correct model to study P $\alpha$ S MSC *in vitro*. I decided to further develop an *in vitro* model to enable me to assess the ability of P $\alpha$ S MSC isolated from C57BL/6 to suppress lymphocyte proliferation in an attempt to confirm or refute the findings in the

naïve lymphocyte assay.

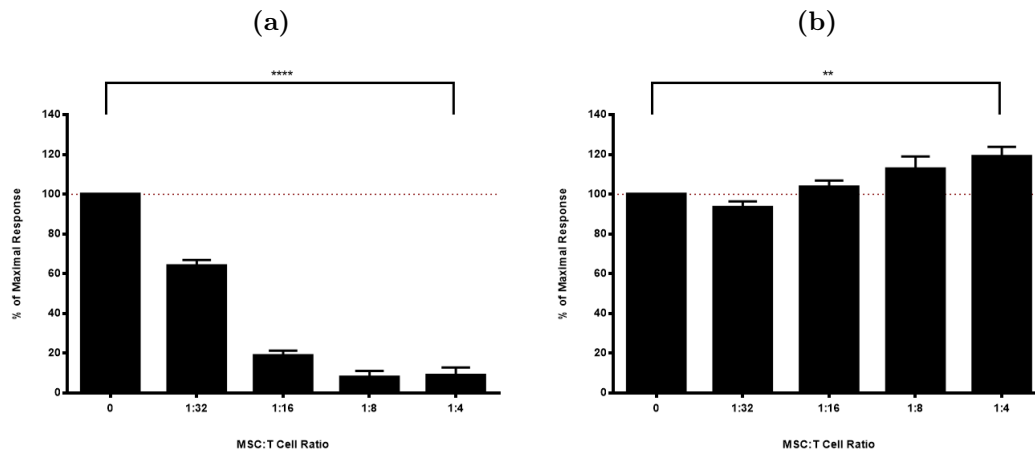


**Figure 3.4 – P $\alpha$ S MSC isolated from C57BL/6 mice do not suppress purified naïve lymphocytes unlike those isolated from BALB/c mice.** (a) MSC isolated from BALB/c mice caused a dose dependent reduction in T lymphocyte proliferation in co-culture experiments ( $p < 0.0001$ ) whereas (b) MSC isolated from C57BL/6 mice showed a significant increase in proliferation ( $P = 0.0011$ ). MSC were isolated from either C57BL/6 ( $n = 6$ ) or BALB/c ( $n = 6$ ) mice. MSC were then co-cultured in increasing concentrations with naïve  $CD4^+CD25^-$  T lymphocytes and  $CD19^+$  B lymphocytes activated with  $0.8 \mu\text{g/ml}$  anti-CD3e (T cell:B cell ratio 2:1). Following 72 hours of culture cells were stained and analysed by flow cytometry. Stimulated controls without MSC were used to calculate the 100% line. Percentage of the maximal calculated response normalised to controls cell counts is represented on the y axis and ratio of MSC to T cells is represented on the x axis. Histograms represent mean and bars represent SEM and the red line represents 100% stimulation. Statistical comparison was carried out using a one way ANOVA.

### 3.2.3.2 Development of a bulk splenocyte reaction to test the efficacy of P $\alpha$ S MSC

Due to the ability of MSC to influence a large number of cell types I investigated the ability of P $\alpha$ S MSC to exert their effect in a bulk splenocyte reaction in order to allow for the use of intermediary cells when responding to inflammatory stimuli. By utilising immune cells extracted from the spleens of transgenic OT-1 mice I was able to use OVA peptide to stimulate T cell proliferation. OT-1 mice are transgenic mice with inserts into the Tcra-V2 and Tcrb-V5 genes which results in a transgenic T cell receptor specifically designed to recognise ovalbumin peptide residues 257-264 (OVA<sub>257-264</sub>) in the context of CD8 co-receptor (H2K<sup>b</sup>) interaction with MHC class I, resulting in an MHC class 1



restricted ovalbumin specific CD8<sup>+</sup> T cell [234].

Lymphocyte stimulation has been achieved with a range of doses of OVA<sub>257-264</sub> peptide in the literature [235] so I decided to test low and high doses (2 µg/ml and 10 µg/ml). Splenocytes were generated by mechanical dissociation of OT-1 spleens and stained with CellTrace™ violet as a proliferation marker. Either 1x10<sup>5</sup> or 2x10<sup>5</sup> cells were seeded onto a 96 well round bottomed plate in C10 media and stimulated with different doses of OVA<sub>257-264</sub> and 50 U/ml of Il-2. After 96 hours in culture cells were stained for surface antigens and analysed by flow cytometry. Wells were pooled to enable more accurate analysis so that 3 wells represent one data point. Stimulation was successful in all groups (figure 3.5a) with a significant increase in CD8<sup>+</sup> lymphocyte number (p<0.0001). A marginally higher number of divided CD8<sup>+</sup> cells was demonstrated when seeding 1x10<sup>5</sup> immune cells however proliferation proved less consistent between replicates so I decided to use 2x10<sup>5</sup> cells for the remaining experiments. Lymphocyte activation was then assessed using CD25 to demonstrate lymphocyte activation. A significantly greater number of activated CD8<sup>+</sup> lymphocytes was demonstrated (figure 3.5b) when CD8<sup>+</sup> cells were stimulated with 2 µg/ml of OVA<sub>257-264</sub> (p<0.0005).

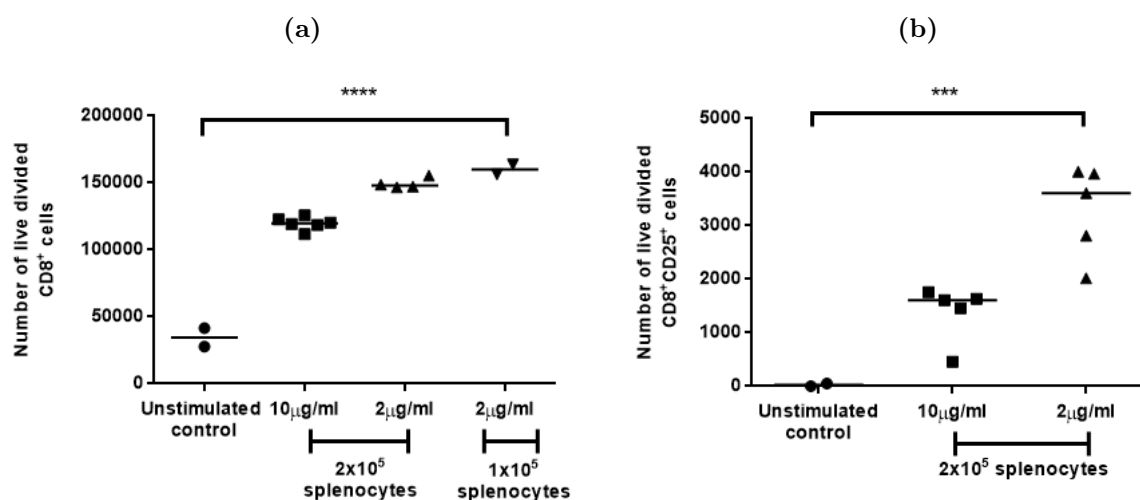


**Figure 3.5 – Optimisation of OVA<sub>257-264</sub> dose and splenocyte number in a bulk splenocyte reaction.** (a) Immune cells were isolated by mechanical dissociation of spleens from OT-1 mice. Either 1x10<sup>5</sup> or 2x10<sup>5</sup> cells were seeded into 96 well plates and either 2 µg/ml or 10 µg/ml of OVA<sub>257-264</sub> was added with 50U/ml of Il-2. At 96 hours analysis by flow cytometry demonstrated a significant increase in live CD8<sup>+</sup> lymphocytes (n=14) with significantly higher numbers of cells when using the lower dose of OVA<sub>257-264</sub> (p<0.0001). A marginally higher number of cells was found when seeding 1x10<sup>5</sup> immune cells however proliferation proved less consistent between replicates. (b) When seeding 2x10<sup>5</sup> cells analysis of activation using CD25 demonstrated a significantly larger number of activated CD8<sup>+</sup> lymphocytes (n=12) when stimulated with 2 µg/ml of OVA<sub>257-264</sub> (p<0.0005). Points on the graphs represent three pooled wells and bars represent the median. Points on the graphs represent three pooled wells and bars represent the median. Statistical analysis was carried out using a one way ANOVA.

CellTrace<sup>TM</sup> violet fluorescence was lower when compared with unstimulated controls that were stimulated with either 2 µg/ml of OVA<sub>257-264</sub> or 10 µg/ml of OVA<sub>257-264</sub> (figure 3.6) in the live CD8<sup>+</sup> population confirming proliferation of lymphocytes in the splenocyte reaction.

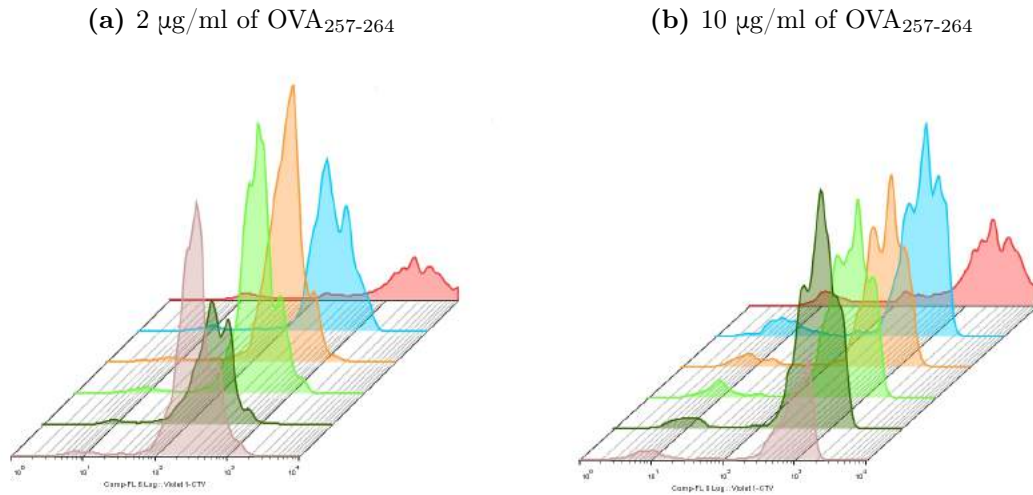


**Figure 3.6 – CellTrace™ violet levels were reduced by similar amounts in CD8<sup>+</sup> cells following stimulation with either 2 µg/ml or 10 µg/ml of OVA<sub>257-264</sub>.** Bulk splenocytes were stained with CellTrace™ violet and stimulated with OVA<sub>257-264</sub> and 50 U/ml of Il-2. After 96 hours staining and then flow cytometry were carried out. After gating for live CD8<sup>+</sup> cells levels of CellTrace™ violet were lower in both the 2 µg/ml (a) group and the 10 µg/ml (b) group confirming cell division of the CD8<sup>+</sup> population. Fluorescence graphs show log<sub>10</sub> fluorescence on the x axis and cell count on the y axis. Each colour represents 3 pooled wells. The red peak represents unstimulated controls and all other colours represent stimulated samples.

The percentage of live divided CD8<sup>+</sup> lymphocytes was significantly higher when stimulated with both 2 µg/ml of OVA<sub>257-264</sub> or 10 µg/ml of OVA<sub>257-264</sub> (figure 3.7) when compared with unstimulated cells. When splenocytes were stimulated with 2 µg/ml of OVA<sub>257-264</sub> the percentage of divided CD8<sup>+</sup> cells as significantly greater than when splenocytes were stimulated with 10 µg/ml of OVA<sub>257-264</sub> (98.4% ± 1.94% vs. 85.68% ± 8.61%, p=0.0039).

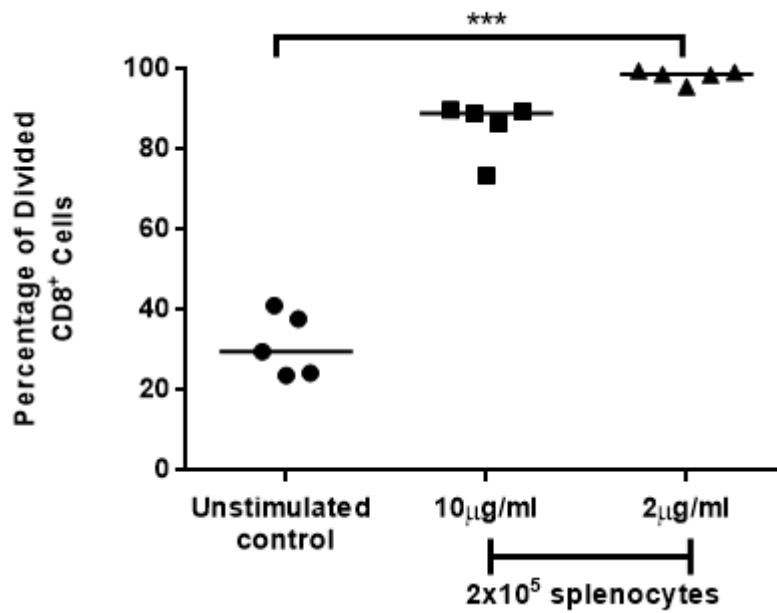


**Figure 3.7 – A significantly greater percentage of CD8 lymphocytes proliferated when stimulated with OVA<sub>257-264</sub>.** Bulk splenocytes cells were isolated by mechanical dissociation of spleens from OT-1 mice.  $2 \times 10^5$  cells were seeded into 96 well plates and either 2 µg/ml or 10 µg/ml of OVA<sub>257-264</sub> was added along with 50U/ml of Il-2. At 96 hours analysis by flow cytometry demonstrated that a significantly greater percentage of CD8<sup>+</sup> lymphocytes proliferated when stimulated with OVA<sub>257-264</sub> with a greater percentage seen in the lower dose group (85.68% ± 8.61% vs. 98.4% ± 1.94%,  $p=0.0039$ ). Points on the graphs represent three pooled wells and bars represent the median. The y axis represents percentage of total CD8<sup>+</sup> cells which have divided. Statistical analysis was carried out using a one way ANOVA.

Having determined a dose of 2 µg/ml of OVA<sub>257-264</sub> and an initial number of  $2 \times 10^5$  splenocytes I next sought to quantify the numbers and activation status of the immune cells at the beginning of the reaction and over the course of 4 days in culture. Following mechanical digestion  $2 \times 10^5$  splenocytes were seeded per well on a 96 well plate and stimulated with 2 µg/ml of OVA<sub>257-264</sub> and 50 U/ml of Il-2. After 1 hour cells were stained and analysed by flow cytometry. The largest cell population was CD19<sup>+</sup> B lymphocytes representing 71.51% ± 5.69% with CD8<sup>+</sup> lymphocytes at 12.56% ± 4.69% and CD4<sup>+</sup> lymphocytes only 4.93% ± 9.32% (figure 3.8). This gives a ratio of almost 6:1 B lymphocytes to CD8<sup>+</sup> T lymphocytes and 15:1 B lymphocytes to CD4<sup>+</sup> lymphocytes, greater than the 2:1 ratio used in purified assays. Natural killer cells (NK1.1) cells represented 4.13% ± 1.01%. Cell activation markers demonstrated cells were not activated at baseline with

CD25<sup>+</sup> representing 0.96%  $\pm$  1.12% of the total CD45<sup>+</sup> cells and CD69<sup>+</sup> representing 1.16%  $\pm$  1.09%. The myeloid population represented a relatively small number of the total cells. CD11b<sup>+</sup>F4/80<sup>+</sup> macrophages were the least prevalent of the myeloid cells at 2.56%  $\pm$  2.04%, with CD11b<sup>+</sup>Gr1<sup>+</sup> monocytes representing 3.33%  $\pm$  2.12% and CD11b<sup>+</sup>Gr1<sup>+</sup> neutrophils the most prevalent myeloid cell type at 5.29%  $\pm$  1.79%.

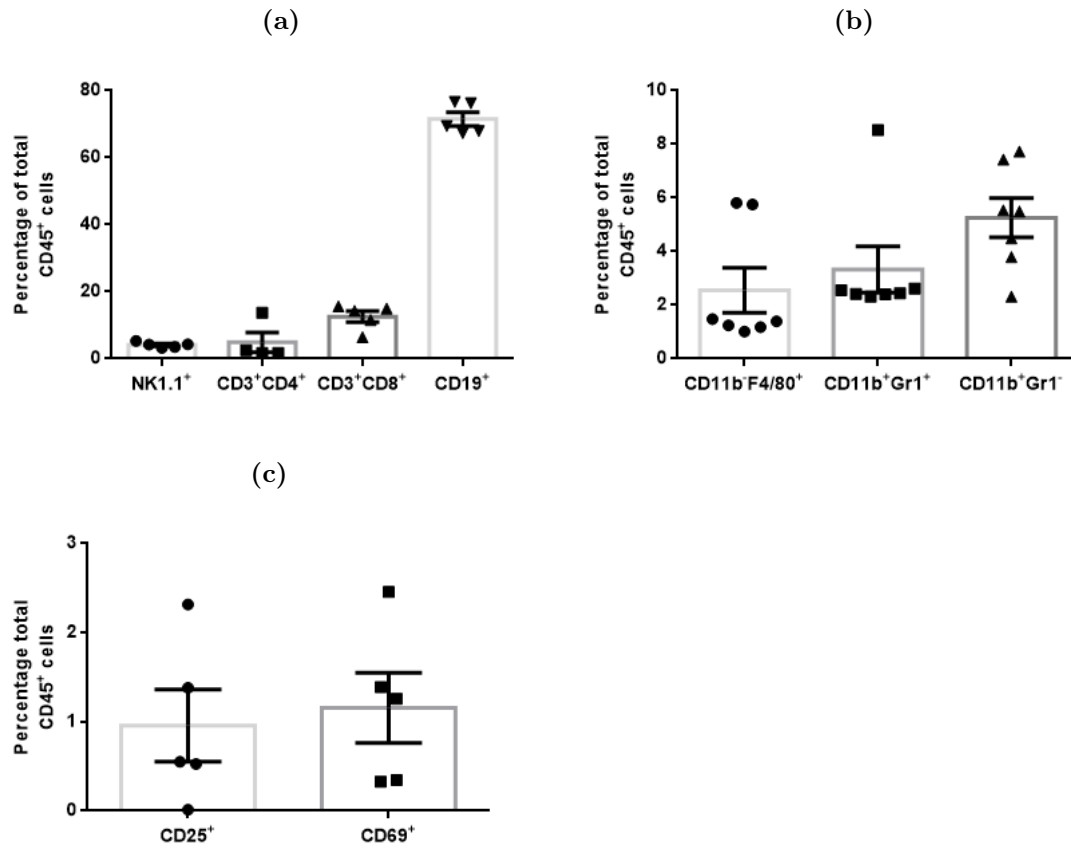


**Figure 3.8 – Quantification of the numbers of immune cells on day 0 of a bulk splenocyte reaction.** (a) Immune cells from the spleen of OT-1 mice were seeded and stimulated with OVA<sub>257-264</sub> and 50U/ml of Il-2. After 1 hour cells were stained and analysed by flow cytometry. CD19<sup>+</sup> B lymphocytes represented the largest population 71.51%  $\pm$  5.69% with CD8<sup>+</sup> lymphocytes at 12.56%  $\pm$  4.69% and CD4<sup>+</sup> lymphocytes only 4.93%  $\pm$  9.32% (n=5). (b) Myeloid cells included CD11b<sup>+</sup>F4/80<sup>+</sup> positive macrophages 2.56%  $\pm$  2.04%, CD11b<sup>+</sup>Gr1<sup>+</sup> monocytes 3.33%  $\pm$  2.12% and CD11b<sup>+</sup>Gr1<sup>+</sup> neutrophils 5.29%  $\pm$  1.79% (n=7). (c) Activation markers were low demonstrating minimal activation at baseline with CD25<sup>+</sup> representing 0.96%  $\pm$  1.12% of the total CD45<sup>+</sup> positive cells and CD69<sup>+</sup> representing 1.16%  $\pm$  1.09%. Histograms represent mean and bars represent SEM. Points represent 3 pooled wells. Percentage of cells was calculated as percentage of total CD45<sup>+</sup> cells.

At 24 hours following stimulation cells were stained and analysed by flow cytometry

(figure 3.9). Divided cells were those whose CellTrace™ violet fluorescence had fallen below the level of unstimulated control. The divided cell population contained a low percentage of CD8<sup>+</sup> cells ( $0.17\% \pm 0.46\%$ ) with low expression of activation markers (CD25<sup>+</sup>  $0.013\% \pm 0.045\%$ , CD69<sup>+</sup>  $0.017\% \pm 0.045\%$ ). Undivided cells contained a higher percentage of CD8<sup>+</sup> cells ( $51\% \pm 93.1\%$ ) and higher levels of activation markers (CD25  $12.55\% \pm 53.76\%$ , CD69  $18.93\% \pm 46.26\%$ ).

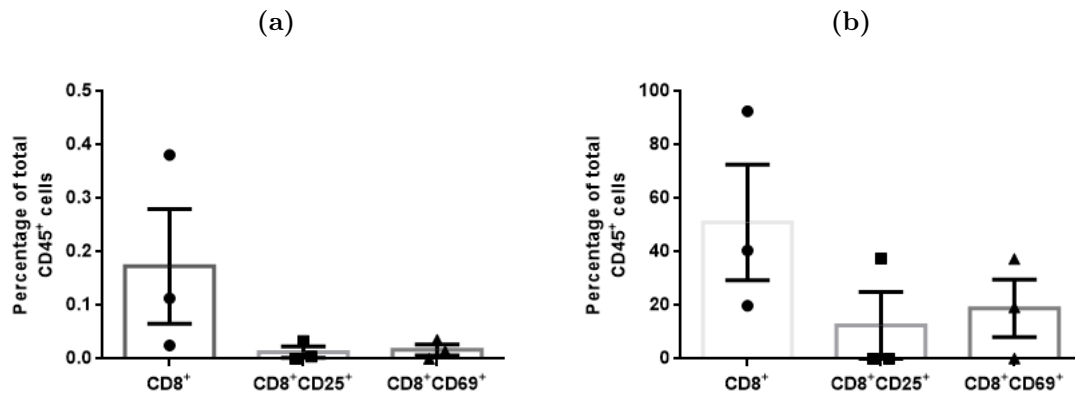


**Figure 3.9 – Quantification of the numbers of immune cells on day 1 of a splenocyte reaction.** Immune cells from the spleen of OT-1 mice were seeded and stimulated with OVA<sub>257-264</sub> and 50U/ml of Il-2. At 24 hours following stimulation cells were stained and analysed by flow cytometry (n=6). Divided cells were those whose CellTrace™ violet had fallen below unstimulated control. The divided cell population (a) contained a low percentage of CD8<sup>+</sup> cells ( $0.17\% \pm 0.46\%$ ) with low expression of activation markers (CD25<sup>+</sup>  $0.013\% \pm 0.045\%$ , CD69<sup>+</sup>  $0.017\% \pm 0.045\%$ ). Undivided cells (b) contained a higher percentage of CD8<sup>+</sup> cells ( $51\% \pm 93.1\%$ ) and higher levels of activation (CD25<sup>+</sup>  $12.55\% \pm 53.76\%$ , CD69<sup>+</sup>  $18.93\% \pm 46.26\%$ ). Histograms represent mean and bars represent SEM. Points represent 3 pooled wells. Percentage of cells was calculated as percentage of total CD45<sup>+</sup> cells.

Further analysis was undertaken at 96 hours following stimulation. Again cells were stained and analysed by flow cytometry (figure 3.10). Divided cells were those whose CellTrace™ violet fluorescence had fallen below the level of unstimulated control. The divided cell population contained a high percentage of CD8<sup>+</sup> cells ( $62.05\% \pm 17.21\%$ ) with high expression of CD25 ( $60.69\% \pm 16.5\%$ ). Undivided cells contained a lower percentage of CD8<sup>+</sup> cells ( $13.43\% \pm 4.6\%$ ) and lower levels of CD25 ( $12.20\% \pm 3.47\%$ ).

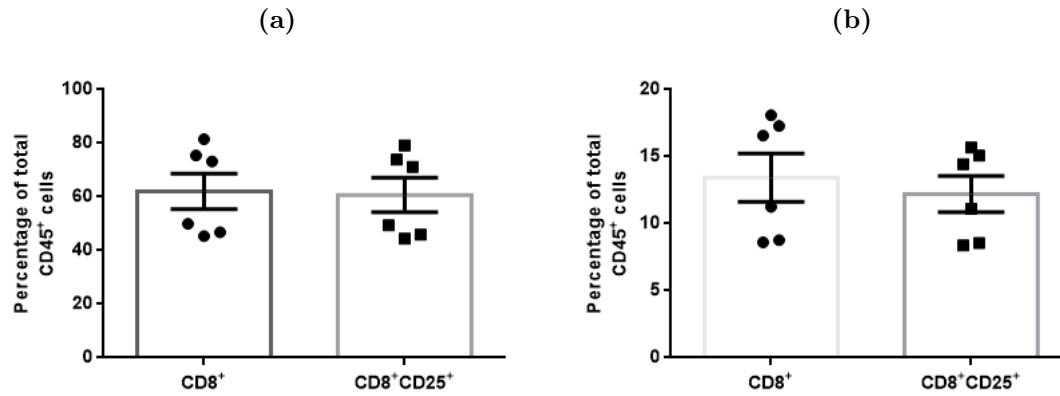


**Figure 3.10 – Quantification of the numbers of immune cells on day 4 of a bulk splenocyte reaction.** Immune cells from the spleen of OT-1 mice were seeded and stimulated with OVA<sub>257-264</sub> and 50 U/ml of Il-2. At 96 hours following stimulation cells were stained and analysed by flow cytometry (n=6). Divided cells were those whose CellTrace<sup>TM</sup> violet had fallen below unstimulated control. (a) The divided cell population contained a high percentage of CD8<sup>+</sup> cells (62.05% ± 17.21%) with high expression of CD25 (60.69% ± 16.5%). (b) Undivided cells contained a lower percentage of CD8<sup>+</sup> cells (13.43% ± 4.6%) and lower levels of CD25 (12.20% ± 3.47%). Histograms represent mean and bars represent SEM. Points represent 3 pooled wells. Percentage of cells was calculated as percentage of total CD45<sup>+</sup> cells.

CellTrace<sup>TM</sup> violet fluorescence at day 4 showed a consistent reduction in all stimulated samples (figure 3.11).

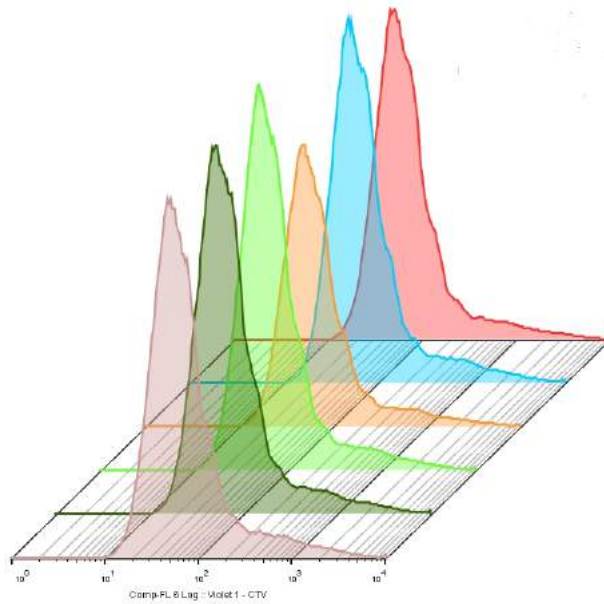


**Figure 3.11 – CellTrace<sup>TM</sup> violet fluorescence was reduced in CD8<sup>+</sup> cells 96 hours after stimulation in the splenocyte reaction.** Cells were stained with CellTrace<sup>TM</sup> violet and stimulated with OVA<sub>257-264</sub> and 50 U/ml of Il-2. After 96 hours staining and then flow cytometry were carried out. After gating for live CD8<sup>+</sup> cells levels of CellTrace<sup>TM</sup> violet were reduced in all samples confirming cell division of the CD8<sup>+</sup> population. Fluorescence graphs show log<sub>10</sub> fluorescence on the x axis and cell count on the y axis. Each colour represents 3 pooled wells, n=6.

### 3.2.3.3 *In vitro* efficacy of PαS MSC in a bulk splenocyte reaction

Having optimised a splenocyte reaction I proceeded to test the ability of PαS MSC to suppress T Cell proliferation in this assay. Immune cells were extraction from the spleens of OT-1 mice, stained with CellTrace<sup>TM</sup> violet and then seeded onto a 96 well plate in C10 media. Cells were stimulated with 2 µg/ml of OVA<sub>257-264</sub> and 50 U/ml of Il-2 and incubated for 24 hours. This was to allow stimulation to occur prior to the addition of PαS MSC. At 24 hours graded numbers of PαS MSC were added and then incubated for a further 72 hours. Immune cells were removed and stained leaving behind the plastic adherent PαS MSC and then analysed by flow cytometry. Proliferation was normalised to stimulated controls with no PαS MSC added. The percentage of live divided CD8<sup>+</sup> lymphocytes was significantly reduced ( $p < 0.0001$ ) in a dose dependent fashion with the greatest number of PαS MSC added leading to the largest reduction in divided CD8<sup>+</sup>



lymphocytes (figure 3.12).

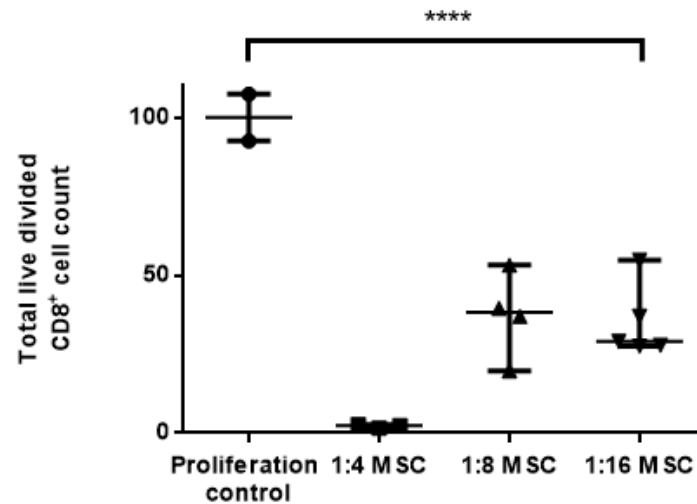


**Figure 3.12 – P $\alpha$ S MSC suppress CD8<sup>+</sup> proliferation in a bulk splenocyte reaction.** Immune cells from the spleen of OT-1 mice were seeded and stimulated with OVA<sub>257-264</sub> and 50 U/ml of Il-2 and after 24 hours graded numbers of P $\alpha$ S MSC were added. After a further 72 hours staining and flow cytometry was undertaken. The percentage of live divided CD8<sup>+</sup> lymphocytes was significantly reduced ( $p < 0.0001$ ) in a dose dependent fashion when normalised to proliferation controls with the greatest number of P $\alpha$ S MSC leading to the largest reduction in divided CD8<sup>+</sup> lymphocytes. Data are shown a median with range,  $n=14$ . Points represent 3 pooled wells. Percentage of cells was calculated as percentage of total stimulated cells from the proliferation controls. Statistical analysis was carried out using a one way ANOVA.

The absolute number of CD8<sup>+</sup> lymphocytes was also significantly reduced (figure 3.13) with the lowest number occurring with the highest number of MSC ( $p < 0.0001$ ). The total number of live divided CD8<sup>+</sup>CD25<sup>+</sup> lymphocytes was significantly reduced ( $p < 0.0001$ ) in a dose dependent fashion when compared to proliferation controls.

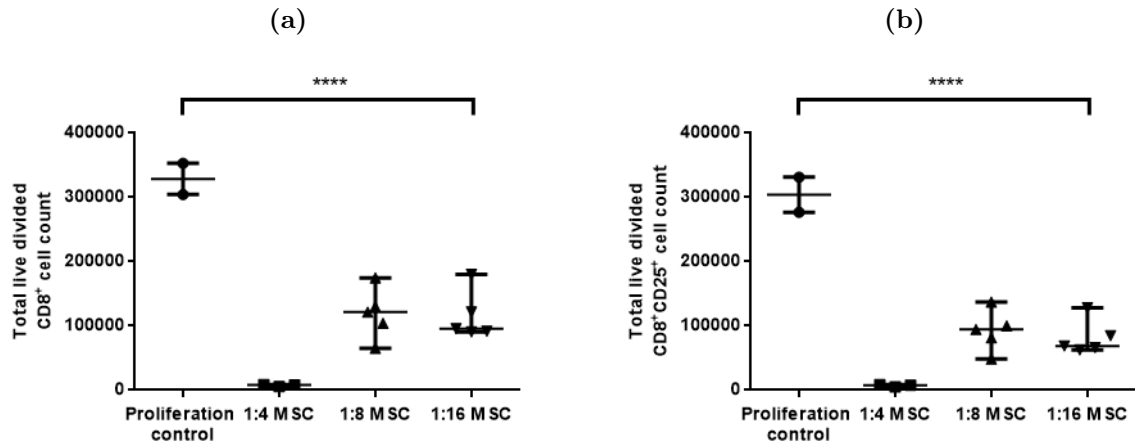


**Figure 3.13 – P $\alpha$ S MSC reduce CD8<sup>+</sup> and CD8<sup>+</sup>CD25<sup>+</sup> numbers in a bulk splenocyte reaction.** Immune cells from the spleen of OT-1 mice were seeded and stimulated with OVA<sub>257-264</sub> and 50 U/ml of Il-2 and after 24 hours graded numbers of P $\alpha$ S MSC were added. After a further 72 hours staining and flow cytometry was undertaken. (a) The total number of live divided CD8<sup>+</sup> lymphocytes was significantly reduced ( $p < 0.0001$ ) in a dose dependent fashion when compared to proliferation controls with the greatest number of MSC leading to the largest reduction in divided CD8<sup>+</sup> lymphocytes. (b) The total number of live divided CD8<sup>+</sup>CD25<sup>+</sup> lymphocytes was also significantly reduced ( $p < 0.0001$ ) in a dose dependent fashion when compared to proliferation controls. Data are shown a median with range,  $n=15$ . Points represent 3 pooled wells. Percentage of cells was calculated as percentage of total stimulated cells from the proliferation controls. Statistical analysis was carried out using a one way ANOVA.

CellTrace<sup>TM</sup> violet fluorescence demonstrates a dose dependent reduction when compared with stimulated control values (figure 3.14) indicating a reduction in proliferation of CD8<sup>+</sup> lymphocytes following the addition of MSC.

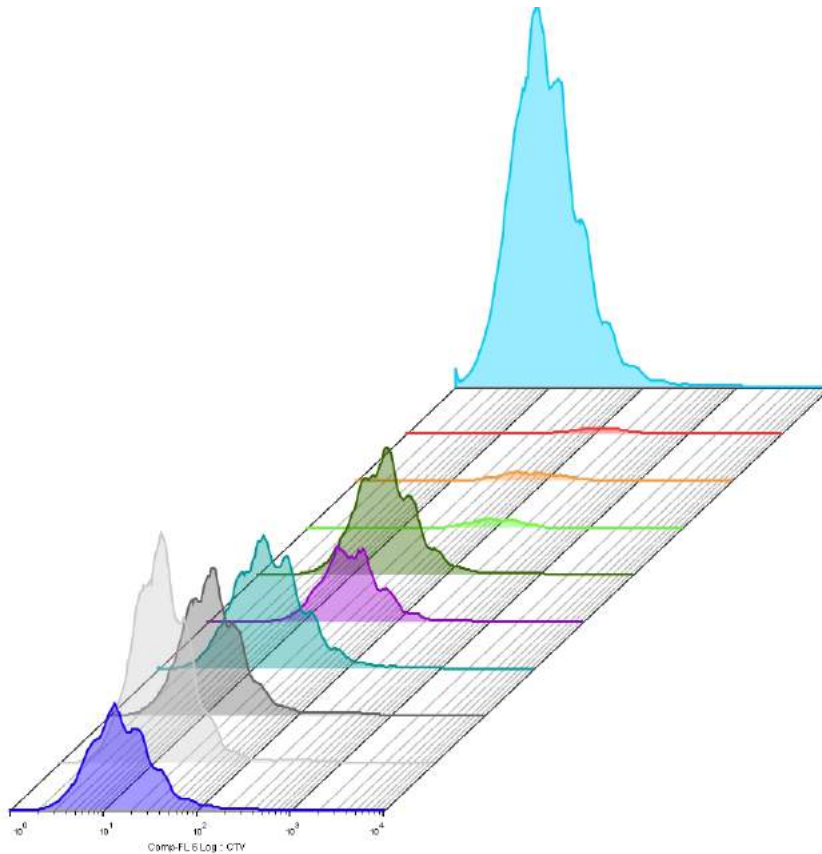


**Figure 3.14 – P $\alpha$ S MSC reduce CellTrace<sup>TM</sup> violet fluorescence in CD8<sup>+</sup> cells in a bulk splenocyte reaction.** Immune cells were stained with CellTrace<sup>TM</sup> violet and stimulated with OVA<sub>257-264</sub> and 50 U/ml of IL-2 and for 24 hours. Graded numbers of P $\alpha$ S MSC were then added and after a further 72 hours staining and flow cytometry was performed. CellTrace<sup>TM</sup> violet fluorescence in CD8<sup>+</sup> cells was reduced in a dose dependent fashion indicating reduction in proliferation when compared with stimulated controls containing no P $\alpha$ S MSC. Fluorescence graphs show log<sub>10</sub> fluorescence on the x axis and cell count on the y axis. Each colour represents 3 pooled wells, n=6. Light blue represents stimulated cells with no P $\alpha$ S MSC added, all other colours indicate stimulated cells with P $\alpha$ S MSC added (top 3 1:4 MSC, middle 3 1:8 MSC and bottom 3 1:16 MSC), n=10).

I next sought to examine the effects of inflammatory stimulus on P $\alpha$ S MSC.

### 3.2.4 The effects of an inflammatory stimulus on P $\alpha$ S MSC

In order to investigate the effects of an inflammatory stimulus on P $\alpha$ S MSC and their secretome I decided to examine medium passage (passage 4) P $\alpha$ S MSC cultured in standard media and stimulated with inflammatory cytokines. I decided to stimulate P $\alpha$ S MSC with TNF $\alpha$  and IFN- $\gamma$  common inflammatory cytokines, as these cytokines are found in the

livers of a number of mouse models of liver injury [247, 98, 248]. Stimulation of MSC has been carried out successfully in other studies [249, 250] and P $\alpha$ S MSC have also been successfully stimulated with these cytokines [237].

#### **3.2.4.1 P $\alpha$ S MSC morphology**

I prospectively isolated P $\alpha$ S MSC as previously described and expanded in culture to passage 4. Stimulation of P $\alpha$ S MSC was undertaken by the addition 20 ng/ml TNF $\alpha$  and IFN- $\gamma$  to the culture media and cells incubated for a further 24 hours. Following incubation supernatant was removed and cells washed, fixed and stained with the cytoskeletal stain Phalloidin and the nuclear stain DAPI. Unstimulated control cells were also stained for comparison.

The unstimulated P $\alpha$ S MSC showed a distinctive spindle shaped morphology. The stimulated P $\alpha$ S MSC showed the same morphological structure with no clear differences between groups (figure 3.2).

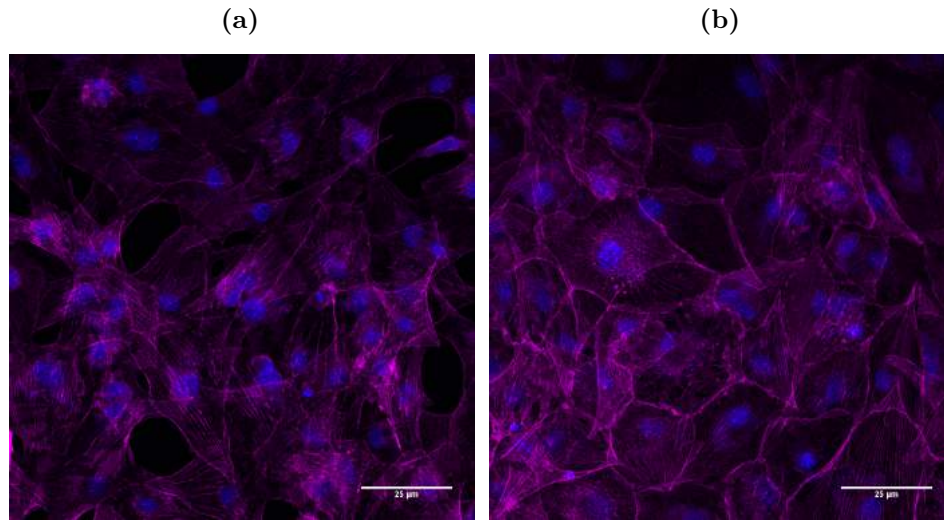


**Figure 3.15 – Representative fluorescent histochemical images of P $\alpha$ S MSC stimulated with TNF $\alpha$  and IFN- $\gamma$ .** P $\alpha$ S MSC were prospectively isolated and expanded in culture to passage 4. Stimulation of P $\alpha$ S MSC was undertaken by the addition 20 ng/ml TNF $\alpha$  and IFN- $\gamma$  added to the culture media and cells incubated for a further 24 hours. Following incubation supernatant was removed and cells washed, fixed and stained with the cytoskeletal stain Phalloidin and the nuclear stain DAPI. Unstimulated control cells were also stained for comparison. (a) The unstimulated P $\alpha$ S MSC showed a distinctive spindle shaped morphology. (b) The stimulated P $\alpha$ S MSC showed the same morphological structure with no clear differences between groups. Images were taken at 400x magnification. Scale bars represent 25  $\mu$ m.

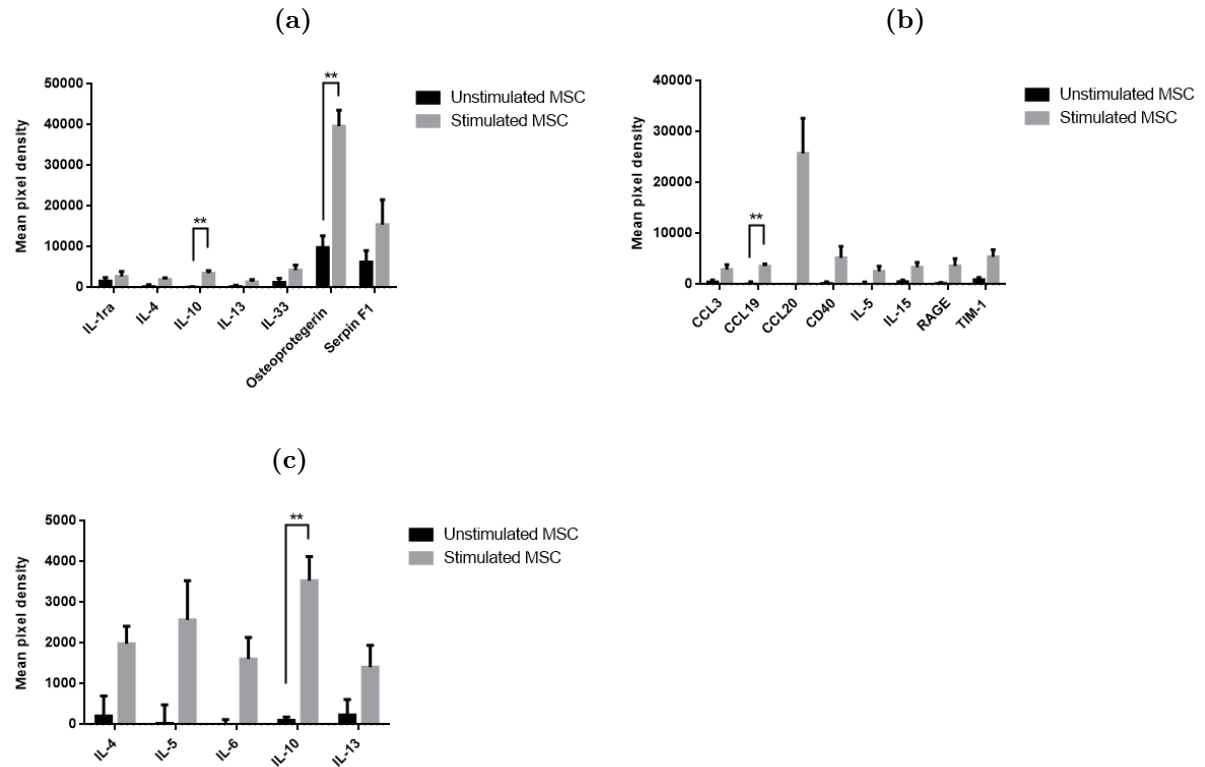
I next sought to assess the cytokines secreted by P $\alpha$ S MSC following stimulation with inflammatory cytokines.

#### 3.2.4.2 Cytokines secreted by P $\alpha$ S MSC

Prospectively isolated P $\alpha$ S MSC were expanded in culture to passage 4. Stimulation of P $\alpha$ S MSC was undertaken by the addition 20 ng/ml TNF $\alpha$  and IFN- $\gamma$  to the culture media and cells incubated for a further 24 hours. Following incubation supernatant was removed and the cytokine profile was assessed using a Proteome Profiler<sup>TM</sup> (R&D Systems, US).

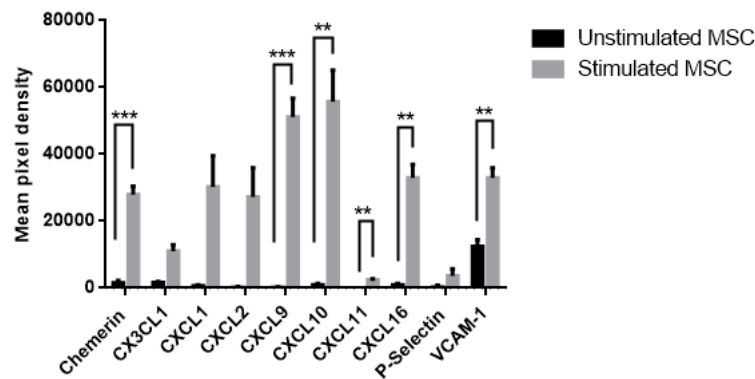
Following stimulation P $\alpha$ S MSC (figure 3.16a) the anti-inflammatory cytokines IL-10 and osteoprotegerin showed a significant increase in their levels ( $p=0.00453$  and  $p=0.00363$ ). The pro-inflammatory cytokine CCL19 also showed a significant increase ( $p=0.00457$ ,

figure 3.16b). When specifically looking at cytokines involved in the Th2 response (figure 3.16c) only Il-10 showed a significant increase ( $p=0.00453$ ).



**Figure 3.16 – Cytokine profile in the secretome of PαS MSC following stimulation with TNFα and IFN-γ.** PαS MSC were prospectively isolated and expanded in culture to passage 4. Stimulation of PαS MSC was undertaken by the addition 20 ng/ml TNFα and IFN-γ to the culture media and cells incubated for a further 24 hours. Following incubation supernatant was removed and the cytokine profile was assessed using a Proteome Profiler™. (a) The anti-inflammatory cytokines Il-10 and osteoprotegerin showed significant increases in their levels ( $p=0.00453$  and  $p=0.00363$ ). (b) The pro-inflammatory cytokine CCL19 also showed a significant increase following stimulation ( $p=0.00457$ ). (c) When specifically looking at cytokines involved in the Th2 response only Il-10 showed a significant increase ( $p=0.00453$ ). Bars represent mean values and lines represent the standard error of the mean. Statistical analysis was undertaken using multiple t-tests with Bonferroni's correction for multiple comparisons.

I also examined the chemokine and adhesion molecule profile using the Proteome Profiler™ (figure 3.17). Chemerin ( $p=0.000533$ ), Chemokine (C-X-C motif) Ligand (CXCL)9 ( $p=0.000780$ ), CXCL10 ( $p=0.00432$ ), CXCL11 ( $p=0.00238$ ), CXCL16 ( $p=0.00132$ ) and VCAM-1 ( $p=0.00497$ ) all showed statistically significant increases following stimulation with TNFα and IFN-γ.



**Figure 3.17 – Chemokine and adhesion molecule profile of P $\alpha$ S MSC following stimulation with TNF $\alpha$  and IFN- $\gamma$ .** P $\alpha$ S MSC were prospectively isolated and expanded in culture to passage 4. Stimulation of P $\alpha$ S MSC was undertaken by the addition 20 ng/ml TNF $\alpha$  and IFN- $\gamma$  to the culture media and cells incubated for a further 24 hours. Following incubation supernatant was removed and the cytokine profile was assessed using a Proteome Profiler<sup>TM</sup>. Chemerin (p=0.000533), CXCL9 (p=0.000780), CXCL10 (p=0.00432), CXCL11 (p=0.00238), CXCL16 (p=0.00132) and VCAM-1 (p=0.00497) all showed statistically significant increases following stimulation with TNF $\alpha$  and IFN- $\gamma$ . Bars represent mean values and lines represent the standard error of the mean. Statistical analysis was undertaken using multiple t-tests with Bonferroni's correction for multiple comparisons.

## 3.3 Discussion

### 3.3.1 Isolation, culture expansion and phenotype of murine P $\alpha$ S MSC

Whilst plastic adherence is a described property of MSC using this as an isolation technique leads to a heterogeneous population of cells and even after a number of passages of culture expansion contaminating cells are still present [251]. Prospective isolation with cell sorting is one way of overcoming this heterogeneity. By utilising a technique originally described by Morikawa [150], and subsequently refined in our lab [233, 245], I was able to isolate purified murine P $\alpha$ S MSC from the bone marrow of C57BL/6 mice using the positive lineage markers SCA-1 and PDGFR $\alpha$  and the negative lineage markers CD45 and Ter119 with a high degree of purity (95-99%). On culture expansion these cells took on a spindle shaped morphology and demonstrated colony forming potential as originally described [150]. The cell yield following isolation was 8-10x10<sup>3</sup> per mouse which was also in keeping with numbers previously described.

By examining surface markers that have been recommended as required for MSC classification by the ISCT [126], I was able to show that murine P $\alpha$ S MSC express all of the positive lineage markers expected of an MSC with a high degree of positivity, with less than 1% expression of the negative haematopoietic lineage markers. These findings, taken alongside other extensive work undertaken in our lab support the published literature in claiming that P $\alpha$ S MSC are MSC as described by the ISCT definition [236, 245, 237].

P $\alpha$ S MSC have not been extensively studied in the literature despite the potential benefits of a highly purified cell type with a repeatable isolation technique. Reasons for this may include difficulty with the isolation technique and a lack of access to the requisite facilities such as a high speed cell sorter. The logistical difficulties with using this technique are also a concern as an isolation requires 8-10 hours and will only yield approximately 1x10<sup>5</sup> cells meaning that culture expansion is a requirement prior to most experiments due to the number of cells needed. There also needs to be a consideration of the number



of mice required in order to yield a useful number of MSC. Each isolation requires the use of 10 mice and multiple isolations may be required for each experiment. As such wherever possible tissue not required for the isolation was used in other experiments in order to be compliant with the 3Rs [252].

### **3.3.2 The ability of murine P $\alpha$ S MSC to suppress lymphocyte proliferation *in vitro***

A key mechanism by which human MSCs exert their effects when used as a cell therapy is a reduction in lymphocyte proliferation [1, 253]. When testing P $\alpha$ S MSC isolated from BALB/c mice in a purified naive lymphocyte assay there was a demonstrable dose dependent reduction in lymphocyte proliferation. When this experiment was repeated with cells isolated from C57BL/6 mice no suppression of lymphocyte proliferation was seen. There are many reasons why this finding might have been true. I undertook enough controlled replications in order to rule out experimental error. BALB/c mice have a tendency towards TH2 responses and have been described as models of the TH2 response [254], they are used in models of asthma due to their ability to generate TH2 type allergic responses in the lungs [255]. With this in mind a possible explanation could be that BALB/c MSC respond differently in an inflammatory micro-environment and release cytokines in keeping with TH2 response such as Il-10, which would inhibit the proliferation of CD4<sup>+</sup> but not CD8<sup>+</sup> T lymphocytes. Yang et al have demonstrated that Il-10 secreted from BALB/c MSC can inhibit T cell proliferation *in vitro* [256]. A limitation of this study is the lack of cytokine data in the splenocyte reaction which would go some way to demonstrate the mechanistic differences between P $\alpha$ S MSC isolated from BALB/c mice and those isolated from C57BL/6 mice. Another explanation for the differences found between the purified naive lymphocyte reaction and the splenocyte reaction is a difference in type of lymphocyte studied. The naive lymphocyte reaction looked at the effects on CD4<sup>+</sup> lymphocytes, whereas the splenocyte reaction directly stimulated CD8<sup>+</sup> lymphocytes, although there was still a considerable number of CD4<sup>+</sup> cells present in the

assay. Whilst the decision to switch cell type was taken due to assay design concerns, it was felt that as an *in vitro* model of the effects of P $\alpha$ S MSC on the proposed models of liver injury the difference would be acceptable as both the MDR2<sup>-/-</sup> model and the hepatic ischaemia reperfusion model have been shown to have immune mediated damage caused by CD4<sup>+</sup> and CD8<sup>+</sup> lymphocytes [98, 74]. Another consideration in the splenocyte reaction is the ratio of other cells found in the splenocyte culture, in particular the large number of CD19<sup>+</sup> B cells, a ratio of 6:1 when compared with CD8<sup>+</sup> cells and almost 15:1 when compared with CD4<sup>+</sup> cells. It has been shown that MSC can exert their effects through the induction of regulatory B cells [257] and it is possible that this mechanism is utilised by P $\alpha$ S MSC. With lower numbers of CD19<sup>+</sup> cells to act as an immune system regulator suppression may not be seen. Further study would be needed to confirm this hypothesis.

P $\alpha$ S MSC isolated from C57BL/6 mice did suppress CD8<sup>+</sup> lymphocyte proliferation and activation when tested in a splenocyte reaction in a dose dependent fashion. By optimising the stimulation and cell number I was able to create a robust means of demonstrating this important effect of P $\alpha$ S MSC, confirming their potential for immunomodulation in models of liver injury with a lymphocyte mediated component and setting the scene for further *in vitro* and *in vivo* work.

### **3.3.3 The secretome of P $\alpha$ S MSC exposed to an inflammatory stimulus**

Various types of MSC have been studied in the literature and a number have papers have postulated mechanisms by which MSC can exert their immunosuppressive effects. A common mechanism of immunomodulation in the MSC literature is suppression of T cell proliferation as discussed earlier. MSC have been shown to exert their suppressive effect on T cells better when they are in direct contact [246] and this interaction can be facilitated by the expression of adhesion molecules including VCAM-1 and ICAM-1 [258]. In this study I have demonstrated that P $\alpha$ S MSC significantly increase their production of VCAM-1 following an inflammatory stimulus, suggesting they also possess the ability

to bind to T cells. Further work would need to be carried out in order to confirm this hypothesis. MSC have also been shown to attract T cells via expression of a number of leucocyte chemokines including CXCL9, CXCL10 and CXCL11 [259], with neutralisation of the T cell chemokine receptor CXCR3 reversing this effect. I have shown that P $\alpha$ S MSC produce significantly higher amounts of CXCL9, CXCL10 and CXCL11 following exposure to an inflammatory stimulus. I have also shown a significant increase CXCL, an NKT cell chemoattractant. This increase in production of leucocyte attractant chemokines could account for the ability of P $\alpha$ S MSC to suppress T lymphocyte proliferation either on its own or in conjunction with the secretion of other immunosuppressive cytokines such as Il-10 [260].

There exists debate in the MSC literature about the ability of MSC to secrete Il-10 with some studies demonstrating that MSC secrete Il-10 [240, 241], whilst other studies suggest that it is the effects of MSC on intermediary cells that leads to an increase in Il-10 levels [242, 243]. It has been suggested that MSC can stimulate the differentiation of macrophages into an M2 phenotype leading to the secretion of Il-10 by M2 macrophages [244, 128]. In this study I have clearly demonstrated that P $\alpha$ S MSC are able to secrete Il-10 following stimulation with TNF $\alpha$  and IFN- $\gamma$ . I did not however study the effects of other inflammatory cytokines on the secretome of P $\alpha$ S MSC and whilst the combination of TNF $\alpha$  and IFN- $\gamma$  seem to lead to the production of Il-10 it is possible that priming with other cytokines may lead to a different response. The choice of TNF $\alpha$  and IFN- $\gamma$  was based on previous studies and an attempt to recapitulate the *in vivo* inflammatory environment in models of liver injury and as such this finding is important and relevant. Increased Il-10 production could lead to a multitude of abilities including induction of TH2 response [261], the ability to inhibit neutrophil and macrophage function [262, 263, 264], inhibit T cell growth [260] and to suppress the secretion of pro-inflammatory cytokines [261]. MSC induced to overexpress Il-10 have been shown to be beneficial in models of graft versus host disease [164] indicating a role for Il-10 in inflammatory conditions and suggesting that MSC with the ability to secrete Il-10 in response to inflammatory stimuli

such as P $\alpha$ S MSC may be beneficial in inflammatory disease.

The chemokine CCL19 has been shown to aid the recruitment of CD4<sup>+</sup> and CD8<sup>+</sup> T lymphocytes into inflamed tissue [265, 266], as well as activating dendritic cells [267]. MSC have been shown to interfere with the CCL19 induced migration and antigen presentation of dendritic cells [268] so it was surprising to find that P $\alpha$ S MSC produce CCL19 in response to inflammatory cytokines. This could be a reflection of the ability of MSC to exert both pro and anti-inflammatory effects *in vivo*, the significance of this response needs further study.

In this chapter I have also demonstrated an increase in the production of osteoprotegerin by P $\alpha$ S MSC. It has previously been demonstrated that human MSC produce osteoprotegerin in response to inflammation [269] and that the interaction between MSC and macrophages may be responsible for MSC mediated inhibition of osteogenesis during inflammation [270]. This finding demonstrates a potential role of P $\alpha$ S MSC in bone remodelling during inflammation. Osteoprotegerin forms a part of the OPG/RANK/RANKL pathway and acts as an inhibitor of RANKL preventing the activation of the RANK signalling pathway [271]. The RANK/RANKL system is present on a number of immune cells and has a modulatory effect on the inflammatory response, and as such the ability of P $\alpha$ S MSC to secrete osteoprotegerin may represent a mechanism by which they are able to suppress the immune system. Further study is need to confirm this hypothesis.

### 3.3.4 Chapter summary

I prospectively isolated Murine P $\alpha$ S MSC from the bone marrow of C57BL/6 mice with cell yields similar to those found in the published literature. Following culture expansion I demonstrated P $\alpha$ S MSC morphology and also demonstrated that there are no morphological changes following an inflammatory stimulus. Following isolation I also demonstrated the expression of cell surface markers for MSC as defined by the ISCT. A splenocyte reaction was developed and optimised which allowed the ability of P $\alpha$ S MSC to suppress lymphocyte proliferation to be adequately demonstrated. P $\alpha$ S MSC were able to

suppress CD8<sup>+</sup> lymphocyte proliferation and activation in a dose dependent fashion with higher numbers of MSC leading to a greater level of suppression. I also demonstrated the secretome of P $\alpha$ S MSC following an inflammatory stimulus which included significantly increased levels of Il-10. These results support the hypothesis that murine P $\alpha$ S MSC may be a viable cell therapy *in vivo* in models of T cell mediated liver injury but further experiments will be is required.

## CHAPTER 4

# THE *IN VIVO* EFFICACY OF P $\alpha$ S MSC IN THE MDR2<sup>-/-</sup> MODEL OF LIVER INJURY

### 4.1 Chapter introduction and aims

I have demonstrated that P $\alpha$ S MSC can be isolated from the bone marrow of C57BL/6 mice and that following culture expansion these cells are able to suppress lymphocyte proliferation in a bulk splenocyte reaction. I have also demonstrated the ability of P $\alpha$ S MSC to secrete a broad range of cytokines in response to an inflammatory stimulus. In this chapter I tested the ability of P $\alpha$ S MSC to modulate the immune system in a mouse model of biliary injury.

#### 4.1.1 Non-anastomotic biliary complications following liver transplantation

Following the development of the surgical technique for liver transplantation in the 1960's it has rapidly become the standard treatment for end stage liver disease and remains so today due to a paucity of other effective therapies. As has always been the case the number of transplantations performed is limited by the number of donor organs meaning that patients often die whilst waiting for a donor liver to become available. In recent years this has led to the use of more marginal donor livers and extension of the donor criteria. A number of UK centres now use Maastricht class III non-heart beating donors [29]. The use

of more marginal donors, in particular DCD livers causes a different complication profile with a greater number of biliary complications when compared with DBD livers with DCD giving a 2-3 fold increased risk of biliary complications (30%-50% vs 10%-25%) [272, 273]. There is conflicting evidence regarding the overall morbidity and mortality of DCD transplantation when compared with DBD transplantation with some centres reporting a difference in mortality [42], and others suggesting that with careful patient selection there is no difference in outcome [31]. Biliary complications include bile leakage, bile duct strictures and ischaemic cholangiopathy. By reducing these complications, in particular in the more marginal grafts, graft survival may be increased and re-transplantation rate reduced thereby increasing the number of available organs for transplantation. I set out to test the ability of P $\alpha$ S MSC to reduce immune mediated injury in the MDR2<sup>-/-</sup> model of liver injury, a model I selected as the phenotype of injury is close to that seen in post DCD transplant liver injury.

#### **4.1.2 MDR2<sup>-/-</sup> mouse model of liver injury**

The MDR2<sup>-/-</sup> Mouse model [95] is a model utilised extensively by Fickert et al [96] to study liver injury. With targeted disruption of the multi-drug resistance gene 2 (Abcb4), an absence of biliary phospholipids is seen, resulting in the leaking of bile acids and cytotoxic injury to the biliary tree. This leads to extra- and intra-hepatic biliary strictures and dilatation with onion skin fibrosis. Whilst proposed as a model of sclerosing cholangitis there are clear parallels with the injury seen in DCD liver transplantation in the medium term and so this model was chosen to test the hypothesis that P $\alpha$ S MSC may reduce this immune mediated damage.

Experiments were limited to male mice due to the propensity of female mice to form bile stones in an unpredictable manner leading to heterogeneous results [99]. An age below 15 weeks was determined as the appropriate time course as peak CD4<sup>+</sup> and CD8<sup>+</sup> cell infiltration within the liver occurs during this time period as does early fibrosis and stricture development [98]. After 14 weeks fibrosis becomes established and the immune

component of the injury appears to be reduced with less infiltrating immune cells present and lower levels of serum markers of liver injury [95, 97, 98]. Formation of gallstones also seems to be more prevalent from 15 weeks of age [99]. Whilst the MDR2<sup>-/-</sup> model has been studied extensively the majority of papers seem to use immunohistochemistry to assess immune cell infiltration in the liver so I decided to complement this with flow cytometry in order to better quantify the immune cell infiltrate in the liver of MDR2<sup>-/-</sup> mice.

### 4.1.3 MSC as a therapy in immune mediated liver injury

MSC from a variety of sources have been extensively studied, however a limitation of the field is the heterogeneity of cell types isolated and cultured and the duplicity of effects often seen. Isolation of more homogeneous populations of cells may enable more robust and repeatable testing of the efficacy of MSC as a cell therapy. With this in mind I have focussed on the use of P $\alpha$ S MSC which represent a more homogeneous group of MSC. Little work has been carried out with these cells as previously discussed and their efficacy as a cell therapy has yet to be tested in the published literature. Previous work in our laboratory has shown that these cells can suppress the immune response in a model of autoimmune hepatitis [237, 245], and I have demonstrated the ability of P $\alpha$ S MSC to suppress lymphocyte proliferation and activation in a previous chapter.

### 4.1.4 Specific chapter aims

Previous chapters have demonstrated the ability of P $\alpha$ S MSC to suppress CD8<sup>+</sup> T cell proliferation *in vitro* in a dose dependent fashion. I have also demonstrated a number of cytokines secreted following stimulation which have the potential to modulate the immune response. The aim of this chapter was to characterise the ability of P $\alpha$ S MSC to modulate the immune system *in vivo* in the MDR2<sup>-/-</sup> model of liver injury. The specific aims of this chapter were:

1. To establish the MDR2<sup>-/-</sup> model of liver injury



2. To optimise techniques to study infiltrating immune cells in the livers of MDR2<sup>-/-</sup> mice
3. To characterise the inflammatory injury seen in the MDR2<sup>-/-</sup> model over time
4. To test the *in vivo* efficacy of PαS MSC in the MDR2<sup>-/-</sup> model

## 4.2 Results

### 4.2.1 Genotyping of MDR2<sup>-/-</sup> breeding pairs

The MDR2<sup>-/-</sup> model is a homozygous knockout model and a colony was maintained at the . Mice were bred on an FVB background as the majority of the published literature using this model is in FVB mice and MDR2<sup>-/-</sup> mice bred on a C57BL/6 background had low litter numbers and as such their use was unfeasible for this study. Whilst this model was a homozygous model and therefore genotyping of all litters was not necessary periodic genotyping was undertaken to confirm no significant genetic drift. Genotyping was undertaken by TransnetXY®. Results demonstrated that all breeding pairs were homozygous for the *mdr2/abcb4* gene.

### 4.2.2 Time course of liver injury in the MDR2<sup>-/-</sup> mouse model

The MDR2<sup>-/-</sup> model of liver injury is a spontaneous and progressive model of liver injury. There is increased flow of toxic bile acids and by 3 weeks of age mice demonstrate ductular proliferation and a mixed inflammatory infiltrate [97]. As the literature describes an inflammatory infiltrate which develops from week 3 to peak at around 8 weeks I decided to look at a number of time points during the peak inflammatory period. By 14 weeks fibrosis should become established and the risk of ductal lithiasis increases so time points beyond this were not considered [99]. ALT has been used as the primary outcome measure in the MDR2<sup>-/-</sup> model in the majority of studies. Given that young mice tend to release ALP during bone turnover which could cloud the results [274] I decided to use ALT as a primary measure but considered ALP and bile acids as secondary measures.

#### 4.2.2.1 Serum markers of liver injury over time

MDR2<sup>-/-</sup> mice were sacrificed at different time points after birth. Samples from male 8 week old uninjured FVB wild type mice were also analysed for control values (figure 4.1).

Serum ALT showed a significant increase over time ( $p < 0.0001$ ) with a peak at 11 weeks ( $801.7 \pm 142.9$  IU/L). There appeared to be a plateau between weeks 8 and 10 where there were no significant changes in ALT value. Serum ALP also demonstrated a significant increase over time ( $p = 0.0012$ ) with a peak at 11 weeks ( $1289 \pm 572$  U/L), although levels were not significantly higher than those between 8 and 10 weeks. Bile acids followed the same pattern with a significant increase over time ( $p = 0.045$ ) with a peak at 11 weeks ( $72.5 \pm 26.9$   $\mu\text{mol/L}$ ), although again levels were not significantly higher than those between 8 and 10 weeks. ALT was the only marker that continued to increase up to 12 weeks with ALP and bile acids remaining relatively unchanged.

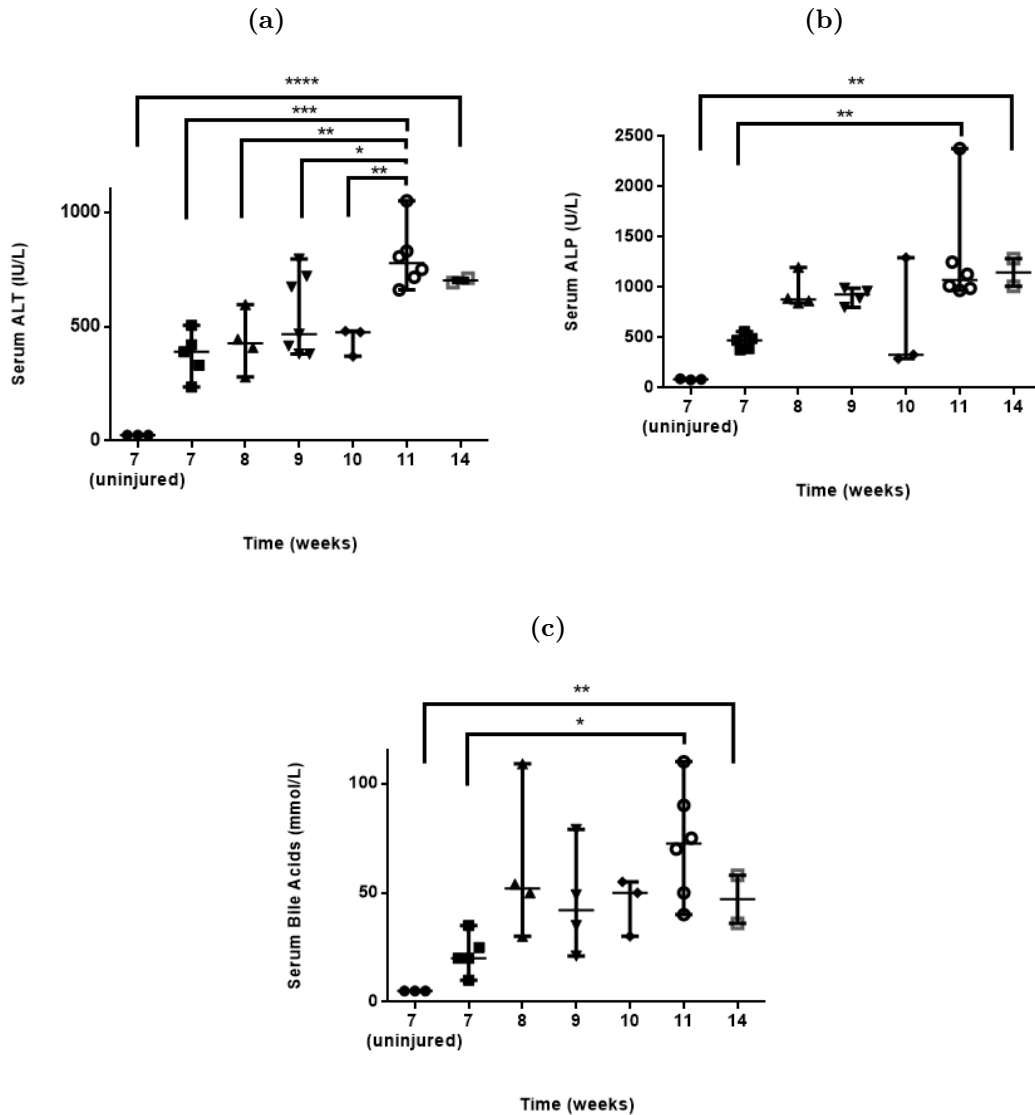


**Figure 4.1 – MDR2<sup>-/-</sup> serum markers of liver injury show changes over time.** Male MDR2<sup>-/-</sup> mice or FVB wild type controls were sacrificed at different time points after birth. MDR2<sup>-/-</sup> mouse serum was analysed at multiple time points for ALT, ALP and bile acids. (a) Serum ALT showed a significant increase over time ( $p < 0.0001$ ) with a peak at 11 weeks ( $801.7 \pm 142.9$  IU/L,  $n=30$ ). (b) Serum ALP also demonstrated a significant increase over time ( $p=0.0012$ ) with a peak at 11 weeks ( $1289 \pm 572$  U/L), although levels were not significantly higher than those between 8 and 10 weeks ( $n=27$ ). (c) Bile acids followed the same pattern with a significant increase over time ( $p=0.045$ ) with a peak at 11 weeks ( $72.5 \pm 26.9$   $\mu$ mol/L), although levels were not significantly higher than those between 8 and 10 weeks ( $n=27$ ). Points represent individual mice, bars represent the median and lines represent the range. Statistical analysis was carried out using a one way ANOVA and multiple comparison testing was undertaken.

#### **4.2.2.2 Liver immunohistochemistry over time**

Following sacrifice of MDR2<sup>-/-</sup> mice liver tissue was removed and fixed in formalin. Fixed liver tissue was embedded in paraffin and processed for immunohistochemistry. H & E staining (figure 4.2) was performed and demonstrated inflammation of the portal regions (zone I) at all time points with inflammatory cell infiltration around the bile ducts as described by Maud et al [97], with sparing of the peri-central (zone III) areas. Quantification was not undertaken as further analysis of infiltrating immune cells was undertaken.

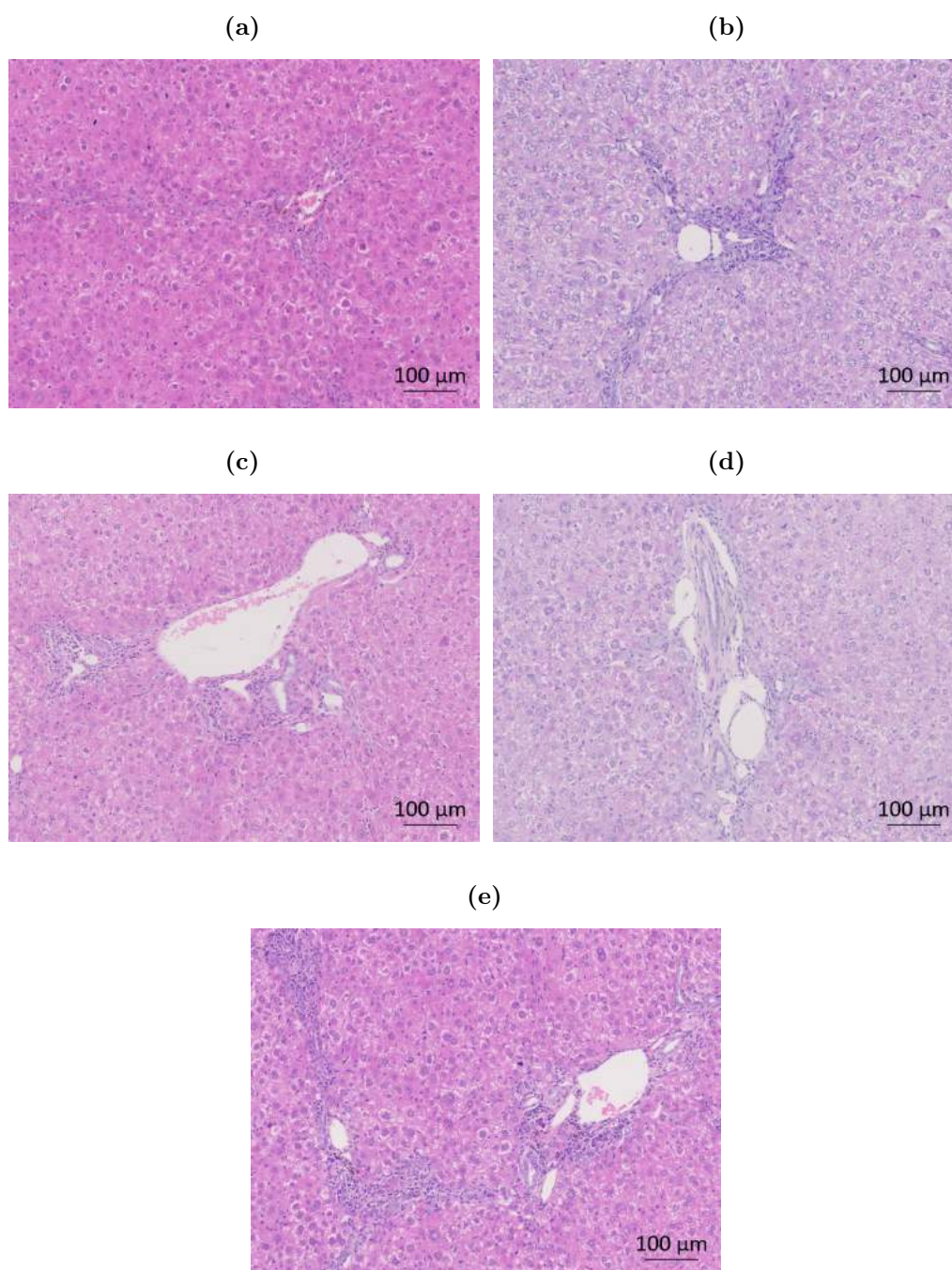


**Figure 4.2 – Representative haematoxylin and eosin staining of MDR2<sup>-/-</sup> livers between 7 and 14 weeks.** Either male MDR2<sup>-/-</sup> mice or FVB wildtype controls were sacrificed at different time points after birth and liver tissue was removed and processed sectioned. H & E staining was performed and demonstrated inflammation of the portal regions (zone I) at (a) 7 weeks, (b) 8 weeks, (c) 9 weeks, (d) 10 weeks and (e) 14 weeks. Quantification was not undertaken. All images are generated from whole slide scans and are at 400x magnification. Scale bars represent 100 μm.

Immunohistochemical staining for CD45 was used to demonstrate total leucocyte infiltration in MDR2<sup>-/-</sup> mouse livers (figure 4.4), and F4/80 staining was used to delineate hepatic macrophages (figure 4.5). Staining was undertaken using a chromogenic technique. Whole slide images from stained slides were captured using a Zeiss AxioScanner. Between 5 and 10 images were taken from each scan to cover the whole slide and quantification of each image was performed using Image J software. CD45 staining was greatest at 7 weeks ( $3.71 \pm 0.31$ ) and significantly lower at weeks 8-10, although there was no difference found in the levels between weeks 8-10 (figures 4.3,4.4). F4/80 staining was greatest at 14 weeks ( $5.06 \pm 11.0$ ) but not significantly different at any time point and showed a large confidence interval (figures 4.3,4.5).

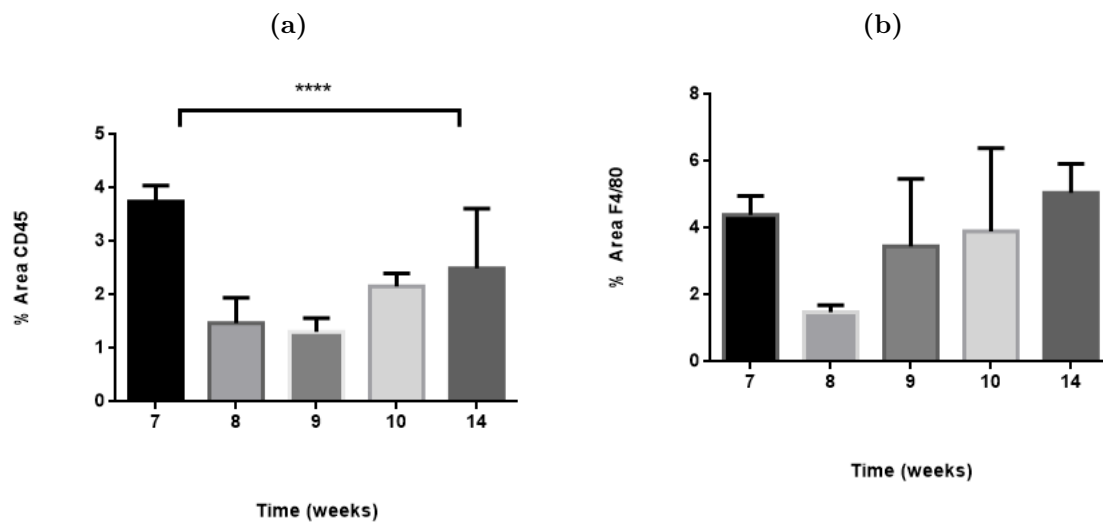


**Figure 4.3 – Time course quantification of CD45 and F4/80 staining levels in MDR2<sup>-/-</sup> mice.** Either male MDR2<sup>-/-</sup> mice or FVB wild type controls were sacrificed at different time points after birth and liver tissue was removed and processed sectioned. Immunohistochemical staining was undertaken using a chromogenic technique. (a) CD45 staining was greatest at 7 weeks and significantly lower at weeks 8-10 (n=19). (b) F4/80 staining was greatest at 14 weeks but not significantly different at any time point (n=18). Slides were captured using a Zeiss AxioScanner. Between 5 and 10 images were taken from each scan to cover the whole slide and quantification of each image was performed using Image J software. Histograms represent the median value and lines represent the range. Statistical analysis was carried out using a one way ANOVA and multiple comparison testing was undertaken.

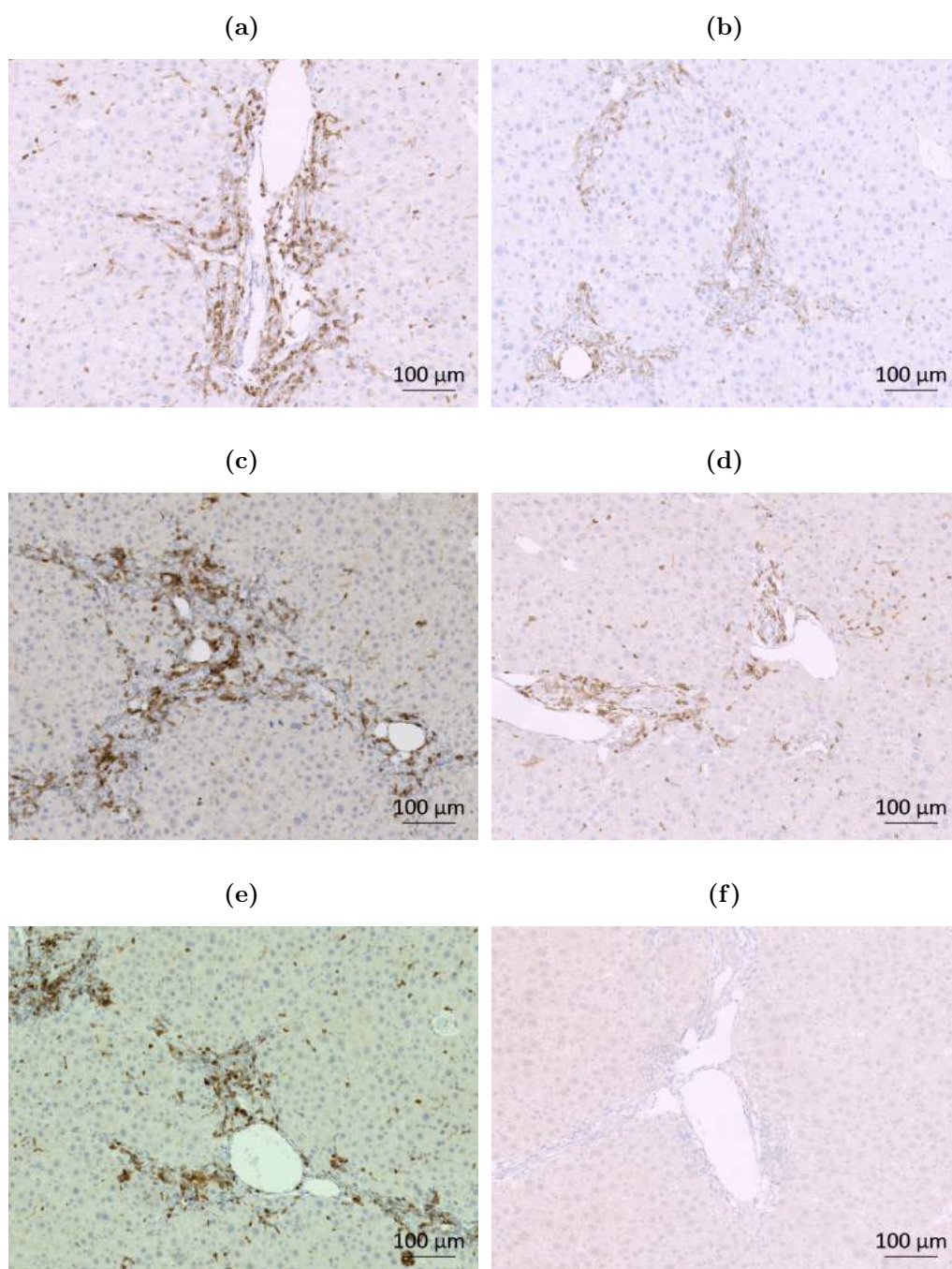


**Figure 4.4 – Representative immunohistochemical staining for CD45 of MDR2<sup>-/-</sup> livers between 7 and 14 weeks.** Either male MDR2<sup>-/-</sup> mice or FVB wild type controls were sacrificed at different time points after birth and liver tissue was removed, processed and sectioned. Immunohistochemical staining was undertaken using a chromogenic technique. Slides were captured using a Zeiss AxioScanner. There was an apparent peri-portal distribution of CD45 positive cells with localisation in zone 1 around the bile ducts present at (a) 7 weeks, (b) 8 weeks, (c) 9 weeks, (d) 10 weeks and (e) 14 weeks. All images are generated from whole slide scans and are at 400x magnification. Scale bars represent 100 µm.



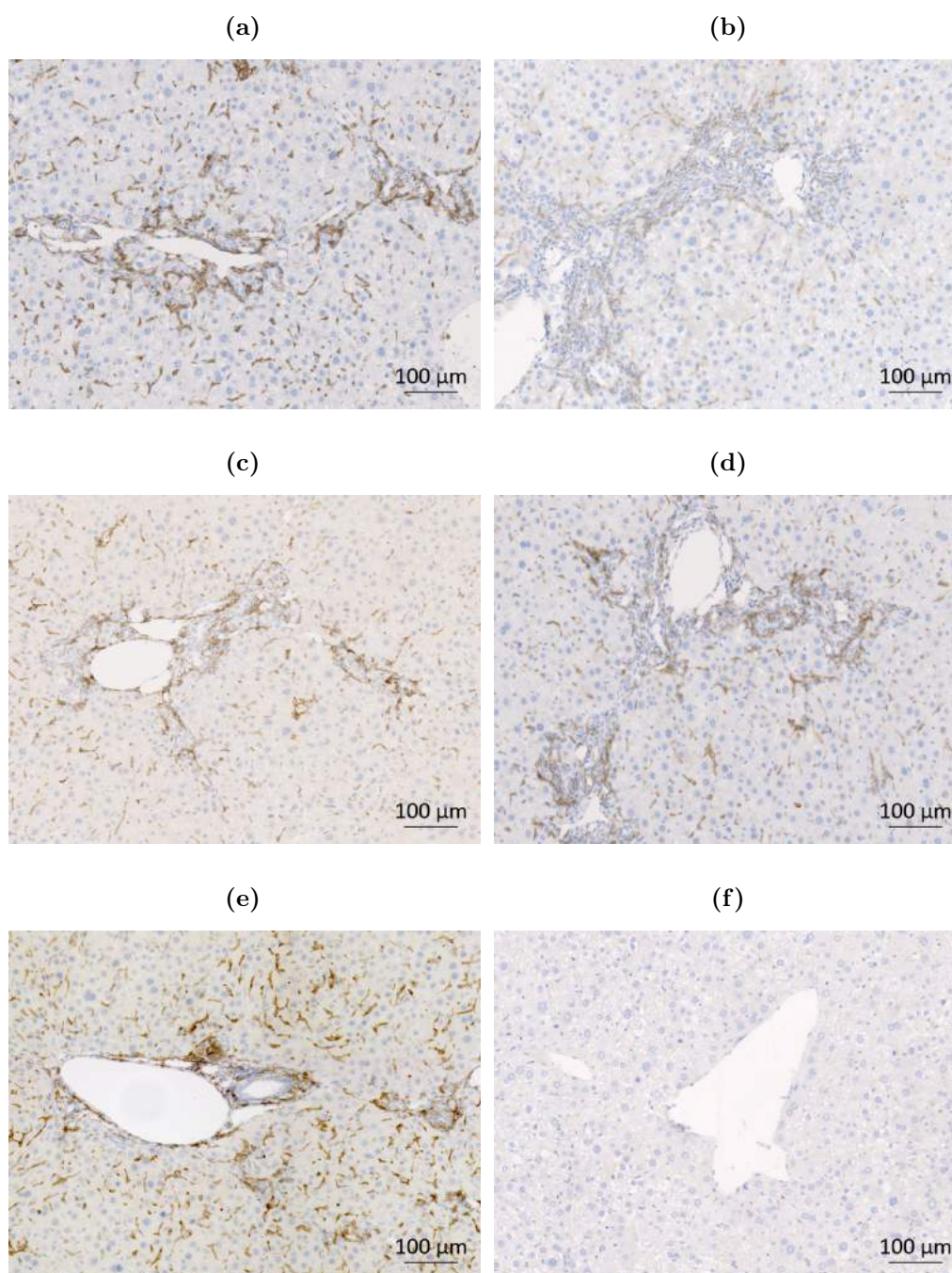


**Figure 4.5 – Representative immunohistochemical staining for F4/80 of MDR2<sup>-/-</sup> livers between 7 and 14 weeks.** Either male MDR2<sup>-/-</sup> mice or FVB wild type controls were sacrificed at different time points after birth and liver tissue was removed, processed and sectioned. Immunohistochemical staining was undertaken using a chromogenic technique. Slides were captured using a Zeiss AxioScanner. There was an apparent peri-portal concentration of F4/80 positive cells with localisation in zone 1 around the bile ducts, however F4/80 cells were also distributed throughout the liver. This pattern was seen at (a) 7 weeks, (b) 8 weeks, (c) 9 weeks, (d) 10 weeks and (e) 14 weeks. All images are generated from whole slide scans and are at 400x magnification. Scale bars represent 100  $\mu$ m.

#### 4.2.2.3 Western blotting for CK19 expression

In the MDR2<sup>-/-</sup> model ductular proliferation has been described as occurring as early as 4 weeks of age [98]. Whilst this can be seen on H & E staining, quantification can be better achieved by investigating levels of the cytoskeletal protein cytokeratin 19 (CK19). I decided to perform western blotting in order to examine CK19 expression levels in keeping with other studies into the MDR2<sup>-/-</sup> model [100]. Mechanical liver tissue homogenisation was undertaken followed by protein lysis. Determination of protein concentration was performed using the Biuret assay. Following optimisation 40 µg of protein was loaded per well and samples run and subsequently transferred to a PVDF membrane. A primary antibody for CK17/19 (New England BioLabs, US) followed by a secondary conjugated to Horseradish Peroxidase (HRP) was used and imaging undertaken using X Ray film. Films were scanned and analysed using ImageStudio Lite (LI-COR Biosciences, GB). Membranes were stripped and re-probed using  $\alpha$ -actinin as a loading control. Samples were normalised to the loading control and represented as fold change using samples from uninjured FVB wild type mice as reference values.

CK19 levels were variable throughout the time course of the MDR2<sup>-/-</sup> model but demonstrated broad confidence intervals (figure 4.6). The only time point which demonstrated a significant increase from the baseline level was 10 weeks (P=0.03).

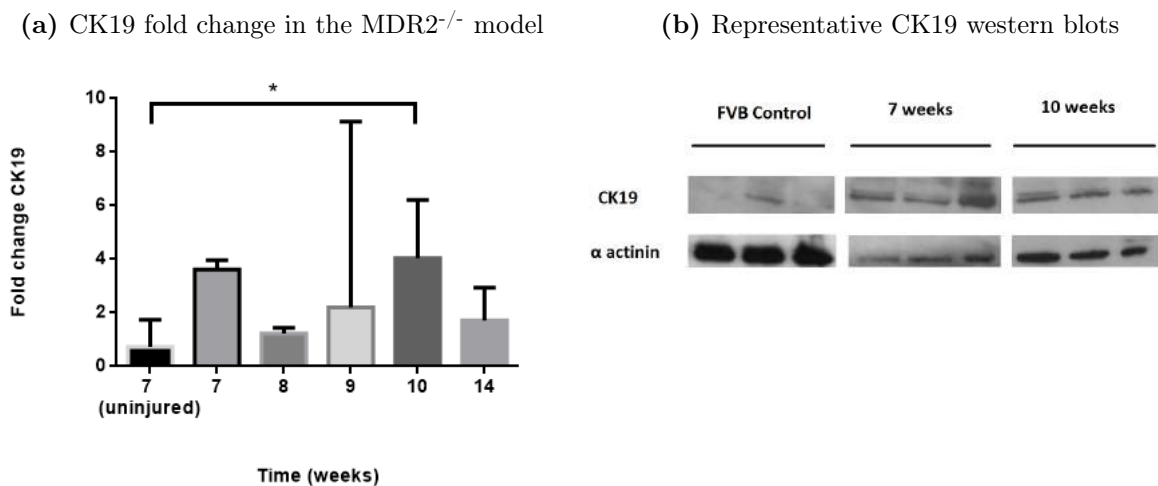


**Figure 4.6 – Western blot of the time course of CK19 levels in the MDR2<sup>-/-</sup> mouse model.** Either male MDR2<sup>-/-</sup> mice or FVB wild type controls were sacrificed at different time points after birth and liver tissue was removed and processed. Protein was extracted from the liver tissue and 40 µg was loaded per well. Blotting was performed and images were scanned and analysed. α-actinin was used as a loading control and samples were normalised to the loading control and represented as fold change using samples from uninjured FVB wild type mice as reference values. (a) CK19 levels were variable throughout the time course of the MDR2<sup>-/-</sup> model but demonstrated broad confidence intervals (n=20). Group analysis showed no significant difference with multiple comparisons however at 10 weeks there was a significant increase in CK19 when compared with uninjured FVB (P=0.03). (b) representative western blots at 7 and 10 weeks compared with FVB controls demonstrate higher expression of CK19. Histograms represent the median value and lines represent the range. Statistical analysis was carried out using a one way ANOVA and multiple comparison testing was undertaken. Individual T-tests were also performed.

Based on these results I decided to focus my investigations at 7, 10 and 11 weeks in order to determine the most beneficial time point for MSC therapy in the MDR2<sup>-/-</sup> model.

#### 4.2.2.4 Characterisation of liver lymphocytes by flow cytometry

I next sought to quantify the immune cell populations in the livers of MDR2<sup>-/-</sup> mice. Male mice aged 8 weeks old were sacrificed and liver lobes were removed and mechanically homogenised and following washing were passed over a density gradient using Lympholyte® (Cedarlane, CA). Cells were stained and analysed by flow cytometry. Values are normalised to liver weight.

Following the first isolation run it was clear that the cell yield was well below what I

expected based on the serum markers of liver injury (figure 4.7). Total CD3<sup>+</sup> cell numbers were low ( $2905 \pm 2951$ ) with CD4<sup>+</sup> and CD8<sup>+</sup> lower still ( $986 \pm 307$ ,  $257.1 \pm 121.4$ ). Whilst I have successfully used this technique to isolate immune cells from the livers of OVA-Bil mice [245], I hypothesised based on that Lympholyte<sup>®</sup> was not the correct gradient to enable isolation of immune cells in the MDR2<sup>-/-</sup> model.

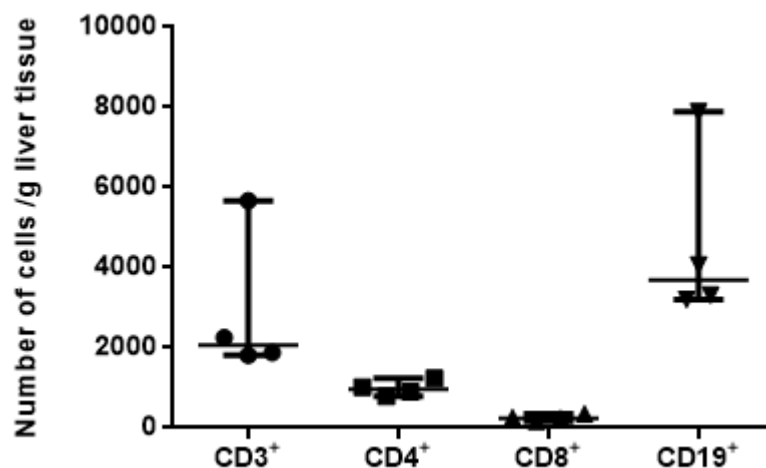


**Figure 4.7 – Flow cytometric analysis of immune cell numbers from 8 week old MDR2<sup>-/-</sup> mouse liver following extraction with Lympholyte<sup>®</sup>.** Male mice aged 8 weeks old were sacrificed and liver lobes were removed and mechanically homogenised and following washing were passed over a density gradient using Lympholyte<sup>TM</sup> (Cedarlane, CA). Cells were stained and analysed by flow cytometry. Following the first isolation run it was clear that the cell yield was well below what I expected based on the serum markers of liver injury. Total CD3<sup>+</sup> cell numbers were low ( $2905 \pm 2951$ ) with CD4<sup>+</sup> and CD8<sup>+</sup> lower still ( $986 \pm 307$ ,  $257.1 \pm 121.4$ ). Values are normalised to liver weight and shown as cells per gramme of liver tissue. Points represent individual mice, bars represent the median and lines represent the range.

Previous studies have reported successful isolation of immune cells from models of liver fibrosis using Optiprep<sup>TM</sup> as the density gradient [275]. I decided to investigate this as an alternative to Lympholyte<sup>®</sup> in the MDR2<sup>-/-</sup> model. Mouse livers from 8 week old male MDR2<sup>-/-</sup> mice were processed as previously described but using Optiprep<sup>TM</sup> as the density gradient.

Cell numbers isolated using the modified protocol were greatly improved (figure 4.8) with a 56 fold increase in the number of CD8<sup>+</sup> lymphocytes isolated using Optiprep<sup>TM</sup> ( $p=0.006$ ). Based on these results I used Optiprep<sup>TM</sup> for all subsequent immune cell

isolation from MDR2<sup>-/-</sup> mouse liver.

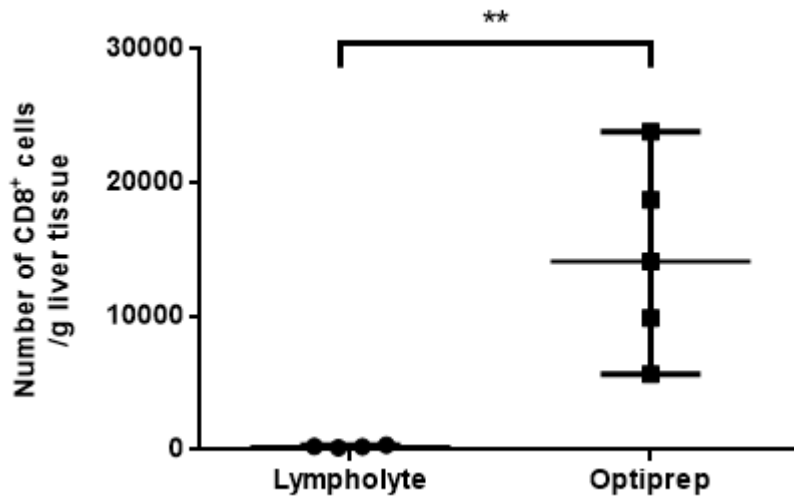


**Figure 4.8 – Optiprep<sup>TM</sup> yields a greater number of immune cells from liver digest than Lympholyte<sup>®</sup> in MDR2<sup>-/-</sup> mice.** Mouse livers from male 8 week old MDR2<sup>-/-</sup> mice were homogenised and immune cells separated using either Optiprep<sup>TM</sup> (n=4) or Lympholyte<sup>®</sup> (n=5) as the density gradient. Immune cells were then stained and analysed by flow cytometry. Cell numbers isolated using Optiprep<sup>TM</sup> were greater than when using with the number of CD8<sup>+</sup> lymphocytes isolated using Optiprep<sup>TM</sup> 56 times higher (p=0.006). Values are normalised to liver weight and shown as cells per gramme of liver tissue. Points represent individual mice, bars represent the median and lines represent the range. Statistical analysis was performed using a Student's t-test.

I next investigated liver immune cell infiltration at 7, 10 and 11 weeks in order to determine the most beneficial time point for MSC therapy in the MDR2<sup>-/-</sup> model (figure 4.9).

Between 7 and 10 weeks there was a significant increase in CD8<sup>+</sup> and CD19<sup>+</sup> lymphocytes with CD8<sup>+</sup> cells falling significantly between 10 and 11 weeks back to a similar level to that seen at 7 weeks of age. Between 10 and 11 weeks CD4<sup>+</sup>, CD19<sup>+</sup> and NK1.1 numbers all fell significantly indicating that the peak immune cell number occurred at around 10 weeks.

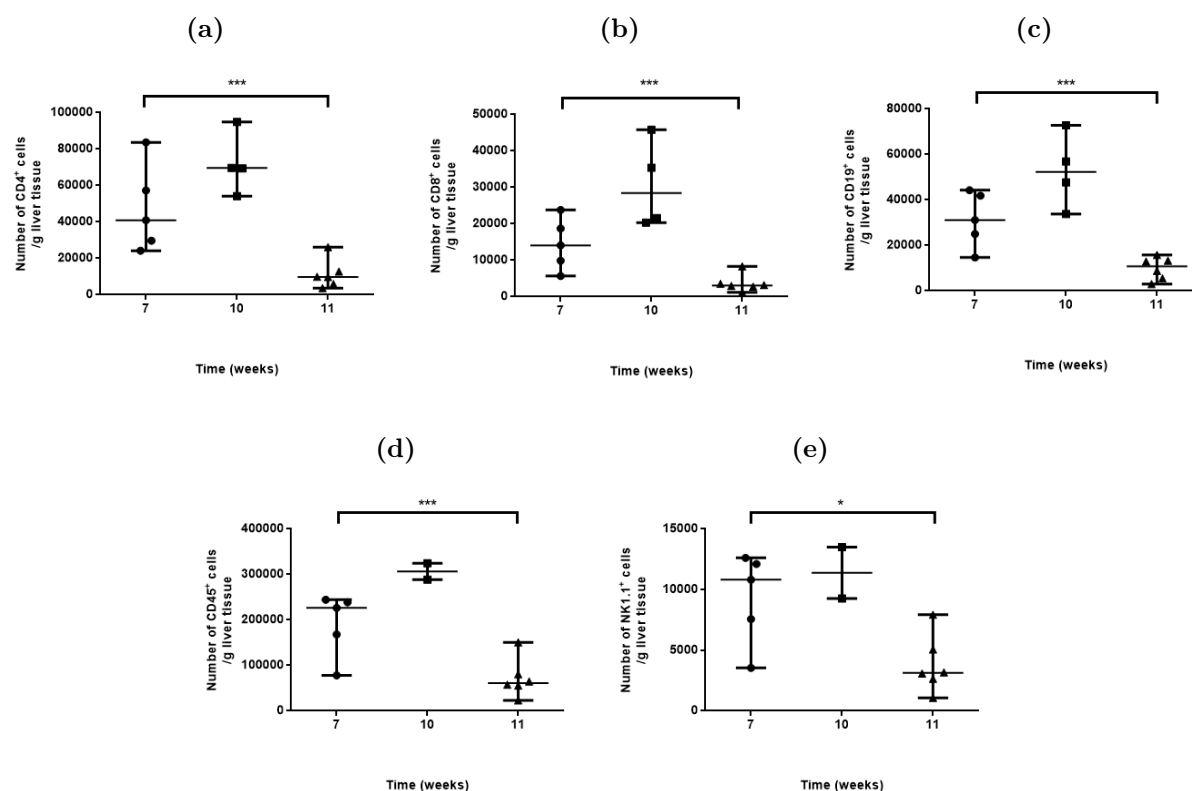


**Figure 4.9 – FACS analysis of MDR2<sup>-/-</sup> mouse livers demonstrating the immune cell profile between 7 and 11 weeks of age.** Liver lobes from MDR2<sup>-/-</sup> mice aged 7 (n=5), 10 (n=2) or 11 (n=6) weeks were mechanically homogenised and following washing were passed over a density gradient using Optiprep<sup>TM</sup>. Cells were stained and analysed by flow cytometry. All cells studied showed significant changes throughout the time course studied and peak values of all immune cells were seen in mice aged 10 weeks. (a) CD4<sup>+</sup> lymphocytes showed a non significant increase between 7 and 10 weeks but fell significantly between 10 and 11 weeks. (b) CD8<sup>+</sup> lymphocytes increased significantly between 7 and 10 weeks and following a significant reduction between 10 and 11 weeks returned below the levels at 7 weeks. (c) CD19<sup>+</sup> lymphocytes increased significantly between 7 and 10 weeks and then decreased significantly between 10 and 11 weeks. (d) Total CD45<sup>+</sup> cells demonstrated a non significant increase between weeks 7 and 10 and then fell significantly between weeks 10 and 11. (e) NK1.1 numbers remained high between weeks 7 and 10 and then fell significantly between weeks 10 and 11. Values are normalised to liver weight and shown as cells per gramme of liver tissue. Points represent individual mice, bars represent the median and lines represent the range. Statistical analysis was carried out using a one way ANOVA and multiple comparison testing was undertaken.

The immune cell profile in the livers of MDR2<sup>-/-</sup> mice showed a peak immune cell infiltration at week 10 with a subsequent fall by week 11, in keeping with the published literature [98]. Levels of CD4<sup>+</sup>, CD45<sup>+</sup> and NK1.1 cells were all high from 7 weeks peaking at 10 weeks and falling by 11 weeks.

### 4.2.3 *In vivo* efficacy of P $\alpha$ S MSC in the MDR2<sup>-/-</sup> model

Having demonstrated that serum markers of liver injury in the MDR2<sup>-/-</sup> model are high between 8 and 10 weeks of age and infiltrating immune cells peak in mice aged 10 weeks old I determined that treating mice aged 6-8 weeks with cell therapy followed by analysis 2 weeks later should allow enough time for cells to exert an anti-inflammatory effect at the time of peak inflammatory liver injury.

In order to test the efficacy of P $\alpha$ S MSC in the MDR2<sup>-/-</sup> model I used MSC cultured in standard media which were expanded to passage 4. This passage was chosen based on my findings when testing their efficacy *in vitro* as well as previous experience with these cells in other models of liver injury [245]. Doses of either 1x10<sup>5</sup> or 2x10<sup>5</sup> P $\alpha$ S MSC suspended in PBS were tested using the intravenous route with control animals receiving PBS alone. Male mice aged between 6 and 8 weeks were injected with P $\alpha$ S MSC and culled 2 weeks later. Analysis of serum markers, liver infiltrating immune cells and immunohistochemistry were performed.

#### 4.2.3.1 Effects of P $\alpha$ S MSC on serum markers of liver injury in the MDR2<sup>-/-</sup> model

Following treatment with P $\alpha$ S MSC mice were culled at 2 weeks and serum analysed for markers of liver injury. Serum ALT showed a significant dose dependent reduction after treatment with MSC (figure 4.10a). Treatment with 1x10<sup>5</sup> showed no difference when compared with PBS treated controls (562 IU/L  $\pm$  87.3 vs 558.1 IU/L  $\pm$  119.5), however treatment with 2x10<sup>5</sup> MSC led to a significant reduction in ALT when compared with controls (325.7 IU/L  $\pm$  191.7 vs 562 IU/L  $\pm$  87.3, p=0.002). Serum ALP demonstrated a similar pattern (figure 4.10b) with the control group and the group treated with 1x10<sup>5</sup> MSC showing similar values (1067 IU/L  $\pm$  319.1 vs 1007 IU/L  $\pm$  92.8) whereas the group treated with 2x10<sup>5</sup> MSC showing a significant reduction in ALP (1067 IU/L  $\pm$  319.1 vs 635.1 IU/L  $\pm$  178.7, p=0.0055). Serum Bile acids did not show any significant changes following treatment (figure 4.10c) with either 1x10<sup>5</sup> MSC (41.47  $\mu$ mol/L  $\pm$  10.14 vs 42.93

$\mu\text{mol/L} \pm 12.85$ ) or  $2 \times 10^5$  MSC ( $39.07 \mu\text{mol/L} \pm 11.27$  vs  $42.93 \mu\text{mol/L} \pm 12.85$ ) when compared with controls.

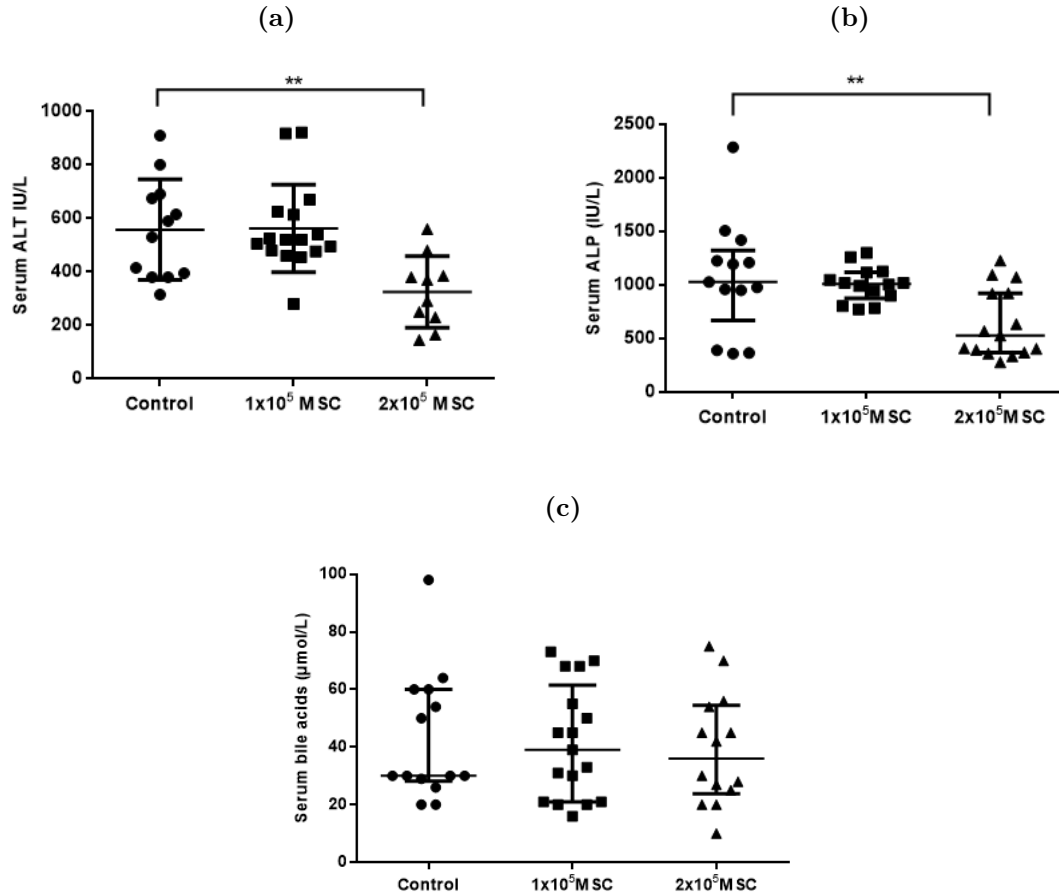


**Figure 4.10 – P $\alpha$ S MSC significantly reduce ALT and ALP but not Bile acids in MDR2<sup>-/-</sup> mice.** MDR2<sup>-/-</sup> mice aged 6-8 weeks were given either  $1 \times 10^5$  or  $2 \times 10^5$  P $\alpha$ S MSC via the tail vein and culled at 2 weeks. Serum ALT (a) showed a non-significant reduction after treatment with  $1 \times 10^5$  MSC compared with PBS treated controls ( $562 \text{ IU/L} \pm 87.3$  vs  $558.1 \text{ IU/L} \pm 119.5$ ), however treatment with  $2 \times 10^5$  MSC led to a significant reduction in ALT ( $325.7 \text{ IU/L} \pm 191.7$  vs  $562 \text{ IU/L} \pm 87.3$ ,  $p=0.002$ ,  $n=38$ ). Serum ALP (b) demonstrated a similar pattern with the control group and the group treated with  $1 \times 10^5$  MSC showing similar values ( $1067 \text{ IU/L} \pm 319.1$  vs  $1007 \text{ IU/L} \pm 92.8$ ) whereas the group treated with  $2 \times 10^5$  MSC showed a significant reduction in ALP ( $1067 \text{ IU/L} \pm 319.1$  vs  $635.1 \text{ IU/L} \pm 178.7$ ,  $p=0.0055$ ,  $n=42$ ). Serum Bile (c) acids did not show any significant changes following treatment with either  $1 \times 10^5$  MSC ( $41.47 \mu\text{mol/L} \pm 10.14$  vs  $42.93 \mu\text{mol/L} \pm 12.85$ ) or  $2 \times 10^5$  MSC ( $39.07 \mu\text{mol/L} \pm 11.27$  vs  $42.93 \mu\text{mol/L} \pm 12.85$ ) when compared with controls ( $n=45$ ). Points represent individual mice, bars represent the median and lines represent the interquartile range. Statistical analysis was carried out using a one way ANOVA.



#### **4.2.3.2 Histological changes in MDR2<sup>-/-</sup> mouse livers when treated with PαS MSC**

Liver tissue from MDR2<sup>-/-</sup> mice treated with PαS MSC was removed, processed and embedded in paraffin and then sectioned and stained. H & E staining was performed in order to demonstrate the morphology of the liver (figure 4.11). There was almost no morphological disruption seen in uninjured FVB control with few infiltrating immune cells. Infiltrating immune cells were demonstrated showing a peri-portal (Zone I) distribution in PBS treated controls as well as mice treated with PαS MSC IV.

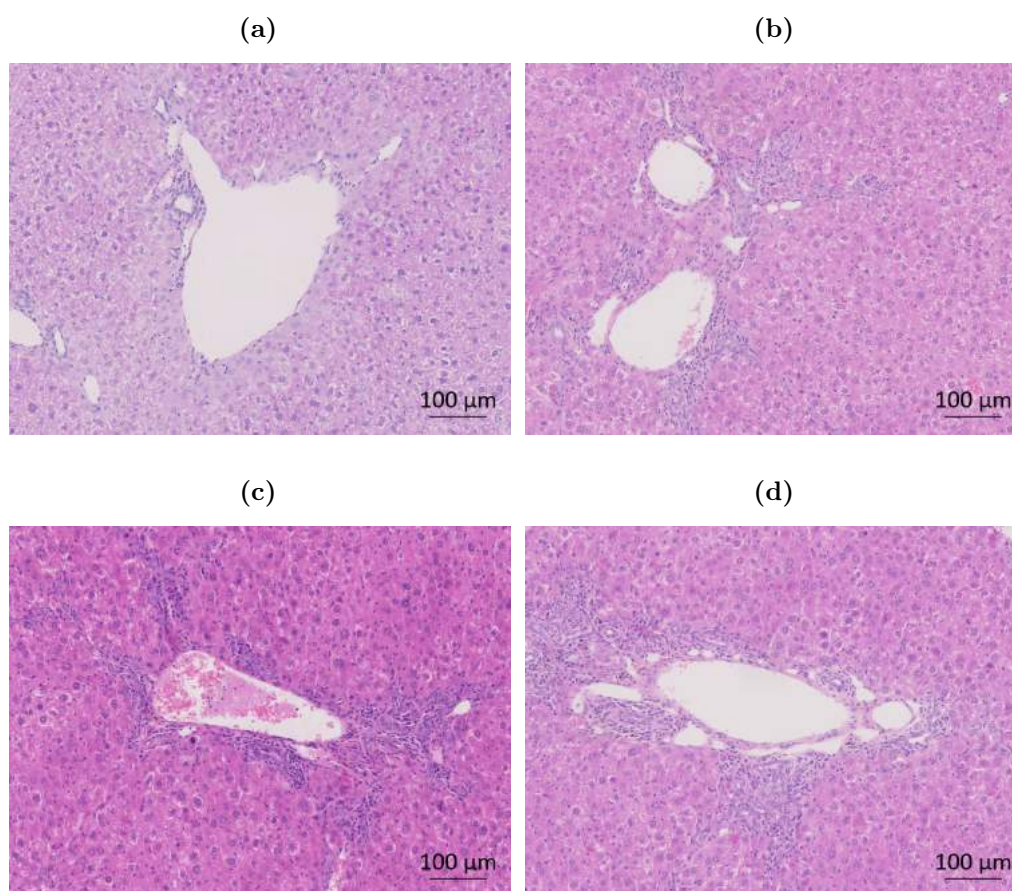


**Figure 4.11 – Representative images of haematoxylin and eosin staining in MDR2<sup>-/-</sup> mice treated with either PBS or PαS MSC at 6-8 weeks of age and culled 2 weeks later.** MDR2<sup>-/-</sup> mice aged 6-8 weeks were given either  $1 \times 10^5$  or  $2 \times 10^5$  PαS MSC via the tail vein and culled at 2 weeks and liver tissue was removed, processed and sectioned. H & E staining was performed. Minimal morphological disruption was seen in (a) uninjured FVB control with almost no infiltrating immune cells seen. Infiltrating immune cells were demonstrated showing a peri-portal (Zone I) distribution in (b) PBS treated controls, (c) mice treated with  $1 \times 10^5$  PαS MSC IV and (d) mice treated with  $2 \times 10^5$  PαS MSC IV. All images are generated from whole slide scans and are at 400x magnification. Scale bars represent 100  $\mu\text{m}$ .

Immunohistochemical antibody staining was undertaken to allow quantification of the expression of the pan-leucocyte marker CD45. Slides were scanned using a Zeiss AxioScanner providing a whole slide image and quantification of the amount of staining was analysed and represented as a percentage total area. MDR2<sup>-/-</sup> control animals showed a marginal increase in CD45 expression (figures 4.12, 4.13) when compared with wild type FVB uninjured controls ( $2.198 \pm 0.947$  vs  $1.90 \pm 0.59$ ). There was a no significant difference in CD45 expression in mice treated with  $1 \times 10^5$  PαS MSC ( $2.198 \pm 0.947$  vs

$2.289 \pm 0.265$ ), but a significant increase in CD45 expression when mice were treated with  $2 \times 10^5$  MSC ( $2.198 \pm 0.947$  vs  $3.432 \pm 1.073$ ,  $p=0.026$ ).

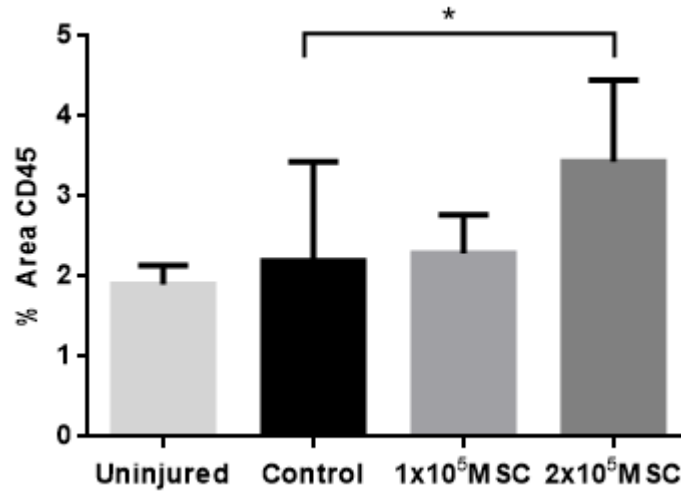


**Figure 4.12 – CD45 expression in the livers of MDR2<sup>-/-</sup> mice treated with either PBS or PαS MSC at 6-8 weeks of age and culled 2 weeks later.** MDR2<sup>-/-</sup> mice aged between 6 and 8 weeks were treated with either  $1 \times 10^5$  or  $2 \times 10^5$  PαS MSC suspended in PBS with control animals receiving PBS alone. Mice were culled 2 weeks later and liver tissue was removed, processed and sectioned. Immunohistochemical staining was undertaken using a chromogenic technique. MDR2<sup>-/-</sup> control animals demonstrated slightly higher CD45 expression when compared with wild type FVB uninjured controls ( $2.198 \pm 0.947$  vs  $1.90 \pm 0.59$ ). There was a no significant difference in CD45 expression in mice treated with  $1 \times 10^5$  PαS MSC when compared with controls ( $2.198 \pm 0.947$  vs  $2.289 \pm 0.265$ ), but a significant increase in CD45 expression when mice were treated with  $2 \times 10^5$  MSC ( $2.198 \pm 0.947$  vs  $3.432 \pm 1.073$ ,  $p=0.026$ )  $n=33$ . Slides were captured using a Zeiss AxioScanner. Between 5 and 10 images were taken from each scan to cover the whole slide and quantification of each image was performed using Image J software. Bars represent median values and lines represent the range. Statistical analysis was carried out using a one way ANOVA and multiple comparison testing was undertaken.

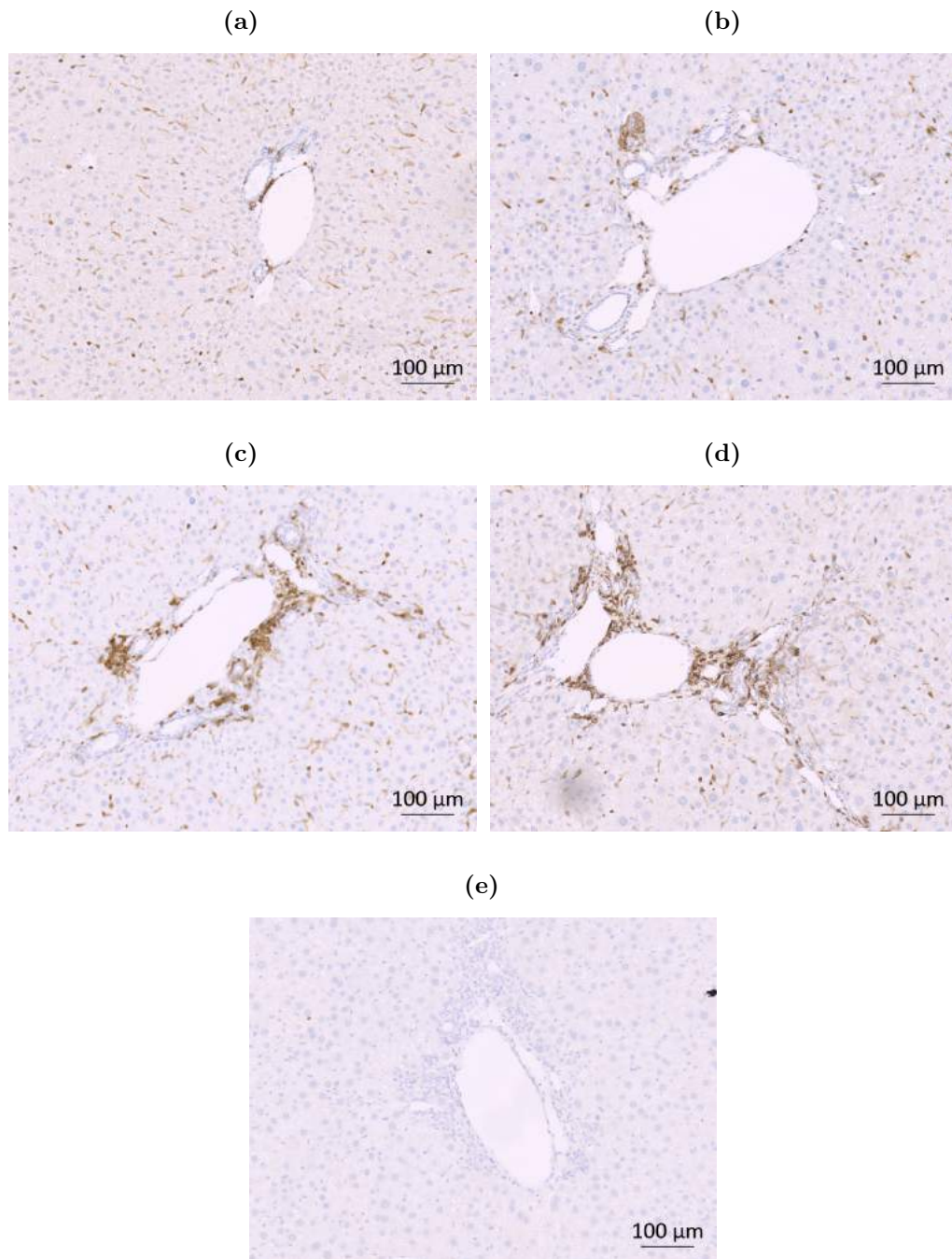


**Figure 4.13 – Representative images of CD45 staining in MDR2<sup>-/-</sup> mice treated with either PBS or PαS MSC at 6-8 weeks of age and culled 2 weeks later.** MDR2<sup>-/-</sup> mice aged between 6 and 8 weeks were treated with either 1x10<sup>5</sup> or 2x10<sup>5</sup> PαS MSC suspended in PBS with control animals receiving PBS alone. Mice were culled 2 weeks later and liver tissue was removed, processed and sectioned. Immunohistochemical staining was undertaken using a chromogenic technique. There were scattered CD45<sup>+</sup> cells distributed across all zones in the (a) uninjured FVB controls. Infiltrating CD45<sup>+</sup> cells were demonstrated showing a peri-portal (Zone I) distribution in (b) PBS treated controls, (c) mice treated with 1x10<sup>5</sup> PαS MSC IV and (d) mice treated with 2x10<sup>5</sup> PαS MSC IV. There was no staining seen in the (e) isotype matched controls. All images are generated from whole slide scans and are at 400x magnification. Scale bars represent 100 μm.

I next sought to quantify the liver macrophage population using the murine antigen F4/80. Staining was undertaken using an F4/80 antibody in order to delineate the hepatic macrophage population (figures 4.14, 4.15). MDR2<sup>-/-</sup> control animals showed a significant increase in F4/80 expression when compared to wild type FVB mice ( $4.257 \pm 0.896$  vs  $2.537 \pm 0.514$ ,  $p=0.0185$ ). Mice treated with  $1 \times 10^5$  P $\alpha$ S MSC showed a significant reduction in F4/80 expression when compared with control animals ( $4.257 \pm 0.896$  vs  $2.725 \pm 0.46$ ,  $p=0.0011$ ), as did those treated with  $2 \times 10^5$  P $\alpha$ S MSC ( $4.257 \pm 0.896$  vs  $2.322 \pm 0.235$ ,  $p=0.0006$ ).

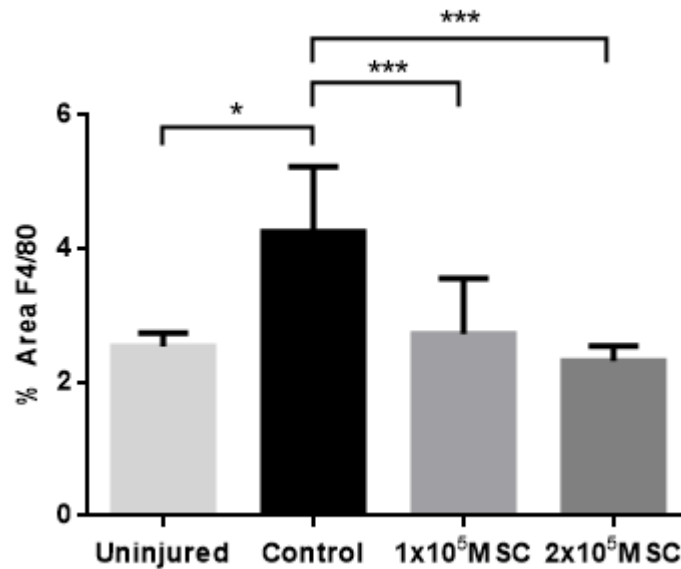


**Figure 4.14 – F4/80 expression in the livers of MDR2<sup>-/-</sup> mice treated with either PBS or P $\alpha$ S MSC at 6-8 weeks of age and culled 2 weeks later.** MDR2<sup>-/-</sup> mice aged between 6 and 8 weeks were treated with either  $1 \times 10^5$  or  $2 \times 10^5$  P $\alpha$ S MSC suspended in PBS with control animals receiving PBS alone. Mice were culled 2 weeks later. Immunohistochemical staining was undertaken using a chromogenic technique. Staining was undertaken using an F4/80 antibody in order to delineate the hepatic macrophage population. MDR2<sup>-/-</sup> control animals showed a significant increase in F4/80 expression when compared to wild type FVB mice ( $4.257 \pm 0.896$  vs  $2.537 \pm 0.514$ ,  $p=0.0185$ ). Mice treated with  $1 \times 10^5$  P $\alpha$ S MSC showed a significant reduction in F4/80 expression when compared with control animals ( $4.257 \pm 0.896$  vs  $2.725 \pm 0.46$ ,  $p=0.0011$ ), as did those treated with  $2 \times 10^5$  P $\alpha$ S MSC ( $4.257 \pm 0.896$  vs  $2.322 \pm 0.235$ ,  $p=0.0006$ )  $n=31$ . Slides were captured using a Zeiss AxioScanner. Between 5 and 10 images were taken from each scan to cover the whole slide and quantification of each image was performed using Image J software. Bars represent median values and lines represent the range. Statistical analysis was carried out using a one way ANOVA and multiple comparison testing was undertaken. Comparison between groups was undertaken using Student's t-test.



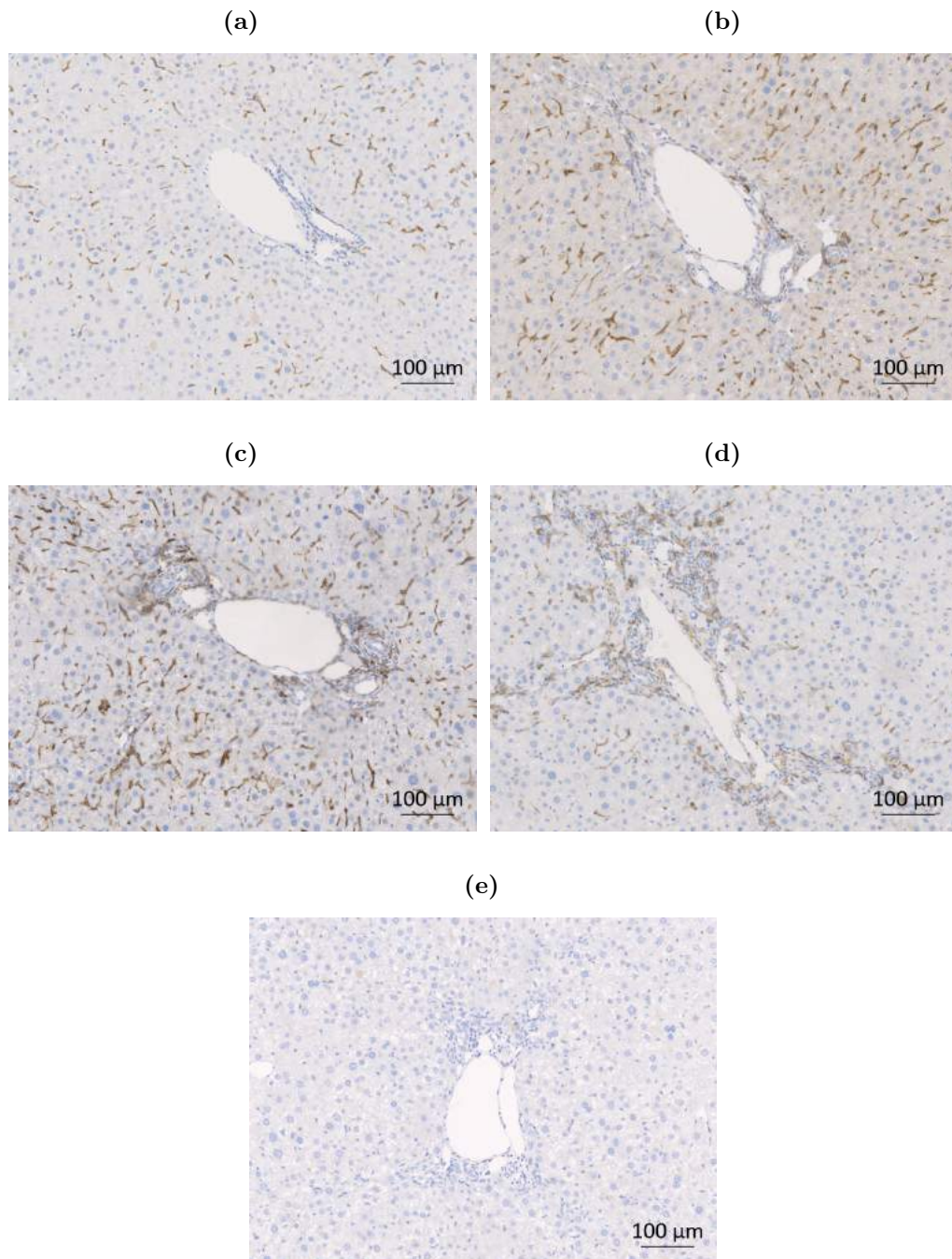


**Figure 4.15 – Representative images of F4/80 staining in MDR2<sup>-/-</sup> mice treated with either PBS or PαS MSC at 6-8 weeks of age and culled 2 weeks later.** MDR2<sup>-/-</sup> mice aged between 6 and 8 weeks were treated with either  $1 \times 10^5$  or  $2 \times 10^5$  PαS MSC suspended in PBS with control animals receiving PBS alone. Mice were culled 2 weeks later and liver tissue was removed, processed and sectioned. Immunohistochemical staining was undertaken using a chromogenic technique. There were scattered F4/80 cells distributed across all zones in the (a) uninjured FVB controls. Some infiltrating F4/80 cells were demonstrated showing a peri-portal (Zone I) distribution on a background of scattered F4/80 cells across all zones were seen in (b) PBS treated controls, (c) mice treated with  $1 \times 10^5$  PαS MSC IV and (d) mice treated with  $2 \times 10^5$  PαS MSC IV. There was no staining seen in the (e) isotype matched controls. All images are generated from whole slide scans and are at 400x magnification. Scale bars represent 100 μm.

In order to assess biliary proliferation I next sought to assess the distribution of CK19 expression. Antibody staining for CK19 was undertaken in selected sections in order to generate representative images of CK19 distribution (figure 4.16). Quantification was not undertaken as this was achieved by western blotting. Distribution of CK19 was limited to the ductular areas.

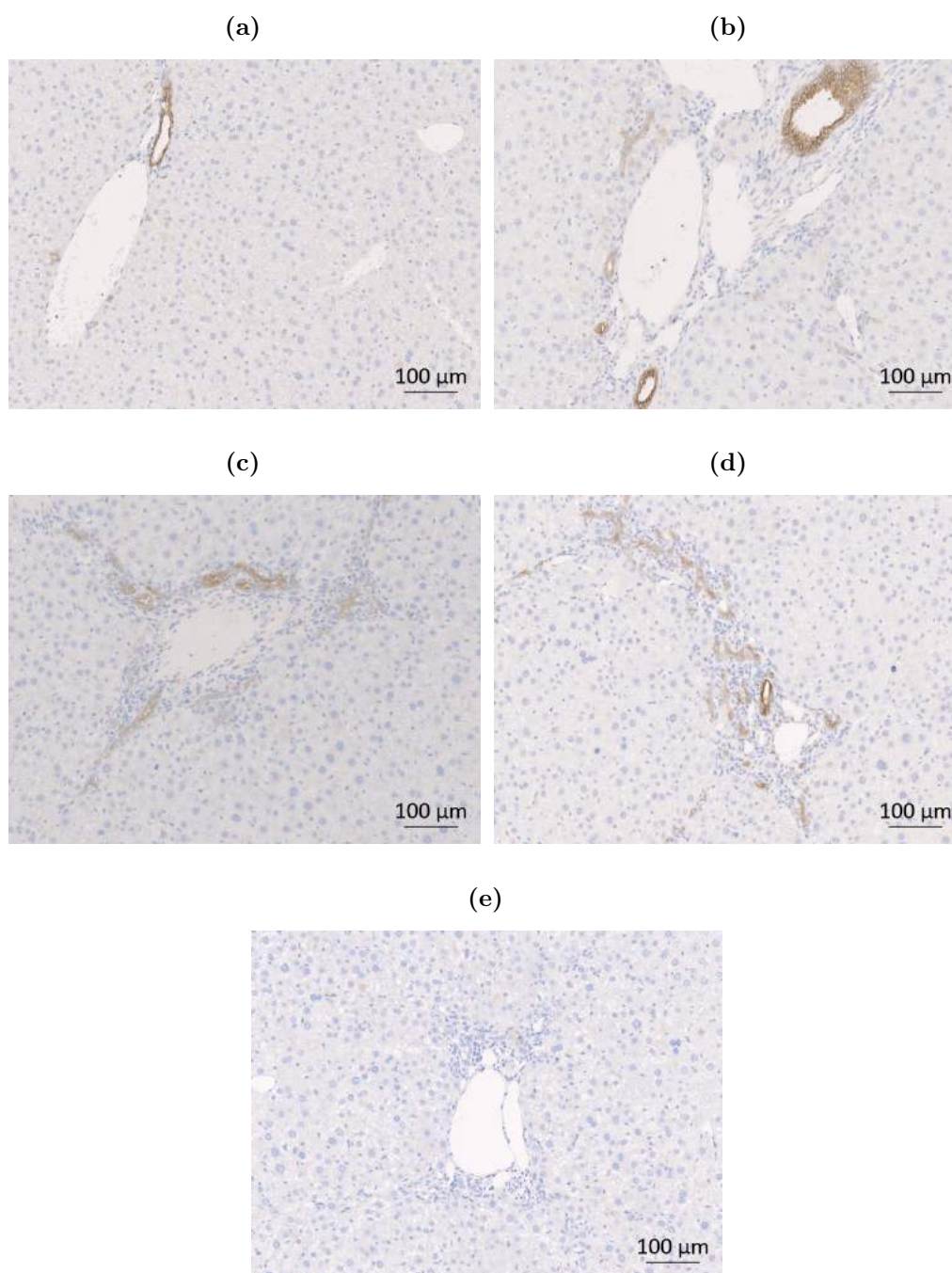


**Figure 4.16 – Representative images of CK19 staining in MDR2<sup>-/-</sup> mice treated with either PBS or PαS MSC at 6-8 weeks of age and culled 2 weeks later.** MDR2<sup>-/-</sup> mice aged between 6 and 8 weeks were treated with either 1x10<sup>5</sup> or 2x10<sup>5</sup> PαS MSC suspended in PBS with control animals receiving PBS alone. Mice were culled 2 weeks later and liver tissue was removed, processed and sectioned. Immunohistochemical staining was undertaken using a chromogenic technique. CK19 expression was demonstrated around the bile ducts in (a) uninjured FVB control, (b) PBS treated control, (c) mice treated with 1x10<sup>5</sup> PαS MSC IV and (d) mice treated with 2x10<sup>5</sup> PαS MSC IV. No staining was demonstrated in (e) isotype matched control. All images are generated from whole slide scans and are at 400x magnification. Scale bars represent 100 μm.



I next undertook western blotting for quantification of CK19 expression.

#### **4.2.3.3 Effects on ductular proliferation in MDR2<sup>-/-</sup> mouse livers when treated with PαS MSC**

In MDR2<sup>-/-</sup> knockout mice cytotoxic biliary injury leads to ductular proliferation. CK19 is a cytoskeletal protein present in biliary cells and is therefore a marker of bile duct proliferation and hence level of injury. CK19 quantification by western blotting is used in the literature to assess for the extent of injury in the MDR2<sup>-/-</sup> model [100].

Following treatment with PαS MSC mice were culled at 2 weeks and liver lobes removed and homogenised. Protein lysis and quantification was undertaken and then western blotting was performed using the lysed protein. A CK17/19 antibody was used for detection of CK19 and α-actinin was used as a loading control.

CK19 expression showed a significant increase between uninjured FVB mice and PBS treated MDR2<sup>-/-</sup> mice (p=0.018). There was also a significant dose dependent reduction in CK19 expression following treatment with PαS MSC (p=0.0185, n=40, figure 4.17).

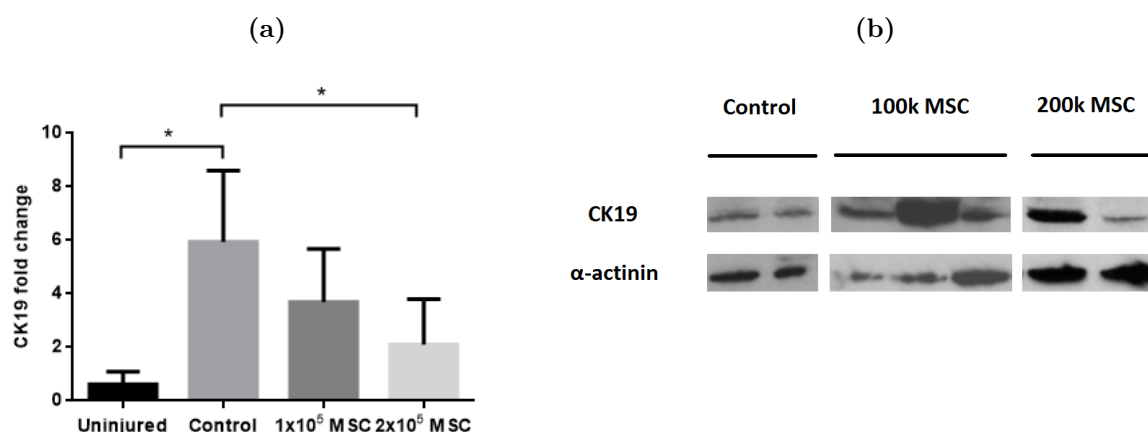


**Figure 4.17 – CK19 quantification by western blotting in MDR2<sup>-/-</sup> mice treated with PαS MSC.** MDR2<sup>-/-</sup> mice aged 6-8 weeks were treated with either 1x10<sup>5</sup> or 2x10<sup>5</sup> PαS MSC and then culled 2 weeks later. Liver lobes were removed and homogenised. Protein lysis and quantification was undertaken and then western blotting was performed using the lysed protein. A CK17/19 antibody was used for detection of CK19 and α-actinin was used as a loading control. Expression levels were normalised to loading controls and are expressed as fold change. (a) CK19 expression showed a significant increase between uninjured FVB mice and PBS treated MDR2<sup>-/-</sup> mice (p=0.018). There was also a significant dose dependent reduction in CK19 expression following treatment with PαS MSC (p=0.0185, n=40). (b) Representative western blots for CK19 expression are shown with loading controls below. Bars represent median values and lines represent the range. Statistical analysis was carried out using a Mann-Whitney U test and Kruskal-Wallis analysis due to the unequal variance and multiple comparison testing was undertaken.

I next sought to quantify the immune cell infiltration in MDR2<sup>-/-</sup> mouse livers by flow cytometry.

#### 4.2.3.4 Characterisation of immune cell populations in MDR2<sup>-/-</sup> mice following treatment with PαS MSC

In order to quantify the infiltrating immune cells in the livers of MDR2<sup>-/-</sup> mice I undertook flow cytometric analysis. Two weeks after treatment with PαS MSC liver lobes were removed, weighed and processed to allow flow cytometry to be performed. Single cell suspensions were stained with relevant antibodies including a live/dead marker. Cell counts were normalised to liver weight and presented as cells per gramme.

There was no difference in infiltrating CD45<sup>+</sup> cells (figure 4.18) between control animals, mice treated with 1x10<sup>5</sup> PαS MSC and mice treated with 2x10<sup>5</sup> PαS MSC (213224 cells/g

$\pm 76453$  vs  $204766$  cells/g  $\pm 105192$  vs  $219788$  cells/g  $\pm 101257$ ). This pattern was also true for  $CD4^+$  ( $69071$  cells/g  $\pm 44144$  vs  $34508$  cells/g  $\pm 14384$  vs  $70588$  cells/g  $\pm 42034$ ),  $CD8^+$  ( $23597$  cells/g  $\pm 16426$  vs  $9790$  cells/g  $\pm 5268$  vs  $27693$  cells/g  $\pm 16303$ ),  $CD19^+$  ( $50651$  cells/g  $\pm 22227$  vs  $36774$  cells/g  $\pm 8540$  vs  $45149$  cells/g  $\pm 29662$ ) and  $NK1.1^+$  ( $8750$  cells/g  $\pm 7612$  vs  $11432$  cells/g  $\pm 5203$  vs  $9001$  cells/g  $\pm 7078$ ) cells. There was however a significant increase in  $F4/80^+$  cells in mice treated with  $1 \times 10^5$  P $\alpha$ S MSC when compared with controls ( $16462$  cells/g  $\pm 4005$  vs  $30571$  cells/g  $\pm 21086$ ,  $p=0.0355$ ) but not when mice were treated with  $2 \times 10^5$  P $\alpha$ S MSC ( $16462$  cells/g  $\pm 4005$  vs  $12712$  cells/g  $\pm 4626$ ). Myeloid Derived Suppressor Cells (MDSC) delineated by  $CD11b$  and  $Gr1$  also followed this pattern with an increase following treatment with  $1 \times 10^5$  P $\alpha$ S MSC ( $13210$  cells/g  $\pm 8300$  vs  $30585$  cells/g  $\pm 18476$ ,  $p=0.0217$ ) but not when mice were treated with  $2 \times 10^5$  P $\alpha$ S MSC ( $13210$  cells/g  $\pm 8300$  vs  $9917$  cells/g  $\pm 3507$ ).

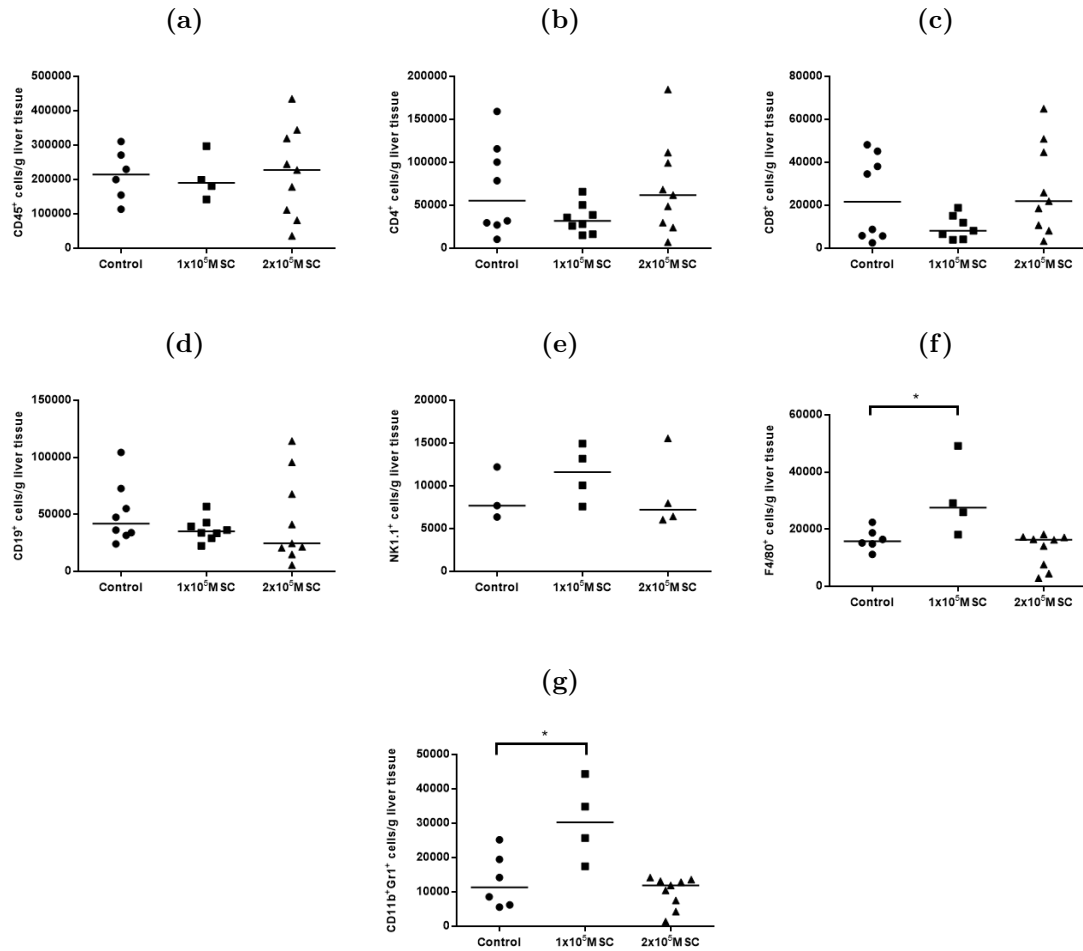


**Figure 4.18 – Flow cytometric analysis of immune cell infiltrates in the livers of MDR2<sup>-/-</sup> mice treated with PαS MSC.** Two weeks following treatment with PαS MSC liver lobes from MDR2<sup>-/-</sup> mice were removed, weighed and processed to allow flow cytometry to be performed. Single cell suspensions were stained with relevant antibodies including a live/dead marker. Cell counts were normalised to liver weight and presented as cells per gramme. There was no difference in infiltrating (a) CD45<sup>+</sup> (213224 cells/g  $\pm$  76453 vs 204766 cells/g  $\pm$  105192 vs 219788 cells/g  $\pm$  101257), (b) CD4<sup>+</sup> (69071 cells/g  $\pm$  44144 vs 34508 cells/g  $\pm$  14384 vs 70588 cells/g  $\pm$  42034) (c) CD8<sup>+</sup> (23597 cells/g  $\pm$  16426 vs 9790 cells/g  $\pm$  5268 vs 27693 cells/g  $\pm$  16303) (d) CD19<sup>+</sup> (50651 cells/g  $\pm$  22227 vs 36774 cells/g  $\pm$  8540 vs 45149 cells/g  $\pm$  29662) (e) NK1.1<sup>+</sup> (8750 cells/g  $\pm$  7612 vs 11432 cells/g  $\pm$  5203 vs 9001 cells/g  $\pm$  7078) cells between control animals, mice treated with 1x10<sup>5</sup> PαS MSC and mice treated with 2x10<sup>5</sup> PαS MSC. There was a significant increase in (f) F4/80 (16462 cells/g  $\pm$  4005 vs 30571 cells/g  $\pm$  21086,  $p=0.0355$ ) and (g) CD11b<sup>+</sup>Gr1<sup>+</sup> (13210 cells/g  $\pm$  8300 vs 30585 cells/g  $\pm$  18476,  $p=0.0217$ ) cells treated with 1x10<sup>5</sup> PαS MSC. Points represent individual mice and bars represent the median value. Statistical analysis was carried out using a one way ANOVA and multiple comparison testing was undertaken. Comparison between groups was undertaken using Student's t-test.

I next decided to examine a subset of regulatory immune cells in order to determine if

the reduction in ALT seen in treated mice was related to a regulatory effect rather than a change in absolute numbers of infiltrating immune cells. Mice aged 6-8 weeks old were treated with  $2 \times 10^5$  P $\alpha$ S MSC and liver lobes removed after 2 weeks. Antibody staining for regulatory cells was undertaken including intra-cytoplasmic staining for FoxP3.

Mice treated with P $\alpha$ S MSC (figure 4.19) showed no significant differences in their defensive macrophage (F4/80<sup>+</sup>CD11b<sup>+</sup>Ly6C<sup>+</sup>) and regulatory macrophage (F4/80<sup>-</sup>Ly6C<sup>-</sup>) populations (7571 cells/g  $\pm$  1178 vs 11867 cells/g  $\pm$  3726 and 176285 cells/g  $\pm$  85463 vs 187871 cells/g  $\pm$  89156). There was however a significant increase in the number of restorative macrophages (F4/80<sup>-</sup>CD11b<sup>+</sup>Ly6C<sup>+</sup>) when compared with controls (7630 cells/g  $\pm$  3758 vs 12597 cells/g  $\pm$  1848). There was no change in CD4<sup>+</sup>CD25<sup>+</sup>FoxP3<sup>+</sup> Tregs (5879 cells/g  $\pm$  764 vs 7870 cells/g  $\pm$  2856) or CD8<sup>+</sup>CD25<sup>+</sup>FoxP3<sup>+</sup> Tregs (3324 cells/g  $\pm$  1920 vs 3894 cells/g  $\pm$  2141).

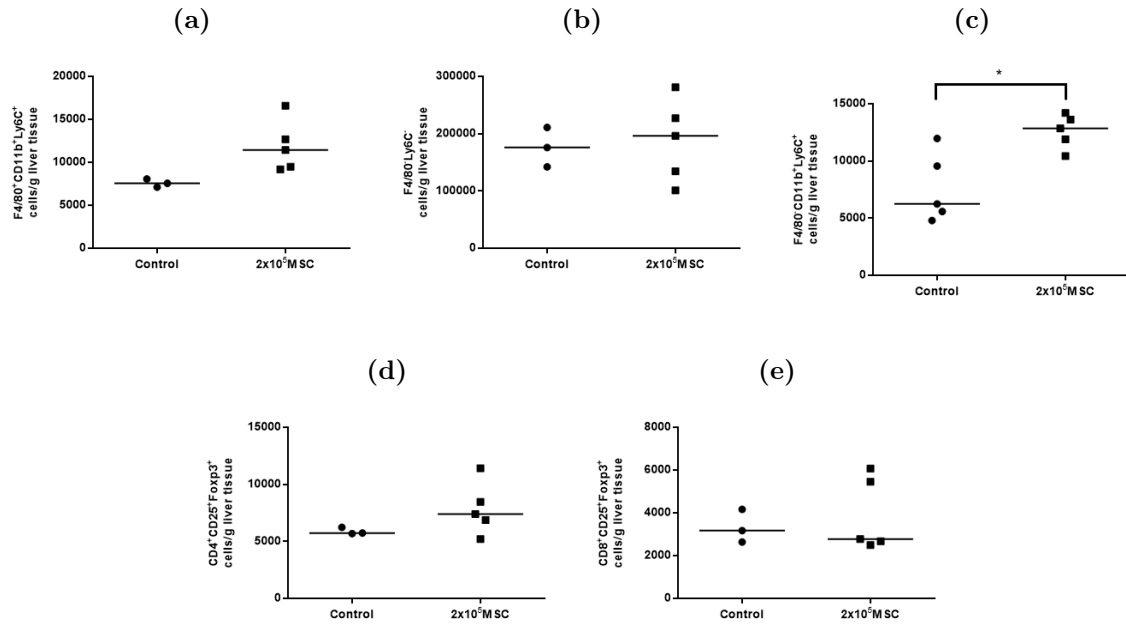


**Figure 4.19 – Flow cytometric analysis of regulatory immune cell infiltrates in the livers of MDR2<sup>-/-</sup> mice treated with P $\alpha$ S MSC.** MDR2<sup>-/-</sup> mice aged 6-8 weeks old were treated with 2x10<sup>5</sup> P $\alpha$ S MSC and liver lobes removed after 2 weeks. Antibody staining for regulatory cells was undertaken. Mice treated with P $\alpha$ S MSC showed no significant differences in their (a) defensive macrophage (F4/80<sup>+</sup>CD11b<sup>+</sup>Ly6C<sup>+</sup>) and (b) regulatory macrophage (F4/80<sup>+</sup>Ly6C<sup>-</sup>) populations (7571 cells/g  $\pm$  1178 vs 11867 cells/g  $\pm$  3726 and 176285 cells/g  $\pm$  85463 vs 187871 cells/g  $\pm$  89156). There was however a significant increase in the number of (c) restorative macrophages (F4/80<sup>-</sup>CD11b<sup>+</sup>Ly6C<sup>+</sup>) when compared with controls (7630 cells/g  $\pm$  3758 vs 12597 cells/g  $\pm$  1848). There was no change in (d) CD4<sup>+</sup>CD25<sup>+</sup>FoxP3<sup>+</sup> Tregs (5879 cells/g  $\pm$  764 vs 7870 cells/g  $\pm$  2856) or (e) CD8<sup>+</sup>CD25<sup>+</sup>FoxP3<sup>+</sup> Tregs (3324 cells/g  $\pm$  1920 vs 3894 cells/g  $\pm$  2141). Points represent individual mice and bars represent the median value. Statistical analysis was carried out using a Student's t-test.

I also analysed whole blood from MDR2<sup>-/-</sup> mice to assess the circulating immune cell populations. Red cells were lysed from whole blood and the remaining immune cells stained and analysed. Results are presented as cells per ml of whole blood.

A similar pattern to that in the liver was seen in whole blood with a significant increase in restorative macrophages (44105 cells/ml  $\pm$  158906 vs 91911 cells/ml  $\pm$  10841, p=0.0036). There was no difference in circulating defensive macrophages (3343 cells/ml  $\pm$  7015 vs 3314 cells/ml  $\pm$  818), regulatory macrophages (675527 cells/ml  $\pm$  444164 vs 876057 cells/ml  $\pm$  436793), CD4<sup>+</sup> Tregs (8818 cells/ml  $\pm$  6617 vs 10385 cells/ml  $\pm$  3808) or CD8<sup>+</sup> Tregs (2292 cells/ml  $\pm$  822 vs 3090 cells/ml  $\pm$  781).

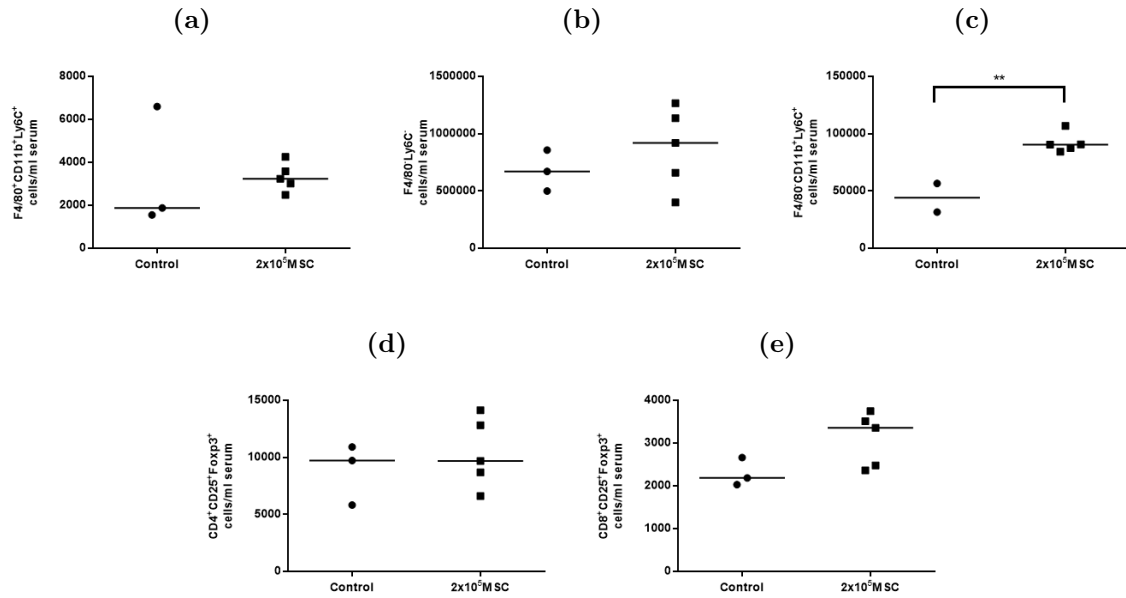


**Figure 4.20 – Flow cytometric analysis of circulating regulatory immune cells in MDR2<sup>-/-</sup> mice treated with PαS MSC.** MDR2<sup>-/-</sup> mice aged 6-8 weeks old were treated with 2x10<sup>5</sup> PαS MSC and culled after 2 weeks. Red cells were lysed from whole blood and the remaining immune cells stained and analysed. Results are presented as cells per ml of whole blood. There was no difference in circulating (a) defensive macrophages (3343 cells/ml ± 7015 vs 3314 cells/ml ± 818) or (b) regulatory macrophages (675527 cells/ml ± 444164 vs 876057 cells/ml ± 436793). There was a significant increase in (c) restorative macrophages (44105 cells/ml ± 158906 vs 91911 cells/ml ± 10841, p=0.0036). There was also no difference in (d) CD4<sup>+</sup> Tregs (8818 cells/ml ± 6617 vs 10385 cells/ml ± 3808) or (e) CD8<sup>+</sup> Tregs (2292 cells/ml ± 822 vs 3090 cells/ml ± 781). Points represent individual mice and bars represent the median value. Statistical analysis was carried out using a Student's t-test.

I also analysed the CD4<sup>+</sup>: CD8<sup>+</sup> ratio in both liver tissue and serum by looking at the ratio of cells analysed by flow cytometry (figure 4.21). In the liver tissue the CD4<sup>+</sup>: CD8<sup>+</sup> ratio showed a significant reduction (p=0.023) in the mice treated with 2x10<sup>5</sup> PαS MSC, whereas the serum ratio was not significantly different (P=0.17).

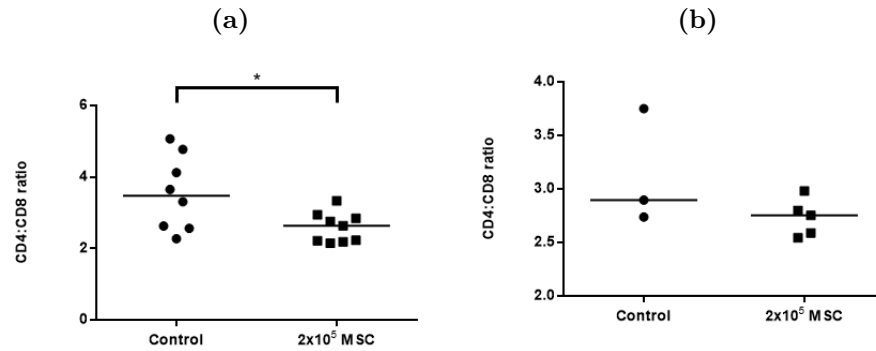


**Figure 4.21 – The CD4/CD8 ratio assessed by flow cytometry in the livers and whole blood of MDR2<sup>-/-</sup> mice aged 6-8 weeks old were treated with P $\alpha$ S MSC and culled after 2 weeks.** Liver lobes removed and antibody staining was undertaken. Red cells were lysed from whole blood and the remaining immune cells stained and analysed. (a) In the liver tissue the CD4/CD8 ratio showed a significant reduction ( $p=0.023$ ) in the mice treated with  $2 \times 10^5$  P $\alpha$ S MSC. (b) The whole blood CD4/CD8 ratio was not significantly different ( $P=0.17$ ) between treated and control mice. Points represent individual mice and bars represent the median value. Statistical analysis was carried out using a Student's t-test.



## 4.3 Discussion

The MDR2<sup>-/-</sup> model of liver injury has been extensively studied, however a lot of the work done uses this model as either a model of PSC or a model of hepatocellular carcinoma, as mice develop an inflammatory type hepatocellular carcinoma by 12 months of age [97, 276]. In this chapter I used the MDR2<sup>-/-</sup> model for its phenotypic similarities to biliary injuries seen more commonly after a DCD liver transplantation. One key undertaking in this chapter was to first characterise the injury pattern in the first 14 weeks in order to determine the time point most representative of DCD liver injury to enable translatable testing of MSC therapy.

### 4.3.1 Characterisation of the injury pattern MDR2<sup>-/-</sup> mouse model

Originally described by Smit [95] the disruption in biliary transport due to a modified P-glycoprotein in the MDR2<sup>-/-</sup> model was shown to cause portal expansion on histological examination and immune cell infiltration. There was also an increase in circulating bile acids. Work by Fickert et al expanded on the description of this model and demonstrated that it could also be used as a model of liver fibrosis and PSC [277].

#### 4.3.1.1 Classical markers of injury in the MDR2<sup>-/-</sup> mouse model

Analysis of the MDR2<sup>-/-</sup> model in the literature has focussed more on markers of hepatic fibrosis such as hydroxyproline levels and picosirius red staining. When immune cells have been examined it is usually by immunohistochemistry and limited to CD4<sup>+</sup> and CD8<sup>+</sup> cells. Fickert [98, 100] used ALT, ALP and serum bile acids as markers of liver injury in the MDR2<sup>-/-</sup> model and demonstrated that concentrations of ALT and ALP peak at 8 weeks of age and remain at a similar level for a further 4 weeks, with serum bile acids peaking at 2 weeks but remaining moderately raised at 8 weeks. I demonstrated a different pattern of serum markers with levels of ALT continuing to rise until 11 weeks and remaining high up to 14 weeks. ALT in this study at 8 weeks was 432.0 IU/ml  $\pm$  207.6, in keeping with

the 406 IU/ml  $\pm$  68 described by Fickert et al, however this continued to climb to a peak of 801 IU/ml  $\pm$  142.9 at 11 weeks. This difference could be explained by the paucity of published data looking at ALT beyond 8 weeks as when used as a model of fibrosis or hepatocellular carcinoma ALT is a less useful marker of disease progression. ALP followed the same pattern described in the published literature with a peak at 8-9 weeks. Serum bile acids also showed a different pattern demonstrating a rise between 7 and 8 weeks with a peak level at 11 weeks. In this study I did not look at time points earlier than 7 weeks, whereas Fickert et al had compared 2 and 4 week old mice. The levels demonstrated at 8 weeks were in keeping with those published.

Analysis of the morphological changes in liver architecture were reassuring in this study and demonstrated the same pattern of injury to that in the original description of the MDR2<sup>-/-</sup> model [95] with portal expansion and infiltration progressing as the mice aged. Immunohistochemical analysis of CD45 expression showed a significant reduction in expression from 7 weeks of age, with F4/80 expression showing no significant changes, again in keeping with published findings that immune cell infiltration is greater around 8 weeks.

Another marker utilised in the literature to demonstrate biliary proliferation is CK19. This intermediate filament forming protein is found in biliary endothelium and is increased in the MDR2<sup>-/-</sup> model. I demonstrated a significant increase in CK19 in the injured MDR2<sup>-/-</sup> mice when compared with wild type FVB mice, again in keeping with the published literature, however over the time course studied there was no significant difference in the levels observed. It is not surprising that the pattern of CK19 injury follows that of serum ALP and serum bile acids as these are all markers of biliary tract injury and regeneration.

#### **4.3.1.2 Liver immune cell profile in the MDR2<sup>-/-</sup> model**

Whilst histological analysis has been commonly used in the MDR2<sup>-/-</sup> model there is little published data using flow cytometry to assess total infiltrating immune cells. Arguably

flow cytometry allows for more accurate quantification of immune cells in mouse livers than immunohistochemistry alone. In this study I modified the usual technique carried out in our laboratory as after initial attempts using Lympholyte<sup>®</sup> as the density gradient to extract immune cells led to a considerably lower yield than expected. By changing to Optiprep<sup>™</sup> and reducing the total number of centrifugation steps I was able to reliably isolate significantly more immune cells per gramme of liver tissue. Whilst I have been successful in isolating immune cells from the livers of injured mice in other models of liver injury such as the OVA-Bil model it is possible that the nature of the MDR2<sup>-/-</sup> model, with fibrosis present from 4 weeks, does not lend itself to the use of Lympholyte<sup>®</sup>. As Lympholyte<sup>®</sup> is patented it is unclear as to what is contained in the gradient formulation and so further hypothesis testing is difficult. A further advantage of using Optiprep<sup>™</sup> was the ability to isolate other immune cells such as granulocytes.

I examined the levels of lymphocyte (CD4<sup>+</sup>, CD8<sup>+</sup> and CD19<sup>+</sup>) as well as natural killer cells (NK1.1<sup>+</sup>) in the livers of MDR2<sup>-/-</sup> mice between 7 and 11 weeks of age. When analysing the immune cell infiltration into the livers of MDR2<sup>-/-</sup> mice over time all cells examined showed a peak at 10 weeks and began to fall again at 11 weeks.

### **4.3.2 P $\alpha$ S MSC reduce markers of injury in the MDR2<sup>-/-</sup> model**

I decided on a systemic route of administration for to the P $\alpha$ S MSC in order test their efficacy in the MDR2<sup>-/-</sup> model based on previous experience and success with this route of administration in other mouse models [245]. Whilst other routes of administration have been published and are feasible intravenous administration is commonly used in the clinical environment and would be easily translatable.

#### **4.3.2.1 Timing and dose of P $\alpha$ S MSC**

Timing of MSC therapy is important, but also challenging. It is likely that after systemic administration MSC are trapped in capillary beds, in particular those in the pulmonary

circulation. It has been demonstrated that in the first 24 hours systemically administered MSC are trapped in the pulmonary capillary bed [278], however after 24 hours MSC appear to redistribute to other organs such as the liver and spleen [279]. This initial 'lung trap' is likely due to the size of cultured MSC being greater than the size of the pulmonary capillaries. Interestingly MSC cultured from humans, mice or other animals appear to be similar in size [280, 281]. It has also been demonstrated that MSC leave the circulation after 24 hours, suggesting that they exert their immunomodulatory effects by exerting a lasting effect on other intermediary cells [279], as the effects of systemic MSC therapy are seen long after this time period.

Given the profile of injury demonstrated in the MDR2<sup>-/-</sup> model in this chapter it is clear that the peak immune cell infiltration, and therefore the peak immune mediated injury occurs between 7 and 11 weeks of age, with markers of hepatocyte death greatest at 11 weeks. Based on these findings I decided to treat mice with PαS MSC between 6 and 8 weeks of age [167]. This would mean that cell therapy would be given as the immune mediated injury occurs. By analysing these mice 14 days later I would then be assessing injury at or close to the peak injury. Whilst it is likely that systemically administered MSC would have been cleared from the mouse, the lasting effects seen in other studies would likely still be present after the first 24 hours based on previous work that we have undertaken [237, 245], whilst giving enough time for those effects to be reflected in markers of liver injury.

Dose of MSC is also an important consideration and a wide range of doses have been employed in the literature with doses in human studies ranging from  $0.5 \times 10^6$  cells/kg to  $8.45 \times 10^8$  cells/kg [1]. It is also unclear if doses between species and even MSC isolated by different techniques are comparable, and given the relative differences in purity of cells achieved by different techniques it is reasonable to conclude that doses are not equivalent. With this in mind the only data to guide doses of PαS MSC available is that generated in our lab [237, 245]. Systemic administration of doses over  $5 \times 10^5$  leads to mortality due to embolic phenomena, and even at doses of  $5 \times 10^5$  occasional problems have been seen. I

decided to test doses of  $1 \times 10^5$  and  $2 \times 10^5$  rather than attempting to tailor dose to weight as this was logistically challenging and almost impossible to perform with any degree of accuracy. This equates to a dose of  $4 \pm 0.7 \times 10^6$  cells/kg and  $8 \pm 1.4 \times 10^6$  cells/kg respectively, doses in the middle and at the top of the dose ranges in human studies.

#### **4.3.2.2 Reduction in markers of liver injury with P $\alpha$ S MSC therapy**

Treatment of MDR2<sup>-/-</sup> mice with P $\alpha$ S MSC led to a significant reduction in ALT and ALP when a high dose was administered via the systemic route. The same was not seen in the lower dose group with no significant changes. As ALT was the primary outcome measure for this study it was encouraging to see a significant reduction following P $\alpha$ S MSC therapy. ALT is a predominantly intracellular enzyme whose concentration is high in the cytoplasm of hepatocytes so an increase in ALT is relatively specific for hepatocyte injury therefore the reduction seen in these experiments is indicative of a decrease in hepatocyte death. Since the half-life of ALT is 47 hours this reduction implies a prolonged action of P $\alpha$ S MSC therapy as the MDR2<sup>-/-</sup> model is a model that continues to develop injury through the study period as demonstrated. ALP is a transport enzyme with the ability to transport metabolites across the cell membrane. ALP is found in a large number of cell types but the greatest concentrations are found in liver and bone. By using mice with an FVB background problems seen with low hepatic production of ALP are not seen [274] and allow interpretation in the context of liver injury. The reduction in ALP in these experiments is suggestive of reduced biliary injury as ALP is found in the biliary endothelium and released when this is damaged. ALP has a longer half life than ALT and tends to remain raised as ALT resolves implying that the reduction in both these markers is due to a sustained effect of P $\alpha$ S MSC therapy. Serum bile acids were not reduced following P $\alpha$ S MSC therapy. Whilst other researchers have used bile acids as a marker of injury in the MDR2<sup>-/-</sup> model this may be inappropriate when assessing immune mediated damage. Excess bile acids occur in the MDR2<sup>-/-</sup> model due to a mutation of a biliary transporter and leads to immune system activation. Suppressing the immune system

should therefore have no effect on serum bile acid concentration. Bile acids are involved in normal signalling pathways for cholesterol metabolism at physiological concentrations by activating the intestinal farnesoid X receptor and intestinal fibroblast growth factor 15 which culminates in the inhibition of CYP7A1 [282]. However at pathological levels bile acids have been shown to drive inflammation and recruit neutrophils into the liver [283]. Whilst reduction in ALT and ALP are an important marker of reduced liver injury the ongoing stimulus in this model is still present and confirmed by the lack of a change in bile acid levels.

The cytokeratin CK19 has been used as a marker of biliary proliferation and hence injury in the MDR2<sup>-/-</sup> model [100] with lower levels representing less injury. In this study there was a significant reduction in CK19 levels with P $\alpha$ S MSC therapy. As a marker of biliary injury the levels of CK19 do not reflect the damage seen in other parts of the liver. I have established that CK19 is localised to the biliary epithelium through chromogenic immunohistochemistry and as such it is the most sensitive marker used for isolated biliary injury. However I have already demonstrated that injury in the MDR2<sup>-/-</sup> model is not confined to the biliary tree and therefore P $\alpha$ S MSC therapy may reduce immune mediated parenchymal and biliary injury in this model.

#### **4.3.2.3 Changes in infiltrating immune cells in MDR2<sup>-/-</sup> mouse livers**

In this study I assessed levels of immune cells in the livers of MDR2<sup>-/-</sup> mice using traditional techniques published in the MDR2<sup>-/-</sup> literature (immunohistochemistry for CD45 and F4/80 expression) as well as flow cytometric analysis of liver tissue. Analysis of CD45 expression showed a significant increase when assessed by immunohistochemistry which was not the case when flow cytometry was used. Whilst an unchanged CD45 expression level can be explained by changes in the ratio of cell types or their function rather than absolute numbers as CD45 is a pan-leucocyte marker, an increase in CD45 expression is not in keeping with the earlier findings that P $\alpha$ S MSC therapy reduces liver injury. The changes in CD45 expression assessed by flow cytometry seem to only be present when therapy

is undertaken with  $1 \times 10^5$  P $\alpha$ S MSC and not when mice were treated with  $2 \times 10^5$  P $\alpha$ S MSC. Flow cytometric analysis demonstrated a significant increase in F4/80 expression with  $1 \times 10^5$  P $\alpha$ S MSC whereas analysis of immunohistochemistry however demonstrated a significant reduction in F4/80 expression. Neutrophil count was also increased in mice treated with  $1 \times 10^5$  P $\alpha$ S MSC. The discrepancies found between the flow cytometric analysis and the immunohistochemical analysis are difficult to explain by a biologically plausible mechanism. In theory flow cytometry should be a more accurate technique for quantifying immune cells, however in this study there were difficulties with optimising the technique to isolate immune cells from MDR2<sup>-/-</sup> livers. The technique for isolating immune cells was also very time consuming and as such proved logistically challenging. This meant that n numbers for flow cytometry were considerably lower than those for immunohistochemistry (n=10-20 vs n=33). It is possible that there is a threshold effect for P $\alpha$ S MSC whereby too few cells can lead to a different effect than the correct treatment dose. Indeed mesenchymal precursor cells, a subset of MSC have been shown to increase myocardial remodelling at lower concentrations when compared with higher concentrations or control [284]. This may explain the increase in neutrophil and macrophage numbers in the lower dose group, however it does not explain the discrepancy between the flow cytometric and immunohistochemical analysis of F4/80 and CD45 expression.

It is possible that the beneficial effects of P $\alpha$ S MSC cannot be described in terms of immune cell numbers as MSC have been shown to alter function as well as proliferation. A change of lymphocyte phenotype has been described in the literature with MSC driving CD4<sup>+</sup> lymphocytes into an anti-inflammatory state [163]. Interestingly the CD4/CD8 ratio significantly decreased following treatment with P $\alpha$ S MSC. The CD4/CD8 ratio has primarily been used in patients with HIV infection as in the chronic phase it gives a better indication of disease status than CD4<sup>+</sup> cell count alone, and in the context of treated HIV a low count is predictive of all cause mortality [285]. The CD4/CD8 ratio has also been suggested as a prognostic factor in fibrotic liver disease secondary to hepatitis C virus infection with a low level being associated with a greater degree of fibrosis [286].

Whilst viral illness appears to reduce the CD4/CD8 ratio, primarily due to a reduction in CD4 count and an increase in CD8 count, in this study the CD4/CD8 ratio never fell below the usual accepted threshold level of 1.5. Despite this being a relative reduction it potentially highlights a move towards a regulatory phenotype and away from a cytotoxic phenotype which supports the hypothesis that P $\alpha$ S MSC reduce injury by changing the function, rather than absolute numbers of immune cells. Further work would need to be done to validate the CD4/CD8 ratio in the context of non-viral liver disease.

The analysis of regulatory immune cells in a subset of experiments showed an increase in both infiltrating and circulating restorative macrophages (F4/80<sup>-</sup>CD11b<sup>+</sup>Ly6C<sup>+</sup>). This finding may support the immunohistochemical analysis that F4/80 cells are reduced in the treated groups as restorative macrophages do not express F4/80 and so a global reduction in expression may be seen if more F4/80<sup>+</sup> monocytes are converted into F4/80<sup>-</sup> restorative macrophages. In acute liver injury circulating pro-inflammatory monocytes infiltrate the liver and eventually mature into a restorative phenotype. These pro-inflammatory monocytes release inflammatory cytokines, whereas the restorative macrophages have a positive effect on recovery from injury and this change in phenotype of monocyte populations could explain the reduction in markers of liver injury following P $\alpha$ S MSC therapy. In a previous chapter I have demonstrated that P $\alpha$ S MSC exposed to an inflammatory environment greatly increase their secretion of Il-10, a cytokine which has anti-inflammatory properties and has been shown to support the generation of restorative macrophages [263]. In models of paracetamol induced liver injury depletion of Ly6C<sup>+</sup> monocytes leads to a worse injury phenotype [287]. The increase in infiltrating neutrophils seen in the lower dose group, whilst seemingly inconsequential in terms of markers of liver injury, may represent a marker of the change in balance of infiltrating and circulating monocytes as infiltrating Ly6C<sup>+</sup> monocytes have been shown to regulate neutrophil recruitment to injured liver [287]. The balance of pro and anti-inflammatory monocyte populations may be dependent on the number of P $\alpha$ S MSC present. Further work would need to be done in order to assess cytokine profiles *in vivo* to see if this hypothesis is born



out.

### 4.3.3 Chapter summary

In this chapter I demonstrated that the MDR2<sup>-/-</sup> model in our institution is a viable and reproducible model of immune cell mediated liver injury. The model shows the same serological and histological pattern of injury to those published, however I have examined markers of hepatocyte injury and immune cell infiltration over a longer time period than usually published. This has enabled me to confirm that the peak injury period for hepatocytes and biliary cells is between 7 and 11 weeks. I have also optimised the isolation of immune cells from MDR2<sup>-/-</sup> mouse livers and used flow cytometry to quantify the infiltrating immune cell populations, demonstrating a peak immune cell infiltration at 10 weeks which rapidly falls by 11 weeks.

Treatment of MDR2<sup>-/-</sup> mice with systemically administered P $\alpha$ S MSC led to a significant reduction in ALT and ALP with bile acids remaining unchanged and CK19 expression was significantly reduced in the treated mice when assessed by western blotting. The immune cell profile in P $\alpha$ S MSC treated mice was difficult to illicit with differences found between immunohistochemical and flow cytometric analysis of these cells. It is likely that global F4/80 expression is significantly reduced, whereas the number of restorative macrophages found in the liver and the serum are significantly increased. Taken together these findings suggest a role for MSC therapy in cholestatic immune mediated liver injury.

## CHAPTER 5

# THE DISTRIBUTION AND REMOTE ACTION OF P $\alpha$ S MSC

### 5.1 Chapter introduction and aims

I have demonstrated the isolation and culture of P $\alpha$ S MSC from murine bone marrow, as well as the ability of P $\alpha$ S MSC to develop an immunomodulatory phenotype followed exposure to a pro-inflammatory micro-environment. I have also demonstrated that intravenous administration of P $\alpha$ S MSC in the MDR2<sup>-/-</sup> model of liver injury leads to a reduction in markers of liver injury. In this chapter I aim to examine the distribution of P $\alpha$ S MSC administered via the intravenous route and to investigate the ability of P $\alpha$ S MSC administered by the subcutaneous route to exert remote immunomodulatory effects.

#### 5.1.1 Distribution of parenterally administered mesenchymal stem cells

There have been varying routes of administration tested when using MSC as a cell therapy. Due to its clear advantage as a translatable route of administration intravenous infusion is a commonly studied route. Bio-distribution of MSC following intravenous infusion is an important consideration both due to its implications when studying mechanism of action, but also as it is a requirement to demonstrate bio-distribution when seeking approval for clinical trials.

Human MSC have been demonstrated to become trapped in the lungs after systemic administration in mouse models [288], with less than 0.1% of cells found in other organs at 48 hours. Tracking MSC in this study was limited by its use of PCR methods and so the resolution was limited to 100 cells. Studies have been undertaken on systemically administered murine MSC and have again demonstrated trapping in the lungs at 24 hours [278]. This study demonstrated that in cardiac injury more cells migrate to the heart, but the majority are still trapped in the lungs. MSC levels in other organs remained low. It has also been demonstrated that murine MSC are rapidly eliminated from mice after systemic administration with the majority of cells disappearing after 24 hours [279]. However when administered to immunocompromised mice MSC appear to persist for a number of weeks [289], although different imaging techniques have been used in all of these studies and different types of MSC have been tested and this may account for the differences seen. Whilst a variety of techniques have been used to study the bio-distribution of systemically administered MSC the resolution and quantification techniques are limited. As yet no research exists on the bio-distribution of systemically administered P $\alpha$ S MSC.

### **5.1.2 Remote effects of mesenchymal stem cells**

MSC as a therapy have been studied in a number of disease states due to their ability to exert their effects on a broad range of immune cells. Whilst a large number of mechanistic studies have been undertaken, due to the broad range of effects it is not clear whether MSC need to be located in the area in which they are to exert their effect or whether they are able to communicate with circulating immune cells and exert their effects through an intermediary cell type. In models of cardiac injury human MSC have been shown to become trapped in the lungs after systemic infusion with in the first 24 hours and exert their effects remotely [288]. It has been demonstrated that murine bone marrow derived MSC can exert their effects via a remote action in a model of graft versus host disease [155], and it has been suggested that subcutaneous injection either with or without encapsulation in a carrier such as alginate may improve the ability of MSC to suppress

immune mediated injury. Study into different sites of intravascular administration in rat models of acute liver failure have demonstrated increased numbers of MSC present in the liver when injection is performed by the hepatic artery, however there was no difference in outcome suggesting that MSC do not need to be at the site of injury to exert their effects [290]. So far there have been limited numbers of studies demonstrating remote effects of MSC when administered by the subcutaneous route and the studies that have been performed seem to be limited to systemic disease such as graft versus host disease. There have been no studies looking at the the remote effects of P $\alpha$ S MSC or subcutaneous administration of these cells.

### 5.1.3 Specific chapter aims

The previous findings have demonstrated that P $\alpha$ S MSC given systemically can lead to a reduction in liver injury in the MDR2<sup>-/-</sup> model. The aims of this chapter are to establish a system to track systemically administered P $\alpha$ S MSC and to test the ability of P $\alpha$ S MSC to exert immunomodulatory effects remotely by subcutaneous injection. The specific aims of this chapter were:

1. To establish and optimise a high resolution method of tracking systemically administered P $\alpha$ S MSC in mice
2. To characterise the distribution of systemically administered P $\alpha$ S MSC in the MDR2<sup>-/-</sup> model over time
3. To test the *in vivo* efficacy of P $\alpha$ S MSC administered subcutaneously in the MDR2<sup>-/-</sup> model

## 5.2 Results

### 5.2.1 *In vivo* tracking of systemically administered P $\alpha$ S MSC

Whilst I have demonstrated that systemically administered P $\alpha$ S MSC can decrease markers of liver injury in the MDR2<sup>-/-</sup> model it is not clear if these cells need to be located in the liver in order to exert their effects. In order to track systemically administered P $\alpha$ S MSC I decided to use a novel block face cryoimaging system which enables the generation of whole mouse images at microscopic resolution [291, 292].

#### 5.2.1.1 The effects of QDot<sub>605</sub> staining on P $\alpha$ S MSC

In order to highlight P $\alpha$ S MSC during processing cells were labelled with QDot<sub>605</sub> prior to injection into MDR2<sup>-/-</sup> mice. I first set out to ensure that QDot<sub>605</sub> would adequately label P $\alpha$ S MSC and to assess the effect that labelling may have on cell survival.

P $\alpha$ S MSC were culture expanded to passage 4 and then stained with QDot<sub>605</sub> as well as a live/dead marker. As quantum dots are an intra-cytoplasmic stain and rely on a carrier to cross the cell membrane, and live/dead staining works on the principle of membrane disruption during cell death to allow positive staining in dead cells, I tested live/dead staining alone and in conjunction with QDot<sub>605</sub> to test if there was any effect on the live/dead stain. There appeared to be no difference between any of the groups with a greater than 95% viability meaning that QDot<sub>605</sub> did not appear to give false positive results when assessing viability using an intra-cytoplasmic live/dead marker, regardless of whether cells were first stained with QDot<sub>605</sub> or the live/dead marker (figure 5.1a). I then proceeded to look at the viability of the cells stained with QDot<sub>605</sub> and in particular ensure dead cells would stain for QDot<sub>605</sub> and a live/dead marker. Four groups of 2x10<sup>5</sup> P $\alpha$ S MSC were stained with QDot<sub>605</sub> and then a live/dead marker. Overall viability of QDot<sub>605</sub> stained cells was 89.57%  $\pm$  10.42 (figure 5.1b). As the percentage of dead cells was low in this series of experiments I decided to confirm that it was possible to accurately identify dead cells using a live/dead marker when staining with QDot<sub>605</sub>. I induced cell

death by heating  $2 \times 10^5$  P $\alpha$ S MSC in a water bath at 40°C for 30 minutes. I then mixed these cells with fresh, live cells and followed the previously described staining protocols. Cell viability was 66% with 95% of live cells and 92% of dead cells staining positive for QDot<sub>605</sub> (figure 5.1c). As my previous analysis of the effects of P $\alpha$ S MSC was carried out over a two week time course I next sought to assess the extent of QDot staining over time. In order to do so I carried out the staining protocol as previously with  $5 \times 10^5$  cells stained and analysed immediately and  $5 \times 10^5$  cells plated onto a T75 culture flask without the addition of a live/dead stain and cultured for 7 days. At day 7 cells were removed and stained with a live/dead marker and analysed. There was a small reduction in the percentage of live QDot positive cells from 98% to 92% but I deemed this an acceptable attrition rate in the context of these experiments.

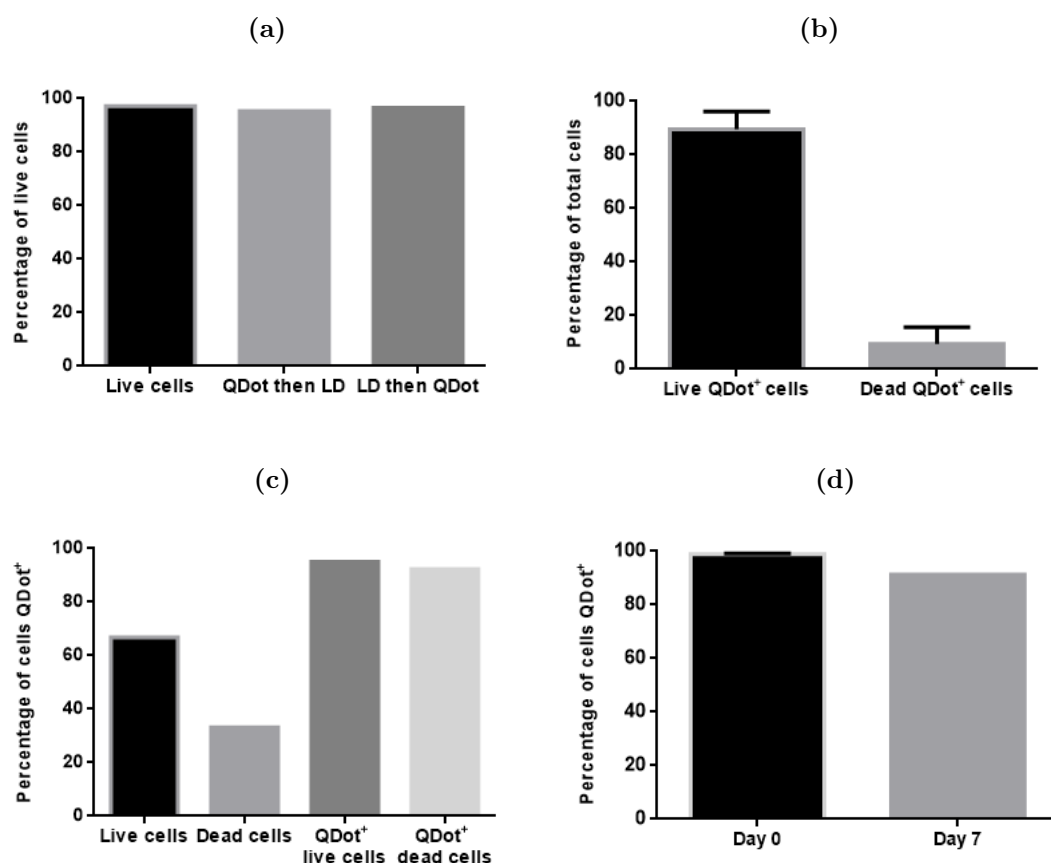


**Figure 5.1 – QDot<sub>605</sub> staining of P $\alpha$ S MSC demonstrates no effect on viability and a small reduction in intensity over a 7 day period.** P $\alpha$ S MSC were cultured to passage 4 and then stained with a live/dead marker with some also being stained with QDot<sub>605</sub>. (a) There was no effect on viability or QDot staining when cells were stained with QDot<sub>605</sub> first or the live/dead marker when compared with cells only stained with a live/dead marker (n=3). (b) Average viability of QDot<sub>605</sub> stained cells was high at 89.57%  $\pm$  10.42 (n=4). (c) Following induced cell death using a water bath set at 60°C for 30 minutes an equal mixture of cells showed a viability of 66% with 95% of live cells and 92% of dead cells staining positive for QDot<sub>605</sub> (n=4). (d) After 7 days in culture following QDot<sub>605</sub> staining 5x10<sup>5</sup> cells demonstrated a small reduction in the percentage of live QDot<sub>605</sub> positive cells from 98% to 92% (n=5). Bars represent median values and lines represent the range.

#### 5.2.1.2 Tracking QDot<sub>605</sub> labelled P $\alpha$ S MSC in the MDR2<sup>-/-</sup> model of liver injury

Having already demonstrated a reduction in liver injury in the MDR2<sup>-/-</sup> model I next sought to track QDot<sub>605</sub> labelled P $\alpha$ S MSC following intravenous injection into the tail vein in order to assess their distribution. In order to calibrate the CryoViz<sup>TM</sup> image analysis software I first needed to ensure I could visualise labelled P $\alpha$ S MSC in individual

organs. Male MDR2<sup>-/-</sup> mice aged 8 weeks old were culled and organs removed by careful dissection. 1x10<sup>5</sup> PαS MSC labelled with QDot<sub>605</sub> were injected into *ex-vivo* lungs, liver, spleen and heart and organs then embedded in OCT and frozen to -80°C. Sectioning and image reconstruction was undertaken by BioInVision Inc (<http://www.bioinvision.com>). Cells were visible in all organs and automatic quantification of cells injected into lung gave a value of 73742 (figure 5.2) which was felt to be an accurate reading in the context of these experiments.

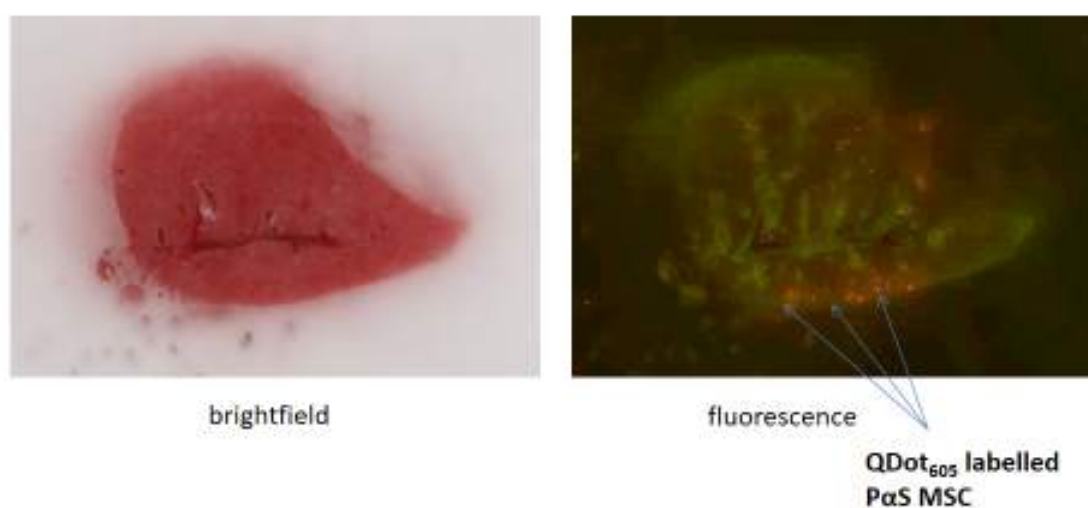


**Figure 5.2 – Representative bright field and fluorescent images of QDot<sub>605</sub> labelled PαS MSC injected *ex-vivo* into MDR2<sup>-/-</sup> lung tissue.** Male MDR2<sup>-/-</sup> mice aged 8 weeks old (n=1) were sacrificed and organs removed by careful dissection. 1x10<sup>5</sup> PαS MSC labelled with QDot<sub>605</sub> were injected *ex-vivo* into explanted lungs. The organ was then embedded in OCT and frozen to -80°C using dry ice. Sectioning and image reconstruction was undertaken by BioInVision Inc (<http://www.bioinvision.com>) using the CryoViz<sup>TM</sup> system. Samples were used for calibration of the imaging system. Cells were visible in all organs and automatic quantification of cells injected into lung gave a value of 73742. Representative paired bright field and fluorescence images from the CryoViz<sup>TM</sup> system are shown with green fluorescence demonstrating liver tissue and red/orange staining highlighting QDot<sub>605</sub> labelled PαS MSC.



I next sought to examine the location of P $\alpha$ S MSC following systemic administration and whether this distribution changes over time. Male 8 week old MDR2<sup>-/-</sup> mice were injected into the tail vein with 1x10<sup>5</sup> passage 4 QDot<sub>605</sub> labelled P $\alpha$ S MSC. Mice were culled at different time points and examined using the CryoViz<sup>TM</sup> imaging system. Whole mouse sectioning and imaging in both bright field and fluorescent microscopy was undertaken and computerised 3 dimensional reconstructions were created. Automatic quantification was undertaken by the CryoViz<sup>TM</sup> system. Representative images are included (figure 5.3).

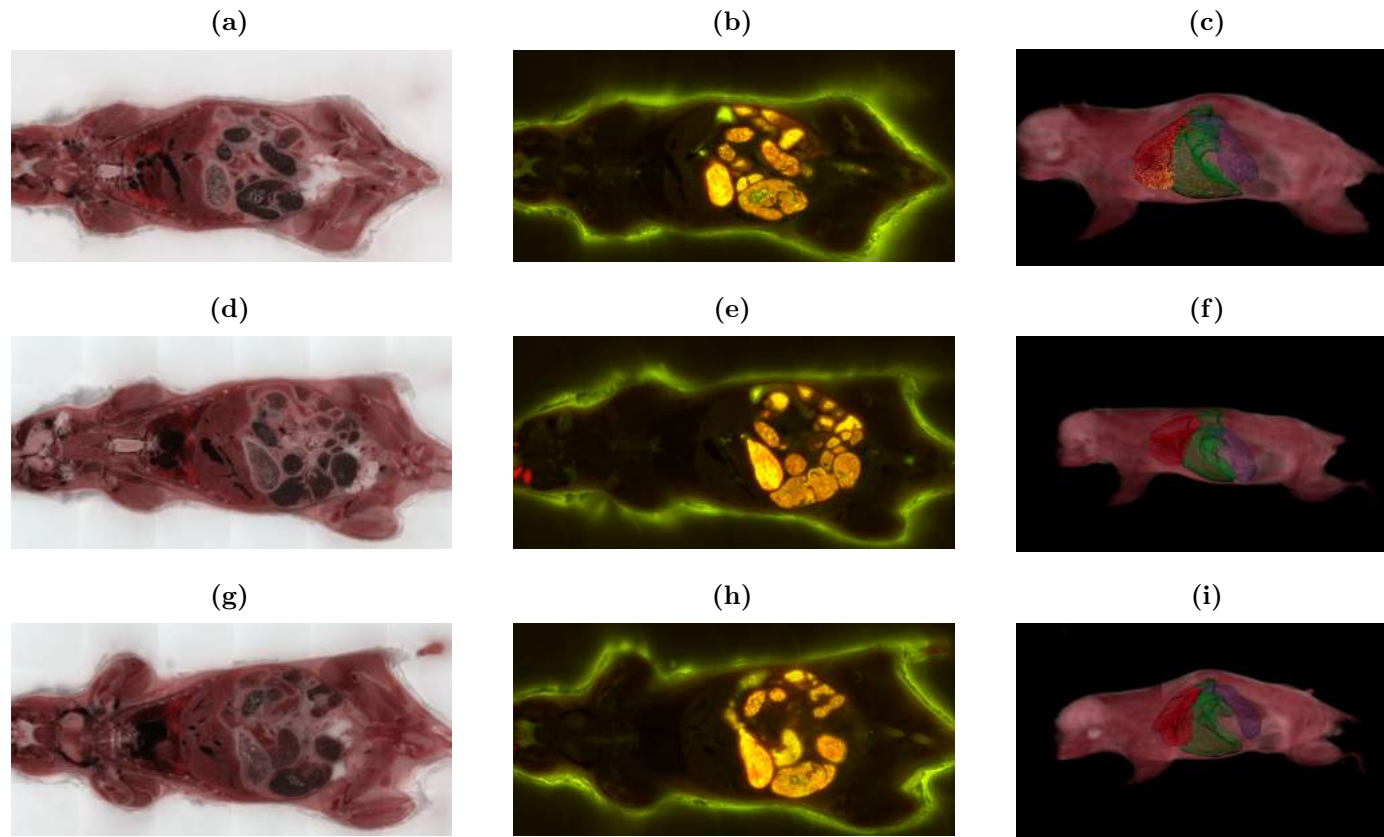


**Figure 5.3 – Representative images from whole mouse CryoViz™ imaging showing bright field, fluorescent and 3 dimensional reconstructions in MDR2<sup>-/-</sup> mice injected with QDot<sub>605</sub> labelled PαS MSC.** Male 8 week old MDR2<sup>-/-</sup> mice were injected into the tail vein with  $1 \times 10^5$  passage 4 QDot<sub>605</sub> labelled PαS MSC. Time points including 1 hour, 1 day, 3 days and 7 days were investigated (n=12). Whole mouse sectioning in 40  $\mu$ m sections and imaging in both bright field and fluorescent microscopy was undertaken and computerised 3 dimensional reconstructions were created. Automatic quantification was undertaken by the CryoViz™ system. Images of (a) 1 hour bright field, (b) 1 hour fluorescent, (c) 1 hour 3 dimensional reconstruction, (d) 24 hour bright field, (e) 24 hour fluorescent, (f) 24 hour 3 dimensional reconstruction, (g) 72 hour bright field, (h) 72 hour fluorescent, and (i) 72 hour 3 dimensional reconstruction are included. Representative paired bright field, fluorescence and 3 dimensional reconstructions are shown. Lungs are highlighted in red, liver green and spleen blue with QDot<sub>605</sub> labelled PαS MSC highlighted in yellow.

At 1 hour following injection there were a total of 8146 cells  $\pm$  4693 detectable in the MDR2<sup>-/-</sup> mice (table 5.1). Over the course of the experiment detectable P $\alpha$ S MSC declined rapidly with only 688.3 cells  $\pm$  439.8 at 24 hours and 494.7 cells  $\pm$  545.3 at day 7 (table 5.1, figure 5.4).

Sample		Global	Lung	Liver	Spleen
1 Hour	1	10,325	7,452	2,321	87
	2	6,964	4,467	1,544	12
	3	7,149	5,466	1,247	4
1 Day	1	509	184	181	25
	2	693	178	100	130
	3	863	123	369	41
3 Day	1	139	4	20	4
	2	1,046	70	395	14
	3	887	15	365	22
7 Day	1	289	144	49	0
	2	469	166	229	2
	3	726	41	264	32

**Table 5.1 – Quantification of QDot<sub>605</sub> labelled P $\alpha$ S MSC in different organs following tail vein injection into MDR2<sup>-/-</sup> mice.** Male 8 week old MDR2<sup>-/-</sup> mice were injected into the tail vein with  $1 \times 10^5$  passage 4 QDot<sub>605</sub> labelled P $\alpha$ S MSC. Mice were culled at different time points and examined using the CryoViz<sup>TM</sup> imaging system (n=12).

Following injection of P $\alpha$ S MSC there was a rapid decline in all organs of QDot<sub>605</sub> labelled cells during the first 24 hours, followed by a slower continuous decline over the 7 days studied (figure 5.4).

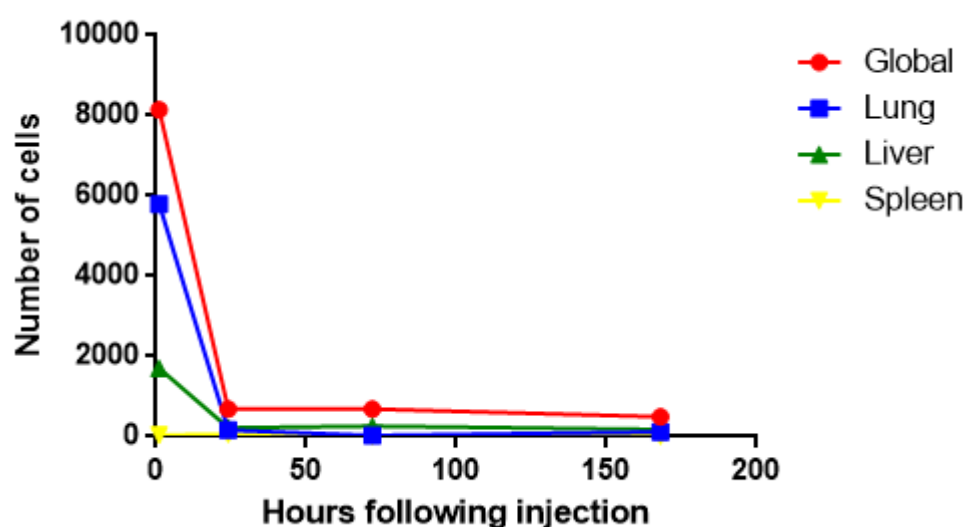


**Figure 5.4 – PαS MSC cell numbers decline rapidly in all organs following systemic administration in MDR2<sup>-/-</sup> mice.** Following injections with  $1 \times 10^5$  passage 4 QDot<sub>605</sub> labelled PαS MSC Male 8 week old MDR2<sup>-/-</sup> mice were culled at different time points and examined using the CryoViz™ imaging system (n=12). There was a rapid decline in all organs of QDot<sub>605</sub> labelled cells during the first 24 hours, followed by a slower continuous decline over across the 7 days studied. Each line represents the mean number of cells in each organ of 3 MDR2<sup>-/-</sup> mice. Point represent mean number of cells, red demonstrates the global number of QDot<sub>605</sub> labelled PαS MSC, blue represents cells found in the lungs, green the liver and yellow the spleen.

Whilst the total number of PαS MSC declines quickly following injection, as does the rate of decline of cells in the lungs the rate of decline of PαS MSC in the liver is 5 times lower in the first 24 hours (table 5.1a). During the subsequent 6 days the rate of decline is slower in all groups with the lungs and the liver declining 4 times sower than the total number of cells. The majority of cells appear to stay in the lungs during the first hour with 71.1% of cells being found in the lungs after 1 hour compared with just 20.9% of cells being found in the liver (table 5.1b). However at 24 hours only 23.5% of cells are found in the lungs, with 31.5% being found in the liver. This trend appear to be maintained over the 7 day period with a greater percentage of cells being found in the liver when compared with the lungs.

(a)

Location	Initial rate of decline (cells/day)	Rate of decline after 1 day (cells/day)
Whole mouse	7457	96
Lung	5633	18
Liver	1487	22
Spleen	31	27

(b)

Time point (hours)	Lung (%)	Liver (%)	Spleen (%)
1	71.1	20.9	0.4
24	23.5	31.5	9.5
72	4.3	37.6	1.9
168	23.7	26.4	2.3

**Table 5.2 – Tables demonstrating the rate of decline and percentages in different organs of P $\alpha$ S MSC when administered to MDR2<sup>-/-</sup> mice.** Male 8 week old MDR2<sup>-/-</sup> mice were injected into the tail vein with 1x10<sup>5</sup> passage 4 QDot<sub>605</sub> labelled P $\alpha$ S MSC. Mice were culled at different time points and examined using the CryoViz<sup>TM</sup> imaging system. (a) The total number of P $\alpha$ S MSC declines quickly following injection, as does the rate of decline of cells in the lungs the rate of decline of P $\alpha$ S MSC in the liver is 5 times lower in the first 24 hours. During the subsequent 6 days the rate of decline is lower in all groups with the lungs and the liver declining 4 times sower than the total number of cells (n=12). (b) The majority of cells appear to stay in the lungs during the first 1 hour with 71.1% of cells being found in the lungs compared with just 20.9% of cells being found in the liver. However at 24 hours only 23.5% of cells are found in the lungs, with 31.5% being found in the liver. This trend appear to be maintained over the 7 day period with a greater percentage of cells being found in the liver when compared with the lungs (n=12).

Having demonstrated that very few cells remain detectable 24 hours after systemic administration I next sought to assess the remote action of subcutaneously administered

P $\alpha$ S MSC.

### **5.2.2 *In vivo* efficacy of subcutaneously administered P $\alpha$ S MSC in the MDR2<sup>-/-</sup> model of liver injury**

It has been demonstrated that MSC may be more efficacious when administered by the subcutaneous route in graft versus host disease [155]. I tested the hypothesis that this may also be true in immune mediated liver injury. As in the previous chapter I treated mice aged 6-8 weeks with cell therapy followed by analysis 2 weeks later.

P $\alpha$ S MSC cultured in standard media were expanded to passage 4. and doses of either  $1 \times 10^5$  or  $2 \times 10^5$  P $\alpha$ S MSC suspended in PBS were tested using the subcutaneous route with control animals receiving PBS alone. Male mice aged between 6 and 8 weeks were injected with P $\alpha$ S MSC and culled after 2 weeks. Analysis of serum markers, liver infiltrating immune cells and immunohistochemistry were performed.

#### **5.2.2.1 Effects of subcutaneous P $\alpha$ S MSC on serum markers of liver injury in the MDR2<sup>-/-</sup> model**

Following subcutaneous injection of P $\alpha$ S MSC mice were analysed 2 weeks later. There was a significant increase in ALT when mice were treated with  $2 \times 10^5$  P $\alpha$ S MSC (figure 5.5a) when compared with controls ( $652.5 \pm 28.8$  vs  $497.8 \pm 46.9$ ), with no significant difference in ALT when mice were treated with  $1 \times 10^5$  P $\alpha$ S MSC. ALP (figure 5.5b) and bile acids (figure 5.5c) showed no significant changes in mice treated with P $\alpha$ S MSC by the subcutaneous route.

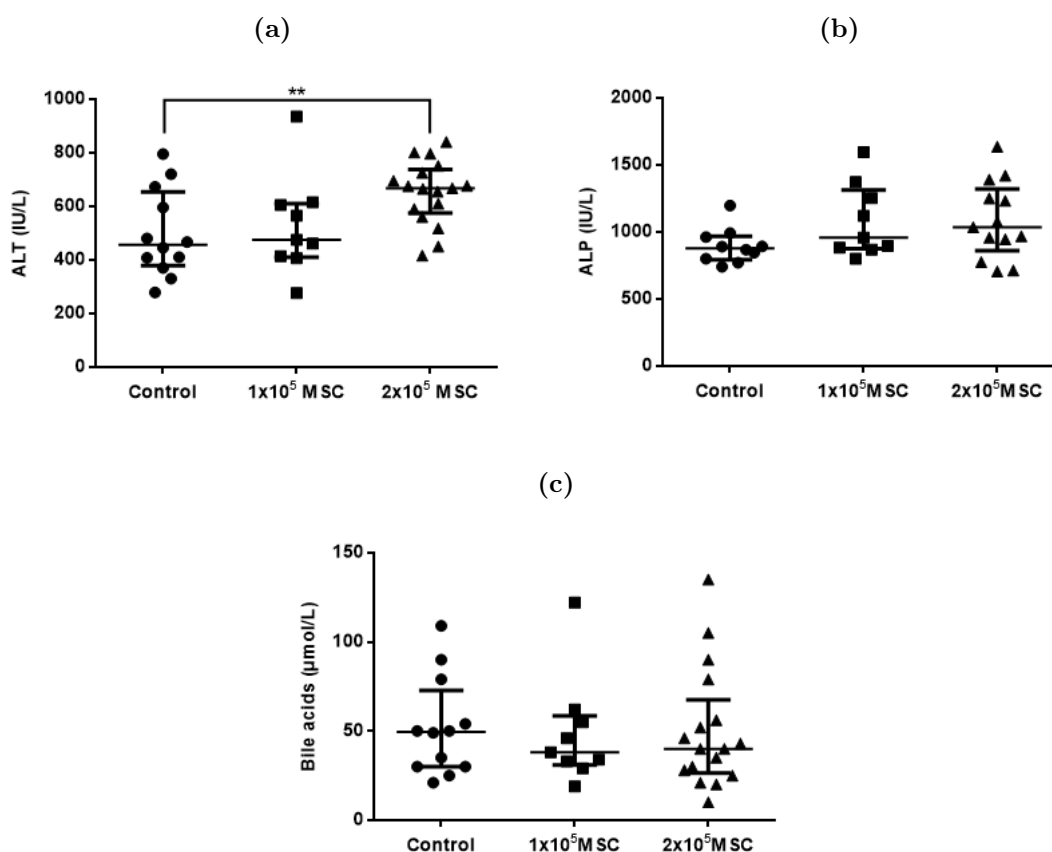


**Figure 5.5 – Subcutaneous treatment with PαS MSC does not reduce ALT, ALP or bile acids in MDR2<sup>-/-</sup> mice.** MDR2<sup>-/-</sup> mice aged between 6 and 8 weeks were treated by subcutaneous injection with either 1x10<sup>5</sup> or 2x10<sup>5</sup> PαS MSC suspended in PBS with control animals receiving PBS alone. Mice were culled 2 weeks later. There was a significant increase in (a) ALT when mice were treated with 2x10<sup>5</sup> PαS MSC when compared with controls (652.5 ± 28.8 vs 497.8 ± 46.9) with no significant difference in ALT when mice were treated with 1x10<sup>5</sup> PαS MSC (528.1 ± 62.2 vs 497.8 ± 46.8). (b) ALP and (c) bile acids showed no significant changes in mice treated with PαS MSC by the subcutaneous route. Points represent individual mice, bars represent the median and lines represent the interquartile range. Statistical analysis was carried out using a one way ANOVA and multiple comparison testing was undertaken.

#### 5.2.2.2 Histological changes in MDR2<sup>-/-</sup> mouse livers when treated with subcutaneous PαS MSC

Liver tissue from MDR2<sup>-/-</sup> mice treated with PαS MSC was removed, processed and embedded in paraffin and then sectioned and stained as previously described. Liver morphology was assessed with H & E staining (figure 5.6). Minimal morphological disruption was seen in uninjured FVB control with almost no infiltrating immune cells seen.

Infiltrating immune cells were demonstrated showing a peri-portal (Zone I) distribution in PBS treated controls as well as mice treated with P $\alpha$ S MSC.

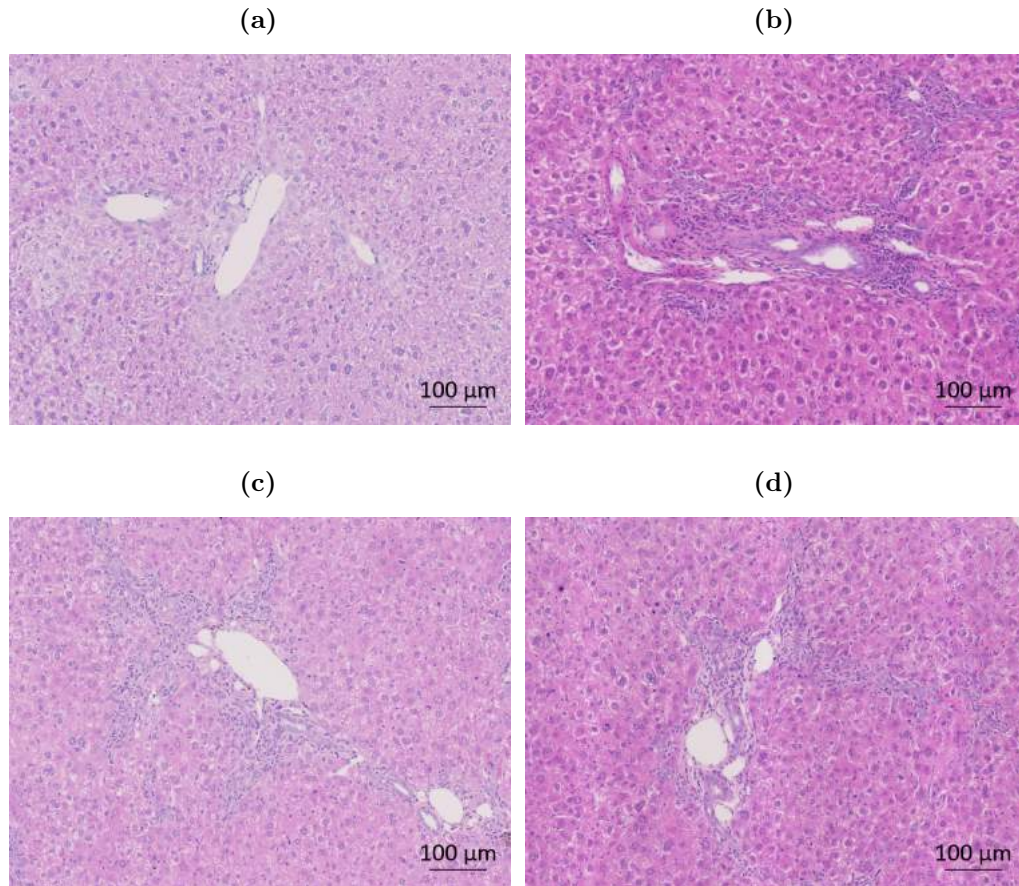


**Figure 5.6 – Representative images of haematoxylin and eosin staining in MDR2<sup>-/-</sup> mice treated with either subcutaneous PBS or P $\alpha$ S MSC at 6-8 weeks of age and culled 2 weeks later.** (a) Minimal morphological disruption was seen in uninjured FVB control with almost no infiltrating immune cells seen. (b) Infiltrating immune cells were demonstrated showing a peri-portal (Zone I) distribution in PBS treated controls, (c) mice treated with 1x10<sup>5</sup> P $\alpha$ S MSC IV and (d) mice treated with 2x10<sup>5</sup> P $\alpha$ S MSC IV. All images are generated from whole slide scans and are at 400x magnification. Scale bars represent 100μm.

The pan-leucocyte marker CD45 was quantified following immunohistochemical staining. Slides were scanned using a Zeiss AxioScanner providing a whole slide image and quantification of the amount of staining was analysed and represented as a percentage total area. MDR2<sup>-/-</sup> control animals showed no difference in CD45 expression (figures 5.7, 5.8) when compared with wild type FVB uninjured controls ( $1.707 \pm 0.312$  vs  $2.173 \pm 0.27$ ). There was no significant difference in CD45 expression in mice treated with 1x10<sup>5</sup>



P $\alpha$ S MSC, but a significant increase in CD45 expression when mice were treated with  $2 \times 10^5$  MSC ( $1.707 \pm 0.312$  vs  $2.640 \pm 0.643$ ,  $p=0.020$ ).

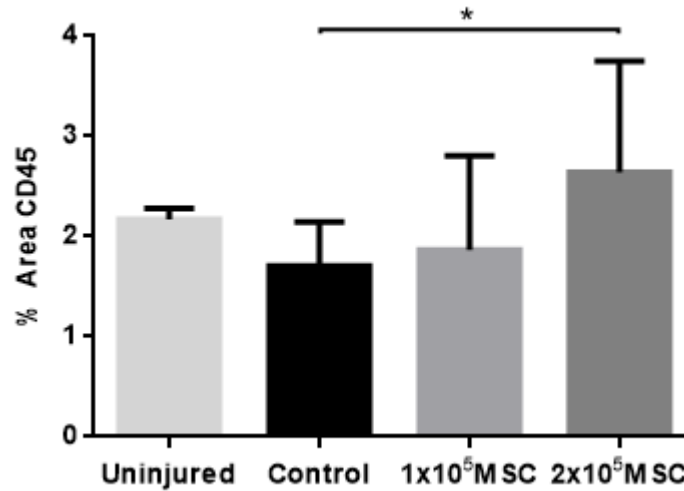


**Figure 5.7 – CD45 expression in the livers of MDR2<sup>-/-</sup> mice treated with either subcutaneous PBS or P $\alpha$ S MSC at 6-8 weeks of age and culled 2 weeks later.** MDR2<sup>-/-</sup> mice aged between 6 and 8 weeks were treated by subcutaneous injection with either  $1 \times 10^5$  or  $2 \times 10^5$  P $\alpha$ S MSC suspended in PBS with control animals receiving PBS alone ( $n=31$ ). Mice were culled 2 weeks later. Immunohistochemical staining was undertaken using a chromogenic technique. MDR2<sup>-/-</sup> control animals demonstrated no difference in CD45 expression when compared with wild type FVB uninjured controls ( $1.707 \pm 0.312$  vs  $2.173 \pm 0.27$ ). There was a no difference in CD45 expression in mice treated with  $1 \times 10^5$  P $\alpha$ S MSC ( $1.707 \pm 0.312$  vs  $1.867 \pm 1.163$ ) when compared with controls, but a significant increase in CD45 expression when mice were treated with  $2 \times 10^5$  MSC ( $1.707 \pm 0.312$  vs  $2.640 \pm 0.643$ ,  $p=0.020$ ). Slides were captured using a Zeiss AxioScanner. Between 5 and 10 images were taken from each scan to cover the whole slide and quantification of each image was performed using Image J software. Bars represent median values and lines represent the range. Statistical analysis was carried out using a one way ANOVA and multiple comparison testing was undertaken.

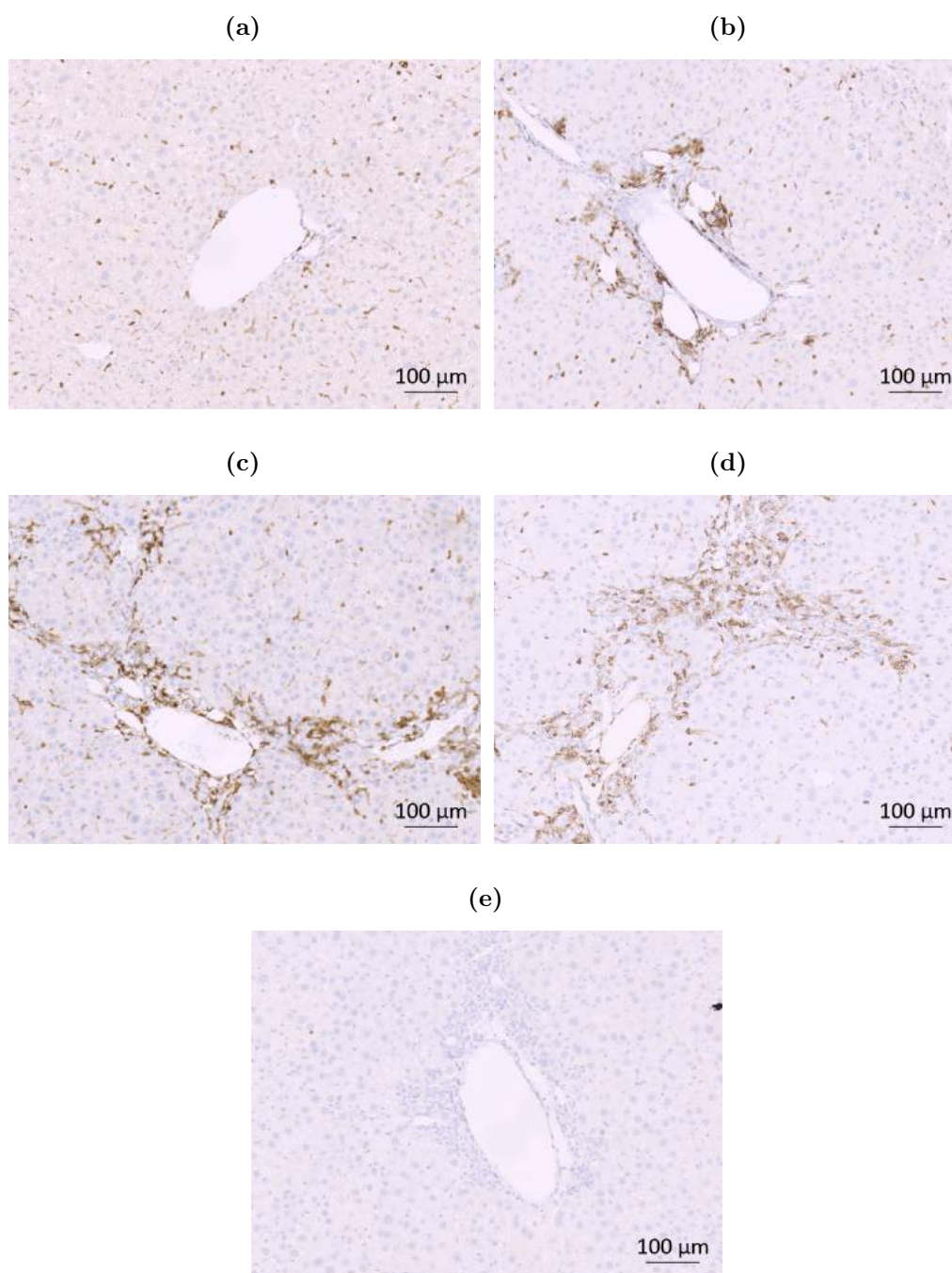


**Figure 5.8 – Representative images of CD45 staining in MDR2<sup>-/-</sup> mice treated with either subcutaneous PBS or PαS MSC at 6-8 weeks of age and culled 2 weeks later.** MDR2<sup>-/-</sup> mice aged between 6 and 8 weeks were treated by subcutaneous injection with either 1x10<sup>5</sup> or 2x10<sup>5</sup> PαS MSC suspended in PBS with control animals receiving PBS alone. Mice were culled 2 weeks later. Immunohistochemical staining was undertaken using a chromogenic technique. (a) There were scattered CD45 cells distributed across all zones in the uninjured FVB controls. (b) Infiltrating CD45<sup>+</sup> cells were demonstrated showing a peri-portal (Zone I) distribution in PBS treated controls, (c) mice treated with 1x10<sup>5</sup> PαS MSC IV and (d) mice treated with 2x10<sup>5</sup> PαS MSC IV. (e) There was no staining seen in the isotype matched controls. All images are generated from whole slide scans and are at 400x magnification. Scale bars represent 100μm.

Staining was next undertaken using an F4/80 antibody in order to delineate the hepatic macrophage population (figures 5.9, 5.10). MDR2<sup>-/-</sup> control animals showed an increase in F4/80 expression when compared to wild type FVB mice. Mice treated with PαS MSC showed a no difference in F4/80 expression when compared with control animals.

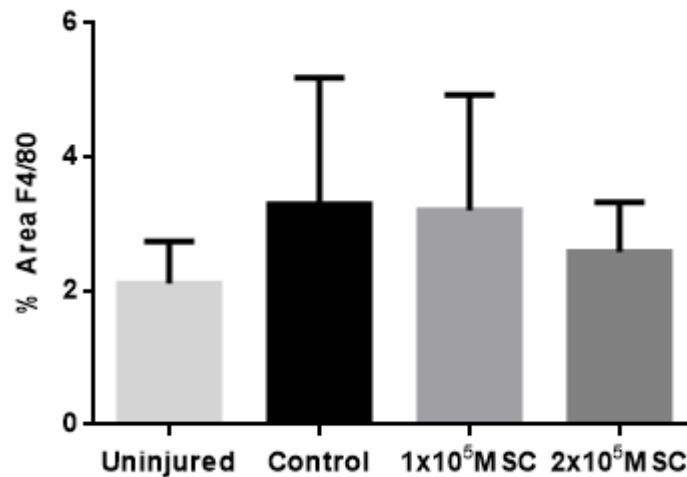


**Figure 5.9 – F4/80 expression in the livers of MDR2<sup>-/-</sup> mice treated with either subcutaneous PBS or PαS MSC at 6-8 weeks of age and culled 2 weeks later.** MDR2<sup>-/-</sup> mice aged between 6 and 8 weeks were treated with either 1x10<sup>5</sup> or 2x10<sup>5</sup> PαS MSC suspended in PBS with control animals receiving PBS alone via the subcutaneous route (n=37). Mice were culled 2 weeks later. Immunohistochemical staining was undertaken using a chromogenic technique. Staining was undertaken using an F4/80 antibody in order to delineate the hepatic macrophage population. MDR2<sup>-/-</sup> control animals showed a no difference in F4/80 expression when compared to wild type FVB mice (3.296 ± 0.598 vs 2.109 ± 0.36, p=0.32). Mice treated with 1x10<sup>5</sup> PαS MSC showed no difference in F4/80 expression when compared with control animals (3.296 ± 0.598 vs 3.209 ± 0.609, p=0.92), neither did those treated with 2x10<sup>5</sup> PαS MSC (3.296 ± 0.598 vs 2.583 ± 0.187, p=0.186). Slides were captured using a Zeiss AxioScanner. Between 5 and 10 images were taken from each scan to cover the whole slide and quantification of each image was performed using Image J software. Bars represent median values and lines represent the range. Statistical analysis was carried out using a one way ANOVA and multiple comparison testing was undertaken. Comparison between groups was undertaken using Student's t-test.

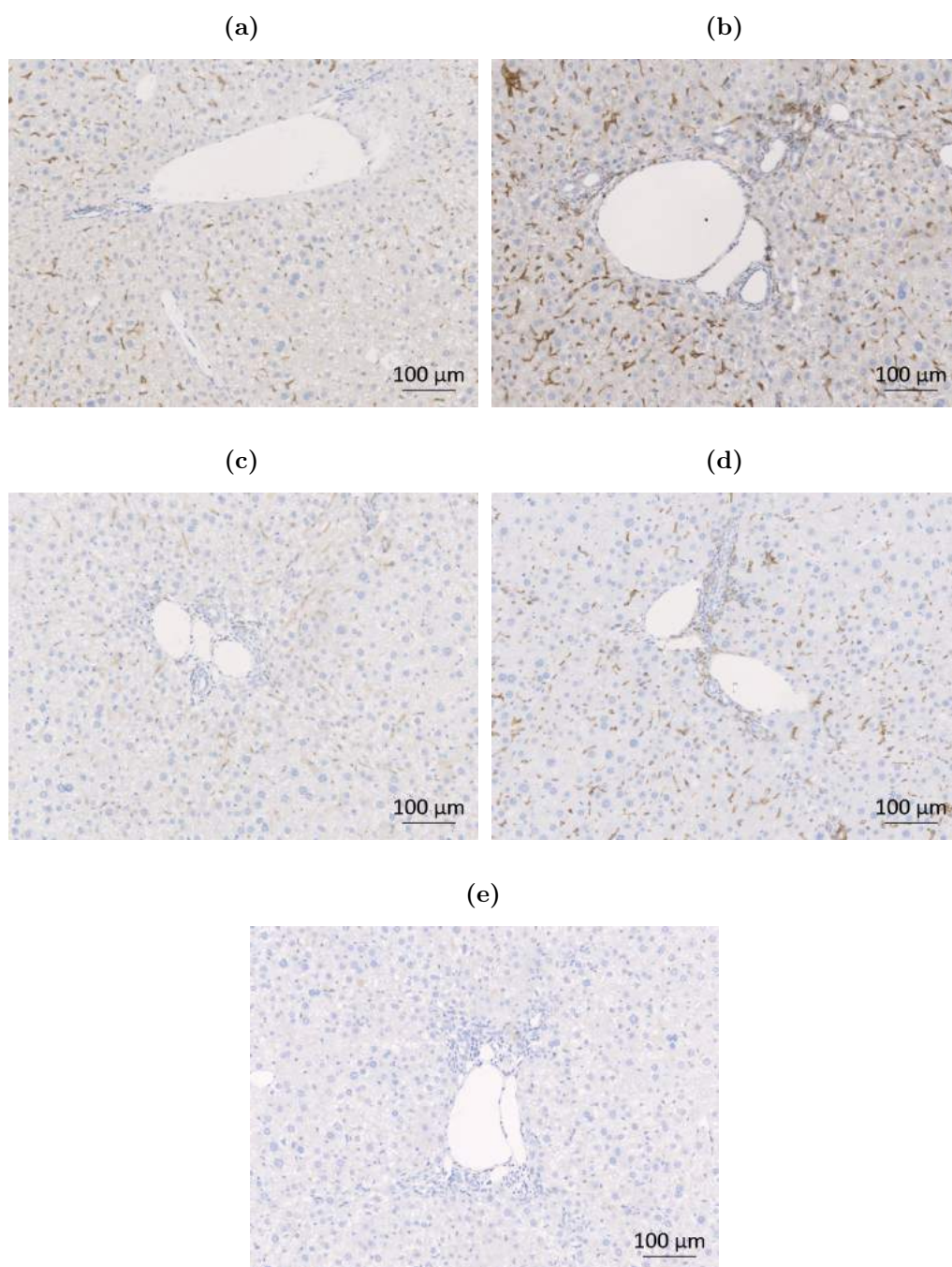


**Figure 5.10 – Representative images of F4/80 staining in MDR2<sup>-/-</sup> mice treated with either subcutaneous PBS or PαS MSC at 6-8 weeks of age and culled 2 weeks later.** MDR2<sup>-/-</sup> mice aged between 6 and 8 weeks were treated by subcutaneous injection with either 1x10<sup>5</sup> or 2x10<sup>5</sup> PαS MSC suspended in PBS with control animals receiving PBS alone. Mice were culled 2 weeks later. Immunohistochemical staining was undertaken using a chromogenic technique. (a) There were scattered F4/80 cells distributed across all zones in the uninjured FVB controls. (b) Some infiltrating F4/80 cells were demonstrated showing a peri-portal (Zone I) distribution on a background of scattered F4/80 cells across all zones were seen in PBS treated controls, (c) mice treated with 1x10<sup>5</sup> PαS MSC IV and (d) mice treated with 2x10<sup>5</sup> PαS MSC IV. There was no staining seen in the (e) isotype matched controls. All images are generated from whole slide scans and are at 400x magnification. Scale bars represent 100μm.

I next sought to quantify CK19 expression using western blotting.

### 5.2.2.3 Effects on ductular proliferation in MDR2<sup>-/-</sup> mouse livers when treated with P $\alpha$ S MSC

Following treatment with P $\alpha$ S MSC mice were culled at 2 weeks and liver lobes removed and homogenised. Protein lysis and quantification was undertaken and then western blotting was performed using the lysed protein. A CK17/19 antibody was used for detection of CK19 and  $\alpha$ -actinin was used as a loading control.

CK19 expression showed no difference between uninjured FVB mice and PBS treated MDR2<sup>-/-</sup> mice. There was no difference CK19 expression following treatment with P $\alpha$ S MSC in either the 1x10<sup>5</sup> or 2x10<sup>5</sup> groups (figure 5.11).

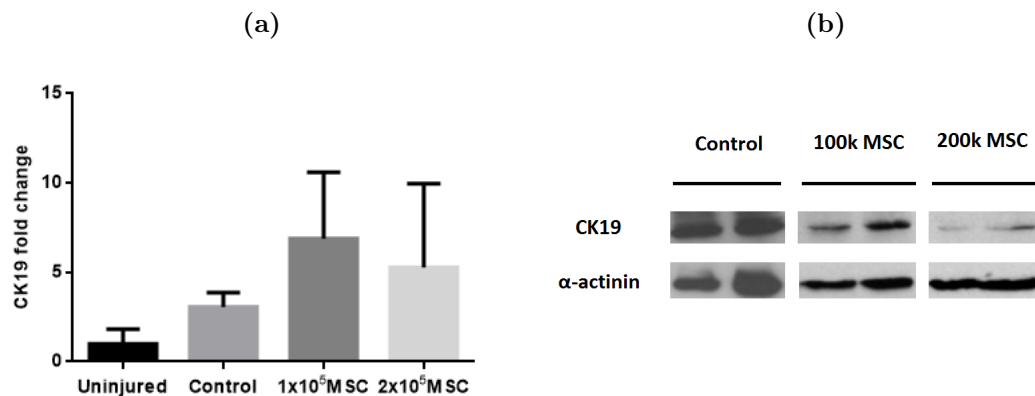


**Figure 5.11 – CK19 quantification by western blotting in MDR2<sup>-/-</sup> mice treated with subcutaneous P $\alpha$ S MSC.** MDR2<sup>-/-</sup> mice aged 6-8 weeks were treated with either 1x10<sup>5</sup> or 2x10<sup>5</sup> P $\alpha$ S MSC via the subcutaneous route and then culled 2 weeks later. Liver lobes were removed and homogenised. Protein lysis and quantification was undertaken and then western blotting was performed using the lysed protein. A CK17/19 antibody was used for detection of CK19 and  $\alpha$ -actinin was used as a loading control. Expression levels were normalised to loading controls and are expressed as fold change. (a) CK19 expression showed no difference between uninjured FVB mice and PBS treated control MDR2<sup>-/-</sup> mice. Mean CK19 expression was not different following treatment with P $\alpha$ S MSC (n=38). (b) Representative western blots for CK19 expression are shown with loading controls below. Bars represent median values and lines represent the range. Statistical analysis was carried out using a one way ANOVA and multiple comparison testing was undertaken.

I next sought to quantify the immune cell infiltration in MDR2<sup>-/-</sup> mouse livers by flow cytometry.

#### 5.2.2.4 Characterisation of liver and serum immune cell populations in MDR2<sup>-/-</sup> mouse livers following sucutaneous treatment with P $\alpha$ S MSC

Infiltrating immune cells in the livers of MDR2<sup>-/-</sup> mice were quantified using flow cytometric analysis. Two weeks after treatment with P $\alpha$ S MSC liver lobes were removed, weighed and processed to allow flow cytometry to be performed. Single cell suspensions were stained with relevant antibodies including a live/dead marker. Cell counts were normalised to liver weight and presented as cells per gramme.

There was a significant reduction in infiltrating CD45<sup>+</sup> cells (figure 5.12) between control animals and mice treated with 2x10<sup>5</sup> P $\alpha$ S MSC (306551 cells/g  $\pm$  18165 vs 194496 cells/g  $\pm$  15135, p=0.009). This pattern was also true for CD8<sup>+</sup> (31855 cells/g  $\pm$  5589 vs 13079 cells/g  $\pm$  4787, p=0.0385) cells. There was a no significant difference in CD4<sup>+</sup> (65013 cells/g  $\pm$  6779 vs 45840 cells/g  $\pm$  9250), CD19<sup>+</sup> (54495 cells/g  $\pm$  6957 vs 42663 cells/g  $\pm$  6514), NK1.1<sup>+</sup> (11390 cells/g  $\pm$  2120 vs 11056 cells/g  $\pm$  802.7), F4/80<sup>+</sup> (19983 cells/g  $\pm$  480.7 vs 28510 cells/g  $\pm$  4616) cells, or neutrophils delineated by CD11b and Gr1 (21037 cells/g  $\pm$  59.53 vs 30634 cells/g  $\pm$  5024).



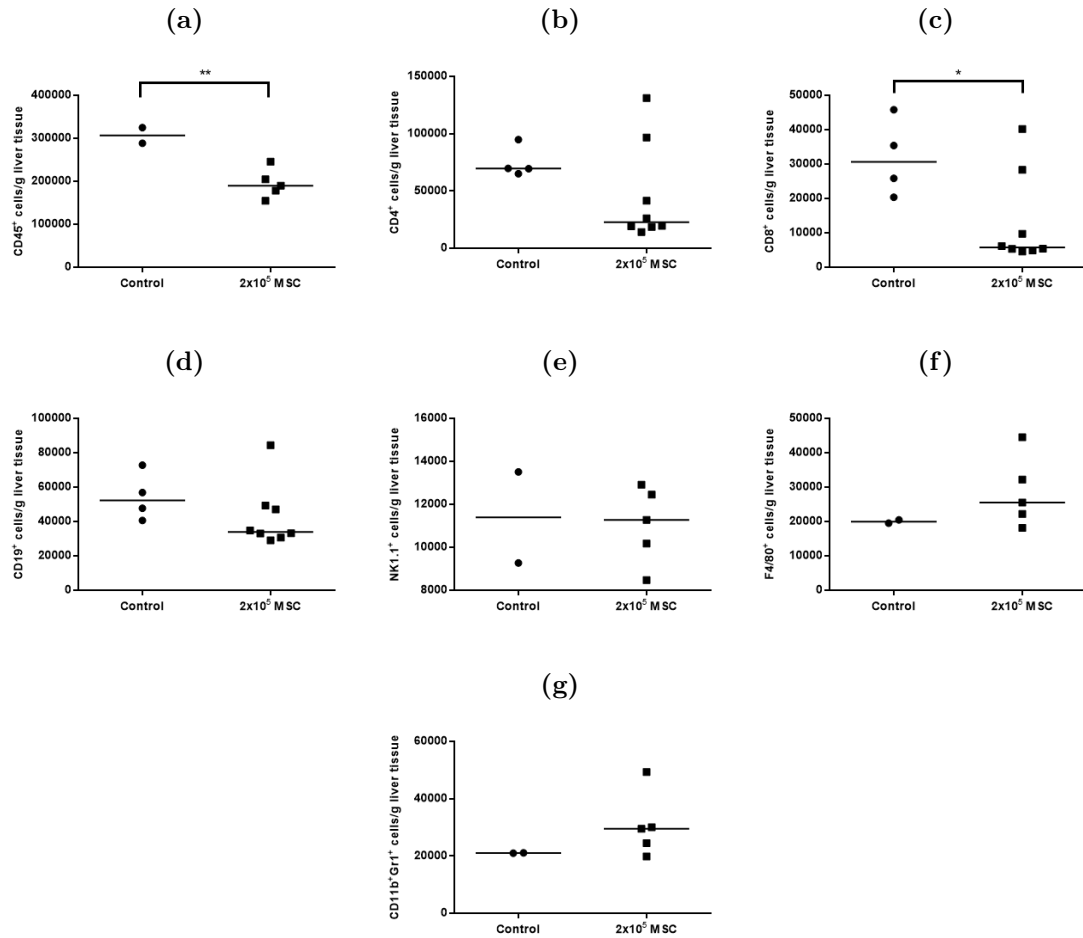


**Figure 5.12 – Flow cytometric analysis of immune cell infiltrates in the livers of MDR2<sup>-/-</sup> mice treated with subcutaneous PαS MSC.** Two weeks following treatment with subcutaneous PαS MSC liver lobes from MDR2<sup>-/-</sup> mice were removed, weighed and processed for cytometry. Single cell suspensions were stained with relevant antibodies including a live/dead marker. Cell counts were normalised to liver weight and presented as cells per gramme. (a) There was a significant reduction in infiltrating CD45<sup>+</sup> cells between control animals and mice treated with 2x10<sup>5</sup> PαS MSC (306551 cells/g ± 18165 vs 194496 cells/g ± 15135, p=0.009, n=7). There was no difference in (b) CD4<sup>+</sup> (65013 cells/g ± 6779 vs 45840 cells/g ± 9250, p=0.235, n=12). (c) CD8<sup>+</sup> cells were also significantly reduced (31855 cells/g ± 5589 vs 13079 cells/g ± 4787, p=0.0385, n=12). There was no difference in (d) CD19<sup>+</sup> (54495 cells/g ± 6957 vs 42663 cells/g ± 6514, p=0.287, n=12), (e) NK1.1<sup>+</sup> (11390 cells/g ± 2120 vs 11056 cells/g ± 802.7, p=0.856, n=7), (f) F4/80<sup>+</sup> (19983 cells/g ± 480.7 vs 28510 cells/g ± 4616, p=0.320, n=7) cells or neutrophils delineated by CD11b<sup>+</sup> and Gr1<sup>+</sup> (21037 cells/g ± 59.53 vs 30634 cells/g ± 5024, p=0.305, n=7). Points represent individual mice and bars represent the median value. Statistical analysis was carried out using a one way ANOVA and multiple comparison testing was undertaken. Comparison between groups was undertaken using Student's t-test.

I also analysed the CD4/CD8 ratio in liver tissue by looking at the ratio of cells analysed by flow cytometry (figure 5.13). In the liver tissue the CD4/CD8 ratio showed a

significant increase ( $p=0.0078$ ) in the mice treated with  $2 \times 10^5$  P $\alpha$ S MSC.

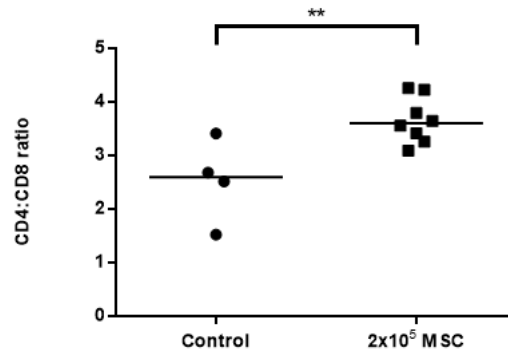


**Figure 5.13** – The CD4/CD8 ratio assessed by flow cytometry in the livers of MDR2<sup>-/-</sup> mice aged 6-8 weeks old were treated with subcutaneous P $\alpha$ S MSC and culled after 2 weeks. MDR2<sup>-/-</sup> mice aged 6-8 weeks were treated with  $2 \times 10^5$  P $\alpha$ S MSC via the subcutaneous route and then culled 2 weeks later. Liver lobes removed and antibody staining was undertaken and analysed by flow cytometry. In the liver tissue the CD4/CD8 ratio showed a significant reduction ( $p=0.0078$ ) in mice treated with  $2 \times 10^5$  P $\alpha$ S MSC compared with control mice. Points represent individual mice and bars represent the median value. Statistical analysis was carried out using a Student's t-test.



## 5.3 Discussion

Systemically administered MSC have been shown to exert a broad range of effects in both organ specific and systemic models of immune mediated disease. A number of techniques have been used to track the location of systemically administered MSC. In this study I opted to use a novel block face cryoimaging technique which enabled quantification and imaging of QDot<sub>605</sub> labelled P $\alpha$ S MSC at a single cell resolution.

### 5.3.1 Tracking systemically administered P $\alpha$ S MSC

In order to examine the distribution of systemically administered P $\alpha$ S MSC I utilised the CryoViz<sup>TM</sup> imaging system which required cells to be stained using quantum dots. Whilst quantum dot technology has been around nearly 20 years [293], its use in MSC research has been limited. CryoViz<sup>TM</sup> is a recently developed technology and studies using this technique to track MSC distribution have only started to be seen in the last 12 months [294, 295]. There are no published papers demonstrating quantum dot staining or CryoViz<sup>TM</sup> imaging using P $\alpha$ S MSC. In this study I have demonstrated that staining P $\alpha$ S MSC is feasible and does not lead to significant cell death. I have also demonstrated that QDot<sub>605</sub> is compatible with live/dead staining using an intra-cytoplasmic viability marker. Whilst it is not a new finding that MSC can be stained with quantum dots there is no literature describing their use with P $\alpha$ S MSC. I have also demonstrated that QDot<sub>605</sub> is persistent at 7 days and therefore can be reliably used to track P $\alpha$ S MSC *in vivo* over this time period. In this study I did not look at the function of P $\alpha$ S MSC following quantum dot staining, and whilst it is conceivable that the use of quantum dots could lead to a change in function of P $\alpha$ S MSC this has not been seen in the literature when quantum dots have been used to stain MSC [296].

In this study I examined the distribution of systemically administered P $\alpha$ S MSC in the MDR2<sup>-/-</sup> model of liver injury. Whilst the aim of this study was to examine the distribution of cells in the MDR2<sup>-/-</sup> model, a benefit of using this model when studying

MSC trafficking is that the model is a spontaneous injury model which was continuous through the studied time course. This means that even with a reduction in injury due to MSC therapy, there should remain an inflammatory stimulus at the site of injury making the localisation of MSC to the liver during the later time periods still valid. One hour following injection of  $1 \times 10^5$  P $\alpha$ S MSC only around 10% of cells were still detectable. Whilst it is possible that cells were left in the syringes during injection, initial testing and calibration using *ex vivo* organs showed nearly 75% of injected cells still visible. Levels were similar between replicates making experimental error unlikely. This reduction in cell number either represents rapid clearance from the mice, an inability to resolve low numbers of cells, cell death and clearance or an inability to quantify cells grouped together. As seen in other studies of MSC the greatest number of cells were found in the lungs (66% total) [279]. As pulmonary 'trapping' is at least in part a physical property of MSC [297], and P $\alpha$ S MSC are similar in size to their human counterparts, this is not surprising. Approximately 20% of the total cells were found in the liver, with very few found in the spleen. There appeared to be a rapid decrease in the number of detectable cells over the first 24 hours. After 24 hours the rate of decline levelled out with the greatest reduction occurring in cells not found in the lung, liver or spleen. The ratio of cells found in the liver, compared with cells found in the lung also changed over the remaining 6 days with the percentage of cells found in the lungs falling below those found in the liver by 24 hours and remaining there throughout the 7 day experiment. Whilst on the surface it appears that this is a retention phenomenon with cells being more readily retained in the liver, it is possible that the clearance rates from each organ are similar, but that those cells leaving the lungs then become redistributed to the liver. It is not possible to determine if this is the case from the data presented in this study, further work would need to be done to confirm this hypothesis. It is also not possible to determine the exact location of MSC within the liver in this study which may be important when trying to understand the interaction between MSC and the immune system. By 7 days there were very few cells remaining in any organ. This finding supports the hypothesis that P $\alpha$ S MSC are

able to reduce injury by the use of intermediary cells, however it does not clearly answer the question as to whether P $\alpha$ S MSC need to be co-located in the injured area in order to exert these effects. To answer this question I examined the effects of subcutaneously administered P $\alpha$ S MSC.

### **5.3.2 The effect of P $\alpha$ S MSC administered subcutaneously in the MDR2<sup>-/-</sup> model**

The ability of MSC to exert an immunomodulatory effect on models of liver disease has been demonstrated in the literature where both human and murine MSC have been tested. In models of acute liver failure murine bone marrow derived MSC have been shown to attenuate liver injury via paracrine effects on regulatory T-cells [298]. It has also been demonstrated that in a fatal model of hepatic failure extracellular vesicles secreted from MSC are able to reduce injury by reducing hepatocyte apoptosis [299]. MSC encapsulated in alginate have also been demonstrated to reduce injury in a model of graft versus host disease [155], suggesting that MSC are able to exert remote effects on the immune system. In this study MDR2<sup>-/-</sup> mice injected with subcutaneous P $\alpha$ S MSC showed a significant increase in injury when examining ALT, the primary outcome measure. ALP and bile acids were unchanged. This is in contrast to the experiments using intravenously administered P $\alpha$ S MSC which showed a significant reduction in both ALT and ALP. Histological examination revealed an increase in total CD45 expression, similar to that seen in the mice treated via the intravenous route. There was no difference in F4/80 expression in these experiments. On the surface these findings appear unusual as the serum markers of injury are contrary to those seen in the intravenous group yet the histological findings appear to be similar. Flow cytometric analysis of liver infiltrating immune cells showed a significant reduction in CD45<sup>+</sup> and CD8<sup>+</sup> cells, with no changes in CD4<sup>+</sup> cells. All other cell types analysed showed no significant changes in numbers. The reduction in CD45 expression is in keeping with a reduction in CD8<sup>+</sup> cells, however this is an unexpected finding given that systemic administration of P $\alpha$ S MSC did not lead to changes in CD8<sup>+</sup>

cells. In the MDR2<sup>-/-</sup> model CD4<sup>+</sup> and CD8<sup>+</sup> lymphocytes have been shown to increase in numbers at time of injury [98], however it has never been conclusively demonstrated that an increase in infiltrating immune cells is responsible for an increase in injury in this model. The CD4/CD8 ratio significantly increased in the mice treated with subcutaneous P $\alpha$ S MSC, the opposite effect to that seen following intravenous injection. The importance of an increase in the CD4/CD8 ratio in this context is difficult to interpret, however it could represent a change towards a cytotoxic rather than restorative phenotype and hence provide an explanation for the increase in ALT after treatment with subcutaneous P $\alpha$ S MSC. The difference between the effects of subcutaneous and intravenous P $\alpha$ S MSC therapy could then be explained by the differing effects of the MSC. The published models which have shown a benefit in encapsulated MSC are models where injury is driven by lymphocytes, and the reduction in lymphocyte numbers mediated by MSC has been possible remotely. In the MDR2<sup>-/-</sup> model I have shown that P $\alpha$ S MSC may decrease injury by a more complex mechanism, specifically a change in macrophage phenotype. It is possible that this change in macrophage type requires cell to cell contact or close proximity in order to reduce injury, this being prevented by subcutaneous administration. Further work would need to be done to confirm this hypothesis including cell tracking to ascertain if subcutaneously administered P $\alpha$ S MSC remain at the site of injection.

### 5.3.3 Chapter summary

In this chapter I have demonstrated that it is feasible to label P $\alpha$ S MSC with quantum dots to facilitate cell tracking with the CryoViz<sup>TM</sup> block face cryoimaging technique without any change in viability. By utilising this technique I have demonstrated that systemically administered P $\alpha$ S MSC rapidly reduce in number over the first hour after injection. I have also demonstrated that in keeping with studies of other types of MSC that P $\alpha$ S MSC are temporarily 'trapped' in the lungs following systemic administration. After 24 hours however there appeared to be a greater reduction in cells found in the lungs when compared with those in the liver. This finding is potentially due to redistribution from

the lungs to the liver.

I have also demonstrated that subcutaneously administered P $\alpha$ S MSC increase liver injury in the MDR2<sup>-/-</sup> mouse model. The mechanism by which this occurs is not clear, although a change in the balance of cytotoxic and restorative cell types is a potential mechanism, however this requires further study. These findings suggest that systemic administration of MSC may be required in complex conditions where injury is not primarily driven by lymphocytes alone.

## CHAPTER 6

# DEVELOPMENT AND *IN VIVO* EFFICACY TESTING OF P $\alpha$ S MSC IN A MODEL OF HEPATIC ISCHAEMIA REPERFUSION INJURY

### 6.1 Chapter introduction and aims

I have so far demonstrated the isolation and culture expansion of P $\alpha$ S MSC as well as their ability to suppress lymphocyte proliferation in a bulk splenocyte reaction. I have also demonstrated the ability of P $\alpha$ S MSC to reduce injury in the MDR2<sup>-/-</sup> model which has a similar injury pattern to the medium term complications seen post liver transplantation. In this chapter I developed a mouse model of hepatic ischaemia reperfusion injury and tested the ability of P $\alpha$ S MSC to modulate the immune system in this model.

#### 6.1.1 Hepatic ischaemia reperfusion injury

Liver transplantation has become a standard of care for suitable patients with end stage liver disease with no other therapies able to prevent the mortality associated with this condition. With a shortage of donor organs worldwide the use of more marginal organs, such as those from Maastricht class III and IV donation after circulatory death donors has increased in recent years [29]. During both liver resection and liver transplantation an inevitable ischaemic injury occurs to the liver, either due to organ preservation and

transport, major haemorrhage or deliberate vascular inflow occlusion with an aim to reduce surgical blood loss [52, 53, 54, 55]. Liver ischaemia can be categorised as warm or cold ischaemia. Cold ischaemia occurs during cold preservation of explanted liver and is defined as occurring from the beginning of cold preservation to the removal from 4°C cold storage. Warm ischaemic time can be subdivided into donor warm ischaemic time, occurring between withdrawal of life support and the initiation of cold storage, or graft warm ischaemic time which occurs between removal from cold storage and establishment of reperfusion [57].

The ischaemic phase of ischaemia reperfusion injury occurs in cells that require mitochondrial oxidative phosphorylation due to a lack of oxygen supply. This initial phase leads to glycogen consumption and depletion of ATP which impairs ATP dependent  $\text{Na}^+$  and  $\text{Ca}^{2+}$  pumps. The resultant electrolyte imbalance, osmotic stress and mitochondrial permeability leads to necrotic/non-apoptotic cell death. Following reperfusion of ischaemic tissue a further injury process has been described which has been characterised as occurring in two phases [300]. The first phase occurs during the first 6 hours following reperfusion injury and is caused by activation of resident Kupffer cells, whereas the later stage which occurs between 6 and 24 hours is characterised by infiltration of polymorphonuclear cells. This description is an oversimplification of the complex cellular interactions occurring in hepatic ischaemia reperfusion injury which are not fully understood but involve both the innate and the adaptive immune system. Whilst a large number of potential therapies have been trialled in animal models with an aim at reducing injury due to warm ischaemia almost none have made the translation into clinical practice. Most therapies focus on oxidative stress and aim to reduce this insult, however given there is a significant immune component to reperfusion injury there is potential for a therapeutic benefit by targetting the immune system. Whilst there has been some preclinical work looking at MSC and their vesicles in liver ischaemia reperfusion injury [301, 302, 299] most of this work has used human MSC into mouse models and there have been no studies looking at P $\alpha$ S MSC in this disease. Earlier work with MSCs in liver ischaemia reperfusion injury focussed on

supporting hepatocyte differentiation rather than immune modulation [186].

### 6.1.2 Mouse models of liver ischaemia reperfusion injury

One of the first descriptions of reperfusion injury as a result of superoxide generation used a feline model of gastrointestinal tract ischaemia and reperfusion [51]. Since this publication nearly 40 years ago there has been a considerable amount of work done to illicit the causes of reperfusion injury. The use of small animal models to investigate liver ischaemia reperfusion injury has predominated over the last 10 years but a variety of techniques still persist making comparison between studies difficult. In this study I decided to use male C57BL/6 mice as these are the same strain of mice from which the P $\alpha$ S MSC were isolated. I used a model of partial hepatic ischaemia to avoid back pressure into the intestines and bacterial translocation. I also chose an inhalational anaesthetic technique using isoflurane with opiate analgesia whilst avoiding Non-Steroidal Anti-Inflammatory Drugs (NSAIDs) as this has a good correlation with liver surgical practice in the clinical environment. Whilst animal models of liver transplantation do exist and can incorporate both cold and warm ischaemia, the logistical challenges and complexity make these difficult to reproduce [303].

### 6.1.3 Specific chapter aims

Previous chapters have demonstrated the ability of P $\alpha$ S MSC to suppress CD8<sup>+</sup> T cell proliferation *in vitro* in a dose dependent fashion. I have also demonstrated a number of cytokines secreted following stimulation which have the potential to modulate the immune response. The aim of this chapter was to develop a model of partial hepatic ischaemia reperfusion injury in which I could adequately test the ability of P $\alpha$ S MSC to modulate the immune system *in vivo*, and to subsequently test the effects of P $\alpha$ S MSC as a therapy for hepatic ischaemia reperfusion injury. The specific aims of this chapter were:

1. To establish a model of hepatic ischaemia reperfusion injury



2. To optimise the duration of ischaemia and reperfusion in the model to provide an adequate testing environment for PαS MSC therapy.
3. To characterise the inflammatory injury seen in the hepatic ischaemia reperfusion injury model
4. To test the *in vivo* efficacy of PαS MSC in the hepatic ischaemia reperfusion injury model

## 6.2 Results

### 6.2.1 Developing a model of hepatic ischaemia reperfusion injury

Models of hepatic ischaemia reperfusion injury are not new and have been carried out in multiple different species using a variety of surgical techniques. In this study 8 week old male C57BL/6 wild type mice were chosen in keeping with other published literature in liver injury [102]. I opted to perform a portal triad clamp of 70% of the liver (figure 6.1), leaving the lower lobes perfused to act as a portal shunt and prevent back pressure into the portal system which has been shown to lead to gut bacterial translocation.

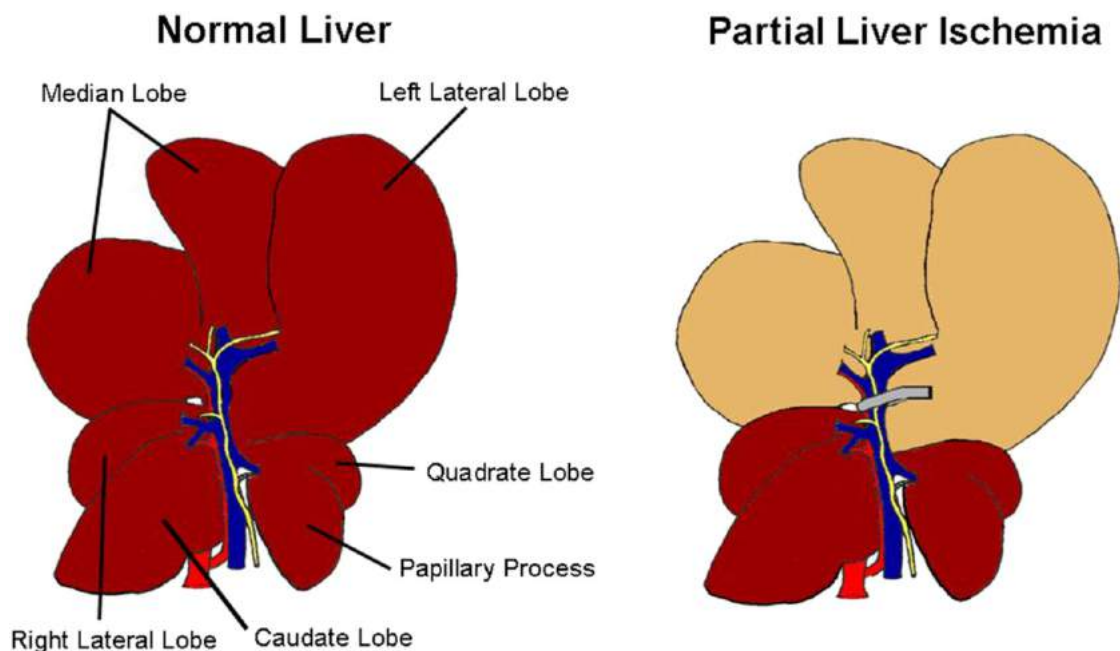


**Figure 6.1 – Graphic of 70% partial liver ischaemia.** Diagrammatic representation of normal murine liver anatomy and the clamp position representing 70% partial ischaemia. Perfused liver is demonstrated as dark brown and ischaemic liver as light brown. The microvascular clamp is shown in silver. Image from Abe et al. [102]

Following a number of cadaveric practice runs in order to optimise the surgical technique I developed a method of administering analgesia before and after surgery using buprenorphine with titrated isoflurane anaesthesia. I used an upper quadrant limited midline laparotomy incision (figure 6.2a) in order to reduce pain and recovery time. Following the initial incision and insertion of a micro-spreader an atraumatic clamp was applied to

the portal triad, sparing the lower liver lobes in order to achieve 70% ischaemia (figures 6.2b and 6.2c). Following reperfusion explanted livers showed a characteristic mottled haemorrhagic appearance in the ischaemic lobes with sparing of the non-ischaemic lobes (figure 6.2d).

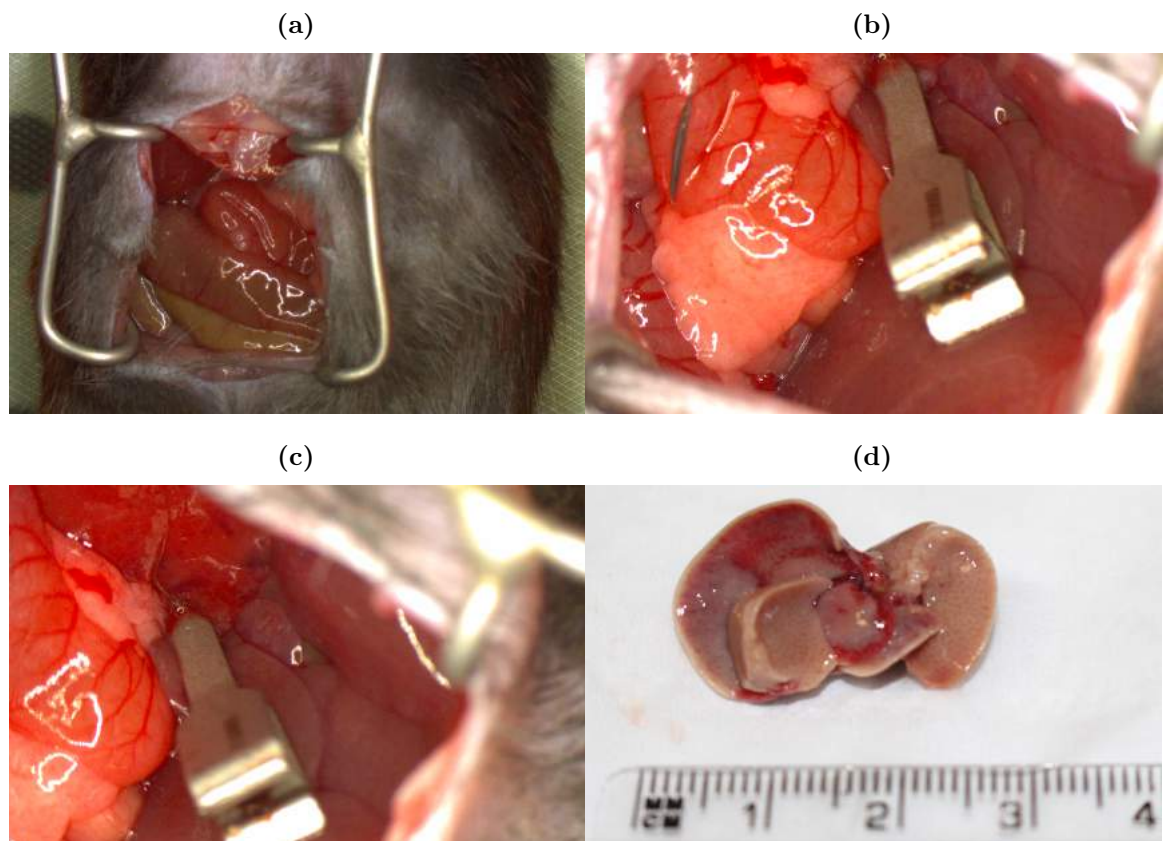


**Figure 6.2 – Images demonstrating hepatic ischaemia reperfusion surgery.** (a) Image demonstrating limited laparotomy of approximately 2cm with micro-spreader inserted. (b) An atraumatic microvascular clamp was inserted into the abdominal cavity superior to the lower liver lobes. (c) Ischaemic liver can be seen as pale in colour whilst perfused liver is red/brown. (d) Following 24 hours of reperfusion, saline flushing and removal of livers, lobes which have undergone ischaemia show a mottled, haemorrhagic appearance whereas non-ischaemic lobes can be seen as homogeneous light brown in colour.

Having optimised the surgical technique I next sought to investigate the effect of different durations of reperfusion on liver injury in the hepatic ischaemia reperfusion injury model.

## **6.2.2 Time course of hepatic ischaemia reperfusion injury**

### **6.2.2.1 Serum transaminases in hepatic ischaemia reperfusion injury**

I decided to use serum ALT as the primary outcome measure in the ischaemia reperfusion injury model as based on the published literature this is a good indicator of degree of liver injury in an ischaemic injury model [102]. Two distinct phases of liver injury have been described following prolonged interruption of blood flow to the liver [304]. The acute phase occurs during the first 6 hours following reperfusion and the sub-acute phase occurs between 6 and 24 hours. I first sought to investigate the profile of transaminases over the first 24 hours of reperfusion following hepatic ischaemia reperfusion injury.

Male C57BL/6 mice aged 8 weeks underwent 60 minutes of 70% ischaemia which was achieved by applying a microvascular clamp across the portal triad via a midline laparotomy incision. Following ischaemia varying durations of reperfusion were undertaken and serum ALT analysed (figure 6.3). Baseline ALT following 60 minutes of ischaemia was taken at 0 hours which demonstrated an increase in ALT ( $647.5 \text{ IU/L} \pm 279.4$ ). There was a time dependent increase in ALT which peaked at 6 hours ( $15893.3 \text{ IU/L} \pm 3059.6$ ). At 24 hours of reperfusion ALT remained raised ( $2825.0 \text{ IU/L} \pm 873.3$ ) with sham controls having an almost normal ALT ( $37.5 \text{ IU/L} \pm 3.2$ ).

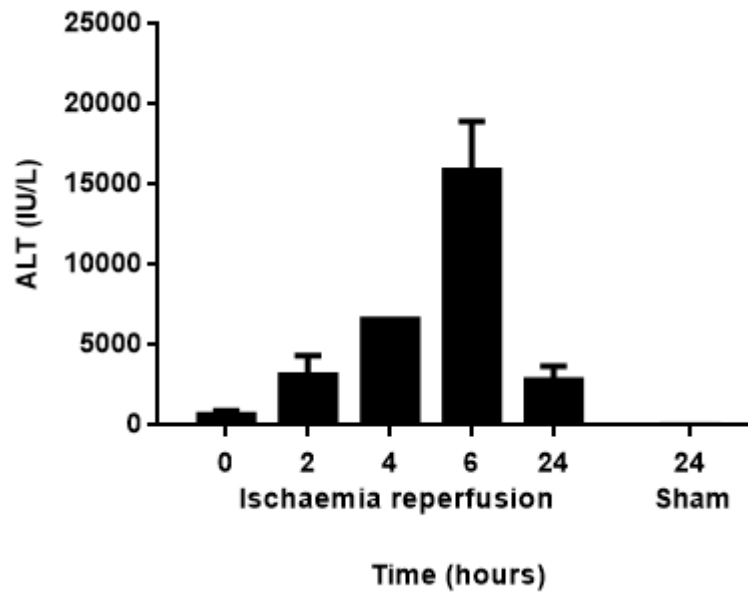


**Figure 6.3 – Time course of serum ALT following 60 minutes of hepatic ischaemia.** Male C57BL/6 mice aged 8 weeks underwent 60 minutes of 70% ischaemia. Following ischaemia varying durations of reperfusion were undertaken. Baseline ALT at 0 hours demonstrated an increase in ALT ( $647.5 \text{ IU/L} \pm 279.4$ ,  $n=4$ ). There is a time dependent increase in ALT which peaked at 6 hours ( $15893.3 \text{ IU/L} \pm 3059.6$ ,  $n=3$ ). At 24 hours of reperfusion ALT remained raised ( $2825.0 \text{ IU/L} \pm 873.3$ ,  $n=4$ ) with sham controls having an almost normal ALT ( $37.5 \text{ IU/L} \pm 3.2$ ,  $n=4$ ). Histograms represent mean values and bars represent standard error of the mean.  $n=18$ .

I next sought to assess the associated histological changes following ischaemia reperfusion injury.

#### 6.2.2.2 Histochemical analysis in hepatic ischaemia reperfusion injury

Various techniques for assessing hepatic necrosis in ischaemia reperfusion injury models have been described including semi-quantitative analysis of H & E stained sections [102] and TUNEL staining [305]. One technique that has been shown to delineate necrotic cells following ischaemia in otherwise well mice is Periodic Acid-Schiff (PAS) staining, a glycogen stain[306]. This stain is used regularly in our clinical lab for assessment of hepatic necrosis in pre and post transplant liver tissue. I undertook H & E staining to assess liver architecture and PAS staining to assess necrosis.

Following sacrifice of C57BL/6 mice liver tissue was removed from the lobes which

underwent ischaemia and the lobes that were spared and fixed in formalin. Fixed liver tissue was embedded in paraffin and processed for histochemistry and H & E staining (figures 6.4 and 6.5) was performed. At baseline 0 hours reperfusion extravasation of red blood cells was seen in the spaces between hepatocytes with minimal apparent necrosis. Between 0 and 6 hours necrosis became more apparent with sparing around the portal vessels. At 24 hours necrotic areas were better delineated with islands of non-necrotic hepatocytes surrounding the portal vessels.

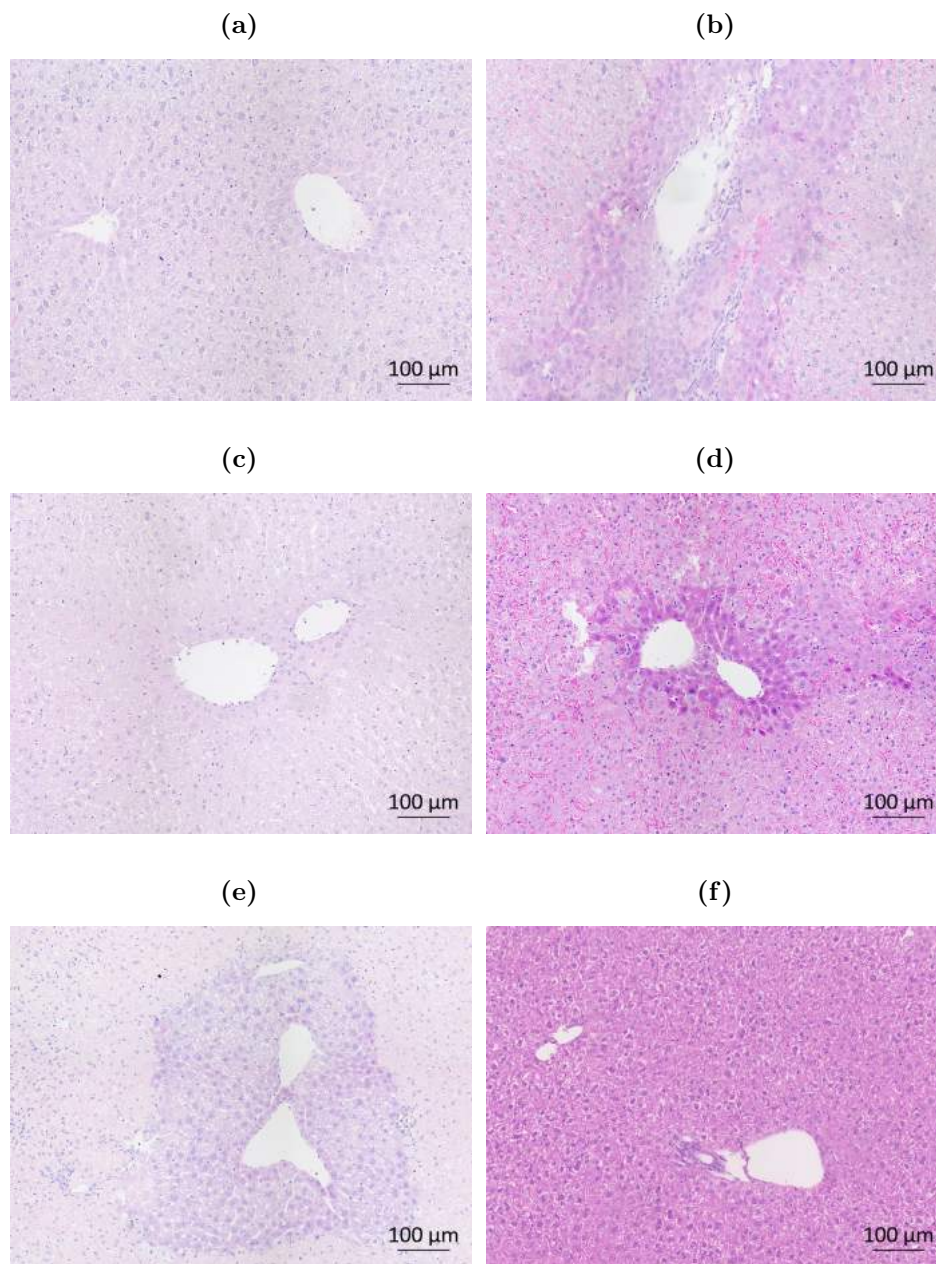


**Figure 6.4 – Representative haematoxylin and eosin staining of ischaemic mouse livers following 60 mins ischaemia and varied reperfusion injury.** Male C57BL/6 mice aged 8 weeks underwent 60 minutes of 70% ischaemia. Following ischaemia varying durations of reperfusion were undertaken. Ischaemic liver lobes were removed and stained with Haematoxylin and Eosin. (a) At baseline 0 hours reperfusion extravasation of red blood cells was seen into the spaces between hepatocytes with minimal apparent necrosis. At (b) 2, (c) 4 and (d) 6 hours necrosis became more apparent with sparing around the portal vessels. (e) At 24 hours necrotic areas were better delineated with islands of non-necrotic hepatocytes surrounding the portal vessels. (f) Sham controls showed no necrosis or abnormalities. All images are generated from whole slide scans and are at 400x magnification. Scale bars represent 100  $\mu\text{m}$ .

In the non-ischaemic lobes at baseline 0 hours reperfusion minimal changes were seen. At 4 hours some morphological changes in hepatocytes were seen and by 6 hours there were small areas of necrosis and some red cell extravasation. At 24 hours the morphological changes in hepatocytes had almost completely resolved and there were no apparent necrotic areas.



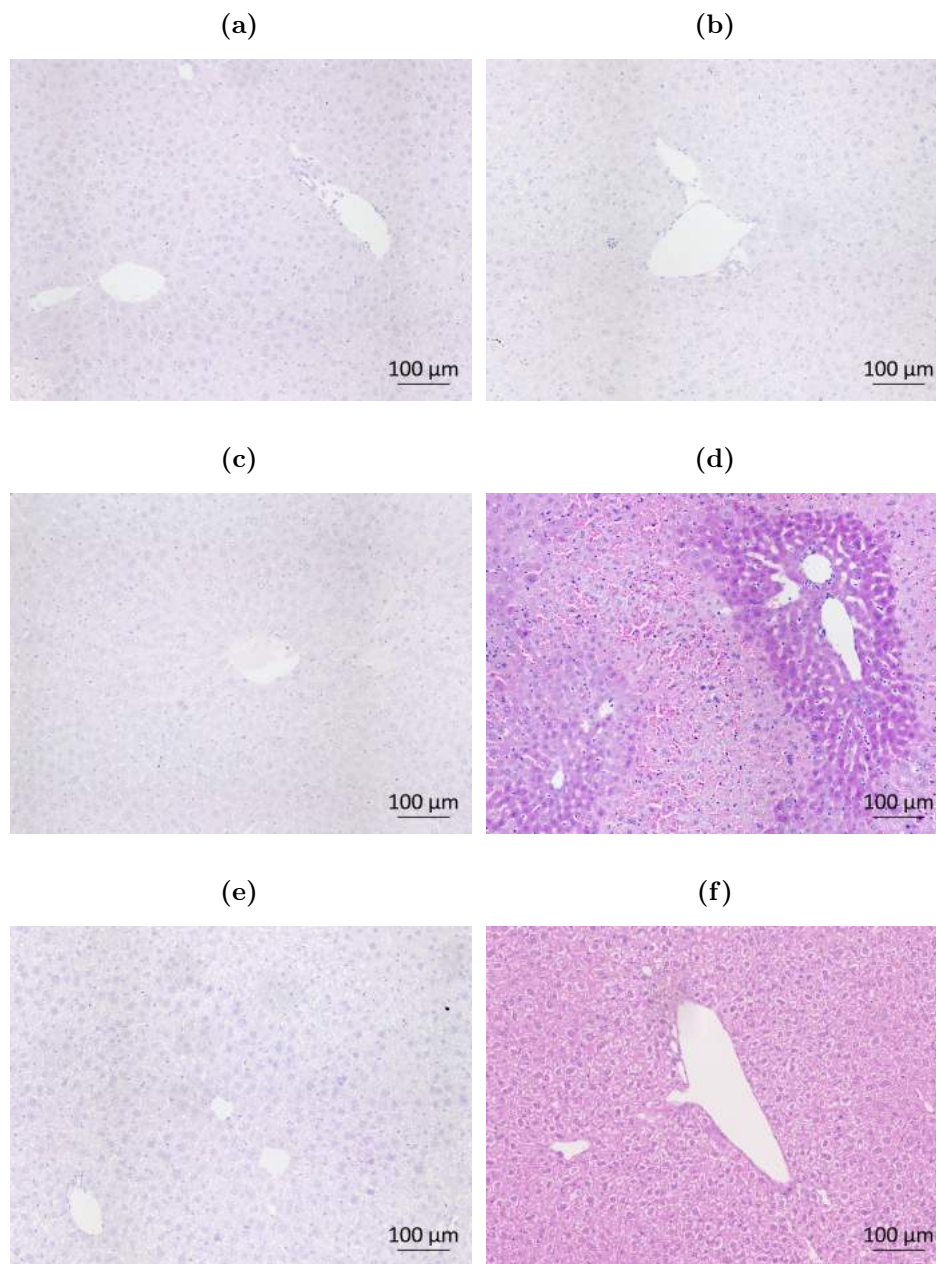


**Figure 6.5 – Representative haematoxylin and eosin staining of non-ischaemic mouse liver lobes following 60 mins ischaemia and varied reperfusion injury.** Male C57BL/6 mice aged 8 weeks underwent 60 minutes of 70% ischaemia. Following ischaemia varying durations of reperfusion were undertaken. Non-ischaemic liver lobes were removed and stained with H & E. (a) At baseline 0 hours reperfusion minimal changes were seen. (b) At 2 and (c) 4 hours some morphological changes in hepatocytes were seen. (d) At 6 hours there were small areas of necrosis and some red cell extravasation. (e) At 24 hours the morphological changes in hepatocytes had almost completely resolved and there were no apparent necrotic areas. (f) Sham controls showed no necrosis or abnormalities. All images are generated from whole slide scans and are at 400x magnification. Scale bars represent 100 µm.

In order to quantify the extent of liver ischaemia I next performed PAS staining (figures 6.6, 6.7 and 6.8). Glycogen depletion was used as a surrogate of hepatic ischaemia and hepatocyte function as previously described [306].

Following 60 minutes of ischaemia (n=17) the baseline 0 hours reperfusion ischaemic liver lobes showed considerable necrosis assessed by glycogen depletion ( $71.00\% \pm 7.69$ ). The amount of glycogen depletion remained relatively constant at 2 hours ( $74.36\% \pm 1.72$ ) and 4 hours ( $69.85\%$ ) with a peak at 6 hours ( $83.26\% \pm 2.69$ ). By 24 hours there was a small reduction in glycogen depletion ( $66.74\% \pm 11.86$ ). Sham controls showed much lower levels of glycogen depletion ( $17.05\% \pm 0.90$ ). In the non-ischaemic lobes there was a similar pattern of injury but with lower levels of glycogen depletion.

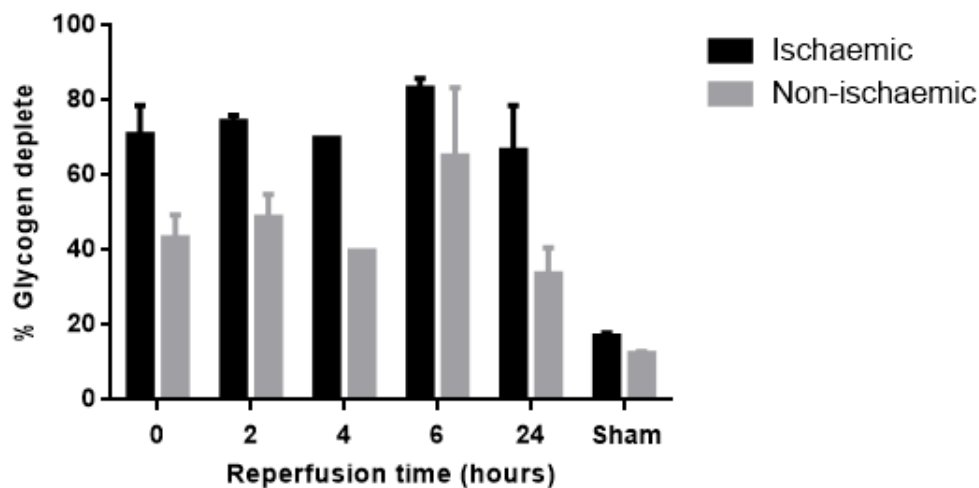


**Figure 6.6 – Histogram showing the time course of glycogen depletion in ischaemic and non-ischaemic livers of mice after hepatic ischaemia reperfusion injury assessed by PAS staining.** Male C57BL/6 mice aged 8 weeks underwent 60 minutes of 70% ischaemia. Following ischaemia varying durations of reperfusion were undertaken. Ischaemic and non-ischaemic liver lobes were removed and stained with PAS. The baseline 0 hours reperfusion ischaemic liver lobes showed considerable glycogen depletion ( $71.00\% \pm 7.69$ ). The amount of glycogen depletion remained constant at 2 hours ( $74.36\% \pm 1.72$ ) and 4 hours ( $69.85\%$ ) with a peak at 6 hours ( $83.26\% \pm 2.69$ ). By 24 hours there was a small reduction in glycogen depletion ( $66.74\% \pm 11.86$ ). Sham controls showed much lower levels of glycogen depletion ( $17.05\% \pm 0.90$ ). The non-ischaemic lobes showed a similar pattern but with lower levels of glycogen depletion at 0 ( $43.31\% \pm 6.16$ ), 2 ( $48.80\% \pm 6.20$ ), 4 ( $39.81\%$ ), 6 ( $65.21\% \pm 18.13$ ) and 24 ( $33.60\% \pm 6.99$ ) hours. Sham controls again showed lower levels of glycogen depletion ( $12.45\% \pm 0.43$ ). Histograms represent mean values and bars represent standard error of the mean, n=17.

In the ischaemic lobes the pattern of PAS staining at baseline 0 hours showed a global reduction in staining when compared with sham controls with no changes in architecture. This pattern continued at 2 and 4 hours. At 6 hours reperfusion there was both global fade in PAS staining as well as some underlying architectural changes in keeping with those seen in the H & E stained livers. At 24 hours of reperfusion there were higher levels of PAS staining seen in the peri-portal regions showing some recovery with widespread necrotic areas throughout the parenchyma. Sham controls demonstrated normal PAS staining.

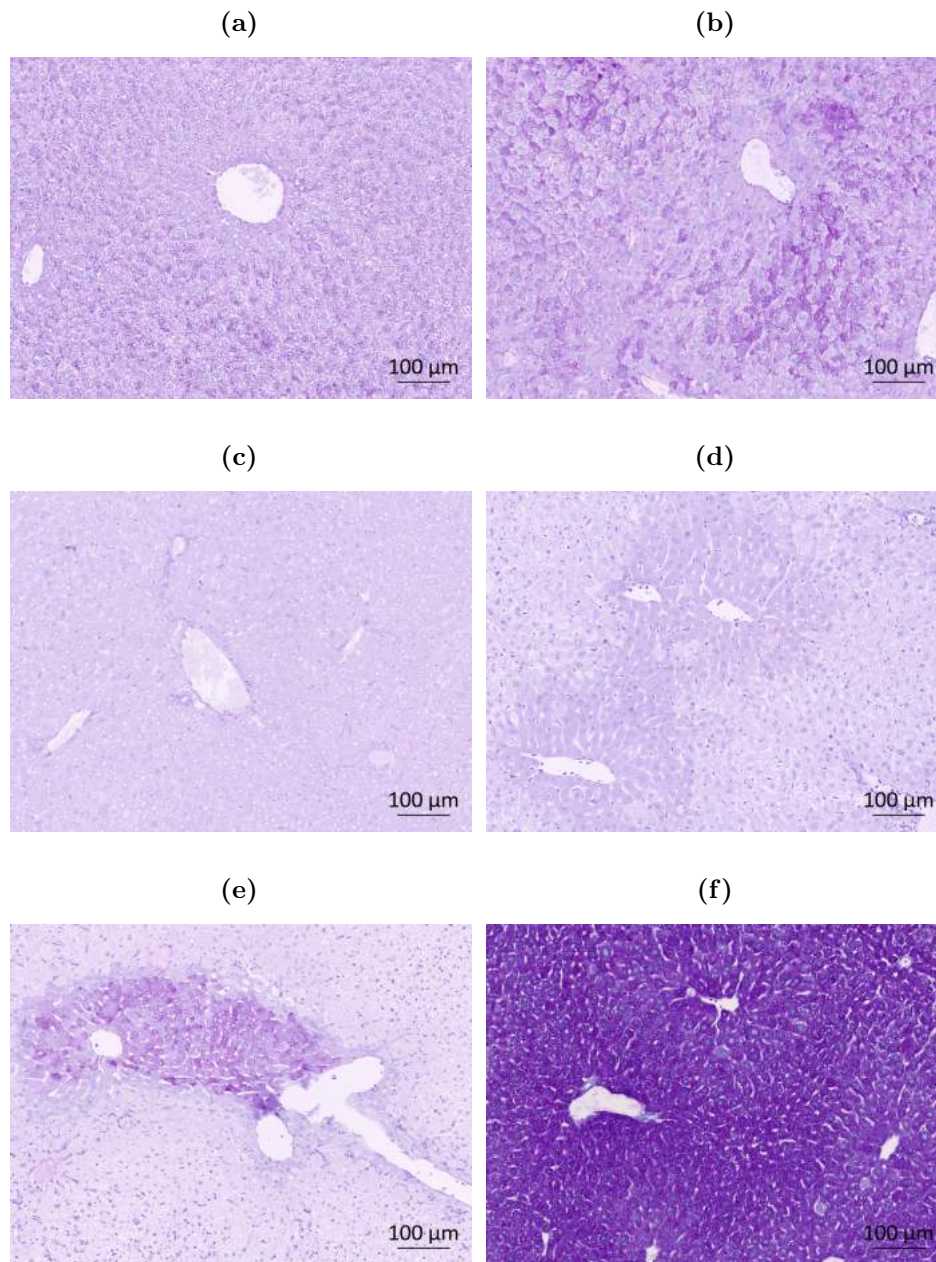


**Figure 6.7 – Representative histology of PAS stained ischaemic liver lobes following 60 minutes of 70% ischaemia.** Male C57BL/6 mice aged 8 weeks underwent 60 minutes of 70% ischaemia. Following ischaemia varying durations of reperfusion were undertaken. Ischaemic and non-ischaemic liver lobes were removed and stained with PAS. (a) The pattern of PAS staining at baseline 0 hours showed a global reduction in PAS staining when compared with sham controls with no changes in architecture. (b) At 2 and (c) 4 hours the same pattern of global reduction in PAS staining was seen. (d) At 6 hours reperfusion there was both global fade in PAS staining as well as some underlying architectural changes in keeping with those seen in the H & E stained livers. (e) At 24 hours of reperfusion there was higher levels of PAS staining seen in the peri-portal regions showing some recovery with widespread necrotic areas throughout the parenchyma. (f) Sham controls demonstrated normal staining. All images are generated from whole slide scans and are at 400x magnification. Scale bars represent 100 µm.

In the non-ischaemic lobes the pattern of PAS staining at baseline 0 hours showed a global patchy reduction in PAS staining when compared with sham controls but less than the ischaemic lobes with no changes in architecture. This pattern continued at 2 and 4 hours. At 6 hours reperfusion there was both global fade in PAS staining as well as some underlying architectural changes in keeping with those seen in the H & E stained livers but again less than the ischaemic lobes. At 24 hours of reperfusion there were higher levels of PAS staining than the earlier time points but less than the sham controls with global involvement across the lobes and no architectural changes. Sham controls demonstrated normal glycogen staining.



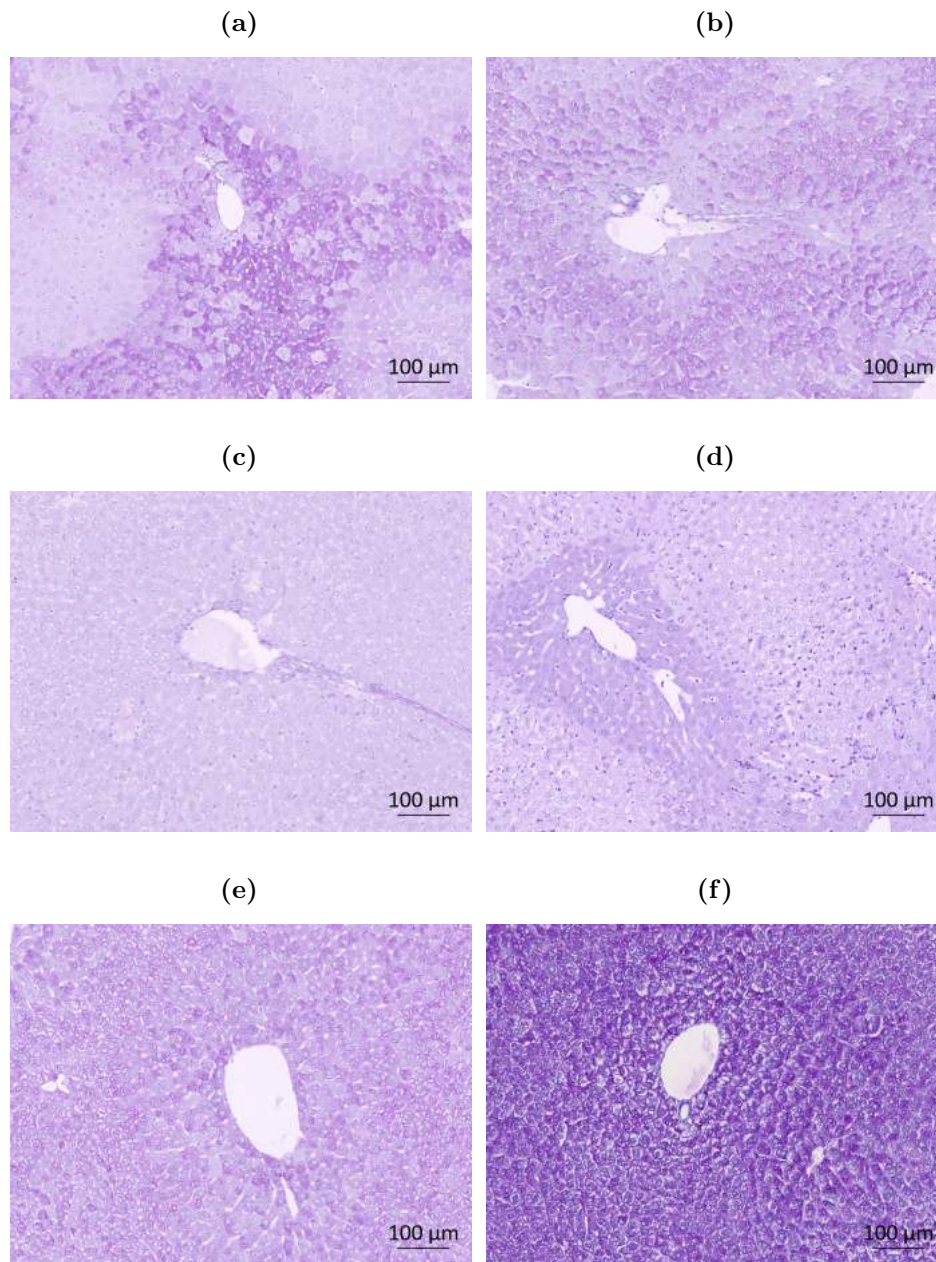


**Figure 6.8 – Representative histology of PAS stained non-ischaemic liver lobes following 60 minutes of 70% ischaemia.** Male C57BL/6 mice aged 8 weeks underwent 60 minutes of 70% ischaemia. Following ischaemia varying durations of reperfusion were undertaken. Ischaemic and non-ischaemic liver lobes were removed and stained with PAS. (a) The pattern of PAS staining at baseline 0 hours showed a global patchy reduction when compared with sham controls but less than the ischaemic lobes with no changes in architecture. (b) At 2 and (c) 4 hours the same pattern of global reduction in PAS staining was seen. (d) At 6 hours reperfusion there was global fade in PAS staining as well as some underlying architectural changes in keeping with those seen in the H & E stained livers but again less than the ischaemic lobes. (e) At 24 hours of reperfusion levels of PAS staining were higher than earlier time points but less than sham controls with global involvement across the lobes and no architectural changes. (f) Sham controls demonstrated normal PAS staining. All images are generated from whole slide scans at 400x magnification. Scale bars represent 100 µm.

I next sought to examine the infiltrating immune cells in livers of mice after ischaemia reperfusion injury by flow cytometry.

#### **6.2.2.3 Analysis of liver infiltrating immune cells by flow cytometry in hepatic ischaemia reperfusion injury**

Whilst the published literature in hepatic ischaemia reperfusion injury has focussed on immunohistochemical analysis of immune cells I decided that utilising flow cytometric analysis would give a more accurate quantification of the immune cells found in the livers of mice following ischaemia reperfusion injury. Following sacrifice liver lobes were mechanically homogenised and following washing were passed over a density gradient using Optiprep™. Cells were stained and analysed by flow cytometry (figure 6.9).

Total CD45<sup>+</sup> cells increased from baseline to peak at 24 hours in the ischaemic lobes, whereas there was a relatively constant level in the non-ischaemic lobes throughout the time course. CD3<sup>+</sup>CD4<sup>+</sup> cells appeared to decrease in number during reperfusion in the ischaemic lobes but levels increased again at 24 hours. The pattern in the non-ischaemic lobes showed a peak at 6 hours with a return to baseline at 24 hours. CD3<sup>+</sup>CD8<sup>+</sup> cell numbers initially fell in the ischaemic lobe but by 24 hours were higher than the baseline levels. In the non-ischaemic lobe levels again remained relatively constant. NK1.1<sup>+</sup> natural killer cell levels appeared unchanged in the ischaemic lobes during reperfusion injury, however in the non-ischaemic lobes NK1.1<sup>+</sup> cells showed relatively high levels at baseline and decreased by 24 hours. Platelets, represented by CD41<sup>+</sup> cells, increased from baseline to a peak at 2 hours in the ischaemic lobes and then fell to below baseline by 24 hours. In the non-ischaemic lobes levels increased from baseline and remained relatively constant throughout the 24 hour time course. Neutrophil cell numbers (SSC<sup>Int</sup>Ly6G<sup>Hi</sup>) remained low for the first 6 hours and then showed a large increase in number by 24 hours in the ischaemic lobes, but remained at low levels in the non-ischaemic lobes for the duration of the 24 hour experiment.

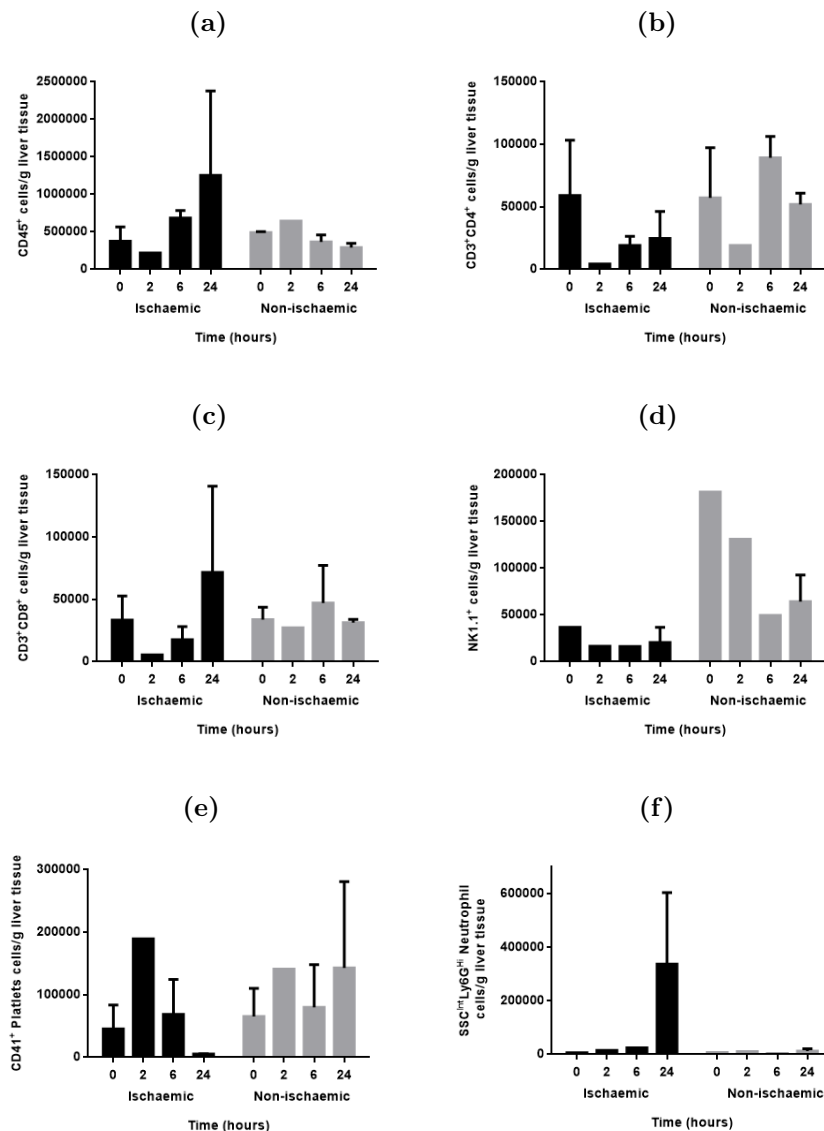


**Figure 6.9 – Flow cytometric analysis of mouse livers following ischaemia reperfusion injury.** Male C57BL/6 mice aged 8 weeks underwent 60 minutes of 70% ischaemia. Liver lobes were homogenised and passed over a density gradient. Cells were stained and analysed by flow cytometry. (a) Total CD45<sup>+</sup> cells increased to peak at 24 hours in the ischaemic lobes, in the non-ischaemic lobe they remained constant. (b) CD3<sup>+</sup>CD4<sup>+</sup> cells decreased initially in the ischaemic lobes increased again at 24 hours. The non-ischaemic lobes showed a peak at 6 hours with a return to baseline at 24 hours. (c) CD3<sup>+</sup>CD8<sup>+</sup> cell numbers initially fell in the ischaemic lobe but by 24 hours were higher than the baseline levels. In the non-ischaemic lobe numbers again remained relatively constant. (d) Nk1.1<sup>+</sup> cell numbers appeared unchanged in the ischaemic lobes during reperfusion injury, however in the non-ischaemic lobes NK1.1<sup>+</sup> cells showed relatively high levels at baseline and decreased by 24 hours. (e) Platelets, represented by CD41<sup>+</sup> cells, increased from baseline to a peak at 2 hours in the ischaemic lobes and then fell to below baseline by 24 hours. In the non-ischaemic lobes levels increased from baseline and remain relatively constant throughout the 24 hour time course. (f) Neutrophils remained low for the first 6 hours but showed a large increase in number by 24 hours in the ischaemic lobes, but remained at low levels in the non-ischaemic lobe for the duration of the 24 hour experiment. Histograms represent mean and bars represent standard error of the mean, n=15.



Having quantified the injury profile during reperfusion I next assessed the impact of clamp duration on injury.

### **6.2.3 The effect of clamp duration in ischaemia reperfusion injury**

In the published literature ischaemia reperfusion injury models in the liver use a broad range of clamp times [307, 308]. I decided to compare clamp times of 30 and 60 minutes in order to determine the minimum duration required to illicit prolonged liver necrosis in keeping with the equivalent clinical picture. As in the previous experiments mice underwent general anaesthesia and a laparotomy with the use of an atraumatic clamp to interrupt the hepatic blood supply at the portal triad. A 70% model was used, however clamp times were varied at either 30 or 60 minutes and analysis was undertaken after different durations of reperfusion.

#### **6.2.3.1 Serum transaminases following different clamp durations in hepatic ischaemia reperfusion injury**

Male C57BL/6 mice aged 8 weeks underwent either 30 minutes or 60 minutes of 70% hepatic ischaemia. Following ischaemia varying durations of reperfusion were undertaken and serum ALT analysed (figure 6.10).

At baseline 0 hours ALT was raised in both the 30 minute ( $368.3 \text{ IU/L} \pm 81.7$ ) and 60 minute ( $647.5 \text{ IU/L} \pm 279.4$ ) clamp group, with the 60 minute group having nearly double the ALT of the 30 minute group. By 6 hours levels in both groups had raised with the 60 minute group demonstrating a considerably higher level ( $15893.3 \text{ IU/L} \pm 3059.6$ ) than the 30 minute group ( $1170.0 \text{ IU/L} \pm 665.1$ ). At 24 hours ALT levels in both groups had decreased with the 30 minute group ( $185.0 \text{ IU/L} \pm 155.0$ ) lower than the 60 minute group ( $2825.0 \text{ IU/L} \pm 873.3$ ).

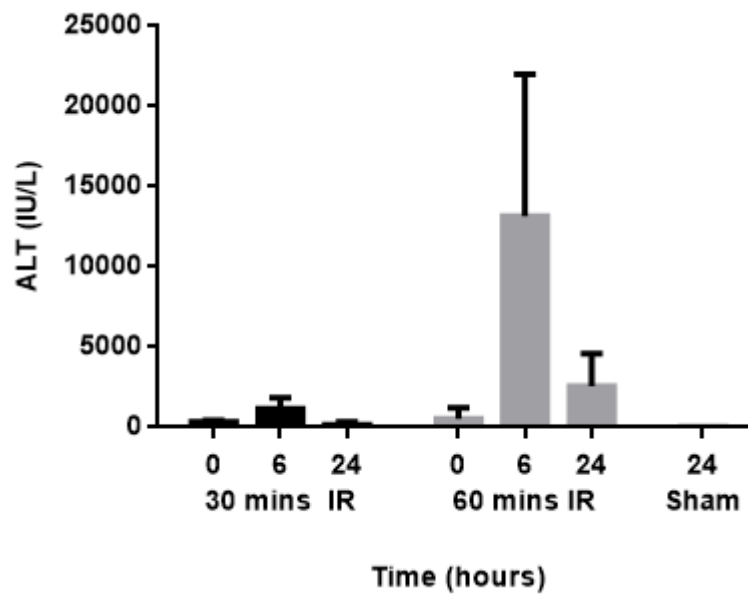


**Figure 6.10 – Time course of serum ALT following either 30 or 60 minutes of hepatic ischaemia.** Male C57BL/6 mice aged 8 weeks underwent either 30 or 60 minutes of 70% ischaemia. Following ischaemia varying durations of reperfusion were undertaken. At baseline 0 hours ALT was raised in both the 30 minute ( $368.3 \text{ IU/L} \pm 81.7$ ) and 60 minute ( $647.5 \text{ IU/L} \pm 279.4$ ) clamp group. By 6 hours levels in both groups had raised with the 60 minute group demonstrating a considerably higher level ( $15893.3 \text{ IU/L} \pm 3059.6$ ) than the 30 minute group ( $1170.0 \text{ IU/L} \pm 665.1$ ). At 24 hours ALT levels in both groups had decreased with the 30 minute group ( $185.0 \text{ IU/L} \pm 155.0$ ) lower than the 60 minute group ( $2825.0 \text{ IU/L} \pm 873.3$ ). Histograms represent mean and bars represent standard error of the mean,  $n=23$ .

I next assessed the histological changes when using different clamp durations in the hepatic ischaemia reperfusion model.

### 6.2.3.2 Histochemical analysis of different clamp durations in hepatic ischaemia reperfusion injury

Following sacrifice of C57BL/6 mice liver tissue was removed from the lobes which underwent ischaemia and the lobes that were spared and fixed in formalin. Fixed liver tissue was embedded in paraffin and processed for histochemistry.

H & E staining (figure 6.11) was performed. At 0 hours baseline there was some red cell extravasation but no necrosis or architectural changes seen in the ischaemic lobe, and no clear change in the non-ischaemic lobe. After 6 hours of reperfusion there were a few small areas which demonstrated fading of the nucleus in hepatocytes along with

small infiltrating cells in both the ischaemic lobes and the non-ischaemic lobes. By 24 hours there was no architectural changes or necrotic areas in either the ischaemic or the non-ischaemic lobes.

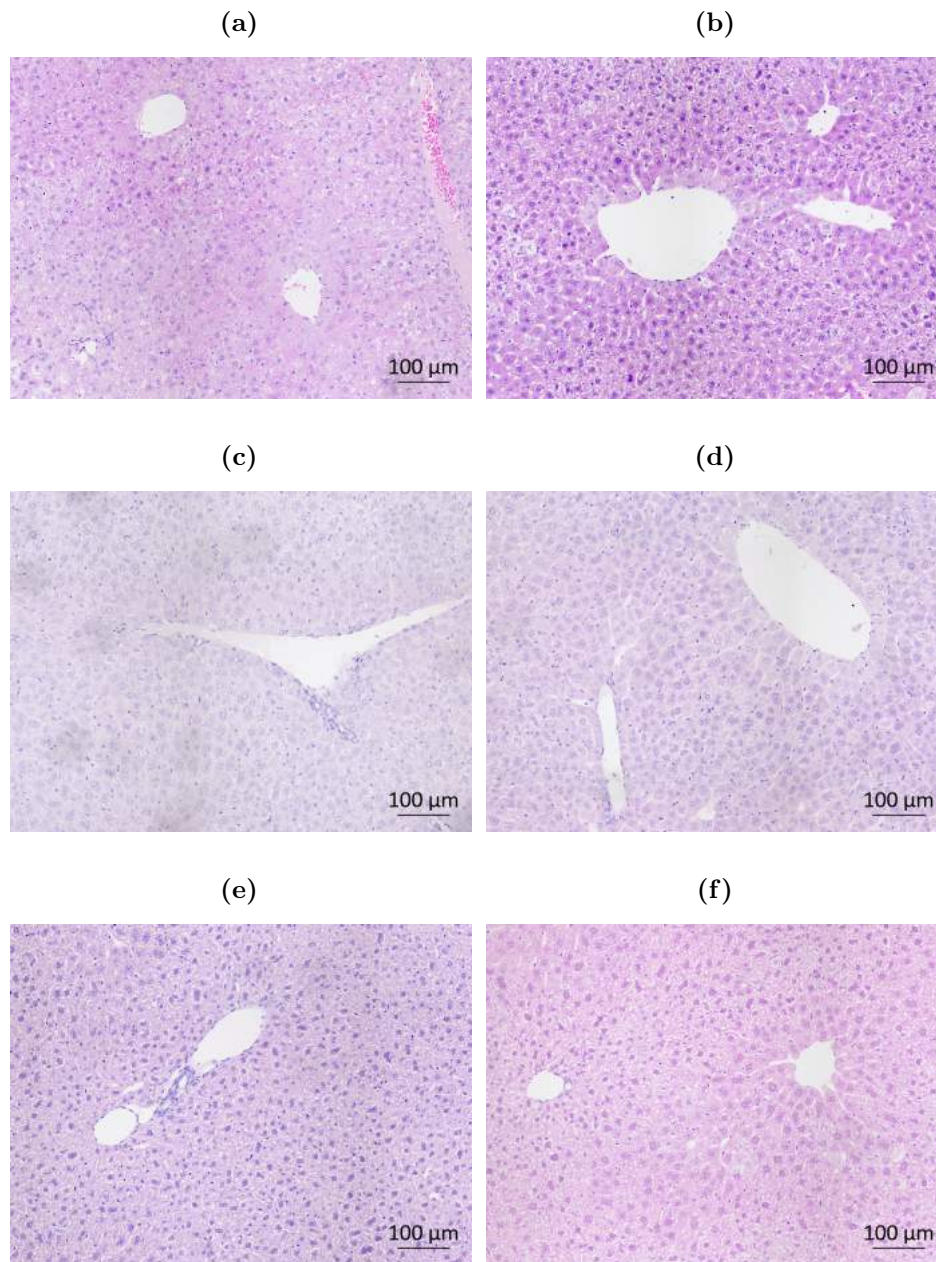


**Figure 6.11 – Representative haematoxylin and eosin staining of non-ischaemic mouse liver lobes following 30 minutes ischaemia and varied duration of reperfusion injury.** Male C57BL/6 mice aged 8 weeks underwent 30 minutes of 70% hepatic ischaemia. Following sacrifice liver tissue was removed and fixed in formalin. H & E staining was performed on processed liver tissue. (a) At 0 hours baseline there was some red cell extravasation but no necrosis or architectural changes seen in the ischaemic lobe, and (b) no clear change in the non-ischaemic lobe. (c) After 6 hours of reperfusion there was a few small areas which demonstrated fading of the nucleus in hepatocytes along with small infiltrating cells in both the ischaemic lobes (d) and the non-ischaemic lobes. (e) By 24 hours there was no architectural changes or necrotic areas in either the ischaemic (f) or the non-ischaemic lobes. All images are generated from whole slide scans and are at 400x magnification. Scale bars represent 100 µm.

In order to quantify the extent of liver ischaemia I next performed PAS staining (figures 6.12 and 6.13). Glycogen depletion was used as a surrogate of ischaemia. Over the 24 hour time course the ischaemic lobe in the 60 minute clamp group showed consistently more glycogen depletion than the 30 minute group ( $66.7\% \pm 11.6$  vs  $64.6\% \pm 15.6$  at 24 hours) however these findings did were not statistically significant. As expected the amount of glycogen depletion was lower in the non-ischaemic lobes when compared with the ischaemic lobes at all time points and for both 30 and 60 minutes clamp duration. At 0 hours the non-ischaemic lobes in the 30 and 60 minute groups were broadly similar ( $47.2\% \pm 1.36$  vs  $43.3\% \pm 6.16$ ), however at 24 hours the non-ischaemic lobe in the 60 minute group showed less glycogen depletion than the 30 minute group ( $33.6\% \pm 7.0$  vs  $56.3\% \pm 0.5$ ) although this also did not reach statistical significance ( $p=0.0957$ ).

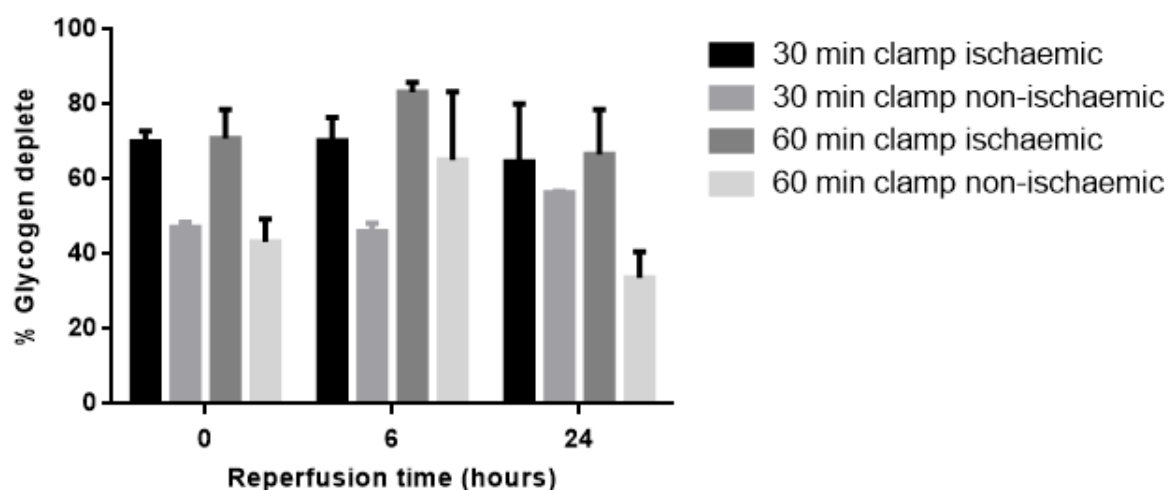


**Figure 6.12 – Histogram showing the time course of glycogen depletion in ischaemic and non-ischaemic livers of mice after either 30 or 60 minutes of hepatic ischaemia reperfusion injury assessed by PAS staining.** Male C57BL/6 mice aged 8 weeks underwent either 30 or 60 minutes of 70% ischaemia. Following ischaemia varying durations of reperfusion were undertaken. Glycogen depletion was used as a surrogate of ischaemia. At 0, 6 and 24 hours the ischaemic lobe in the 30 minute clamp group showed consistently less glycogen depletion than the 60 minute group ( $70.0\% \pm 2.8$  vs  $71.0\% \pm 7.7$ ,  $70.3\% \pm 6.2$  vs  $83.3\% \pm 2.7$  and  $64.6\% \pm 15.6$  vs  $66.7\% \pm 11.6$ ) however these findings did not reach statistical significance. The amount of glycogen depletion was lower in the non-ischaemic lobes when compared with the ischaemic lobes at all time points and for both 30 and 60 minutes clamp duration. At 0 hours the non-ischaemic lobes in the 30 and 60 minute groups were broadly similar ( $47.2\% \pm 1.36$  vs  $43.3\% \pm 6.16$ ), however at 24 hours the non-ischaemic lobe in the 30 minute group showed more glycogen depletion than the 60 minute group ( $56.3\% \pm 0.5$  vs  $33.6\% \pm 7.0$ ) although this also did not reach statistical significance ( $p=0.0957$ ). Statistical analysis was undertaken using Student's t-test. Histograms represent mean and bars represent standard error of the mean,  $n=19$ .

In the livers of mice undergoing 30 minutes of ischaemia there was visibly more glycogen staining than in the mice undergoing 60 minutes of ischaemia at all time points. The pattern of staining showed a global patchy reduction in staining in the ischaemic lobes of the 30 minute group at baseline 0 hours and 6 hours. By 24 hours there was visually more glycogen staining across all of the liver lobe. The non-ischaemic lobes of the mice in the 30 minute group showed a similar pattern to those in the 60 minute group with a reduction in glycogen deposition in the parenchyma with some sparing of the peri-portal region. There did appear to be less recovery of glycogen staining in the 30 minute group when compared with the 60 minute group.



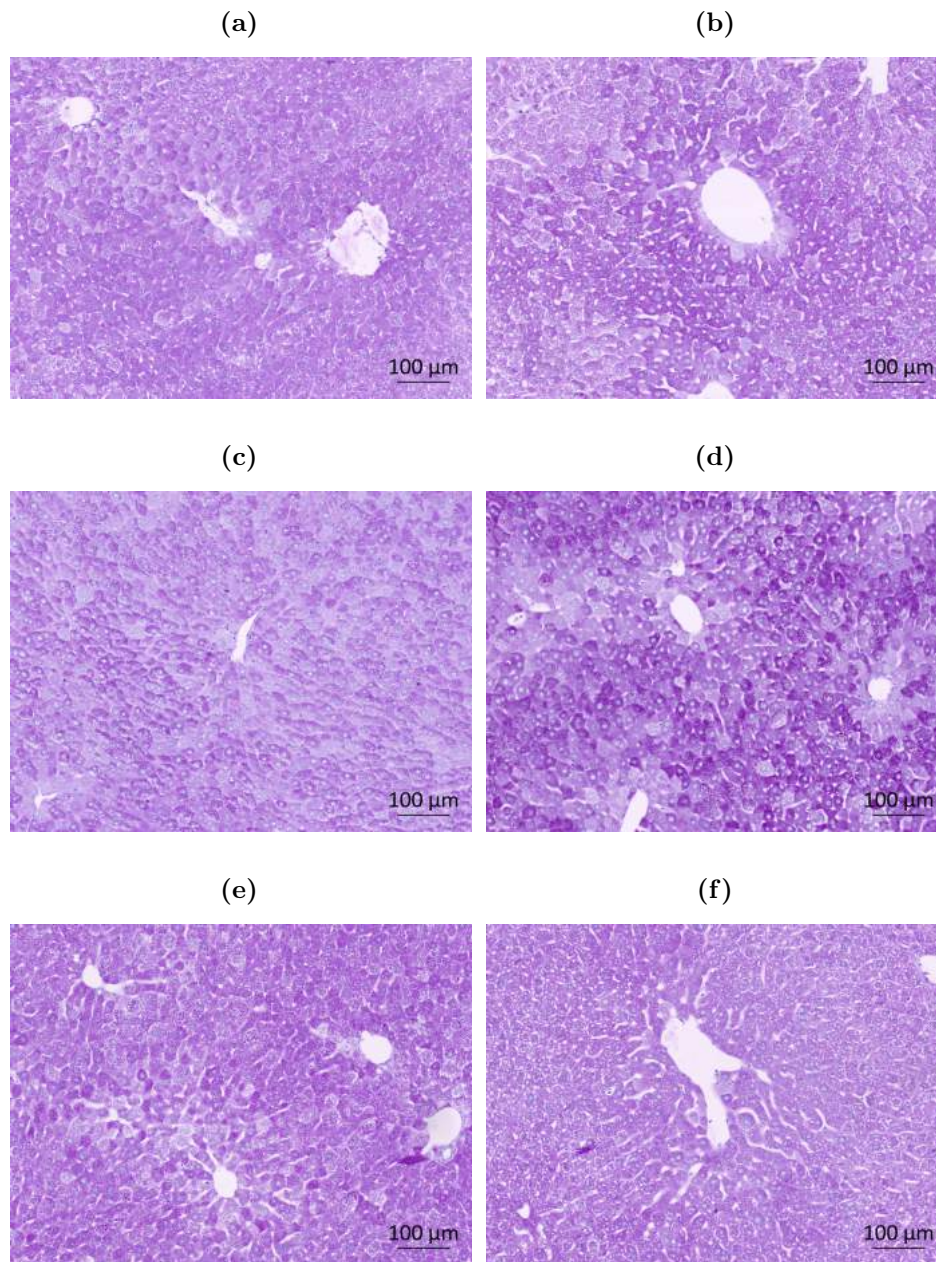


**Figure 6.13 – Representative PAS staining of ischaemic and non-ischaemic mouse liver lobes following 30 minutes of ischaemia and varied duration of reperfusion injury.** Male C57BL/6 mice aged 8 weeks underwent 30 minutes of 70% hepatic ischaemia. Following sacrifice liver tissue was removed and fixed in formalin. PAS staining was performed on processed liver tissue. (a) At baseline 0 hours there was a patchy reduction in staining in the ischaemic lobe with the (b) non-ischaemic lobe showing a reduction in staining with some peri-portal sparing. (c) at 6 hours a similar pattern in the ischaemic and (d) non-ischaemic lobes was present with less overall staining in both. At (e) 24 hours there was an increase in overall staining in the ischaemic lobe but the (f) non-ischaemic lobe appeared to show less recovery of staining. Images are generated from whole slide scans and are at 400x magnification. Scale bars represent 100 µm.

I next sought to assess the effects of clamp duration on infiltrating immune cells in the livers of mice undergoing hepatic ischaemia reperfusion injury.

#### **6.2.3.3 The effect of clamp duration on liver infiltrating immune cells in hepatic ischaemia reperfusion injury**

Male C57BL/6 mice aged 8 weeks underwent 30 minutes of 70% hepatic ischaemia. Following sacrifice liver lobes were mechanically homogenised and following washing were passed over a density gradient using Optiprep<sup>TM</sup>. Cells were stained and analysed by flow cytometry (figure 6.14).

Mice that had undergone 30 minutes of ischaemia showed peak levels of CD45<sup>+</sup>, CD4<sup>+</sup>, CD8<sup>+</sup>, NK1.1<sup>+</sup> cells and platelets (CD41<sup>+</sup>) in their livers at baseline 0 hours with levels reducing at 6 hours and again at 24 hours. This pattern was repeated in the non-ischaemic lobes with the exception of CD8<sup>+</sup> cells which appeared to continue to increase at 6 hours and then decrease at 24 hours. Neutrophils (SSC<sup>int</sup>Ly6G<sup>Hi</sup>) in the ischaemic lobes were static between 0 and 6 hours, but then increased at 24 hours, whereas the non-ischaemic lobes the levels decreased between 0 and 24 hours.



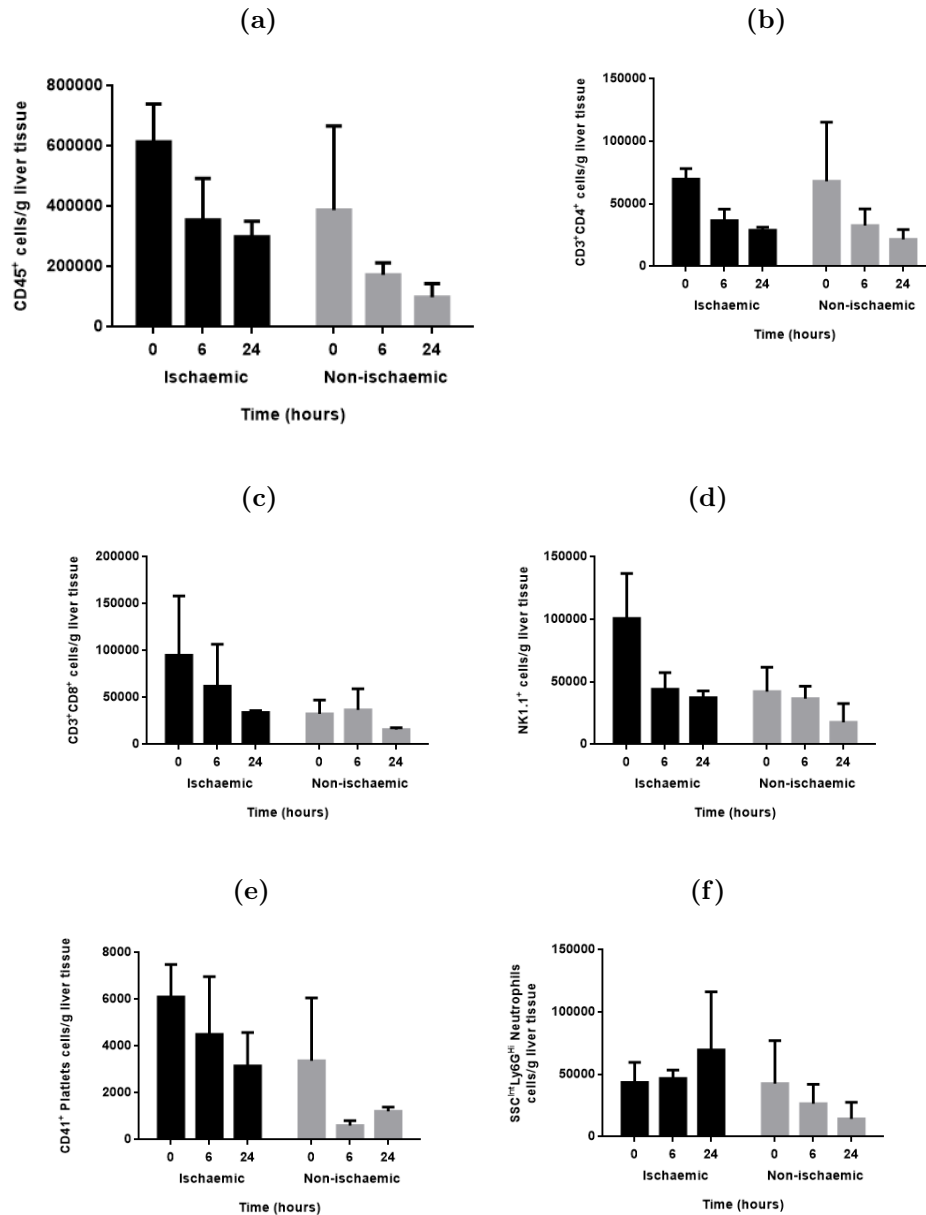


**Figure 6.14 – Flow cytometric analysis of mouse livers following 30 minutes of ischaemia and a variable duration of reperfusion injury.** Male C57BL/6 mice aged 8 weeks underwent 30 minutes or 60 of 70% hepatic ischaemia. Following sacrifice liver lobes were mechanically homogenised and following washing were passed over a density gradient. Cells were stained and analysed by flow cytometry. In the ischaemic and non-ischaemic lobes peak levels of cells occurred at 0 hours baseline and decreased at 6 and 24 hours in the (a) CD45<sup>+</sup> and (b) CD3<sup>+</sup>CD4<sup>+</sup> populations. (c) This pattern was present in the ischaemic lobes of CD3<sup>+</sup>CD8<sup>+</sup> cells but the non-ischaemic lobes showed a peak at 6 hours and a decrease again at 24 hours. (d) NK1.1<sup>+</sup> cells decreased in number in the ischaemic and non-ischaemic lobes at 6 and 24 hours. (e) Platelets (CD41<sup>+</sup>) decreased in number in the ischaemic lobes at 6 and 24 hours, however in the non-ischaemic lobes there was an initial reduction between 0 hours and 6 hours followed by an increase at 24 hours. (f) Neutrophils (SSC<sup>int</sup>Ly6G<sup>Hi</sup>) showed an increase between 0, 6 and 24 hours in the ischaemic lobes, and a reduction in the non-ischaemic lobes. Histograms represent mean and bars represent standard error of the mean, n=8.

I next sought to test the hypothesis that P $\alpha$ S MSC could reduce the injury in hepatic ischaemia reperfusion injury. Based on the above results I decided to use a clamp time of 60 minutes rather than 30 minutes as this represented a more stable injury pattern with less recovery and a duration of 24 hours.

#### **6.2.4 *In vivo* efficacy of P $\alpha$ S MSC in the hepatic ischaemia reperfusion model**

Bone marrow derived MSC have been shown to reduce hepatocyte apoptosis in a rat model of hepatic ischaemia reperfusion injury and hepatectomy [193]. Given the findings earlier in this chapter I decided to use a clamp time of 60 minutes in order to induce a persistent severe injury. Given the amount of injury induced and the findings of the previous chapter demonstrating low numbers of P $\alpha$ S MSC in the liver after systemic injection I decided that a higher dose would be required in order to adequately test the hypothesis that P $\alpha$ S MSC reduce injury in a model of hepatic ischaemia reperfusion injury. I chose a dose of  $1 \times 10^6$  P $\alpha$ S MSC and based on previous experience with doses in this range and the risk of embolic complications [245] I opted to administer the P $\alpha$ S MSC via the intra-peritoneal route. Experience with this route has demonstrated efficacy in other models of liver injury with P $\alpha$ S MSC [237], has been shown to improve MSC engraftment [309], and in the context of liver surgery this route is feasible in the clinical environment and therefore readily translatable. Whilst the use of the portal venous route has potential advantages [310], other studies have shown that MSC can embolise and cause worse outcomes [311], due to the potential risk I decided to avoid this route of administration.

Male C57BL/6 mice aged 8 weeks were injected via the intra-peritoneal route with  $1 \times 10^6$  P $\alpha$ S MSC 1 hour prior to undergoing surgery. Mice were then subjected to 60 minutes of 70% hepatic ischaemia followed by 24 hours of reperfusion.

#### 6.2.4.1 Serum transaminases in hepatic ischaemia reperfusion injury following P $\alpha$ S MSC therapy

Following injection with P $\alpha$ S MSC and 60 minutes of ischaemia mice were allowed 24 hours of reperfusion and then culled and serum analysed for ALT. There was no significant difference in ALT between control and treated mice following treatment with P $\alpha$ S MSC (4585 IU/L  $\pm$  1567 vs 5877 IU/L  $\pm$  1491).

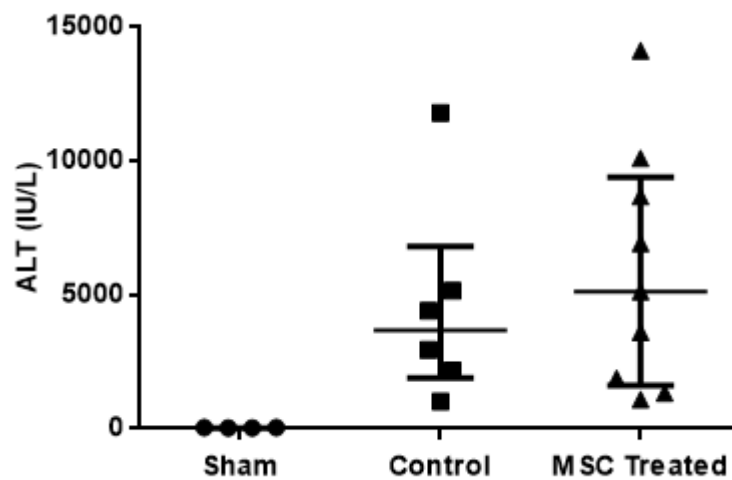


**Figure 6.15 – Serum ALT in mice following 60 minutes of ischaemia and treatment with P $\alpha$ S MSC.** Male C57BL/6 mice aged 8 weeks were injected via the intra-peritoneal route with  $1 \times 10^6$  P $\alpha$ S MSC. Mice were then subjected to 60 minutes of 70% hepatic ischaemia followed by 24 hours of reperfusion and then culled and serum analysed for ALT. There was no significant difference in ALT between control and treated mice following treatment with P $\alpha$ S MSC (4585 IU/L  $\pm$  1567 vs 5877 IU/L  $\pm$  1491). Points represent individual mice, bars represent the median and lines represent the interquartile range. Statistical analysis was carried out using a Student's t-test.

#### 6.2.4.2 Histochemical analysis in hepatic ischaemia reperfusion injury following P $\alpha$ S MSC therapy

Liver tissue from mice who have undergone hepatic ischaemia and treatment with P $\alpha$ S MSC was removed, processed and embedded in paraffin and then sectioned and stained. Haematoxylin and eosin staining was performed in order to demonstrate the morphology of the liver (figure 6.16). Both ischaemic and non-ischaemic lobes in the sham controls showed normal morphology. The ischaemic lobes in the PBS control mice showed widespread

necrosis with sparing around the portal region with red cell extravasation. The non-ischaemic lobes showed some ischaemia but less than the ischaemic lobes and again demonstrated portal sparing. The ischaemic and non-ischaemic lobes in mice treated with P $\alpha$ S MSC showed a similar pattern to their PBS treated control counterparts.

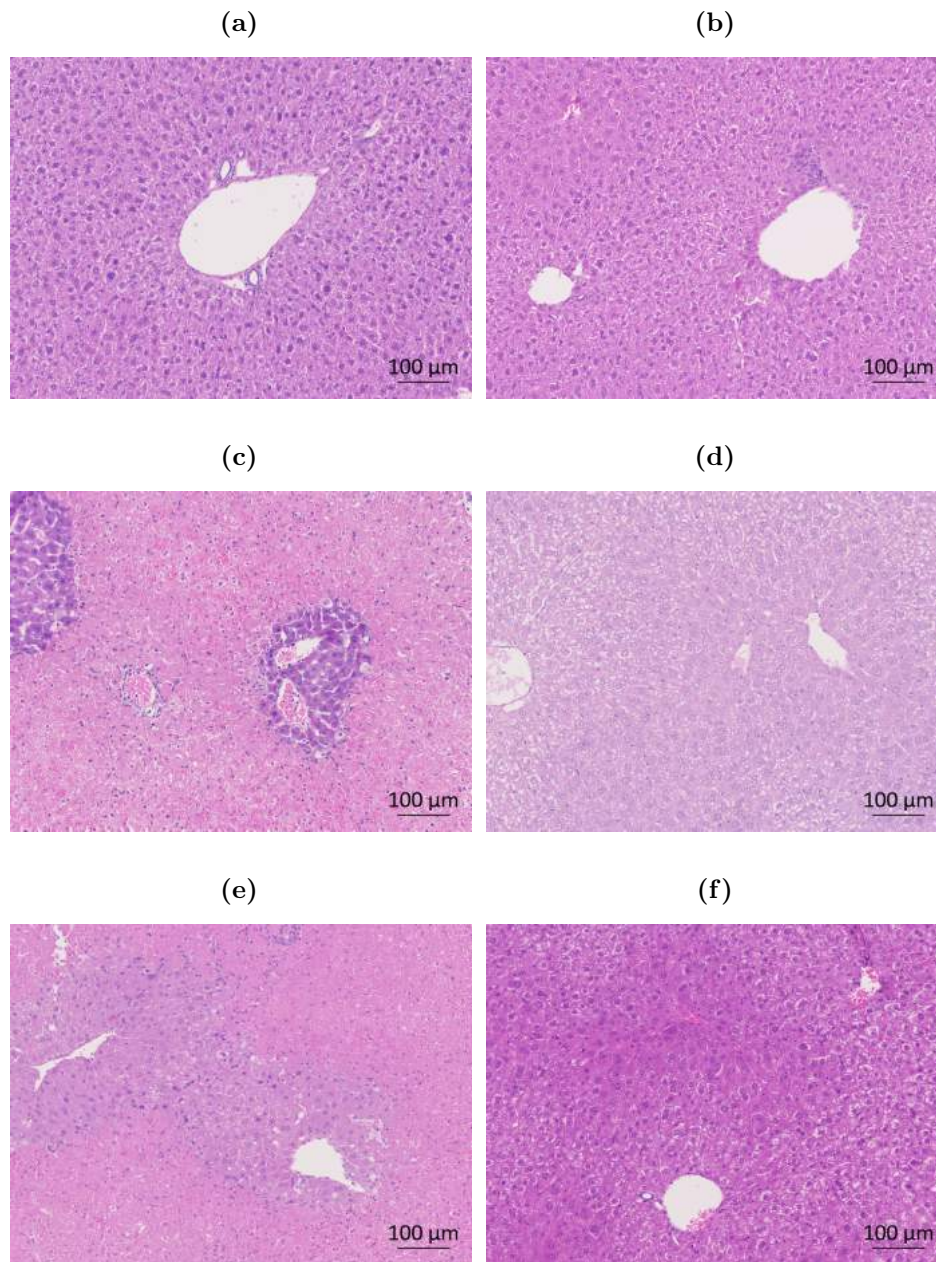


**Figure 6.16 – Representative images of haematoxylin and eosin staining in C57BL/6 mice having undergone 60 minutes of ischaemia treated with either PBS or PαS MSC.** C57BL/6 mice aged 8 weeks were injected via the intra-peritoneal route with  $1 \times 10^6$  PαS MSC. Mice were then subjected to 60 minutes of 70% hepatic ischaemia followed by 24 hours of reperfusion and following sacrifice liver tissue was removed and fixed in formalin. H and E staining was performed on processed liver tissue. (a) Ischaemic lobes in sham controls showed normal morphology as did (b) non-ischaemic lobes in sham controls. (c) Ischaemic lobes in PBS controls showed widespread necrosis with sparing around the portal region with red cell extravasation. (d) Non-ischaemic lobes in PBS controls showed some ischaemia but less than the ischaemic lobes and again demonstrated portal sparing. (e) Ischaemic lobes in mice treated with PαS MSC showed a similar pattern to PBS controls and (f) non-ischaemic lobes in mice treated with PαS MSC showed a similar pattern to their non-ischaemic PBS counterparts. Images are generated from whole slide scans and are at 400x magnification. Scale bars represent 100 μm.

PAS staining was also carried out on paraffin embedded sections (figures 6.17 and 6.18). Quantification was undertaken using ImageJ software. Glycogen depletion was used as a surrogate of ischaemia. Sham surgical controls showed a low amount of glycogen depletion in the ischaemic and non-ischaemic lobes. In the mice undergoing ischaemia those treated with P $\alpha$ S MSC showed a significant reduction in glycogen depletion in the ischaemic lobes when compared with controls ( $91.7\% \pm 2.8$  vs  $80.1\% \pm 4.6$ ,  $p=0.03$ ), whereas the non-ischaemic lobes showed no significant difference ( $43.6\% \pm 6.4$  vs  $48.4\% \pm 2.7$ ).

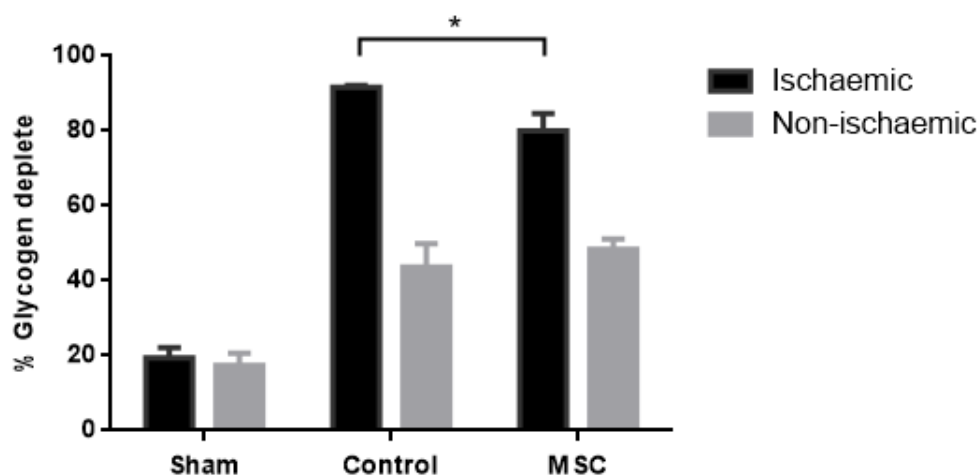


**Figure 6.17 – PAS staining in the livers of C57BL/6 mice following 60 minutes 70% ischaemia and treatment with either PBS or P $\alpha$ S MSC.** C57BL/6 mice aged 8 weeks were injected via the intra-peritoneal route with  $1 \times 10^6$  P $\alpha$ S MSC. Mice were then subjected to 60 minutes of 70% hepatic ischaemia followed by 24 hours of reperfusion and following sacrifice liver tissue was removed and fixed in formalin. PAS staining was performed on processed liver tissue. Sham surgical controls showed a low amount of glycogen depletion in the ischaemic and non-ischaemic lobes ( $19.4\% \pm 2.8$  vs  $17.5\% \pm 3.2$ ). In the mice undergoing ischaemia mice treated with P $\alpha$ S MSC showed a significant reduction in glycogen depletion in the ischaemic lobes when compared with controls ( $91.7\% \pm 2.8$  vs  $80.1\% \pm 4.6$ ,  $p=0.03$ ), whereas the non-ischaemic lobes showed no significant difference ( $43.6\% \pm 6.4$  vs  $48.4\% \pm 2.7$ ). Statistical analysis was undertaken using Welch's t-test. Histograms represent mean and bars represent standard error of the mean,  $n=12$ .

Mice undergoing sham surgery showed no reduction staining in either the ischaemic or non-ischaemic lobes. Mice treated with P $\alpha$ S MSC showed a reduction in staining in the liver parenchyma with sparing of the portal regions in the ischaemic lobe. A less pronounced reduction in staining was seen in the non-ischaemic lobe with no clear sparing

of the portal region. A similar pattern was also seen in the PBS treated controls.



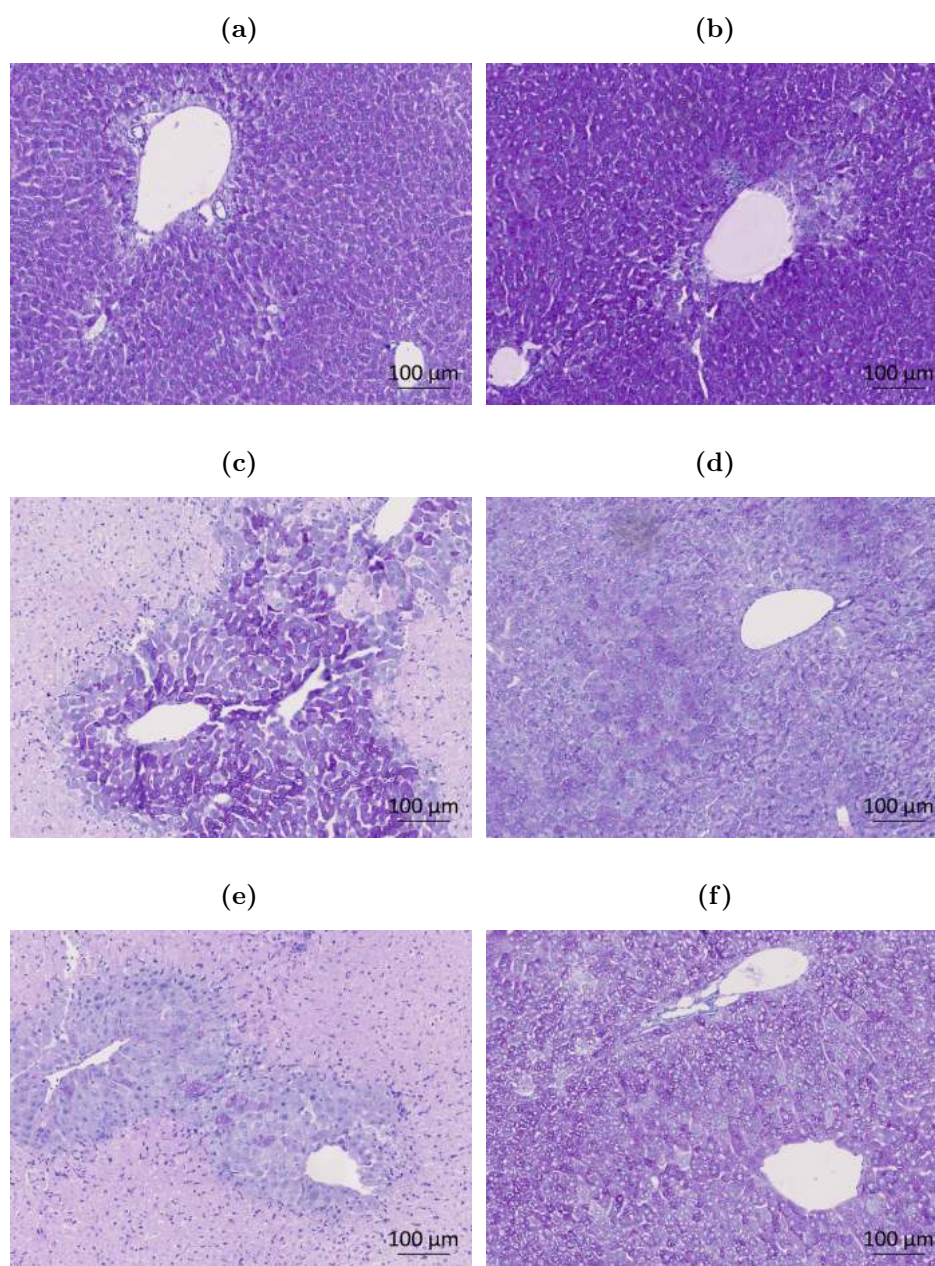


**Figure 6.18 – Representative images of PAS staining in C57BL/6 mice having undergone 60 minutes of ischaemia treated with either PBS or PαS MSC.** C57BL/6 mice aged 8 weeks were injected via the intra-peritoneal route with  $1 \times 10^6$  PαS MSC. Mice were then subjected to 60 minutes of 70% hepatic ischaemia followed by 24 hours of reperfusion and following sacrifice liver tissue was removed and fixed in formalin. PAS staining was performed on processed liver tissue. (a) Mice undergoing sham surgery showed no reduction staining in either the ischaemic or (b) non-ischaemic lobes. (c) Mice treated with PαS MSC showed a reduction in staining in the liver parenchyma with sparing of the portal regions in the ischaemic lobe. (d) A less pronounced reduction in staining was seen in the non-ischaemic lobe with no clear sparing of the portal region. (e) A reduction in staining in the liver parenchyma with sparing of the portal regions in the ischaemic lobe of the PBS treated controls, (f) with a less pronounced reduction in staining in the non-ischaemic lobe with no clear sparing of the portal region. Images are generated from whole slide scans and are at 400x magnification. Scale bars represent 100 μm.



#### **6.2.4.3 The effect of P $\alpha$ S MSC therapy on circulating and liver infiltrating immune cells in hepatic ischaemia reperfusion injury**

Male C57BL/6 mice aged 8 weeks were treated with either PBS or P $\alpha$ S MSC and then underwent 60 minutes of 70% hepatic ischaemia. Following sacrifice whole blood was sampled and liver lobes were mechanically homogenised and following washing were passed over a density gradient using Optiprep<sup>TM</sup>. Cells were stained and analysed by flow cytometry (figures 6.19, 6.20 and 6.21).

There were no significant differences in the infiltrating immune cell populations in mice treated with P $\alpha$ S MSC in either the ischaemic or non-ischaemic liver lobes or circulating in the serum.

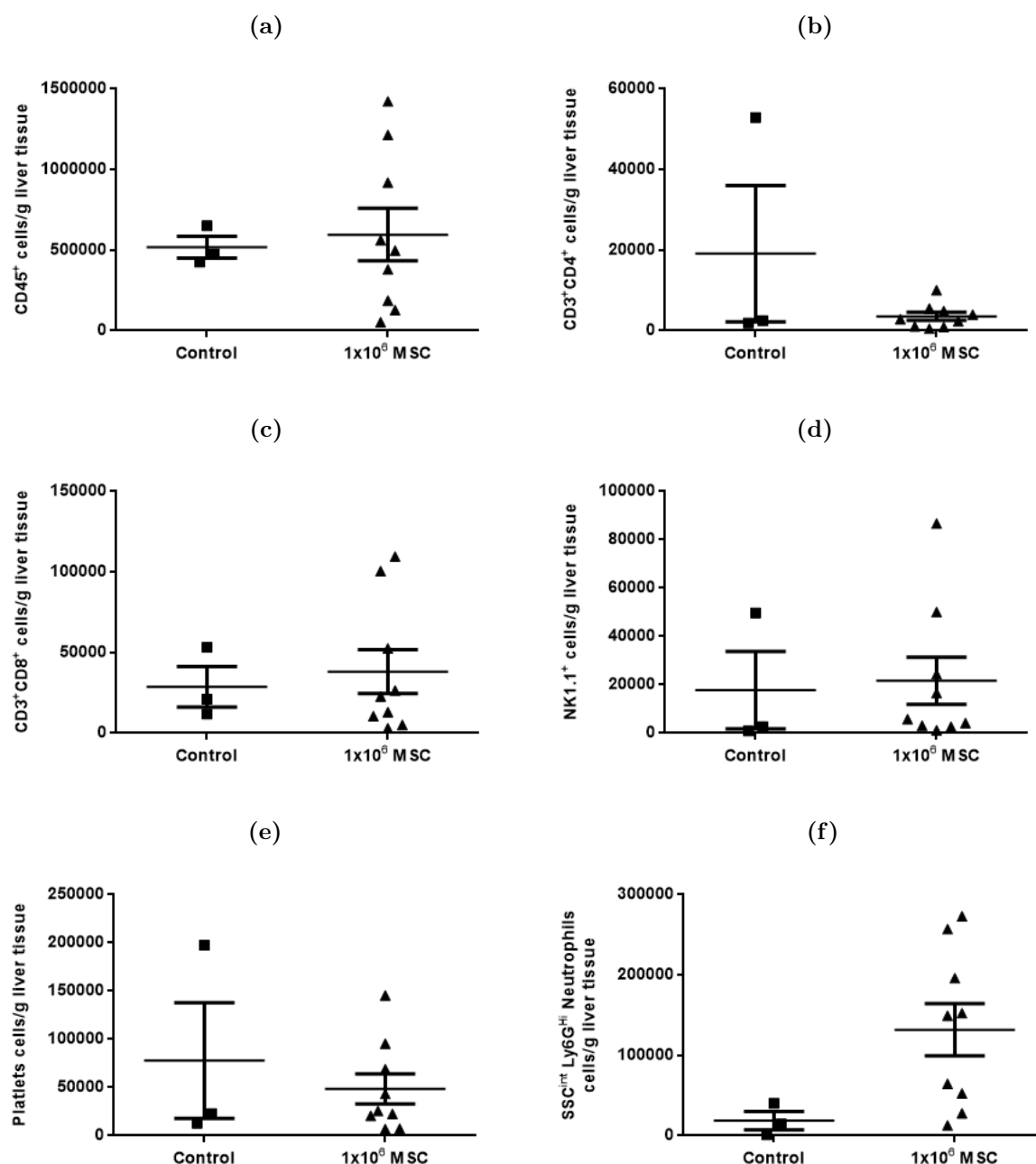


**Figure 6.19 – Flow cytometric analysis of ischaemic liver lobes of mice treated with P $\alpha$ S MSC and undergoing 60 minutes of 70% hepatic ischaemia.** Male C57BL/6 mice aged 8 weeks were treated with either PBS or P $\alpha$ S MSC and then underwent 60 minutes of 70% hepatic ischaemia. Following sacrifice liver lobes were mechanically homogenised and following washing were passed over a density gradient using Optiprep<sup>TM</sup>. Cells were stained and analysed by flow cytometry. There were no significant changes in (a) CD45<sup>+</sup>, (b) CD3<sup>+</sup>CD4<sup>+</sup>, (c) CD3<sup>+</sup>CD8<sup>+</sup>, (d) NK1.1<sup>+</sup> cells, (e) CD41<sup>+</sup> platelets or (f) Neutrophils (SSC<sup>Int</sup>Ly6G<sup>Hi</sup>). Points represent individual mice and bars represent the mean value with the standard error of the mean. Statistical analysis was carried out using a Student's t-test.

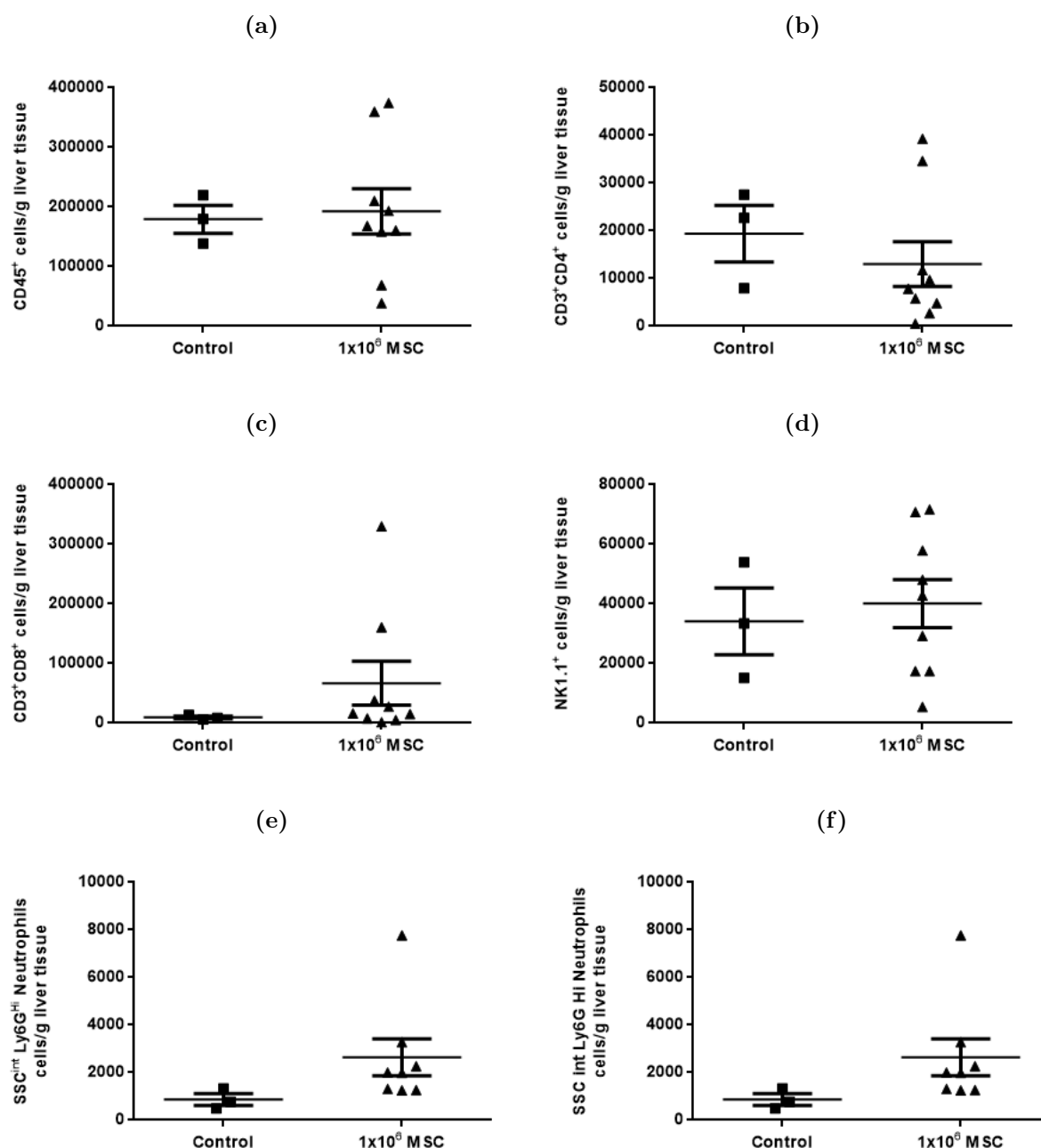


**Figure 6.20 – Flow cytometric analysis of the non-ischaemic liver lobes of mice treated with P $\alpha$ S MSC and undergoing 60 minutes of 70% hepatic ischaemia.** Male C57BL/6 mice aged 8 weeks were treated with either PBS or P $\alpha$ S MSC and then underwent 60 minutes of 70% hepatic ischaemia. Following sacrifice liver lobes were mechanically homogenised and following washing were passed over a density gradient using Optiprep<sup>TM</sup>. Cells were stained and analysed by flow cytometry. There were no significant changes in (a) CD45<sup>+</sup> (b) CD3<sup>+</sup>CD4<sup>+</sup>, (c) CD3<sup>+</sup>CD8<sup>+</sup>, (d) NK1.1<sup>+</sup> cells, (e) CD41<sup>+</sup> platelets or (f) Neutrophils (SSC<sup>Int</sup>Ly6G<sup>Hi</sup>). Points represent individual mice and bars represent the mean value with the standard error of the mean. Statistical analysis was carried out using a Student's t-test, n=12.

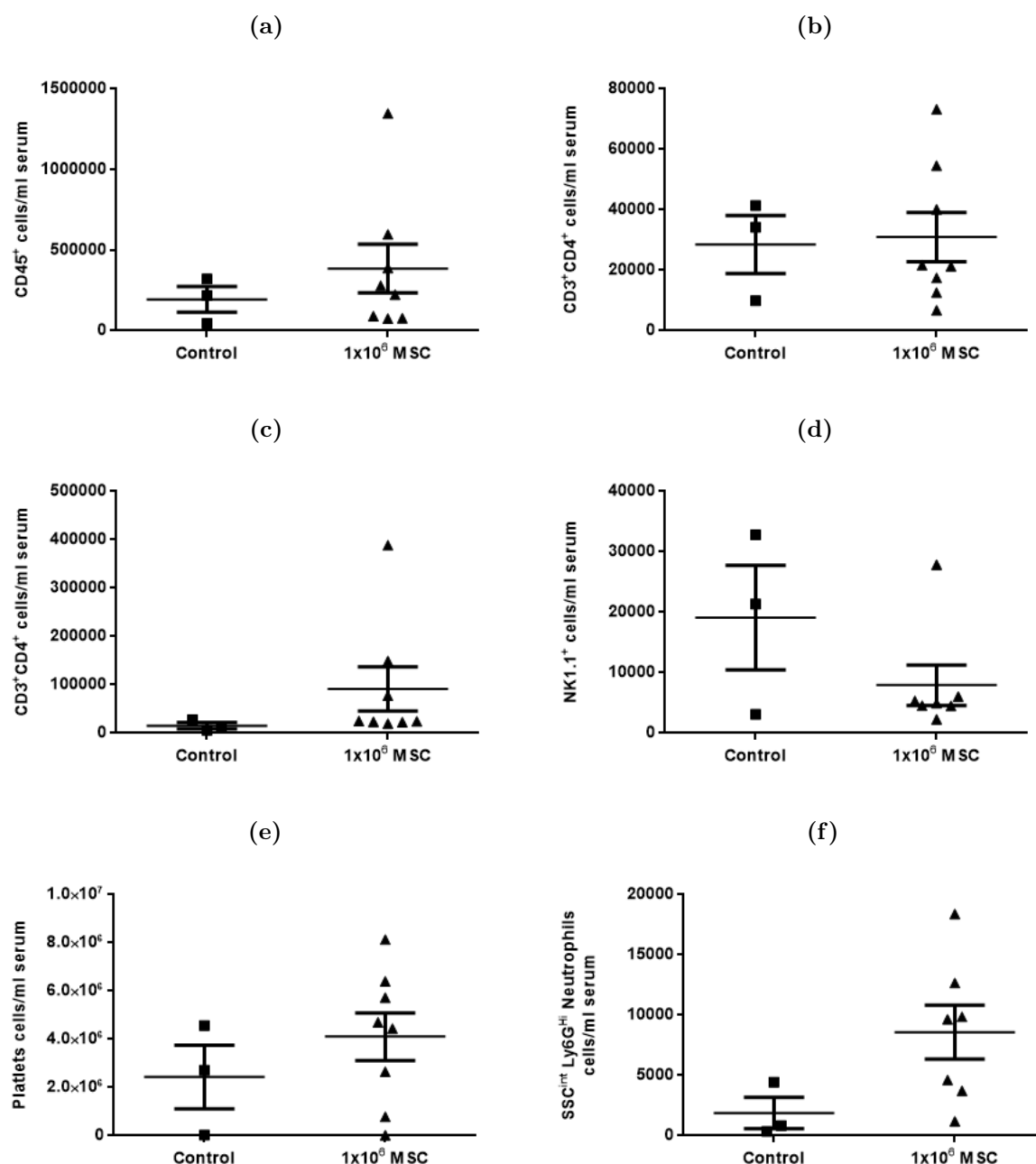


**Figure 6.21 – Flow cytometric analysis of the whole blood of mice treated with P $\alpha$ S MSC and undergoing 60 minutes of 70% hepatic ischaemia.** Male C57BL/6 mice aged 8 weeks were treated with either PBS or P $\alpha$ S MSC and then underwent 60 minutes of 70% hepatic ischaemia. Following sacrifice whole blood was sampled and following washing was passed over a density gradient using Optiprep<sup>TM</sup>. Cells were stained and analysed by flow cytometry. There were no significant changes in (a) CD45<sup>+</sup>, (b) CD3<sup>+</sup>CD4<sup>+</sup>, (c) CD3<sup>+</sup>CD8<sup>+</sup>, (d) NK1.1<sup>+</sup> cells, (e) CD41<sup>+</sup> or, (f) Neutrophils (SSC<sup>Int</sup>Ly6G<sup>Hi</sup>). Points represent individual mice and bars represent the mean value with the standard error of the mean. Statistical analysis was carried out using a Student's t-test.

## 6.3 Discussion

Models of ischaemia reperfusion injury have been around for nearly 40 years and extensive study has been undertaken in murine hepatic ischaemia reperfusion injury. When comparing studies however, there is a considerable amount of variation in the methodology [101] making direct comparisons between studies challenging. Some of the common variables are listed in table 6.1.

Variable	Range in the published literature
Age (weeks)	5-12
Gender	Male/Female
Strain	C57BL/6
	BALB/c
	C3H/HeJ
	Genetic knockout mice
Weight (g)	20-30
Anaesthetic technique	Isoflurane
	Ketamine
	Pentobarbitol
	Methoxyflurane
	Ether
Ischaemic time (mins)	20-180
Liver ischaemia (%)	40-100

**Table 6.1 – A table of methodological variables seen in hepatic ischaemia reperfusion injury in the published literature.**

In this study I sought to develop a model based on the published literature in which

the surgical insult was limited as much as possible to the introduction of a surgical clamp and induction of ischaemia and reperfusion injury. Techniques performed describe the exteriorisation of the liver or bowel contents in order to facilitate clamp placement [102, 101]. In studies in which this technique is used and recapitulated in sham controls the ALT levels in the sham group tend to be over 100 IU/L indicating liver injury. In this study the sham controls had near normal ALT levels ( $37.5 \text{ IU/L} \pm 3.2$ ). In order to achieve this I applied best clinical practice to mouse surgery [312]. This included some of the principles of enhanced recovery (table 6.2), an evidence based strategy employed in a number of surgical specialities. This strategy coupled with a surgical technique that did not involve externalising organs led to minimal surgical insult above and beyond that intended.

Preoperative	Intraoperative	Postoperative
Minimal starvation time	Minimal anaesthetic	Early mobilisation
Good preoperative nutrition	Normovolaemia	Early oral intake
Active pre-warming	Normothermia	Good analgesia
Pre-emptive analgesia	Blood conservation	
Minimal surgical insult		
Minimal surgical incision		

**Table 6.2 – A list of considerations to improve recovery from surgery.**

### 6.3.1 Injury pattern in the hepatic ischaemia reperfusion model

In this study having developed a reproducible surgical technique to induce hepatic ischaemia I investigated clamp duration and injury profile over time. As expected ALT was raised throughout the reperfusion period. In this study I found an ALT peak at 6 hours ( $15893.3 \text{ IU/L} \pm 3059.6$ ). Confidence intervals at all time points studied were wide although did not overlap, an expected finding and one that has been shown previously [101]. Reasons

for the wide confidence intervals in this type of model have been previously suggested and include variations in age and weight. Whilst age was tightly controlled in this study weight was variable between previously published ranges (20-30g), but may have led to the variation seen. Whilst most studies don't provide a time course of injury there is evidence that in mouse models the peak ALT rise is at 12 hours [307]. As I did not look at a 12 hour time point it is possible that this is also the case for the model in this study. Due to the logistical challenges and local policy it would have been difficult to undertake a 12 hour model in our institution as it would entail overnight working in order to collect samples. As two distinct phases of injury occur in hepatic ischaemia reperfusion injury, one in the first 6 hours and the other in the remaining 18 hours, this study almost certainly represents the injury patterns occurring in each phase. Serum ALT levels were lower at 24 hours after an initial peak at 6 hours ( $2825.0 \text{ IU/L} \pm 873.3$ ), however levels were still 100-200 fold higher than normal and nearly 100 times higher than sham surgical controls.

Histochemical analysis demonstrated an evolving injury pattern in the ischaemic lobes over the time course studied with H and E staining demonstrating an initial extravasation of red blood cells into the spaces between hepatocytes, followed by morphological changes in the liver parenchyma. PAS staining confirmed glycogen depletion from the beginning of the reperfusion period. This is to be expected as after 60 minutes of ischaemia the glycogen stores will have been used up. The depletion showed a peak at 6 hours indicating ongoing cell death as glycogen will be lost as cells die. Levels at 24 hours were marginally lower indicating some recovery, although sham surgical controls showed considerably less glycogen depletion ( $17.05\% \pm 0.90$  vs  $66.74\% \pm 11.86$ ). Considering these findings along with the reduction in ALT seen at 24 hours it is likely less cell death is occurring at this point as the majority of cells have been injured earlier on in the time course of this experiment.

Interestingly the non-ischaemic lobes also showed considerable injury throughout the time period studied. With a 70% clamp blood supply should be maintained through the remaining 30% without mechanical obstruction. H and E staining in the non-ischaemic

lobes showed red cell extravasation and necrosis at 6 hours following clamp removal, however by 24 hours these changes had resolved with no apparent necrotic areas visible. PAS staining also showed glycogen depletion with a peak at 6 hours and a reduction at 24 hours, although levels were considerably lower than those seen in the ischaemic lobes ( $33.60\% \pm 6.99$  vs  $66.74\% \pm 11.86$  at 24 hours).

#### **6.3.1.1 Liver immune cell populations in ischaemia reperfusion injury**

The liver infiltrating immune cell profile seen in this study shows an interesting pattern of immune cell infiltration in keeping with other published works, although very few studies have used flow cytometric analysis of digested liver tissue so direct comparison is difficult. A variety of descriptions exist in the published literature regarding reperfusion injury and there is perhaps a lack of clarity as to the timings of when different immune cell populations are present in an ischaemia organ, and what the significance of these cells are. The ischaemic insult sustained in hepatic reperfusion injury has been shown to cause a large number of pathways to activate, but two important processes which have been extensively described are the generation of superoxide and reactive oxygen species [313], and the activation of TLR4 [314]. The majority of publications describe the first six hours of reperfusion as the 'acute phase' of reperfusion injury and characterise this as a time when lymphocyte numbers increase [73], followed by the 'sub-acute phase' over the next 18 hours which is characterised by a rapid rise in neutrophil number [315]. In this study the number of CD45<sup>+</sup> cells rose following reperfusion in the ischaemic lobes and continued to rise during the 24 hour study period, whereas the CD45<sup>+</sup> cells in the non-ischaemic lobe remained relatively constant.

Unlike other studies which describe a rise in the lymphocyte populations in the first 6 hours, I showed a decrease in both CD4<sup>+</sup> and CD8<sup>+</sup> cells. However in the non-ischaemic lobes CD4<sup>+</sup> and CD8<sup>+</sup> cell numbers increased in the first 6 hours, with a reduction again by 24 hours. The difference between my findings and those in the published literature could be related to technique. There are very few studies in murine hepatic ischaemia



reperfusion injury which use flow cytometry to assess immune cell numbers, and studies that have use low n numbers and only looked at the first 4 hours of reperfusion [316]. Most studies use immunohistochemistry which may not give an accurate representation of the cell numbers seen. It is biologically plausible that immune cell populations fall in the first few hours due to two factors. Ischaemia reperfusion injury has been shown to lead to microvascular occlusion and platelet activation in the hepatic sinusoids [317], and in large animal models of warm ischaemia microvascular occlusion coupled with cell oedema has been shown to lead to an arterial shunt [318]. In my study there was a large increase in platelet numbers in both the ischaemic and non-ischaemic lobes during the first 2 hours after reperfusion. All other immune cell numbers remain static or decrease during this time period. With such large platelet numbers it is likely that microvascular occlusion is present and as such access to the liver by immune cell populations is likely to be restricted. Platelet numbers rapidly decrease following a peak at 2 hours and this is accompanied by an increase in almost all cell types measured between 2 and 6 hours after reperfusion. Further study would be needed to confirm this finding in small animal models as whilst functional studies which block platelet adhesion to the endothelium have been shown to reduce liver injury, it is unclear what effect this has on immune cell infiltration as there was no effect seen on inflammatory cytokine levels [317]. It is worth noting that CD4<sup>+</sup> T cell depletion has been shown to reduce hepatic ischaemia reperfusion injury in mouse models, implying that CD4<sup>+</sup> cell function is important in hepatic ischaemia reperfusion injury [319], as such the function of the immune cell populations is almost certainly more important than the absolute numbers present.

In keeping with other studies I showed a large increase in neutrophil numbers in the ischaemic lobes of mice undergoing hepatic ischaemia reperfusion injury at 24 hours following reperfusion. No increase in neutrophil recruitment was seen in the non-ischaemic lobes. It is worth noting that this finding is important as most of the papers published have used either myeloperoxidase as a surrogate for neutrophil numbers or immunohistochemistry [320]. By using flow cytometry with a neutrophil specific staining and gating strategy

[321], I have been able to confirm this finding in a more accurate way than previously described. This finding also suggests that neutrophil recruitment is not dependent on CD4<sup>+</sup> numbers alone.

In this study natural killer cell numbers remained fairly constant in the ischaemic lobe, however there was a large increase in the non-ischaemic lobe at reperfusion with levels gradually declining over the 24 hours study period. It has been suggested that natural killer cells play an important role in hepatic ischaemia reperfusion injury with a protective effect seen when using a CD39 depletion technique [322], however contradictory evidence also suggests that it is natural killer T-cells that are responsible [323]. It is interesting then that in this study levels appear to increase in the non-ischaemic lobe. An explanation for this could be that local leakage of inflammatory mediators during the ischaemic phase coupled with a lack of access to the ischaemic lobe due to the portal clamp led to an increase in natural killer cells in the non-ischaemic lobe which persisted during the reperfusion period.

### **6.3.2 The effects of clamp duration on ischaemic injury in the hepatic ischaemia reperfusion injury model**

Due to the wide range of ischaemic time studied in the literature I opted to assess a shorter clamp time of 30 minutes to ascertain if a suitable injury pattern for testing P&S MSC could be elicited, further reducing the overall surgical burden and therefore reducing the confounding factors associated with a longer operating time.

A clamp duration of 30 minutes greatly reduced the injury seen compared to 60 minutes when assessing serum ALT with peak levels again occurring at 6 hours (1170.0 IU/L  $\pm$  665.1 vs 15893.3 IU/L  $\pm$  3059.6). At 24 hours of reperfusion levels had fallen to 185.0 IU/L  $\pm$  155.0, with some mice having normal levels of ALT. Histochemical analysis showed little structural change on H & E staining, but PAS staining gave similar levels of glycogen depletion to those found in mice undergoing 60 minutes of ischaemia. This suggests that ischaemia has occurred in the same number of hepatocytes, but has not progressed to

necrosis and highlights the limitations of using PAS staining alone as a surrogate for necrosis. Flow cytometric analysis showed a reduction in total CD45<sup>+</sup> cells as well as CD4<sup>+</sup>, CD8<sup>+</sup> and NK1.1<sup>+</sup> cells in both the ischaemic and non-ischaemic lobes with a similar pattern seen in platelets. Neutrophil numbers did increase at 24 hours in the ischaemic lobe but the degree of rise was considerably less than mice undergoing 60 minutes of ischaemia. Taken together these findings indicate that the 30 minute clamp time was not sufficient to cause lasting damage and would make testing the efficacy of P $\alpha$ S MSC difficult in this model. As such I decided to use a 60 minute clamp time for the MSC experiments.

### **6.3.3 The effects of P $\alpha$ S MSC therapy on hepatic ischaemia reperfusion injury**

In this chapter I have demonstrated that the model of ischaemia reperfusion injury employed leads to a rise in neutrophils by 24 hours of reperfusion, but a reduction in lymphocyte numbers in the first 6 hours of reperfusion. MSC have been shown to reduce neutrophil recruitment to ischaemic gut [324], inhibit neutrophil extracellular trap and reactive oxygen species formation [325], and reduce lymphocyte activation and proliferation [246], indeed in earlier chapters I have confirmed that P $\alpha$ S MSC can have similar effects in CD8<sup>+</sup> lymphocytes *in vitro*. This makes MSC a potentially beneficial therapy in hepatic ischaemia reperfusion injury. However treatment of mice undergoing hepatic ischaemic reperfusion injury with P $\alpha$ S MSC did not lead to a significant change in ALT or glycogen depletion. There were also no significant changes in immune cell populations in either the liver or the whole blood when assessed by flow cytometry. There are a number of possible reasons for these findings. It is possible the P $\alpha$ S MSC are unable to reduce the injury in hepatic ischaemia reperfusion injury. Whilst I have shown the ability of P $\alpha$ S MSC to reduce lymphocyte proliferation *in vitro*, as well as their ability to reduce liver injury in the MDR2<sup>-/-</sup> model, the mechanisms responsible for hepatic reperfusion injury are more complex and not fully understood. The inflammatory micro-environment to which MSC

are exposed is critical in determining the effects that they exert on the immune system [249], and the inflammatory environment seen in ischaemia reperfusion injury is different to those in other models due to high levels of reactive oxygen species and relative hypoxia. Whilst MSC have been shown to support antioxidant systems in colitis [326], they have also been shown to undergo senescence and their functions can be impaired by reactive oxygen species [327]. As P $\alpha$ S MSC were given prior to induction of ischaemia then it is conceivable that they were already localised in the liver and underwent a period of hypoxia. Whilst there have been studies into the effects of hypoxia on MSC survival [328], further work needs to be done in order to ascertain if MSC retain their immunosuppressive actions or indeed if their immunosuppressive phenotype is significantly altered by exposure to extreme hypoxia. It is also conceivable that the dose given was inappropriate in this study. A higher dose was used compared with previous work [237] in order to give the best chance of efficacy as this model was logistically more challenging so numbers had to be limited as best possible. MSC have been shown to have no greater effects once a threshold dose is reached, and in ARDS this dose has been shown to be  $2 \times 10^6$  cells/kg. Whilst threshold doses are likely to be different between MSC types and disease processes the dose used in this study equated to  $3\text{--}5 \times 10^7$  cells/kg which is likely to be above the threshold level. The route of administration used in this study was different to that used in the MDR2<sup>-/-</sup> in order to facilitate administration of a higher dose of P $\alpha$ S MSC which may also explain why the cells did not have the desired effects. The intra-peritoneal route has been shown to increase MSC engraftment in gut injury models [309], and has also been shown to be efficacious in mouse models of liver injury using P $\alpha$ S MSC [237], although further work would need to be done to confirm viability of P $\alpha$ S MSC in this model and also to assess their location and trafficking. Finally it is possible that this study was not powered to detect a beneficial effect of P $\alpha$ S MSC therapy. Whilst the primary outcome measure in this study was ALT, levels of immune cells or their function may undergo more subtle changes and whilst I did see some interesting trends in immune cell numbers these did not reach statistical significance. Whilst it is possible to undertake more repetitions to confirm

this hypothesis and undertake cytokine analysis this model is costly and time consuming and so further work would need to be targetted at specific outcomes which would be most likely to show a significant difference with P $\alpha$ S MSC therapy.

### **6.3.4 Chapter summary**

In this chapter I have developed a repeatable mouse model of hepatic ischaemia reperfusion injury which enables portal vessel clamping with minimal surgical insult. I have demonstrated that this model shows a significant injury as assessed by a large ALT rise over the 24 hour time course with some resolution at 24 hours. I have also demonstrated that by assessing immune cell populations using flow cytometry that whilst neutrophil cell numbers follow a similar pattern to those described by other techniques, lymphocyte numbers appear to remain similar to those at induction of injury. One explanation for this could be microvascular occlusion by platelets which I have shown to be raised in the first few hours following ischaemia. Following treatment with P $\alpha$ S MSC there was no significant difference in primary outcome measure (ALT) at 24 hours between treatment and control animals. There was also no significant difference found in immune cell populations in either the liver or whole blood of mice undergoing ischaemia reperfusion injury. This makes it likely that P $\alpha$ S MSC do not reduce the injury seen in hepatic ischaemia reperfusion injury although further work is needed to confirm that this holds true.

## CHAPTER 7

# DISCUSSION AND CONCLUSIONS

### 7.1 Summary of the main findings

End stage liver disease is a clinical condition with a high level of morbidity and mortality and its incidence is still increasing in the developed world [6]. Whilst liver transplantation offers a viable therapy it is a major surgical undertaking and the paucity of donor organs has led to the use of more marginal organs with an increased complication rate [42]. There is an urgent need to increase the available pool of donor organs and improving the outcomes from the transplantation of marginal donors is one way to achieve this [329]. One possible strategy to improve the outcomes from [32, 330] organ donation is to reduce the amount of ischaemia and reperfusion injury sustained by these organs. A number of promising therapies have been demonstrated in pre-clinical models of reperfusion injury however few have made the translation into clinical practice in part due to the complexity of the injury sustained during ischaemia and reperfusion [189]. As reperfusion injury is a combination of oxidative stress and immune mediated damage involving both the innate and adaptive immune systems, a broad acting and adaptable therapy is likely to yield the greatest effect. Medium term complications from marginal donation show a different pattern to those from organs having undergone less ischaemia with a greater incidence of non-anastomotic biliary complications [331, 43]. There have so far been no therapies proposed to enable the treatment of non-anastomotic biliary complications with more focus being placed on

reducing ischaemic time and donor and recipient selection in order to improve outcomes [31, 332].

MSC represent a potential therapy for both early and medium term complications in marginal organ liver transplantation due to their ability to modulate a number of different pathways and cell types in the innate and adaptive immune system. Whilst a number of clinical trials have been performed in liver disease there are as yet no definitive positive results that have led to clinical translation [1]. Whilst some pre-clinical trials have demonstrated a reduction in liver injury and increased regeneration following liver ischaemia with partial hepatectomy there have been limited mechanistic insights and these studies have used human cells into mouse models [301]. The use of MSC in liver transplantation appears to be viewed as an acceptable and potentially useful therapy with ongoing early phase trials currently being undertaken [333]. The use of prospectively isolated murine MSC has the potential to yield a beneficial therapy in post transplantation liver injury and allow for mechanistic studies of MSC. In order to meet these needs this thesis focusses on the use of prospectively isolated murine P $\alpha$ S MSC in models of liver ischaemia reperfusion injury and biliary injury.

### **7.1.1 Phenotype and immunosuppressive action of P $\alpha$ S MSC *in vitro***

The original paper describing the isolation of P $\alpha$ S MSC was published in 2009 [150], however since this paper little further work has been carried out using these cells outside of our laboratory. Whilst previous work has characterised P $\alpha$ S MSC extensively and demonstrated that they meet the ISCT criteria for MSC [237, 236], limited *in vitro* and *in vivo* studies have been carried out to demonstrate their immunomodulatory abilities. Reasons for this are unclear but are likely due to the difficulty of replicating the isolation technique described in the original paper. Difficulty has also been found as using P $\alpha$ S MSC isolated from C57BL/6 mice in *in vitro* assays with purified immune cells did not show any effect of the P $\alpha$ S MSC. In this study I was able to successfully isolate P $\alpha$ S

MSC from murine bone marrow and grow them in culture. I also developed an *in vitro* immunosuppression assay which allowed for the testing of P $\alpha$ S MSC isolated from C57BL/6 mice. I was able to demonstrate suppression of CD8<sup>+</sup> T cell proliferation by P $\alpha$ S MSC and following stimulation with inflammatory cytokines P $\alpha$ S MSC were able to secrete anti-inflammatory cytokines, in particular Il-10. This is an important finding as a number of studies have suggested that MSC do not directly secrete Il-10 but instead stimulate other intermediary cells to do so [334]. In this study I have demonstrated that a purified population of prospectively isolated murine MSC are able to secrete significantly higher amounts of Il-10 following an inflammatory stimulus, an important finding given the functions of Il-10 as an immune regulator. It is not clear however whether this is indeed the mechanism by which P $\alpha$ S MSC exert their effects *in vivo*, or whether priming of P $\alpha$ S MSC is required to guarantee their effects.

### **7.1.2 The *in vivo* effects of P $\alpha$ S MSC in hepatic ischaemia reperfusion injury**

In order to examine the effects of P $\alpha$ S MSC on ischaemia reperfusion injury in the liver I developed a surgical model of hepatic ischaemia. Whilst not a new model by limiting the surgical insult I was able to show a large increase in markers of liver injury with little confounding injury due to surgical technique. By utilising flow cytometry I have been able to demonstrate the profile of infiltrating immune cells in the liver in a different way to those commonly published [335], and whilst infiltrating neutrophils followed a similar pattern to that seen in the majority of the hepatic ischaemia reperfusion literature, infiltrating CD4<sup>+</sup> and CD8<sup>+</sup> lymphocytes appeared to show a different pattern. I also analysed the lobes not undergoing ischaemia, something not commonly published. This also yielded some interesting findings showing high levels of a number of immune cells including platelets and natural killer cells. This finding is important as natural killer cells have been implicated in both liver injury and neutrophil recruitment following ischaemia and transplantation [336]. Remote immune mediated damage to the kidney and liver



following ischaemic injury to other areas has been described in the literature and is likely due to the systemic transport of reactive oxygen species to well perfused organs [337, 338]. Understanding the implications of this and the effects of more local immune mediated damage in liver ischaemia requires further study but is important to help develop therapies that can improve patient outcomes from liver transplantation.

In this study P $\alpha$ S MSC did not show a significant reduction in liver injury following ischaemia and reperfusion. Due to the complexity of the injury seen following hepatic ischaemia it is difficult to make definite conclusions based on this study alone. Indeed systemically administered MSC are able to engraft in the liver and may differentiate into hepatocytes although this finding has been disputed [186]. Mice undergoing hepatic ischaemia reperfusion injury and hepatectomy seemed to benefit from the administration of MSC with a reduction in ALT [301] and mice with acute liver failure injected with MSC via the portal vein seemed to show an increased benefit compared with other routes of administration [339]. Whilst these studies show a different outcome to this study there are important differences. In particular the use of human MSCs in these studies may account for the difference in response seen. A large proportion of the MSC literature use human MSC into mouse or rat models of disease as arguably this represents the ultimate therapy to be delivered to patients. Whilst true this ignores the issue of xenotransplantation and whilst MSC are thought to be relatively immunoprivileged due to their low expression of MHC class II [340], there remain concerns about use between species and whilst most work has been carried out assessing the potential use of non-human MSC in human patients [341, 342] it stands to reason that the use of human MSC in animal models may lead to results which cannot be translated into clinical practice. In a recent paper using human MSC in a model of graft versus host disease Galleu demonstrated that the infused MSC are attacked by the host immune system and shortly after transfer cytotoxic cells render MSC apoptotic. Following phagocytosis IDO is released and exerts an immunosuppressive effect [167].

### 7.1.3 The *in vivo* effects of P $\alpha$ S MSC in biliary injury

Non-anastomotic biliary complications represent a significant problem following marginal organ transplantation and a major cause of retransplantation [42]. As yet there are no models of non-anastomotic biliary injury, however in this study I used the MDR2<sup>-/-</sup> mouse model as the injury pattern and mechanism of toxic bile injury seen in this model is similar that seen in patients with non-anastomotic biliary injury [343]. Treatment with systemically administered P $\alpha$ S MSC led to a reduction in markers of liver injury in the MDR2<sup>-/-</sup> model. Despite this reduction the total number of infiltrating immune cells appeared to remain unchanged. P $\alpha$ S MSC therapy led to a change in the balance of macrophage types with an increase in the number of restorative macrophages. Macrophage biology in the liver is complex with a number of different populations of cells present. Broadly speaking there are resident hepatic macrophages and infiltrating macrophages from the systemic circulation. Whilst resident macrophages seem to be important in sensing injury and initiating the inflammatory process, circulating monocytes seem to be involved in chronic inflammation and fibrosis [344]. Restorative macrophages have been shown to resolve fibrosis in pre-clinical models of fibrosis [345], and monocyte differentiation into restorative macrophages is driven in part by the production of Il-10 [346]. Given the findings in this study that P $\alpha$ S MSC secrete Il-10 in response to an inflammatory stimulus it is indeed conceivable that this mechanism is responsible for the improvement seen in the MDR2<sup>-/-</sup> model. It would also explain why the improvement in ALT persisted at 2 weeks following therapy despite very few cells remaining in the liver in the first few days following injection of P $\alpha$ S MSC as restorative macrophages are able to secrete Il-10 and maintain the stimulus for a restorative phenotype after MSC have been cleared. Further work will be needed to confirm this hypothesis.

#### 7.1.4 P $\alpha$ S MSC trafficking and remote effects in biliary injury

The understanding of how MSC are able to exert their immunosuppressive effects is still incomplete with debate over whether direct cell contact is required or whether effects can be exerted from remote locations. MSC encapsulated in alginate have been shown to reduce inflammation in models of graft versus host disease [155], and MSC administered subcutaneously are able to reduce injury in a cardiac ischaemia model [347]. Following systemic administration P $\alpha$ S MSC appeared to be trapped in the lungs, however a proportion of the cells administered were present in the liver. This proportion seemed to increase after 24 hours indicating either slower clearance from the liver or redistribution from the lungs. It was not possible in this study to quantify the exact location of MSC within the liver, and further investigation to demonstrate the location of MSC and whether they are present at the site of injury or immune cell recruitment following administration will be required. In cardiac injury MSC trapped in the lungs appear to be able to exert an immunomodulatory effect [288] via a remote action. It is possible that the same process is occurring in this study although remote action was not confirmed in the experiments using other routes of administration.

In this study subcutaneously administered P $\alpha$ S MSC did not reduce liver injury unlike experiments using systemic administration. Whilst this is contrary to some of the published literature there are key differences between this study and others. Models which have shown a beneficial effect from encapsulated MSC use systemic models such as graft versus host disease rather than organ specific models. Also the encapsulation process may confer beneficial effects on MSC such as prolonged survival. Whilst subcutaneously administered MSC were beneficial in a cardiac ischaemia model, these were human MSC and it is possible that either a different secretome is found in these cells or a local reaction to xenotransplantation leads to the effects rather than the MSC themselves as no human cellular controls were used in these studies. Further work would be needed to explore this.

## 7.2 Future work

The results of this study have demonstrated some interesting findings and a number of questions which may benefit from future work in order to answer them. The main areas of potential further study are summarised below.

### 7.2.1 What is the mechanism of P $\alpha$ S MSC mediated immunosuppression in the MDR2<sup>-/-</sup> model?

In this study I showed a beneficial effect of systemic but not subcutaneously administered P $\alpha$ S MSC in the MDR2<sup>-/-</sup> with an increase in restorative macrophages. Due to their ability to secrete Il-10 demonstrated *in vitro* it is possible that this represents the mechanism of action, however further study is required. Firstly the significance of macrophages in the MDR2<sup>-/-</sup> should be elicited and one way of achieving this would be to knockout macrophages. This can be achieved by using clodronate liposomes [348] or diphtheria toxin mediated depletion [349]. Treating macrophage deplete MDR2<sup>-/-</sup> with P $\alpha$ S MSC would give further mechanistic insight. Further experiments using P $\alpha$ S MSC isolated from Il-10 deficient mice would enable the investigation of the effects of Il-10 secreted by P $\alpha$ S MSC.

### 7.2.2 Can P $\alpha$ S MSC be primed to respond depending on the inflammatory microenvironment?

P $\alpha$ S MSC secrete a variety of cytokines following stimulation with TNF $\alpha$  and IFN- $\gamma$ . The importance of an inflammatory stimulus to lead to MSC taking on an immunosuppressive phenotype has been studied previously [350]. Whilst the majority of the MSC literature use naive MSC it is possible that cytokine priming may improve the efficacy of MSC therapy by reprogramming them to exert an anti-inflammatory effect. Further work examining the effects of other pro-inflammatory cytokines on cultured P $\alpha$ S MSC may yield a different secretome and aid in predicting how cells will respond to different inflammatory microenvironments *in vivo*. Using cytokines in culture media throughout culture likely

leads to a change in phenotype of P $\alpha$ S MSC [237]. There may be additional benefit in this approach as one advantage of cell therapy is the ability to modulate the immune system rather than completely suppress it allowing the host the ability to fight opportunistic infection [351] and may even improve immune function in viral infection [352], an advantage not seen by conventional immunosuppressant therapies.

### **7.2.3 Can P $\alpha$ S MSC reduce injury in ischaemia reperfusion injury?**

In this study P $\alpha$ S MSC did not reduce injury in a model of hepatic ischaemia reperfusion injury. However some studies have shown a potential benefit of MSC therapy in hepatic ischaemia reperfusion injury [193, 186, 301, 353]. One study has demonstrated an effect of rat MSC given into a rat model of hepatic ischaemia reperfusion injury, however these cells were isolated using plastic adherence and culture expansion and not prospective isolation meaning that the population of cells was certainly more heterogeneous than P $\alpha$ S MSC [353]. In order to confirm the effects of P $\alpha$ S MSC in hepatic ischaemia reperfusion injury further work is certainly needed using different routes of administration. As previously discussed the inflammatory microenvironment may determine the way in which MSC act and so *in vitro* testing of P $\alpha$ S MSC and their secretome following exposure to reactive oxygen species may yield further information to guide future experiments.

### **7.2.4 Is MSC therapy a double edged sword?**

The description of MSC as a double edged sword was coined by Li et al [354] to describe the dual effects of MSC to both suppress and promote inflammation. In this study I have demonstrated the potential for pro-inflammatory effects with a significant worsening of markers of liver injury following subcutaneous administration of P $\alpha$ S MSC in the MDR2<sup>-/-</sup> model and an increase in CCL19 secretion following an inflammatory stimulus. Other studies have demonstrated pro-inflammatory effects, in graft versus host disease MSC

have both increased and decreased disease severity [165]. Before further clinical trials are undertaken a better understanding of why and how MSC exert pro-inflammatory effects, and what the clinical significance of this is need to be undertaken. One approach with P $\alpha$ S MSC could be to expose cultured cells to different pro and anti-inflammatory cytokines and assess their response including phenotype and secretome. Genomics may be able to help and sequencing the MSC transcriptome following exposure to different microenvironments may yield further information to help understand the dual effects seen *in vivo*.

### **7.2.5 What are the effects of xenotransplantation and are murine cells a better model for further study?**

As discussed earlier a potential problem with the current approach in the MSC literature is the use of human MSC in mouse small animal models of injury. Whilst this is seemingly a sensible approach in order to reduce the number of steps to translation there are potential problems related to the use of xenotransplanted cells. Recent work has shown the human MSC can still exert an anti-inflammatory effect when killed prior to injection [355] and tracking of systemically administered MSC has shown that cells migrating to the liver are often dead cells [356]. These findings suggest that either surface marker expression on MSC is all that is required to modulate immune responses as secretion of cytokines does not occur in dead cells, or there is an immune response generated by the injection of xenotransplanted cells. This work needs to be repeated with P $\alpha$ S MSC to confirm if the effect is due to xenotransplantation and further work eliciting the response of rodents to the injection of human cells needs to be carried out.

## **7.3 Final conclusions**

In summary I have isolated and expanded in cell culture a purified population of murine bone marrow MSC based on the markers PDGFR $\alpha$  and SCA-1. These cells were used in

a series of *in vitro* and *in vivo* experiments to demonstrated their ability to modulate the immune system and their potential as a therapy for post transplant liver injury. I have demonstrated that P $\alpha$ S MSC are able to suppress lymphocyte proliferation and that following stimulation with pro-inflammatory cytokines they are able to secrete a number of lymphocyte chemoattractants as well as the immunomodulatory cytokine Il-10.

In the MDR2<sup>-/-</sup> model of biliary injury systemically administered P $\alpha$ S MSC were able to reduce the injury seen by increasing the population of restorative macrophages whilst subcutaneous administration did not yield the same results. Tracking experiments showed that P $\alpha$ S MSC were mainly trapped in the lungs but persisted in the liver for up to 7 days following systemic administration. In a model of hepatic ischaemia reperfusion injury P $\alpha$ S MSC were unable to reduce the injury seen.

Taken together these findings indicate a potential role for MSC therapy in post transplantation liver injury however further work is required in order to confirm the mechanism of action before clinical translation is undertaken.

## BIBLIOGRAPHY

- [1] Owen A, Newsome PN. Mesenchymal Stromal Cell Therapy in liver disease opportunities and lessons to be learnt? *American Journal of Physiology - Gastrointestinal and Liver Physiology*. 2015 Aug;309(10):ajpgi.00036.2015.
- [2] Hernandez-Gea V, Friedman SL. Pathogenesis of Liver Fibrosis. *Annual Review of Pathology: Mechanisms of Disease*. 2011 Feb;6(1):425–456.
- [3] Beers B, Materne R, Annet L, Hermoye L, Sempoux C, Peeters F, et al. Capillarization of the sinusoids in liver fibrosis: Noninvasive assessment with contrast-enhanced MRI in the rabbit. *Magnetic Resonance in Medicine*. 2003;49(4):692–699.
- [4] Jung YK, Yim HJ. Reversal of liver cirrhosis: current evidence and expectations. *The Korean Journal of Internal Medicine*. 2017 Mar;32(2):213–228.
- [5] Popper H. Pathologic aspects of cirrhosis. *The American journal of medicine*. 1977;87(1).
- [6] Williams R, Aspinall R, Bellis M, Ginette C, Cramp M, Dhawan A, et al. Addressing liver disease in the UK: a blueprint for attaining excellence in health care and reducing premature mortality from lifestyle issues of excess consumption of alcohol, obesity, and viral hepatitis. *The Lancet*. 2005;384(9958):1953 – 1997.
- [7] Si-Tayeb K, Lemaigre FP, Duncan SA. Organogenesis and Development of the Liver. *Developmental Cell*. 2010 feb;18(2):175–189.



- [8] Dooley JS, Lok A, Burroughs AK, Heathcote J. *Sherlock's Diseases of the Liver and Biliary System*. Wiley; 2011.
- [9] Anon. Wikimedia Commons; 2018. Available from: [https://commons.wikimedia.org/wiki/Main\\_Page](https://commons.wikimedia.org/wiki/Main_Page).
- [10] Gray H, Lewis W. *Gray's Anatomy of the Human Body*. 20th ed. Lewis WH, editor. Bartleby.com; 2000.
- [11] Anon. Easy Notecards; 2018. Available from: [http://www.easynotecards.com/print\\_list/83431](http://www.easynotecards.com/print_list/83431).
- [12] Sapirstein LA. *Human Biology in Health and Disease*. Sapirstein J, editor. None; 1969.
- [13] Fiebig T, Boll H, Figueiredo G, Kerl HU, Nittka S, Groden C, et al. Three-dimensional in vivo imaging of the murine liver: a micro-computed tomography-based anatomical study. *PLoS ONE*. 2012;7(2):e31179.
- [14] Yang L, Bataller R, Dulyx J, Coffman TM, Ginès P, Rippe RA, et al. Attenuated hepatic inflammation and fibrosis in angiotensin type 1a receptor deficient mice. *Journal of Hepatology*. 2005;43(2):317 – 323.
- [15] Lin RS, Lee FY, Lee SD, Tsai YT, Lin HC, Rei-Hwa L, et al. Endotoxemia in patients with chronic liver diseases: relationship to severity of liver diseases, presence of esophageal varices, and hyperdynamic circulation. *Journal of Hepatology*. 1995 feb;22(2):165–172.
- [16] Isayama F, Hines IN, Kremer M, Milton RJ, Byrd CL, Perry AW, et al. LPS signaling enhances hepatic fibrogenesis caused by experimental cholestasis in mice. *American Journal of Physiology-Gastrointestinal and Liver Physiology*. 2006 jun;290(6):G1318–G1328.

- [17] Seki E, Minicis S, Österreicher CH, Kluwe J, Osawa Y, Brenner DA, et al. TLR4 enhances TGF- signaling and hepatic fibrosis. *Nature Medicine*. 2007;13(11):1324.
- [18] Michalopoulos GK. Liver regeneration: alternative epithelial pathways. *International Journal of Biochemistry & Cell Biology*. 2011;43(2):173–9.
- [19] Dubuquoy L, Louvet A, Lassailly G, Truant S, Boleslawski E, Artru F, et al. Progenitor cell expansion and impaired hepatocyte regeneration in explanted livers from alcoholic hepatitis. *Gut*. 2015;64(12):1949–1960.
- [20] Alison MR, Poulsom R, Jeffery R, Dhillon AP, Quaglia A, Jacob J, et al. Hepatocytes from non-hepatic adult stem cells. *Nature*. 2000;406(6793):257.
- [21] Kobayashi N, Ito M, Nakamura J, Cai J, Gao C, Hammel J, et al. Hepatocyte transplantation in rats with decompensated cirrhosis. *Hepatology*. 2000;31(4):851–857.
- [22] Dhawan A, Mitry RR, Hughes RD. Hepatocyte transplantation for liver-based metabolic disorders. *Journal of Inherited Metabolic Disease*. 2006;29(2):431 – 435.
- [23] Spahr L, Lambert J, Laura R, Chalandon Y, Frossard J, Giostra E, et al. Granulocyte-colony stimulating factor induces proliferation of hepatic progenitors in alcoholic steatohepatitis: a randomized trial. *Hepatology*. 2008;48(1):221–229.
- [24] King A, Houlihan DD, Kavanagh D, Haldar D, Luu N, Owen A, et al. Sphingosine-1-Phosphate Prevents Egress of Hematopoietic Stem Cells From Liver to Reduce Fibrosis. *Gastroenterology*. 2017 Jul;153(1):233–248.e16.
- [25] Newsome P, Fox R, King A, Barton D, Than N, Moore J, et al. Granulocyte colony-stimulating factor and autologous CD133-positive stem-cell therapy in liver cirrhosis (REALISTIC): an open-label, randomised, controlled phase 2 trial. *Lancet Gastroenterology Hepatology*. 2018;3(1):25–36.

- [26] Cholongitas E, Germani G, Burroughs AK. Prioritization for liver transplantation. *Nature Reviews Gastroenterology & Hepatology*. 2010;7(12):659.
- [27] Neuberger J, Gimson A, Davies M, Akyol M, J O, Burroughs A, et al. Selection of patients for liver transplantation and allocation of donated livers in the UK. *Gut*. 2008;57(2):252.
- [28] NHSBT. Transplant activity report; 2018.
- [29] Koostra G, Daemen J, Oomen A. Categories of non-heart-beating donors. *Transplantation Proceedings*. 1995;27(5):2893–4.
- [30] Haring TR, Nguyen TN, Cotton RT, Guiteau JJ, de Armas IA, Liu H, et al. Liver transplantation with donation after cardiac death donors: A comprehensive update. *Journal of Surgical Research*. 2012;178(1):502 – 511.
- [31] Grewal H, Willingham D, Nguyen J, Hewitt W, Taner B, Cornell D, et al. Liver transplantation using controlled donation after cardiac death donors: An analysis of a large single-center experience. *Liver Transplant*. 2009;15(9):1028–1035.
- [32] Zhai Y, Busuttil R, J K. Liver Ischemia and Reperfusion Injury: New Insights into Mechanisms of Innate—Adaptive Immune-Mediated Tissue Inflammation. *American Journal of Transplantation*. 2011;11(8):1563–1569.
- [33] Pan X, Apinyachon W, Xia W, Hong J, Busuttil R, Steadman R, et al. Perioperative complications in liver transplantation using donation after cardiac death grafts: A propensity-matched study. *Liver Transplant*. 2014;20(7):823–830.
- [34] Devi A. Transfusion practice in orthotopic liver transplantation. *Indian Journal of Critical Care Medicine : Peer-reviewed, Official Publication of Indian Society of Critical Care Medicine*. 2009;13(3):120 – 128.
- [35] Ponnudurai RN, Koneru B, Akhtar SA, Wachsberg RH, Fisher A, Wilson DJ, et al. Vasopressor administration during liver transplant surgery and its effect on endo-

- tracheal reintubation rate in the postoperative period: A prospective, randomized, double-blind, placebo-controlled trial. *Clinical Therapeutics*. 2005;27(2):192 – 198.
- [36] Aggarwal S, Kang Y, Freeman J, Fortunato F, Pinsky M. Postreperfusion syndrome: cardiovascular collapse following hepatic reperfusion during liver transplantation. *Transpl P*. 1987;19(4 Suppl 3):54–5.
- [37] Fukazawa K, Yamada Y, Gologorsky E, Arheart KL, Pretto JA. Hemodynamic Recovery Following Postreperfusion Syndrome in Liver Transplantation. *Journal of Cardiothoracic and Vascular Anesthesia*. 2014;28(4):994 – 1002.
- [38] Rodríguez-Perálvarez M, Rico-Juri JM, Tsochatzis E, Burra P, la Mata MD, Lerut J. Biopsy-proven acute cellular rejection as an efficacy endpoint of randomized trials in liver transplantation: a systematic review and critical appraisal. *Transplant International*. 2016 jan;29(9):961–973.
- [39] Neil DAH, Hübscher SG. Current views on rejection pathology in liver transplantation. *Transplant International*. 2010 apr;23(10):971–983.
- [40] Wiesner RH, Demetris AJ, Belle SH, Seaberg EC, Lake JR, Zetterman RK, et al. Acute hepatic allograft rejection: incidence, risk factors, and impact on outcome. *Hepatology*. 1998 Sep;28(3):638–645.
- [41] Blakolmer K, Clouston A, Paul A. Update of the International Banff Schema for Liver Allograft Rejection: working recommendations for the histopathologic staging and reporting of chronic rejection. *Hepatology*. 2000;p. 792–799.
- [42] Foley D, Fernandez L, Levenson G, Anderson M, Mezrich J, Sollinger H, et al. Biliary Complications After Liver Transplantation From Donation After Cardiac Death Donors: An Analysis of Risk Factors and Long-term Outcomes From a Single Center. *Annals of Surgery*. 2011;253(4):817.

- [43] Cursio R, Gugenheim J. Ischemia-Reperfusion Injury and Ischemic-Type Biliary Lesions following Liver Transplantation. *Journal of Transplantation*. 2012;2012:1–17.
- [44] Nishida S, Nakamura N, Kadono J, Komokata T, Sakata R, Madariaga JR, et al. Intrahepatic biliary strictures after liver transplantation. *Journal of Hepato-Biliary-Pancreatic Surgery*. 2006;13(6):511–6.
- [45] Skaro A, Jay C, Baker T, Wang E, Pasricha S, Lyuksemburg V, et al. The impact of ischemic cholangiopathy in liver transplantation using donors after cardiac death: The untold story. *Surgery*. 2009;146(4):543–553.
- [46] Scanga AE, Kowdley KV. Management of biliary complications following orthotopic liver transplantation. *Current Gastroenterology Reports*. 2007;9(1):31–8.
- [47] Sharma S, Gurakar A, Jabbour N. Biliary strictures following liver transplantation: past, present and preventive strategies. *Liver Transplantation*. 2008;14(6):759–69.
- [48] Verdonk RC, Buis CI, Porte RJ, van der Jagt EJ, Limburg AJ, van den Berg AP, et al. Anastomotic biliary strictures after liver transplantation: causes and consequences. *Liver Transplantation*. 2006;12(5):726–35.
- [49] Peralta C, Mónica J, Jordi G. Hepatic ischemia and reperfusion injury: Effects on the liver sinusoidal milieu. *Journal of Hepatology*. 2013;59(5):1094–1106.
- [50] Dictionary O. "ischaemia {} ischemia, n."; 2018.
- [51] Granger ND, Rutili G, M MJ. Superoxide radicals in feline intestinal ischemia. *Gastroenterology*. 1981;81(1):22–29.
- [52] Makuuchi M, Mori T, Gunven P, Yamazaki S, Hasegawa H. Safety of hemihepatic vascular occlusion during resection of the liver. *Surg Gynecol Obstetrics*. 1987;164(2):155–8.
- [53] Rushing G, Britt L. Reperfusion injury after hemorrhage: a collective review. *Annals of Surgery*. 2008;247(6):929.

- [54] Kim YI. Ischemia-reperfusion injury of the human liver during hepatic resection. *Journal of Hepato-Biliary-Pancreatic Surgery*. 2003 jun;10(3):195–199.
- [55] Kupiec-Weglinski JW, Busuttil RW. Ischemia and Reperfusion Injury in Liver Transplantation. *Transplantation Proceedings*. 2005 may;37(4):1653–1656.
- [56] Pringle J. Notes on the arrest of hepatic hemorrhage due to trauma. *Annals of surgery*. 1908;p. 541–549.
- [57] Hong JC. Liver Transplantation Using Organ Donation After Cardiac Death. *Archives of Surgery*. 2011 sep;146(9):1017.
- [58] Kalogeris T, Baines CP, Krenz M, Korthuis RJ. Cell Biology of Ischemia/Reperfusion Injury. In: *International Review of Cell and Molecular Biology Volume 298*. Elsevier; 2012. p. 229–317.
- [59] Chen GY, Nuñez G. Sterile inflammation: sensing and reacting to damage. *Nature Reviews Immunology*. 2010;10(12):826–37.
- [60] Pike MM, Luo CS, Clark MD, Kirk KA, Kitakaze M, Madden MC, et al. NMR measurements of Na and cellular energy in ischemic rat heart: role of Na<sup>+</sup>-H exchange. *American Journal of Physiology-Heart and Circulatory Physiology*. 1993 dec;265(6):H2017–H2026.
- [61] Peralta C, Bartrons R, Riera L, Manzano A, Xaus C, Gelpí E, et al. Hepatic preconditioning preserves energy metabolism during sustained ischemia. *American Journal of Physiology-Gastrointestinal and Liver Physiology*. 2000 jul;279(1):G163–G171.
- [62] Sanada S, Komuro I, Kitakaze M. Pathophysiology of myocardial reperfusion injury: preconditioning, postconditioning, and translational aspects of protective measures. *American Journal of Physiology-Heart and Circulatory Physiology*. 2011 nov;301(5):H1723–H1741.

- [63] Honda HM, Korge P, Weiss JN. Mitochondria and Ischemia/Reperfusion Injury. *Annals of the New York Academy of Sciences*. 2005 jun;1047(1):248–258.
- [64] Buckley G. Free radical-mediated reperfusion injury: a selective review. *British Journal of Cancer*. 1987;8:66–73.
- [65] Jennings R, Sommers H, Yth G, Flack H, Linn H. Myocardial necrosis induced by temporary occlusion of a coronary artery in the dog. *Archives of Pathology*. 1960;70:68–78.
- [66] Jaeschke H. Reactive oxygen and ischemia/reperfusion injury of the liver. *Chemico-Biological Interactions*. 1991;79(2):115 – 136.
- [67] Huang H, Evankovich J, Yan W, Nace G, Zhang L, Ross M, et al. Endogenous histones function as alarmins in sterile inflammatory liver injury through Toll-like receptor 9 in mice. *Hepatology*. 2011 aug;54(3):999–1008.
- [68] Nakashima H, Ogawa Y, Shono S, Kinoshita M, Nakashima M, Sato A, et al. Activation of CD11b+ Kupffer cells/macrophages as a common cause for exacerbation of TNF/Fas-ligand-dependent hepatitis in hypercholesterolemic mice. *PLoS ONE*. 2013 jan;8(1):e49339.
- [69] Miyashita T, Nakanuma S, Ahmed A, Surgery MI. Ischemia reperfusion-facilitated sinusoidal endothelial cell injury in liver transplantation and the resulting impact of extravasated platelet aggregation. *European Surgery*. 2016;48(2):92–98.
- [70] Zhai Y, Shen XdD, Ryan O, Gao F, Lassman C, Busuttil RW, et al. Cutting edge: TLR4 activation mediates liver ischemia/reperfusion inflammatory response via IFN regulatory factor 3-dependent MyD88-independent pathway. *Journal of Immunology*. 2004;173(12):7115–9.
- [71] MacDonald KA, Huang H, Tohme S, Loughran P, Ferrero K, Billiar T, et al. Toll-like Receptor 4 (TLR4) Antagonist Eritoran Tetrasodium Attenuates Liver Ischemia

and Reperfusion Injury through Inhibition of High-Mobility Group Box Protein B1 (HMGB1) Signaling. *Molecular Medicine*. 2014;.

- [72] Shen X, Ke B, Zhai Y, Amersi F, Gao F, Anselmo DM, et al. CD154-CD40 T-cell costimulation pathway is required in the mechanism of hepatic ischemia/reperfusion injury, and its blockade facilitates and depends on heme oxygenase-1 mediated cytoprotection. *Transplantation*. 2002;74(3).
- [73] Zwacka R, Zhang Y, Halldorson J, Schlossberg H, Dudus L, Engelhardt J. CD4(+) T-lymphocytes mediate ischemia/reperfusion-induced inflammatory responses in mouse liver. *Journal of Clinical Investigation*. 1997;100(2):279–289.
- [74] Moine O, Louis H, Demols A, Desalle F, Demoor F, Quertinmont E, et al. Cold liver ischemia-reperfusion injury critically depends on liver T cells and is improved by donor pretreatment with interleukin 10 in mice. *Hepatology*. 2000;31(6):1266–1274.
- [75] Kuboki S, Sakai N, Tschöp J, Edwards MJ, Lentsch AB, Caldwell CC. Distinct contributions of CD4(+) T cell subsets in hepatic ischemia/reperfusion injury. *American Journal of Physiology - Gastrointestinal and Liver Physiology*. 2009;296(5):G1054 – G1059.
- [76] Liesz A, Elisabeth S, Veltkamp C, Doerr H, Sommer C, Rivest S, et al. Regulatory T cells are key cerebroprotective immunomodulators in acute experimental stroke. *Nature Medicine*. 2009;15:192.
- [77] Rao J, Lu L, Zhai Y. T cells in Organ Ischemia Reperfusion Injury. *Current Opinions in Organ Transplantation*. 2014 Apr;19(2):115–120.
- [78] Lesurtel M. Platelet-Derived Serotonin Mediates Liver Regeneration. *Science*. 2006 apr;312(5770):104–107.
- [79] Farmer DG, Amersi F, Jerzy K, Busuttil RW. Current status of ischemia and reperfusion injury in the liver. *Transplantation Reviews*. 2000;14(2):106 – 126.



- [80] Shiki K, Hearse D. Preconditioning of ischemic myocardium: reperfusion-induced arrhythmias. *American Journal of Physiology*. 1987;253(6 Pt 2):H1470–6.
- [81] Yadav SS, Sindram D, Perry DK, Clavien PA. Ischemic preconditioning protects the mouse liver by inhibition of apoptosis through a caspase-dependent pathway. *Hepatology*. 1999 nov;30(5):1223–1231.
- [82] Peralta C, Hotter G, Closa D, Gelpí E, Bulbena O, Rosello-Catafau J. Protective effect of preconditioning on the injury associated to hepatic ischemia-reperfusion in the rat: Role of nitric oxide and adenosine. *Hepatology*. 1997 apr;25(4):934–937.
- [83] Peralta C, Closa D, Xaus C, Gelpí E, Roselló-catafau J, Hotter G. Hepatic preconditioning in rats is defined by a balance of adenosine and xanthine. *Hepatology*. 1998 sep;28(3):768–773.
- [84] Clavien PA, Yadav S, Sindram D, Bentley RC. Protective Effects of Ischemic Preconditioning for Liver Resection Performed Under Inflow Occlusion in Humans. *Annals of Surgery*. 2000 aug;232(2):155–162.
- [85] Chu MJJ, Vather R, Hickey AJR, Phillips ARJ, Bartlett ASJR. Impact of Ischemic Preconditioning on Outcome in Clinical Liver Surgery: A Systematic Review. *BioMed Research International*. 2015;2015:1–13.
- [86] Gurusamy KS, Kumar Y, Sharma D, Davidson BR. Ischaemic preconditioning for liver transplantation. *Cochrane Database of Systematic Reviews*. 2008 jan;.
- [87] Fernández L. Preconditioning protects liver and lung damage in rat liver transplantation: Role of xanthine/xanthine oxidase. *Hepatology*. 2002 sep;36(3):562–572.
- [88] Nordstrom G, Seeman T, Hasselgren P. Beneficial effect of allopurinol in liver ischemia. *Surgery*. 1985;97(6):679–84.
- [89] Jeon BR, Yeom DH, Lee SM. Protective Effect of Allopurinol on Hepatic Energy Metabolism in Ischaemic and Reperfused Rat Liver. *Shock*. 2001 Feb;15(2):112–117.

- [90] Jaeschke H, Smith CV, Mitchell JR. Reactive oxygen species during ischemia-reflow injury in isolated perfused rat liver. *Journal of Clinical Investigation*. 1988 apr;81(4):1240–1246.
- [91] Lemasters JJ, Qian T, He L, Kim JS, Elmore SP, Cascio WE, et al. Role of Mitochondrial Inner Membrane Permeabilization in Necrotic Cell Death, Apoptosis, and Autophagy. *Antioxidants & Redox Signaling*. 2002 oct;4(5):769–781.
- [92] Theruvath TP, Zhong Z, Pediaditakis P, Ramshesh VK, Currin RT, Tikunov A, et al. Minocycline and N-methyl-4-isoleucine cyclosporin (NIM811) mitigate storage/reperfusion injury after rat liver transplantation through suppression of the mitochondrial permeability transition. *Hepatology*. 2008 nov;47(1):236–246.
- [93] Pierce R, Glaug M, Greco R, Mackenzie J, Boyd C, Deak S. Increased procollagen mRNA levels in carbon tetrachloride-induced liver fibrosis in rats. *Journal of Biological Chemistry*. 1987;262(4):1652–8.
- [94] Ohta Y, Mutsumi K, Matsura T, Yamada K, Kitagawa A, Kishikawa T. Melatonin prevents disruption of hepatic reactive oxygen species metabolism in rats treated with carbon tetrachloride. *Journal of Pineal Research*. 2004;36(1).
- [95] Smit J, Schinkel A, Elferink R, Groen A, Wagenaar E, van Deemter L, et al. Homozygous disruption of the murine *MDR2* P-glycoprotein gene leads to a complete absence of phospholipid from bile and to liver disease. *Cell*. 1993;75(3):451 – 462.
- [96] Fickert P, Zollner G, Fuchsbichler A, Stumptner C, Weiglein A, Lammert F, et al. Ursodeoxycholic acid aggravates bile infarcts in bile duct-ligated and *Mdr2* knockout mice via disruption of cholangioles. *Gastroenterology*. 2002;123(4):1238–1251.
- [97] Mauad T, Nieuwkerk C, Dingemans K, Smit J, Schinkel A, Notenboom R, et al. Mice with homozygous disruption of the *mdr2* P-glycoprotein gene. A novel animal model

for studies of nonsuppurative inflammatory cholangitis and hepatocarcinogenesis. *Am J Pathology*. 1994;145(5):1237–45.

- [98] Fickert P, Fuchsbichler A, Wagner M, Zollner G, Kaser A, Tilg H, et al. Regurgitation of bile acids from leaky bile ducts causes sclerosing cholangitis in Mdr2 (Abcb4) knockout mice. *Gastroenterology*. 2004;127(1):261–274.
- [99] Lammert F, Wang DQH, Hillebrandt S, Geier A, Fickert P, Trauner M, et al. Spontaneous cholecysto- and hepatolithiasis in Mdr2<sup>-/-</sup> mice: A model for low phospholipid-associated cholelithiasis. *Hepatology*. 2004 jan;39(1):117–128.
- [100] Fickert P, Wagner M, Marschall H, Fuchsbichler A, Zollner G, Tsybrovskyy O, et al. 24-norUrsodeoxycholic Acid Is Superior to Ursodeoxycholic Acid in the Treatment of Sclerosing Cholangitis in Mdr2 (Abcb4) Knockout Mice. *Gastroenterology*. 2006;130(2):465–481.
- [101] van Golen RF, Reiniers MJ, Heger M, Verheij J. Solutions to the discrepancies in the extent of liver damage following ischemia/reperfusion in standard mouse models. *Journal of Hepatology*. 2015;62:975–989.
- [102] Abe Y, Hines IN, Zibari G, Pavlick K, Gray L, Kitagawa Y, et al. Mouse model of liver ischemia and reperfusion injury: method for studying reactive oxygen and nitrogen metabolites in vivo. *Free Radic Biol Med*. 2009;46(1):1–7.
- [103] Yano K, Fukuda Y, Sumimoto R, Ito H, Asahara T, Dohi K. Development of a rat model for orthotopic liver transplantation for hepatocellular carcinoma. *Surgery*. 1995;118(3):539 – 546.
- [104] Zhang Y, He Y, Praseedom RK, Zheng S, Dong J, Chen H. Establishment of animal model of dual liver transplantation in rat. *PLoS ONE*. 2012;7(7):e40818.
- [105] Qian S, Fung JJ, Demetris AJ, Ildstad ST, Starzl TE. Orthotopic liver transplantation in the mouse. *Transplantation*. 1991;.

- [106] Tian Y, Rudiger H, Jochum W, Clavien P. Comparison of arterialized and non-arterialized orthotopic liver transplantation in mice: prowess or relevant model? Transplantation. 2002;74(9):1242–1246.
- [107] Anastassova-Kristeva M. The Origin and Development of the Immune System with a View to Stem Cell Therapy. Journal of Hematotherapy & Stem Cell Research. 2003 apr;12(2):137–154.
- [108] Akira S, Uematsu S, Takeuchi O. Pathogen Recognition and Innate Immunity. Cell. 2006;124(4):783 – 801.
- [109] Akira S, Takeda K. Toll-like receptor signalling. Nature Reviews Immunology. 2004 jul;4(7):499–511.
- [110] Janeway CA, Travers P, Walport M, Shlomchik MJ. Immunobiology. Garland Science; 2001.
- [111] Vivier E, Tomasello E, Baratin M, Walzer T, Ugolini S. Functions of natural killer cells. Nature Immunology. 2008 may;9(5):503–510.
- [112] Clambey ET, Davenport B, Kappler JW, Marrack P, Homann D. Molecules in medicine mini review: the  $\alpha\beta$  T cell receptor. Journal of molecular medicine. 2014;92(7):735 – 741.
- [113] Zúñiga-Pflücker JC. When Three Negatives Made a Positive Influence in Defining Four Early Steps in T Cell Development. J Immunol. 2012 Nov;189(9):4201. Available from: <http://www.jimmunol.org/content/189/9/4201.abstract>.
- [114] Ciofani M, Zúñiga-Pflücker JC. The Thymus as an Inductive Site for T Lymphopoiesis. Annu Rev Cell Dev Biol. 2007 Nov;23(1):463–493. Available from: <https://doi.org/10.1146/annurev.cellbio.23.090506.123547>.
- [115] Ciofani M, Zuniga-Pflucker JC. Determining gammadelta versus alphass T cell development. Nature reviews Immunology. 2010 Sep;10:657–63.

- [116] Klein L, Kyewski B, Allen PM, Hogquist KA. Positive and negative selection of the T cell repertoire: what thymocytes see and don't see. *Nature reviews Immunology*. 2014 May;14(6):377–391. Available from: <http://www.ncbi.nlm.nih.gov/pmc/articles/PMC4757912/>.
- [117] Weber BN, Chi AWS, Chavez A, Yashiro-Ohtani Y, Yang Q, Shestova O, et al. A critical role for TCF-1 in T-lineage specification and differentiation. *Nature*. 2011 Aug;476:63–8.
- [118] Greenwald RJ, Freeman GJ, Sharpe AH. The B7 family revisited. *Annual review of immunology*. 2005;23:515–48.
- [119] Wucherpennig KW, Gagnon E, Call MJ, Huseby ES, Call ME. Structural Biology of the T-cell Receptor: Insights into Receptor Assembly, Ligand Recognition, and Initiation of Signaling. *Cold Spring Harbor Perspectives in Biology*. 2010 mar;2(4):a005140–a005140.
- [120] Chen L, Flies DB. Molecular mechanisms of T cell co-stimulation and co-inhibition. *Nature Reviews Immunology*. 2013 mar;13(4):227–242.
- [121] Bonilla FA, Oettgen HC. Adaptive immunity. *Journal of Allergy and Clinical Immunology*. 2010 feb;125(2):S33–S40.
- [122] Sakaguchi S, Wing K, Onishi Y, Paz P, Yamaguchi T. Regulatory T cells: how do they suppress immune responses? *International Immunology*. 2009;21(10):1105 – 1111.
- [123] Allen C, Okada T, Cyster JG. Germinal-Center Organization and Cellular Dynamics. *Immunity*. 2007;27(2):190 – 202.
- [124] Liao C, Zimmer MI, Wang C. The Functions of Type I and Type II Natural Killer T (NKT) Cells in Inflammatory Bowel Diseases. *Inflammatory bowel diseases*. 2013;19(6):1330 – 1338.

- [125] Horwitz E, Blanc K, Dominici M, Mueller I, I S, Marini F, et al. Clarification of the nomenclature for MSC: The International Society for Cellular Therapy position statement. *Cytotherapy*. 2005;7(5):393–395.
- [126] Dominici M, Blanc K, Mueller I, I S, Marini F, Krause D, et al. Minimal criteria for defining multipotent mesenchymal stromal cells. The International Society for Cellular Therapy position statement. *Cytotherapy*. 2006;8(4):315–317.
- [127] Mendicino M, Bailey AM, Wonnacott K, Puri RK, Bauer SR. MSC-Based Product Characterization for Clinical Trials: An FDA Perspective. *Cell Stem Cell*. 2014 feb;14(2):141–145.
- [128] Bernardo M, Fibbe W. Mesenchymal Stromal Cells: Sensors and Switchers of Inflammation. *Cell Stem Cell*. 2013;13(4):392–402.
- [129] Haniffa MA, Collin MP, Buckley CD, Dazzi F. Mesenchymal stem cells: the fibroblasts' new clothes? *Haematologica*. 2008 dec;94(2):258–263.
- [130] Bianco P, Robey PG, Simmons PJ. Mesenchymal stem cells: revisiting history, concepts, and assays. *Cell Stem Cell*. 2008;2(4):313–9.
- [131] Pittenger MF, Mackay AM, Beck SC, Jaiswal RK, Douglas R, Mosca JD, et al. Multilineage Potential of Adult Human Mesenchymal Stem Cells. *Science*. 1999;284(5411):143.
- [132] Sacchetti B, Funari A, Michienzi S, Cesare SD, Piersanti S, Saggio I, et al. Self-Renewing Osteoprogenitors in Bone Marrow Sinusoids Can Organize a Hematopoietic Microenvironment. *Cell*. 2007 oct;131(2):324–336.
- [133] Friedenstein AJ, Chailakhjan RK, Lalykina KS. The Developpment of Fibroblast Colonies in Monolayer Cultures og Guinea-pig Bone Marrow and Spleen Cells. *Cell Proliferation*. 1970 oct;3(4):393–403.

- [134] Friedenstein A. Stromal-Hematopoietic Interrelationships: Maximov's Ideas and Modern Models. In: Haematology and Blood Transfusion / Hämatologie und Bluttransfusion. vol. 32. Springer Berlin Heidelberg; 1989. p. 159–167.
- [135] Maximov A. Über experimentelle Erzeugung von Knochenmarks-Gewebe. Anatomischer Anzeiger. 1906;28:24–38.
- [136] Tavassoli M, Crosby WH. Transplantation of Marrow to Extramedullary Sites. Science. 1968;161(3836):54.
- [137] Tavassoli M, Friedenstein A. Hemopoietic stromal microenvironment. American Journal of Hematology. 1983;15(2):195–203.
- [138] Owen M, Friedenstein AJ. Stromal Stem Cells: Marrow-Derived Osteogenic Precursors. In: Ciba Foundation Symposium 136 - Cell and Molecular Biology of Vertebrate Hard Tissues. vol. 136. John Wiley & Sons, Ltd.; 1988. p. 42–60.
- [139] Méndez-Ferrer S, Michurina TV, Ferraro F, Mazloom AR, MacArthur BD, Lira SA, et al. Mesenchymal and haematopoietic stem cells form a unique bone marrow niche. Nature. 2010 aug;466(7308):829–834.
- [140] Caplan AI. Mesenchymal stem cells. Journal of Orthopaedic Research. 1991;9(5):641 – 650.
- [141] Tormin A, Li O, Walsh S, Ehinger M, Brune JC, Scheduling S. CD146 Expression in Primary Bone Marrow MSC Progenitor/Stem Cells Is Dependent On Their In Vivo Location. Blood. 2009 Nov;114(22):251. Available from: <http://www.bloodjournal.org/content/114/22/251.abstract>.
- [142] Bianco P, Cao X, Frenette PS, Mao JJ, Robey PG, Simmons PJ, et al. The meaning, the sense and the significance: translating the science of mesenchymal stem cells into medicine. Nature Medicine. 2013;19(1):35–42.

- [143] Peister A, Mellad JA, Larson BL, Hall BM, Gibson LF, Prockop DJ. Adult stem cells from bone marrow (MSCs) isolated from different strains of inbred mice vary in surface epitopes, rates of proliferation, and differentiation potential. *Blood*. 2004;103(5):1662–8.
- [144] Mabuchi Y, Morikawa S, Harada S, Niibe K, Suzuki S, Renault-Mihara F, et al. LNGFR+THY-1+VCAM-1hi+ Cells Reveal Functionally Distinct Subpopulations in Mesenchymal Stem Cells. *Stem Cell Reports*. 2013 Aug;1(2):152–165.
- [145] Zhou B, Yue R, Murphy M, Peyer J, Morrison S. Leptin-Receptor-Expressing Mesenchymal Stromal Cells Represent the Main Source of Bone Formed by Adult Bone Marrow. *Cell Stem Cell*. 2014 Aug;15:154–168.
- [146] Frenette PS, Pinho S, Lucas D, Scheiermann C. Mesenchymal Stem Cell: Keystone of the Hematopoietic Stem Cell Niche and a Stepping-Stone for Regenerative Medicine. *Annual Review of Immunology*. 2013;31(1):285 – 316.
- [147] Nadri S, Soleimani M. Isolation murine mesenchymal stem cells by positive selection. *In Vitro Cellular & Developmental Biology - Animal*. 2007 sep;43(8-9):276–282.
- [148] Phinney D, Kopen G, Isaacson R, Prockop D. Plastic adherent stromal cells from the bone marrow of commonly used strains of inbred mice: variations in yield, growth, and differentiation. *Journal of Cellular Biochemistry*. 1999;72(4):570–585.
- [149] Baddoo M, Hill K, Wilkinson R, Gaupp D, Hughes C, Kopen GC, et al. Characterization of mesenchymal stem cells isolated from murine bone marrow by negative selection. *Journal of Cellular Biochemistry*. 2003;89(6):1235–1249.
- [150] Morikawa S, Mabuchi Y, Kubota Y, Nagai Y, Niibe K, Hiratsu E, et al. Prospective identification, isolation, and systemic transplantation of multipotent mesenchymal stem cells in murine bone marrow. *The Journal of Experimental Medicine*. 2009 oct;206(11):2483–2496.



- [151] Pinho S, Lacombe J, Hanoun M, Mizoguchi T, Bruns I, Kunisaki Y, et al. PDGFR and CD51 mark human Nestinsphere-forming mesenchymal stem cells capable of hematopoietic progenitor cell expansion. *The Journal of Experimental Medicine*. 2013 jun;210(7):1351–1367.
- [152] Hass R, Kasper C, Böhm S, Jacobs R. Different populations and sources of human mesenchymal stem cells (MSC): A comparison of adult and neonatal tissue-derived MSC. *Cell Commun Signal*. 2011;9(1):1–14.
- [153] Ranganath SH, Levy O, Inamdar MS, Karp JM. Harnessing the mesenchymal stem cell secretome for the treatment of cardiovascular disease. *Cell Stem Cell*. 2012;10(3):244–58.
- [154] Wang Y, Chen X, Cao W, Shi Y. Plasticity of mesenchymal stem cells in immunomodulation: pathological and therapeutic implications. *Nature Immunology*. 2014 oct;15(11):1009–1016.
- [155] Zanotti L, Sarukhan A, Dander E, Castor M, Cibella J, Soldani C, et al. Encapsulated mesenchymal stem cells for in vivo immunomodulation. *Leukemia*. 2012 jul;27(2):500–503.
- [156] Glennie S, Soeiro I, Dyson P, Lam E, Dazzi F. Bone marrow mesenchymal stem cells induce division arrest anergy of activated T cells. *Blood*. 2005;105(7):2821–2827.
- [157] Rasmusson I, Ringdén O, Sundberg B, Blanc K. Mesenchymal stem cells inhibit lymphocyte proliferation by mitogens and alloantigens by different mechanisms. *Experimental Cell Research*. 2005;305(1):33–41.
- [158] Zappia E, Casazza S, Pedemonte E, Benvenuto F, Bonanni I, Gerdoni E, et al. Mesenchymal stem cells ameliorate experimental autoimmune encephalomyelitis inducing T-cell anergy. *Blood*. 2005;106(5):1755–1761.

- [159] Najjar M, Rouas R, Raicevic G, Boufker H, Lewalle P, Meuleman N, et al. Mesenchymal stromal cells promote or suppress the proliferation of T lymphocytes from cord blood and peripheral blood: the importance of low cell ratio and role of interleukin-6. *Cytotherapy*. 2009;11(5):570–583.
- [160] Ramasamy R, Fazekasova H, Lam E, Soeiro I, Lombardi G, Dazzi F. Mesenchymal Stem Cells Inhibit Dendritic Cell Differentiation and Function by Preventing Entry Into the Cell Cycle. *Transplantation*. 2007;83(1):71.
- [161] Chiesa S, Morbelli S, Morando S, Massollo M, Marini C, Bertoni A, et al. Mesenchymal stem cells impair in vivo T-cell priming by dendritic cells. *Proceedings of the National Academy of Sciences*. 2011 sep;108(42):17384–17389.
- [162] Jiang X, Zhang Y, Liu B, Zhang S, Wu Y, Yu X, et al. Human mesenchymal stem cells inhibit differentiation and function of monocyte-derived dendritic cells. *Blood*. 2005;105(10):4120–4126.
- [163] Aggarwal S, Pittenger MF. Human mesenchymal stem cells modulate allogeneic immune cell responses. *Blood*. 2005;105(4):1815–22.
- [164] Min CK, Kim BG, Park G, Cho B, Oh IH. IL-10-transduced bone marrow mesenchymal stem cells can attenuate the severity of acute graft-versus-host disease after experimental allogeneic stem cell transplantation. *Bone Marrow Transplantation*. 2007 mar;39(10):637–645.
- [165] Blanc KL, Frassoni F, Ball L, Locatelli F, Roelofs H, Lewis I, et al. Mesenchymal stem cells for treatment of steroid-resistant, severe, acute graft-versus-host disease: a phase II study. *The Lancet*. 2008 may;371(9624):1579–1586. Available from: [http://dx.doi.org/10.1016/S0140-6736\(08\)60690-X](http://dx.doi.org/10.1016/S0140-6736(08)60690-X).
- [166] Spaggiari G, Capobianco A, Becchetti S, Mingari M, Moretta L. Mesenchymal stem cell-natural killer cell interactions: evidence that activated NK cells are capable of

killing MSCs, whereas MSCs can inhibit IL-2-induced NK-cell proliferation. *Blood*. 2006;107(4):1484–1490.

- [167] Galleu A, Riffo-Vasquez Y, Trento C, Lomas C, Dolcetti L, Cheung TS, et al. Apoptosis in mesenchymal stromal cells induces in vivo recipient-mediated immunomodulation. *Science Translational Medicine*. 2017 nov;9(416):eaam7828.
- [168] Hashemi S, Hassan Z, Pourfathollah A, Soudi S, Shafiee A, Soleimani M. Comparative immunomodulatory properties of adipose-derived mesenchymal stem cells conditioned media from BALB/c, C57BL/6, and DBA mouse strains. *Journal of Cellular Biochemistry*. 2013;114(4):955–965.
- [169] Barzilay R, Sadan O, Melamed E, Offen D. Comparative characterization of bone marrow-derived mesenchymal stromal cells from four different rat strains. *Cytotherapy*. 2009;11(4):435–442.
- [170] François M, Raphaëlle R, Li M, Galipeau J. Human MSC Suppression Correlates With Cytokine Induction of Indoleamine 2,3-Dioxygenase and Bystander M2 Macrophage Differentiation. *Molecular Therapy*. 2012;20(1):187–195.
- [171] Friedman SL. Liver fibrosis – from bench to bedside. *Journal of Hepatology*. 2003 jan;38:38–53.
- [172] Friedman SL. Mechanisms of Disease: mechanisms of hepatic fibrosis and therapeutic implications. *Nature Clinical Practice Gastroenterology & Hepatology*. 2004 dec;1(2):98–105.
- [173] Lin N, Hu K, Chen S, Xie S, Tang Z, Lin J, et al. Nerve growth factor-mediated paracrine regulation of hepatic stellate cells by multipotent mesenchymal stromal cells. *Life Sciences*. 2009 aug;85(7-8):291–295.
- [174] Parekkadan B, van Poll D, Megeed Z, Kobayashi N, Tilles AW, Berthiaume F, et al.

- Immunomodulation of activated hepatic stellate cells by mesenchymal stem cells. *Biochemical and Biophysical Research Communications*. 2007 nov;363(2):247–252.
- [175] Jung KH, Shin HP, Lee S, Lim YJ, Hwang SH, Han H, et al. Effect of human umbilical cord blood-derived mesenchymal stem cells in a cirrhotic rat model. *Liver International*. 2009;29(6):898–909.
- [176] Higashiyama R, Inagaki Y, Hong YY, Kushida M, Nakao S, Niioka M, et al. Bone marrow-derived cells express matrix metalloproteinases and contribute to regression of liver fibrosis in mice. *Hepatology*. 2007;45(1):213–22.
- [177] Oh S, Witek RP, Bae S, Zheng D, Jung Y, Piscaglia AC, et al. Bone Marrow - Derived Hepatic Oval Cells Differentiate Into Hepatocytes in 2-Acetylaminofluorene/Partial Hepatectomy-Induced Liver Regeneration. *Gastroenterology*. 2007;132(3):1077 – 1087.
- [178] Mohamadnejad M, Alimoghaddam K, Bagheri M, Ashrafi M, Abdollahzadeh L, Akhlaghpour S, et al. Randomized placebo-controlled trial of mesenchymal stem cell transplantation in decompensated cirrhosis. *Liver International*. 2013 Jun;33(10):1490–1496.
- [179] Kim JK, Park YN, Kim JS, Park MS, Paik YH, Seok JY, et al. Autologous bone marrow infusion activates the progenitor cell compartment in patients with advanced liver cirrhosis. *Cell Transplantation*. 2010;19(10):1237–46.
- [180] Bernal W, Wendon J. Acute Liver Failure. *New England Journal of Medicine*. 2013 dec;369(26):2525–2534.
- [181] Reuben A, Koch DG, Lee WM. Drug-induced acute liver failure: Results of a U.S. multicenter, prospective study. *Hepatology*. 2010 oct;52(6):2065–2076.
- [182] Bernal W, Auzinger G, Dhawan A, Wendon J. Acute liver failure. *The Lancet*. 2010 jul;376(9736):190–201.

- [183] Chen Y, Chen S, Liu LY, Zou ZL, Cai YJ, Wang JG, et al. Mesenchymal stem cells ameliorate experimental autoimmune hepatitis by activation of the programmed death 1 pathway. *Immunology Letters*. 2014 dec;162(2):222–228.
- [184] Jung J, Choi JH, Lee Y, Park JW, Oh IH, Hwang SG, et al. Human Placenta-Derived Mesenchymal Stem Cells Promote Hepatic Regeneration in CCl<sub>4</sub>-Injured Rat Liver Model via Increased Autophagic Mechanism. *STEM CELLS*. 2013 aug;31(8):1584–1596.
- [185] Zhu X, He B, Zhou X, Ren J. Effects of transplanted bone-marrow-derived mesenchymal stem cells in animal models of acute hepatitis. *Cell and Tissue Research*. 2012 nov;351(3):477–486.
- [186] Kuo T, Hung S, Chuang C, Chen C, Shih Y, Fang S, et al. Stem Cell Therapy for Liver Disease: Parameters Governing the Success of Using Bone Marrow Mesenchymal Stem Cells. *Gastroenterology*. 2008;134(7):2111–2121.e3.
- [187] Gunawan BK, Liu Z, Han D, Hanawa N, Gaarde WA, Kaplowitz N. c-Jun N-Terminal Kinase Plays a Major Role in Murine Acetaminophen Hepatotoxicity. *Gastroenterology*. 2006;131(1):165 – 178.
- [188] Salomone F, Barbagallo I, Puzzo L, Piazza C, Volti G. Efficacy of adipose tissue-mesenchymal stem cell transplantation in rats with acetaminophen liver injury. *Stem Cell Research*. 2013;11(3):1037–1044.
- [189] Bellanti F. Ischemia-reperfusion injury: evidences for translational research. *Annals of Translational Medicine*. 2016 oct;4(S1):S55–S55.
- [190] Vardanian A, Busuttil R. Molecular mediators of liver ischemia and reperfusion injury: a brief review. *Molecular Medicine*. 2008;14(5-6):1.
- [191] Joshi M, Patil PB, He Z, Holgersson J, Olausson M, Suchitra S. Fetal liver-derived

mesenchymal stromal cells augment engraftment of transplanted hepatocytes. *Cytotherapy*. 2012;14(6):657 – 669.

- [192] van Poll D, Parekkadan B, Cho CH, Berthiaume F, Nahmias Y, Tilles AW, et al. Mesenchymal stem cell-derived molecules directly modulate hepatocellular death and regeneration in vitro and in vivo. *Hepatology*. 2008 apr;47(5):1634–1643.
- [193] Kanazawa H, Fujimoto Y, Teratani T, Iwasaki J, Kasahara N, Negishi K, et al. Bone Marrow-Derived Mesenchymal Stem Cells Ameliorate Hepatic Ischemia Reperfusion Injury in a Rat Model. *PLoS ONE*. 2011 apr;6(4):e19195.
- [194] Raffaghello L, Bianchi G, Bertolotto M, Montecucco F, Busca A, Dallegri F, et al. Human Mesenchymal Stem Cells Inhibit Neutrophil Apoptosis: A Model for Neutrophil Preservation in the Bone Marrow Niche. *Stem Cells*. 2008 jan;26(1):151–162.
- [195] Yu Y, Lu L, Qian X, Chen N, Yao A, Pu L, et al. Antifibrotic Effect of Hepatocyte Growth Factor-Expressing Mesenchymal Stem Cells in Small-for-Size Liver Transplant Rats. *Stem Cells and Development*. 2010 jun;19(6):903–914.
- [196] Yu Y, Yao AH, Chen N, Pu LY, Fan Y, Lv L, et al. Mesenchymal Stem Cells Over-expressing Hepatocyte Growth Factor Improve Small-for-size Liver Grafts Regeneration. *Molecular Therapy*. 2007 jul;15(7):1382–1389.
- [197] Du Z, Wei C, Cheng K, Han B, Yan J, Zhang M, et al. Mesenchymal stem cell-conditioned medium reduces liver injury and enhances regeneration in reduced-size rat liver transplantation. *Journal of Surgical Research*. 2013 aug;183(2):907–915.
- [198] Wan C, Cheng R, Wang HB, Liu T. Immunomodulatory effects of mesenchymal stem cells derived from adipose tissues in a rat orthotopic liver transplantation model. *Hepatobiliary Pancreat Dis Int*. 2008;7(1):29–33.
- [199] Perico N, Casiraghi F, Gotti E, Inrona M, Todeschini M, Cavinato R, et al. Mesenchymal stromal cells and kidney transplantation: pretransplant infusion protects

from graft dysfunction while fostering immunoregulation. *Transplant International*. 2013;26(9):867 – 878.

- [200] Reinders MEJ, de Fijter JW, Roelofs H, Bajema IM, de Vries DK, Schaapherder AF, et al. Autologous Bone Marrow-Derived Mesenchymal Stromal Cells for the Treatment of Allograft Rejection After Renal Transplantation: Results of a Phase I Study. *STEM CELLS Translational Medicine*. 2013 jan;2(2):107–111.
- [201] Kar P, Budhiraja S, Narang A, Chakravarthy A. Etiology of sporadic acute and fulminant non-A, non-B viral hepatitis in north India. *Indian Journal of Gastroenterology*. 1997;16(2):43–5.
- [202] Shah U, Habib Z. Liver Failure Attributable to Hepatitis A Virus Infection in a Developing Country. *PEDIATRICS*. 2000 feb;105(2):436–438.
- [203] Hoofnagle JH, Nelson KE, Purcell RH. Hepatitis E. *New England Journal of Medicine*. 2012;367(13):1237–44.
- [204] Schiødt FV, Atillasoy E, Shakil AO, Schiff ER, Caldwell C, Kowdley KV, et al. Etiology and outcome for 295 patients with acute liver failure in the united states. *Liver Transplantation and Surgery*. 1999 jan;5(1):29–34.
- [205] Shi M, Zhang Z, Xu R, Lin H, Fu J, Zou Z, et al. Human Mesenchymal Stem Cell Transfusion Is Safe and Improves Liver Function in Acute-on-Chronic Liver Failure Patients. *STEM CELLS Translational Medicine*. 2012 oct;1(10):725–731.
- [206] Peng L, ying Xie D, Lin BL, Liu J, peng Zhu H, Xie C, et al. Autologous bone marrow mesenchymal stem cell transplantation in liver failure patients caused by hepatitis B: Short-term and long-term outcomes. *Hepatology*. 2011 jul;54(3):820–828.
- [207] Xu L, Gong Y, Wang B, Shi K, Hou Y, Wang L, et al. Randomized trial of autologous bone marrow mesenchymal stem cells transplantation for hepatitis B virus cirrhosis:

regulation of Treg/Th17 cells. *Journal of Gastroenterology and Hepatology*. 2014 jul;29(8):1620–1628.

- [208] Salama H, Zekri ARN, Medhat E, Alim SAA, Ahmed OS, Bahnassy AA, et al. Peripheral vein infusion of autologous mesenchymal stem cells in Egyptian HCV-positive patients with end-stage liver disease. *Stem Cell Research & Therapy*. 2014;5(3):70.
- [209] Ma R, Xing Q, Shao L, Wang D, Hao Q, Li X, et al. Hepatitis B virus infection and replication in human bone marrow mesenchymal stem cells. *Virology Journal*. 2011;8(1):486.
- [210] Beckermann BM, Kallifatidis G, Groth A, Frommhold D, Apel A, Mattern J, et al. VEGF expression by mesenchymal stem cells contributes to angiogenesis in pancreatic carcinoma. *British Journal of Cancer*. 2008 jul;99(4):622–631.
- [211] Hernanda PY, Pedroza-Gonzalez A, van der Laan LJW, Bröker MEE, Hoogduijn MJ, Ijzermans JNM, et al. Tumor promotion through the mesenchymal stem cell compartment in human hepatocellular carcinoma. *Carcinogenesis*. 2013 jun;34(10):2330–2340.
- [212] Klopp AH, Gupta A, Spaeth E, Andreeff M, Marini F. Concise Review: Dissecting a Discrepancy in the Literature: Do Mesenchymal Stem Cells Support or Suppress Tumor Growth? *STEM CELLS*. 2011 jan;29(1):11–19.
- [213] Rubio D, Garcia-Castro J, Martín MC, de la Fuente R, Cigudosa JC, Lloyd AC, et al. Spontaneous Human Adult Stem Cell Transformation. *Cancer Research*. 2005 apr;65(8):3035–3039.
- [214] Rosland GV, Svendsen A, Torsvik A, Sobala E, McCormack E, Immervoll H, et al. Long-term Cultures of Bone Marrow-Derived Human Mesenchymal Stem Cells Frequently Undergo Spontaneous Malignant Transformation. *Cancer Research*. 2009 jun;69(13):5331–5339.



- [215] Torsvik A, Rosland GV, Svendsen A, Molven A, Immervoll H, McCormack E, et al. Spontaneous Malignant Transformation of Human Mesenchymal Stem Cells Reflects Cross-Contamination: Putting the Research Field on Track - Letter. *Cancer Research*. 2010 jul;70(15):6393–6396.
- [216] de la Fuente R, Bernad A, Garcia-Castro J, Martin MC, Cigudosa JC. Retraction: Spontaneous Human Adult Stem Cell Transformation. *Cancer Research*. 2010 aug;70(16):6682–6682.
- [217] Jeong JO, Han JW, Kim JM, Cho HJ, Park C, Lee N, et al. Malignant Tumor Formation After Transplantation of Short-Term Cultured Bone Marrow Mesenchymal Stem Cells in Experimental Myocardial Infarction and Diabetic Neuropathy. *Circulation Research*. 2011 Apr;108(11):1340–1347.
- [218] Rangarajan A, Hong S, Gifford A, Weinberg R. Species- and cell type-specific requirements for cellular transformation. *Cancer Cell*. 2004;6(2):171–183.
- [219] Barbash IM. Systemic Delivery of Bone Marrow-Derived Mesenchymal Stem Cells to the Infarcted Myocardium: Feasibility, Cell Migration, and Body Distribution. *Circulation*. 2003 aug;108(7):863–868.
- [220] Aldridge V, Garg A, Davies N, Bartlett DC, Youster J, Beard H, et al. Human mesenchymal stem cells are recruited to injured liver in a  $\beta$ 1-integrin and CD44 dependent manner. *Hepatology*. 2012;56(3):1063–1073.
- [221] Honczarenko M, Le Y, Swierkowski M, Ghiran I, Glodek AM, Silberstein LE. Human Bone Marrow Stromal Cells Express a Distinct Set of Biologically Functional Chemokine Receptors. *STEM CELLS*. 2006 apr;24(4):1030–1041.
- [222] Hung SC, Pochampally RR, Hsu SC, Sanchez C, Chen SC, Spees J, et al. Short-Term Exposure of Multipotent Stromal Cells to Low Oxygen Increases Their Expression of CX3CR1 and CXCR4 and Their Engraftment In Vivo. *PLoS ONE*. 2007 may;2(5):e416.

- [223] Sackstein R. Glycosyltransferase-programmed stereosubstitution (GPS) to create HCELL: engineering a roadmap for cell migration. *Immunology Reviews*. 2009;230(1):51–74.
- [224] Parekkadan B, van Poll D, Suganuma K, Carter EA, Berthiaume F, Tilles AW, et al. Mesenchymal Stem Cell-Derived Molecules Reverse Fulminant Hepatic Failure. *PLoS ONE*. 2007 sep;2(9):e941.
- [225] Bai L, Lennon DP, Caplan AI, DeChant A, Hecker J, Kranso J, et al. Hepatocyte growth factor mediates mesenchymal stem cell-induced recovery in multiple sclerosis models. *Nature Neuroscience*. 2012 may;15(6):862–870.
- [226] Pan BT, Johnstone RM. Fate of the transferrin receptor during maturation of sheep reticulocytes in vitro: Selective externalization of the receptor. *Cell*. 1983 jul;33(3):967–978.
- [227] Valadi H, Ekström K, Bossios A, Sjöstrand M, Lee JJ, Lötvall JO. Exosome-mediated transfer of mRNAs and microRNAs is a novel mechanism of genetic exchange between cells. *Nature Cell Biology*. 2007 May;9(6):654–659.
- [228] Tan C, Lai R, Wong W, Dan Y, Lim SK, Ho H. Mesenchymal stem cell-derived exosomes promote hepatic regeneration in drug-induced liver injury models. *Stem Cell Research & Therapy*. 2014;5(3):76.
- [229] Walczak P, Kedziorek D, Gilad A, Lin S, Bulte J. Instant MR labeling of stem cells using magnetoelectroporation. *Magnetic Resonance in Medicine*. 2005;54(4):769 – 774.
- [230] Schafer R, Kehlbach R, Muller M, Bantleon R, Kluba T, Ayturan M, et al. Labeling of human mesenchymal stromal cells with superparamagnetic iron oxide leads to a decrease in migration capacity and colony formation ability. *Cytotherapy*. 2009;11(1):68–78.

- [231] Huang J, Xie J, Chen K, Bu L, Lee S, Cheng Z, et al. HSA coated MnO nanoparticles with prominent MRI contrast for tumor imaging. *Chemical Communications*. 2010;46(36):6684–6686.
- [232] Schmuck EG, Koch JM, Centanni JM, Hacker TA, Braun RK, Eldridge M, et al. Biodistribution and Clearance of Human Mesenchymal Stem Cells by Quantitative Three-Dimensional Cryo-Imaging After Intravenous Infusion in a Rat Lung Injury Model. *STEM CELLS Translational Medicine*. 2016 jul;5(12):1668–1675.
- [233] Houlihan DD, Mabuchi Y, Morikawa S, Niibe K, Araki D, Suzuki S, et al. Isolation of mouse mesenchymal stem cells on the basis of expression of Sca-1 and PDGFR-. *Nature Protocols*. 2012 nov;7(12):2103–2111.
- [234] Hogquist KA, Jameson SC, Heath WR, Howard JL, Bevan MJ, Carbone FR. T cell receptor antagonist peptides induce positive selection. *Cell*. 1994;76(1):17–27.
- [235] Huang H, Ostroff GR, Lee CK, Specht CA, Levitz SM. Robust Stimulation of Humoral and Cellular Immune Responses following Vaccination with Antigen-Loaded -Glucan Particles. *mBio*. 2010 jul;1(3):e00164–10–e00164–16.
- [236] Houlihan DD. Growth factors direct mesenchymal stem cell fate and therapeutic potential. University of Birmingham; 2013.
- [237] Suresh S. Growth factor priming of murine mesenchymal stem cells critically determines their functionality. University of Birmingham; 2014.
- [238] Németh K, Leelahavanichkul A, Yuen PS, Mayer B, Parmelee A, Doi K, et al. Bone marrow stromal cells attenuate sepsis via prostaglandin E<sub>2</sub>-dependent reprogramming of host macrophages to increase their interleukin-10 production. *Nature medicine*. 2008;15(1):42–49.
- [239] Chen L, Tredget EE, Wu PYG, Wu Y. Paracrine Factors of Mesenchymal Stem Cells

Recruit Macrophages and Endothelial Lineage Cells and Enhance Wound Healing. PLoS ONE. 2008 apr;3(4):e1886.

- [240] Blaber SP, Webster RA, Hill CJ, Breen EJ, Kuah D, Vesey G, et al. Analysis of in vitro secretion profiles from adipose-derived cell populations. *Journal of Translational Medicine*. 2012;10(1):172.
- [241] Engela AU, Baan CC, Dor FJMF, Weimar W, Hoogduijn MJ. On the interactions between mesenchymal stem cells and regulatory T cells for immunomodulation in transplantation. *Frontiers in Immunology*. 2012;3:126.
- [242] Ivanova-Todorova E, Bochev I, Dimitrov R, Belemezova K, Mourdjeva M, Kyurkchiev S, et al. Conditioned Medium from Adipose Tissue-Derived Mesenchymal Stem Cells Induces CD4FOXP3 Cells and Increases IL-10 Secretion. *Journal of Biomedicine and Biotechnology*. 2012;2012:1–8.
- [243] Solovyeva VV, Salafutdinov II, Martynova EV, Khaiboullina SF, Rizvanov AA. Human adipose derived stem cells do not alter cytokine secretion in response to the genetic modification with pEGFP-N2 plasmid DNA. *World Journal of Applied Sciences*. 2013;26(7):968–972.
- [244] Melief SM, Schrama E, Brugman MH, Tiemessen MM, Hoogduijn MJ, Fibbe WE, et al. Multipotent stromal cells induce human regulatory T cells through a novel pathway involving skewing of monocytes toward anti-inflammatory macrophages. *STEM CELLS*. 2013 sep;31(9):1980–1991.
- [245] Owen AP. The effects of mesenchymal stem cells on a model of autoimmune liver disease. University of Birmingham; 2014.
- [246] Di Nicola M, Carmelo C, Magni M, Milanesi M, Longoni PD, Matteucci P, et al. Human bone marrow stromal cells suppress T-lymphocyte proliferation induced by cellular or nonspecific mitogenic stimuli. *Blood*. 2002;99(10):3838–43.

- [247] Buxbaum J, Qian P, Khuu C, Shneider B, Daikh D, Gershwin M, et al. Novel Model of Antigen-Specific Induction of Bile Duct Injury. *Gastroenterology*. 2006;131(6):1899–1906.
- [248] Wei H, Wei H, Wang H, Tian Z, Sun R. Activation of natural killer cells inhibits liver regeneration in toxin-induced liver injury model in mice via a tumor necrosis factor--dependent mechanism. *American Journal of Physiology-Gastrointestinal and Liver Physiology*. 2010 jul;299(1):G275–G282.
- [249] Waterman RS, Tomchuck SL, Henkle SL, Betancourt AM. A New Mesenchymal Stem Cell (MSC) Paradigm: Polarization into a Pro-Inflammatory MSC1 or an Immunosuppressive MSC2 Phenotype. *PLoS ONE*. 2010 apr;5(4):e10088.
- [250] Krampera M, Glennie S, Dyson J, Scott D, Laylor R, Simpson E, et al. Bone marrow mesenchymal stem cells inhibit the response of naive and memory antigen-specific T cells to their cognate peptide. *Blood*. 2003;101(9):3722–3729.
- [251] da Silva Meirelles L, Nardi NB. Murine marrow-derived mesenchymal stem cell: isolation, in vitro expansion, and characterization. *British Journal of Haematology*. 2003 nov;123(4):702–711.
- [252] Flecknell P. Replacement, reduction and refinement. *ALTEX*. 2002;19(2):73–78.
- [253] Uccelli A, Moretta L, Pistoia V. Mesenchymal stem cells in health and disease. *Nature Reviews Immunology*. 2008;8(9):726–736.
- [254] Gessner A, Blum H, Röllinghoff M. Differential Regulation of IL-9-Expression after Infection with *Leishmania major* in Susceptible and Resistant Mice. *Immunobiology*. 1993;189(5):419 – 435.
- [255] Gueders MM, Paulissen G, Crahay C, Florence Q, Hacha J, Hove C, et al. Mouse models of asthma: a comparison between C57BL/6 and BALB/c strains regarding

- bronchial responsiveness, inflammation, and cytokine production. *Inflammation Research*. 2009;58(12):845–854.
- [256] Yang S, Park M, Yoon I, Kim S, Hong S, Shin J, et al. Soluble mediators from mesenchymal stem cells suppress T cell proliferation by inducing IL-10. *Exp Mol Medicine*. 2009;41(5):315–324.
- [257] Qin Y, Zhou Z, Zhang F, Wang Y, Shen B, Liu Y, et al. Induction of Regulatory B-Cells by Mesenchymal Stem Cells is Affected by SDF-1-CXCR7. *Cellular Physiology and Biochemistry*. 2015;37(1):117–130.
- [258] Majumdar MK, Keane-Moore M, Buyaner D, Hardy WB, Moorman MA, McIntosh KR, et al. Characterization and functionality of cell surface molecules on human mesenchymal stem cells. *Journal of Biomedical Science*. 2003 mar;10(2):228–241.
- [259] Ren G, Zhang L, Zhao X, Xu G, Zhang Y, Roberts A, et al. Mesenchymal Stem Cell-Mediated Immunosuppression Occurs via Concerted Action of Chemokines and Nitric Oxide. *Cell Stem Cell*. 2008;2(2):141–150.
- [260] Taga K, Mostowski H, Tosato G. Human interleukin-10 can directly inhibit T-cell growth. *Blood*. 1993;81(11):2964–2971.
- [261] Oral H, Kotenko S, Yilmaz M, Mani O, Zumkehr J, Blaser K, et al. Regulation of T cells and cytokines by the interleukin-10 (IL-10)-family cytokines IL-19, IL-20, IL-22, IL-24 and IL-26. *European Journal of Immunology*. 2006 feb;36(2):380–388.
- [262] de Waal Malefyt R. Interleukin 10(IL-10) inhibits cytokine synthesis by human monocytes: an autoregulatory role of IL-10 produced by monocytes. *Journal of Experimental Medicine*. 1991 nov;174(5):1209–1220.
- [263] Shouval D, Biswas A, Goettel J, Katelyn M, Conaway E, Redhu N, et al. Interleukin-10 Receptor Signaling in Innate Immune Cells Regulates Mucosal Immune Tolerance and Anti-Inflammatory Macrophage Function. *Immunity*. 2014;40(5):706–719.

- [264] Sun L, Guo RF, Newstead MW, Standiford TJ, Macariola DR, Shanley TP. Effect of IL-10 on Neutrophil Recruitment and Survival after *Pseudomonas aeruginosa* Challenge. *American Journal of Respiratory Cell and Molecular Biology*. 2009 jul;41(1):76–84.
- [265] Nossent AY, Bastiaansen AJNM, Peters EAB, de Vries MR, Aref Z, Welten SMJ, et al. CCR7-CCL19/CCL21 Axis is Essential for Effective Arteriogenesis in a Murine Model of Hindlimb Ischemia. *Journal of the American Heart Association*. 2017 mar;6(3):e005281.
- [266] Takamura K, Fukuyama S, Nagatake T, Kim DY, Kawamura A, Kawauchi H, et al. Regulatory Role of Lymphoid Chemokine CCL19 and CCL21 in the Control of Allergic Rhinitis. *The Journal of Immunology*. 2007 oct;179(9):5897–5906.
- [267] Marsland BJ, Bättig P, Bauer M, Ruedl C, Lässig U, Beerli RR, et al. CCL19 and CCL21 Induce a Potent Proinflammatory Differentiation Program in Licensed Dendritic Cells. *Immunity*. 2005 apr;22(4):493–505.
- [268] English K, Barry FP, Mahon BP. Murine mesenchymal stem cells suppress dendritic cell migration, maturation and antigen presentation. *Immunology Letters*. 2008;115(1):50 – 58.
- [269] Corallini F, Celeghini C, Rimondi E, di Iasio M, Gonelli A, Secchiero P, et al. Trail down-regulates the release of osteoprotegerin (OPG) by primary stromal cells. *Journal of Cellular Physiology*. 2011;226(9):2279 – 2286.
- [270] Zhu H, Jiang XX, Guo ZK, Li H, Su YF, Yao HY, et al. Tumor necrosis factor- $\alpha$  alters the modulatory effects of mesenchymal stem cells on osteoclast formation and function. *Stem Cells and Development*. 2009 dec;18(10):1473–1484.
- [271] Ferrari-Lacraz S, Ferrari S. Do RANKL inhibitors (denosumab) affect inflammation and immunity? *Osteoporosis International*. 2011 Feb;22(2):435–446. Available from: <https://doi.org/10.1007/s00198-010-1326-y>.

- [272] Welling T, Heidt D, Englesbe M, Magee J, Sung R, Campbell D, et al. Biliary complications following liver transplantation in the model for end-stage liver disease era: Effect of donor, recipient, and technical factors. *Liver Transplant*. 2008;14(1):73–80.
- [273] Foley DP, Fernandez LA, Leverson G, Chin LT, Krieger N, Cooper JT, et al. Donation After Cardiac Death. *Annals of Surgery*. 2005 nov;242(5):724–731.
- [274] Linder C, Englund U, Narisawa S, Millán J, Magnusson P. Isozyme profile and tissue-origin of alkaline phosphatases in mouse serum. *Bone*. 2013;53(2):399–408.
- [275] Connolly M, Bedrosian A, Clair J, Mitchell A, Ibrahim J, Stroud A, et al. In liver fibrosis, dendritic cells govern hepatic inflammation in mice via TNF- $\alpha$ . *Journal of Clinical Investigation*. 2009;119(11):3213–3225.
- [276] Katzenellenbogen M, Pappo O, Barash H, Klopstock N, Mizrahi L, Olam D, et al. Multiple Adaptive Mechanisms to Chronic Liver Disease Revealed at Early Stages of Liver Carcinogenesis in the Mdr2-Knockout Mice. *Cancer Research*. 2006;66(8):4001–4010.
- [277] Popov Y, Patsenker E, Fickert P, Trauner M, Schuppan D. Mdr2 (Abcb4)-/- mice spontaneously develop severe biliary fibrosis via massive dysregulation of pro- and antifibrogenic genes. *Journal of Hepatology*. 2005 dec;43(6):1045–1054.
- [278] Assis ACM, Carvalho JL, Jacoby BA, Ferreira RLB, Castanheira P, Diniz SOF, et al. Time-Dependent Migration of Systemically Delivered Bone Marrow Mesenchymal Stem Cells to the Infarcted Heart. *Cell Transplantation*. 2010 feb;19(2):219–230.
- [279] Eggenhofer E, Benseler V, Kroemer A, Popp FC, Geissler EK, Schlitt HJ, et al. Mesenchymal stem cells are short-lived and do not migrate beyond the lungs after intravenous infusion. *Frontiers in Immunology*. 2012;3:297.



- [280] Ge J, Guo L, Wang S, Zhang Y, Cai T, Zhao RC, et al. The Size of Mesenchymal Stem Cells is a Significant Cause of Vascular Obstructions and Stroke. *Stem Cell Reviews and Reports*. 2014;10(2):295 – 303.
- [281] Hoogduijn MJ, van den Beukel JC, Wiersma LCM, Ijzer J. Morphology and size of stem cells from mouse and whale: observational study. *BMJ*. 2013 dec;347(dec12 1):f6833–f6833.
- [282] Allen K, Jaeschke H, Copple BL. Bile Acids Induce Inflammatory Genes in Hepatocytes. *The American Journal of Pathology*. 2011 jan;178(1):175–186.
- [283] Huang W, Ma K, Zhang J, Qatanani M, Cuvillier J, Liu J, et al. Nuclear Receptor-Dependent Bile Acid Signaling Is Required for Normal Liver Regeneration. *Science*. 2006;312(5771):233–236.
- [284] Dixon JA, Gorman RC, Stroud RE, Bouges S, Hirotsugu H, Gorman JH, et al. Mesenchymal Cell Transplantation and Myocardial Remodeling After Myocardial Infarction. *Circulation*. 2009 sep;120(11\_suppl\_1):S220–S229.
- [285] Serrano-Villar S, Sainz T, Lee SA, Hunt PW, Sinclair E, Shacklett BL, et al. HIV-Infected Individuals with Low CD4/CD8 Ratio despite Effective Antiretroviral Therapy Exhibit Altered T Cell Subsets, Heightened CD8 T Cell Activation, and Increased Risk of Non-AIDS Morbidity and Mortality. *PLoS Pathogens*. 2014 may;10(5):e1004078.
- [286] Feuth T, van Baarle D, van Erpecum KJ, Siersema PD, Hoepelman AIM, Arends JE. CD4/CD8 ratio is a promising candidate for non-invasive measurement of liver fibrosis in chronic HCV-monoinfected patients. *European Journal of Clinical Microbiology & Infectious Diseases*. 2014 jan;33(7):1113–1117.
- [287] Zigmond E, Samia-Grinberg S, Pasmanik-Chor M, Brazowski E, Shibolet O, Halpern Z, et al. Infiltrating Monocyte-Derived Macrophages and Resident Kupffer Cells

Display Different Ontogeny and Functions in Acute Liver Injury. *The Journal of Immunology*. 2014 jun;193(1):344–353.

- [288] Lee R, Pulin A, Seo M, Kota D, Ylostalo J, Larson B, et al. Intravenous hMSCs Improve Myocardial Infarction in Mice because Cells Embolized in Lung Are Activated to Secrete the Anti-inflammatory Protein TSG-6. *Cell Stem Cell*. 2009;5(1):54–63.
- [289] Vilalta M, Dégano IR, Bagó J, Gould D, Santos M, García-Arranz M, et al. Biodistribution, Long-term Survival, and Safety of Human Adipose Tissue-derived Mesenchymal Stem Cells Transplanted in Nude Mice by High Sensitivity Non-invasive Bioluminescence Imaging. *Stem Cells and Development*. 2008 Oct;17(5):993–1004.
- [290] SUN L, FAN X, ZHANG L, SHI G, AILI M, LU X, et al. Bone mesenchymal stem cell transplantation via four routes for the treatment of acute liver failure in rats. *International Journal of Molecular Medicine*. 2014 aug;34(4):987–996.
- [291] Wilson D, Roy D, Steyer G, Gargasha M, Stone M, McKinley E. Whole mouse cryo-imaging. In: Hu XP, Clough AV, editors. *Medical Imaging 2008: Physiology, Function, and Structure from Medical Images*. SPIE; 2008. p. 69161I–69161I–9.
- [292] Roy D, Steyer GJ, Gargasha M, Stone ME, Wilson DL. 3D Cryo-Imaging: A Very High-Resolution View of the Whole Mouse. *The Anatomical Record: Advances in Integrative Anatomy and Evolutionary Biology*. 2009 mar;292(3):342–351.
- [293] Jr MB. Semiconductor Nanocrystals as Fluorescent Biological Labels. *Science*. 1998 sep;281(5385):2013–2016.
- [294] Saat TC, van den Engel S, Bijman-Lachger W, Korevaar SS, Hoogduijn MJ, IJzermans JNM, et al. Fate and Effect of Intravenously Infused Mesenchymal Stem Cells in a Mouse Model of Hepatic Ischemia Reperfusion Injury and Resection. *Stem Cells International*. 2016;2016:1–9.

- [295] Gargesha M, de Witte S, Newsome P, Hirschfield G, Clissmann C, Macarthur V, et al. 3D biodistribution of pre-treated MSC in mouse model of liver disease using CryoViz™. *Journal of Immunology*. 2016;196(1 Supplement):56.2.
- [296] Rosen AB, Kelly DJ, Schuldt AJT, Lu J, Potapova IA, Doronin SV, et al. Finding Fluorescent Needles in the Cardiac Haystack: Tracking Human Mesenchymal Stem Cells Labeled with Quantum Dots for Quantitative In Vivo Three-Dimensional Fluorescence Analysis. *Stem Cells*. 2007 aug;25(8):2128–2138.
- [297] Schrepfer S, Deuse T, Reichenspurner H, Fischbein M, Robbins R, Pelletier M. Stem Cell Transplantation: The Lung Barrier. *Transplantation Proceedings*. 2007;39(2):573 – 576.
- [298] Milosavljevic N, Gazdic M, Markovic B, Arsenijevic A, Nurkovic J, Dolicanin Z, et al. Mesenchymal stem cells attenuate acute liver injury by altering ratio between interleukin 17 producing and regulatory natural killer T cells. *Liver Transplant*. 2017;23(8):1040–1050.
- [299] Haga H, Yan IK, Takahashi K, Matsuda A, Patel T. Extracellular Vesicles from Bone Marrow-Derived Mesenchymal Stem Cells Improve Survival from Lethal Hepatic Failure in Mice. *STEM CELLS Translational Medicine*. 2017 feb;6(4):1262–1272.
- [300] Victorino GP, Ramirez RM, Chong TJ, Curran B, Sadjadi J. Ischemia-reperfusion injury in rats affects hydraulic conductivity in two phases that are temporally and mechanistically separate. *American Journal of Physiology-Heart and Circulatory Physiology*. 2008 nov;295(5):H2164–H2171.
- [301] Saidi RF, Rajeshkumar B, Sharifabrizi A, Bogdanov AA, Zheng S, Dresser K, et al. Human adipose derived mesenchymal stem cells attenuate liver ischemia reperfusion injury and promote liver regeneration. *Surgery*. 2014;156(5):1225 – 1231.
- [302] Lu W, Si Y, Ding J, Chen X, Zhang X, Dong Z, et al. Mesenchymal stem cells

attenuate acute ischemia-reperfusion injury in a rat model. *Experimental and Therapeutic Medicine*. 2015 Oct;10(6):2131–2137.

- [303] Shen X, Gao F, Ke B, Zhai Y, Lassman CR, Tsuchihashi S, et al. Inflammatory responses in a new mouse model of prolonged hepatic cold ischemia followed by arterialized orthotopic liver transplantation. *Liver Transplant*. 2005;11(10):1273–1281.
- [304] Hines IN, Hoffman JM, Scheerens H, Day BJ, Harada H, Pavlick KP, et al. Regulation of postischemic liver injury following different durations of ischemia. *American Journal of Physiology-Gastrointestinal and Liver Physiology*. 2003 mar;284(3):G536–G545.
- [305] Yang M, Antoine D, Weemhoff J, Jenkins R, Farhood A, Park B, et al. Biomarkers distinguish apoptotic and necrotic cell death during hepatic ischemia/reperfusion injury in mice. *Liver Transplant*. 2014;20(11):1372–1382.
- [306] Jessica G, Drucker C, Malchow S, Scheller J, Stefan R. Role of IL-6 trans-signaling in CCl<sub>4</sub> induced liver damage. *Biochimica Et Biophysica Acta Bba - Mol Basis Dis*. 2010;1802(11):1054–1061.
- [307] Gong J, Wang J, Tian Y, Zhang J, Liang W, Li Z, et al. Expression of tubulin folding cofactor B in mouse hepatic ischemia-reperfusion injury. *Biomed Reports*. 2017;6(5):525–531.
- [308] Richards JA, Wigmore SJ, Anderton SM, Howie SEM. NKT cells are important mediators of hepatic ischemia-reperfusion injury. *Transplant Immunology*. 2017 dec;45:15–21.
- [309] Wang M, Liang C, Hu H, Zhou L, Xu B, Wang X, et al. Intraperitoneal injection (IP), Intravenous injection (IV) or anal injection (AI)? Best way for mesenchymal stem cells transplantation for colitis. *Scientific Reports*. 2016 aug;6(1):srep30696.

- [310] Kurtz A. Mesenchymal Stem Cell Delivery Routes and Fate. *International Journal of Stem Cells*. 2008 nov;1(1):1–7.
- [311] Uemoto S, Fujimoto Y, Teratani T, Kanazawa H, Iwasaki J, Xiangdong Z, et al. Introduction of Mesenchymal Stem Cells for Liver Surgery (Hepatectomy and Transplantation). In: *Innovative Medicine*. Springer Japan; 2015. p. 281–293.
- [312] Melloul E, Hübner M, Scott M, Snowden C, Prentis J, Dejong C, et al. Guidelines for Perioperative Care for Liver Surgery: Enhanced Recovery After Surgery (ERAS) Society Recommendations. *World Journal of Surgery*. 2016;40(10):2425–2440.
- [313] Jaeschke H, Farhood A. Neutrophil and Kupffer cell-induced oxidant stress and ischemia-reperfusion injury in rat liver. *American Journal of Physiology-Gastrointestinal and Liver Physiology*. 1991 mar;260(3):G355–G362.
- [314] Tsung A, Hoffman RA, Izuishi K, Critchlow ND, Nakao A, Chan MH, et al. Hepatic Ischemia/Reperfusion Injury Involves Functional TLR4 Signaling in Nonparenchymal Cells. *The Journal of Immunology*. 2005 nov;175(11):7661–7668.
- [315] Jaeschke H. Mechanisms of Liver Injury. II. Mechanisms of neutrophil-induced liver cell injury during hepatic ischemia-reperfusion and other acute inflammatory conditions. *American Journal of Physiology-Gastrointestinal and Liver Physiology*. 2006 jun;290(6):G1083–G1088.
- [316] Caldwell CC, Okaya T, Martignoni A, Husted T, Schuster R, Lentsch AB. Divergent functions of CD4 T lymphocytes in acute liver inflammation and injury after ischemia-reperfusion. *American Journal of Physiology-Gastrointestinal and Liver Physiology*. 2005 nov;289(5):G969–G976.
- [317] Pak S, Kondo T, Nakano Y, Murata S, Fukunaga K, Tatsuya O, et al. Platelet adhesion in the sinusoid caused hepatic injury by neutrophils after hepatic ischemia reperfusion. *Platelets*. 2010;21(4):282 – 288.

- [318] Hanboon BK, Ekataksin W, Alsfasser G, Schemmer P, Urbaschek B, McCuskey RS, et al. Microvascular dysfunction in hepatic ischemia–reperfusion injury in pigs. *Microvascular Research*. 2010 jul;80(1):123–132.
- [319] Caldwell CC, Tschoep J, Lentsch AB. Lymphocyte function during hepatic ischemia/reperfusion injury. *Journal of Leukocyte Biology*. 2007;82(3):457 – 464.
- [320] Datta G. Molecular mechanisms of liver ischemia reperfusion injury: Insights from transgenic knockout models. *World Journal of Gastroenterology*. 2013;19(11):1683.
- [321] Rose S, Misharin A, Perlman H. A novel Ly6C/Ly6G-based strategy to analyze the mouse splenic myeloid compartment. *Cytometry Part A*. 2011 dec;81A(4):343–350.
- [322] Beldi G, Banz Y, Kroemer A, Sun X, Wu Y, Graubardt N, et al. Deletion of CD39 on natural killer cells attenuates hepatic ischemia/reperfusion injury in mice. *Hepatology*. 2010;51(5):1702–1711.
- [323] Shimamura K, Kawamura H, Nagura T, Kato T, Naito T, Kameyama H, et al. Association of NKT cells and granulocytes with liver injury after reperfusion of the portal vein. *Cellular Immunology*. 2005;234(1):31 – 38.
- [324] Kavanagh DPJ, Suresh S, Newsome PN, Frampton J, Kalia N. Pretreatment of Mesenchymal Stem Cells Manipulates Their Vasculoprotective Potential While Not Altering Their Homing Within the Injured Gut. *STEM CELLS*. 2015 jun;33(9):2785–2797.
- [325] Magaña-Guerrero FS, Domínguez-López A, Martínez-Aboytes P, Buentello-Volante B, Garfias Y. Human Amniotic Membrane Mesenchymal Stem Cells inhibit Neutrophil Extracellular Traps through TSG-6. *Scientific Reports*. 2017 sep;7(1):12426.
- [326] da Costa Gonçalves F, Grings M, Nunes NS, Pinto FO, Garcez TNA, Visioli F, et al. Antioxidant properties of mesenchymal stem cells against oxidative stress in a murine model of colitis. *Biotechnology Letters*. 2016 dec;39(4):613–622.

- [327] Ko E, Lee K, Hwang D. Human Umbilical Cord Blood–Derived Mesenchymal Stem Cells Undergo Cellular Senescence in Response to Oxidative Stress. *Stem Cells and Development*. 2012;21(11):1877–1886.
- [328] Deschepper M, Oudina K, David B, Myrtil V, Collet C, Bensidhoum M, et al. Survival and function of mesenchymal stem cells (MSCs) depend on glucose to overcome exposure to long-term, severe and continuous hypoxia. *Journal of Cellular and Molecular Medicine*. 2011;15(7):1505–1514.
- [329] Pezzati D. Strategies to optimize the use of marginal donors in liver transplantation. *World Journal of Hepatology*. 2015;7(26):2636.
- [330] Zhai Y, Petrowsky H, Hong JC, Busuttil RW, W KJ. Ischaemia–reperfusion injury in liver transplantation—from bench to bedside. *Nature Reviews Gastroenterology & Hepatology*. 2012;10(2):79.
- [331] Wojcicki M, Milkiewicz P, Silva M. Biliary Tract Complications after Liver Transplantation: A Review. *Digestive Surgery*. 2008;25(4):245–257.
- [332] Routh D, Sharma S, Naidu CS, Rao PP, Sharma AK, Ranjan P. Comparison of outcomes in ideal donor and extended criteria donor in deceased donor liver transplant: A prospective study. *International Journal of Surgery*. 2014 aug;12(8):774–777.
- [333] Detry O, Vandermeulen M, Delbouille M, Somja J, Bletard N, Briquet A, et al. Infusion of mesenchymal stromal cells after deceased liver transplantation: A phase I–II, open-label, clinical study. *Journal of Hepatology*. 2017;67(1):47–55.
- [334] Kyurkchiev D. Secretion of immunoregulatory cytokines by mesenchymal stem cells. *World Journal of Stem Cells*. 2014;6(5):552.
- [335] Karatzas T, Neri AA, Baibaki ME, Dontas IA. Rodent models of hepatic ischemia–reperfusion injury: time and percentage-related pathophysiological mechanisms. *Journal of Surgical Research*. 2014 oct;191(2):399–412.

- [336] Kimura S, Ozaki K, Ueki S, Zhang M, Yokota S, Stolz D, et al. Contribution of alloantigens to hepatic ischemia/reperfusion injury: Roles of natural killer cells and innate immune recognition of nonself. *Liver Transplant*. 2016;22(1):80–90.
- [337] dos Santos CHM, Dourado DM, da Silva BAK, Pontes HBD, de Azevedo-Neto E, da Cruz Vendas GS, et al. Atorvastatin Can Prevent Hepatic Remote Reperfusion Injury. *ABCD Arquivos Brasileiros de Cirurgia Digestiva (São Paulo)*. 2017 sep;30(3):197–200.
- [338] Santos C, Dourado D, Silva B, Pontes H, Neto E, Vendas G, et al. Atorvastatin Protects Kidney from Remote Reperfusion Injury. *Annals of Vascular Surgery*. 2018;46:351–356.
- [339] Amer MEM, El-Sayed SZ, El-Kheir WA, Gabr H, Gomaa AA, El-Noomani N, et al. Clinical and laboratory evaluation of patients with end-stage liver cell failure injected with bone marrow-derived hepatocyte-like cells. *European Journal of Gastroenterology & Hepatology*. 2011 oct;23(10):936–941.
- [340] Jacobs SA, Roobrouck VD, Verfaillie CM, Gool SWV. Immunological characteristics of human mesenchymal stem cells and multipotent adult progenitor cells. *Immunology and Cell Biology*. 2013 jan;91(1):32–39.
- [341] Li J, Ezzelarab MB, Cooper DKC. Do mesenchymal stem cells function across species barriers? Relevance for xenotransplantation. *Xenotransplantation*. 2012 sep;19(5):273–285.
- [342] Vadori M, Cozzi E. Immunological Challenges and Therapies in Xenotransplantation. *Cold Spring Harbor Perspectives in Medicine*. 2014 mar;4(4):a015578–a015578.
- [343] Pirenne J, Monbaliu D, Aerts R, Desschans B, Liu Q, Cassiman D, et al. Biliary Strictures After Liver Transplantation: Risk Factors and Prevention by Donor Treatment With Epoprostenol. *Transplantation Proceedings*. 2009 oct;41(8):3399–3402.



- [344] Tacke F, Zimmerman H. Macrophage heterogeneity in liver injury and fibrosis. *Journal of hepatology*. 2014;60(5):1090–1096.
- [345] Ramachandran P, Pellicoro A, Vernon MA, Boulter L, Aucott RL, Ali A, et al. Differential Ly-6C expression identifies the recruited macrophage phenotype, which orchestrates the regression of murine liver fibrosis. *Proceedings of the National Academy of Sciences*. 2012 oct;109(46):E3186–E3195.
- [346] Dal-Secco D, Wang J, Zeng Z, Kolaczowska E, Wong CHY, Petri B, et al. A dynamic spectrum of monocytes arising from the in situ reprogramming of CCR2 monocytes at a site of sterile injury. *The Journal of Experimental Medicine*. 2015 mar;212(4):447–456.
- [347] Preda MB, Rønningen T, Burlacu A, Simionescu M, Moskaug JØ, Valen G. Remote Transplantation of Mesenchymal Stem Cells Protects the Heart Against Ischemia-Reperfusion Injury. *STEM CELLS*. 2014 jul;32(8):2123–2134.
- [348] Mönkkönen J, Taskinen M, Auriola S, Urtti A. Growth Inhibition of Macrophage-Like and Other Cell Types by Liposome-Encapsulated, Calcium-Bound, and Free Bisphosphonates In Vitro. *Journal of Drug Targeting*. 1994;2(4):299 – 308.
- [349] Buch T, Heppner FL, Tertilt C, Heinen TJAJ, Kremer M, Wunderlich FT, et al. A Cre-inducible diphtheria toxin receptor mediates cell lineage ablation after toxin administration. *Nature Methods*. 2005 jun;2(6):419–426.
- [350] Sheng H, Wang Y, Jin Y, Zhang Q, Zhang Y, Wang L, et al. A critical role of IFN in priming MSC-mediated suppression of T cell proliferation through up-regulation of B7-H1. *Cell Research*. 2008 jul;18(8):846–857.
- [351] Thanunchai M, Hongeng S, Thitithanyanont A. Mesenchymal Stromal Cells and Viral Infection. *Stem Cells International*. 2015;2015:1–8.

- [352] Zhang Z, Fu J, Xu X, Wang S, Xu R, Zhao M, et al. Safety and immunological responses to human mesenchymal stem cell therapy in difficult-to-treat HIV-1-infected patients. *AIDS*. 2013 may;27(8):1283–1293.
- [353] zheng Pan G, Yang Y, Zhang J, Liu W, ying Wang G, cai Zhang Y, et al. Bone marrow mesenchymal stem cells ameliorate hepatic ischemia/reperfusion injuries via inactivation of the MEK/ERK signaling pathway in rats. *Journal of Surgical Research*. 2012 dec;178(2):935–948.
- [354] Li W, Ren G, Huang Y, Su J, Han Y, Li J, et al. Mesenchymal stem cells: a double-edged sword in regulating immune responses. *Cell Death and Differentiation*. 2012;19(9):1505–1513.
- [355] Luk F, de Witte SFH, Korevaar SS, van Rhijn MR, Franquesa M, Strini T, et al. Inactivated Mesenchymal Stem Cells Maintain Immunomodulatory Capacity. *Stem Cells and Development*. 2016 sep;25(18):1342–1354.
- [356] de Witte SF, Gargasha M, Merino A, Elliman SJ, Newsome PN, Roy D, et al. In vivo tracking of live and dead mesenchymal stromal cells. *Cytotherapy*. 2017 may;19(5):S155.